

NOTTINGHAM TRENT UNIVERSITY

Synthesis and functionalization of metal and metal oxide nanoparticles for theranostics

PhD Thesis 2009-2013

Victoria Jane Mundell

A thesis submitted in partial fulfilment of the requirements of Nottingham Trent University for the degree of Master of Philosophy.

6/1/2013

This work is the intellectual property of the author. You may copy up to 5% of this work for private study, or personal, non-commercial research. Any re-use of the information contained within this document should be fully referenced, quoting the author, title, university, degree level and pagination. Queries or requests for any other use, or if a more substantial copy is required, should be directed to the owner of the Intellectual Property Rights.

Acknowledgments

First and foremost I would like to thank my supervisor Dr Gareth Cave for giving me the opportunity to do this PhD and for his continuing support.

I would like to thank Nottingham Trent University for the funding that allowed me to carry out this research project.

Next my thanks go to the other people at Nottingham Trent University who helped me through this phase of my life. To Muriel, for her songs, wisdom, advice, and patience when I didn't get my washing up or cleaning done when I should. To Dan for entertaining me, and for finding solutions when things broke, like the time my precious products got stuck in the centrifuge and they were going to autoclave them. To Matteo for singing, for espresso and for being contagiously cheerful. To Bob Rees and Martin Bencsik for their guidance on the biology and physics; I would have been lost without your input. To Shraddha, Jamie, Graham, Stephanie, Naomi and David for help with the practical biology, and to Rob for his explanation of MRI relaxation. To Gary Hix, for asking me such difficult questions that it made me look at my work in a new light, although it was stressful at the time I really appreciated it in the long run. And to Barbara, for processing my orders so quickly that I was rarely without what I needed.

My masters students also deserve both my thanks and my praise. They have kept me on track and constantly tested my understanding as well as helping in the formulation of methods. So to Dipen, Sahar, Uche, Eyman, and Kinjal; Thank you.

I would also like to thank everyone else in the NSRC lab 113 who have either distracted me with conversation when I was feeling overwhelmed, or who offered me advice when I needed a fresh perspective. So to John, Alberth, Chris, Andy, Gary, Adam, Pat, Fathi, Ismael and Sammy; thank you.

My utmost thanks goes to my parents and step-parents who have always supported and believed in me. Just knowing that you thought I could do it meant that I could.

To my wonderful husband Carl without whom I would have had to give up at the first hurdle. You took over all of the childcare and housework, put up with my stomping around when I was fed up of writing, put up with the late nights and early mornings, and even managed to keep me fed, clothed and sane. My love to you always, you were my saviour through all of this.

And finally I dedicate this to my children. To Sean and Maia, my reason for doing anything in this world. This is for you, to show you that if you put your mind to anything then you really can do it, and to let you know that I will always be behind you 100 %.

Abstract

Metal and metal oxide nanoparticles including calcium oxide, gold, and superparamagnetic iron oxide nanoparticles (SPIOs) were synthesised using a range of techniques including reduction, co-precipitation and spinning disc technology. SPIOs were primarily synthesised *via* a co-precipitation method using iron (II) chloride, iron (III) chloride and ammonia; a spinning disc reactor and gaseous ammonia were trialled successfully for scale up, producing spherical particles of 10-40 nm in diameter as analysed by TEM.

Nanoparticles were coated *via* a novel solvent-free grinding process which was successful for drug molecules, immunogenic peptides and amino acids; the mode of binding theorised to be taking place *via* an electrostatic interaction between the SPIO and the carboxyl, amine or hydroxyl groups on the coating materials. Recrystallisation of the coating materials to form HCl salts, was found to increase the binding efficiency with no detrimental effects to the particles. These coated SPIOs were found to be stable in a range of buffered solutions as well as blood and cell culture media.

Separation of particles by size exclusion chromatography (SEC), dialysis and magnetic separation was only effective for a small range of coatings, with high speed centrifugation at a speed of 60 000 rpm being confirmed as the only universally successful method.

Imaging of citrate capped gold nanoparticles using a CT phantom revealed that gold concentrations of 3700 mg.l⁻¹ were required for *in vivo* use and so this was not continued. Coated SPIOs however produced relaxation times comparable with Endorem[®], as well as being non-toxic. SPIOs coated in this way were more stable than Endorem[®] and stayed in solution retaining their superparamagnetic properties for periods in excess of 72 days with only a negligible degree of degradation.

Various peptides were synthesised using an optimised microwave assisted solid-phase peptide synthesis (SPPS) method using double the suggested coupling times, all of which were analysed for purity and structure using MALDI-TOF MS and HPLC. A cell-penetrating peptide (CPP) synthesised *via* this method was coated onto SPIOs and mixed into a gel for transdermal delivery using porcine skin. An NMR profile of the skin using a 0.25T NMR MOUSE[®] before and after application of the gel showed that after an incubation period of 2 hrs the CPP-SPIOs had penetrated the skin leading to a reduction in signal. This has potential applications for subcutaneous drug delivery and hyperthermia.

Cell studies using U937 and BMDCs indicated by both ICP and fluorescence microscopy that SPIOs coated with fluorescently labelled peptides were successfully taken up into cells. SPIOs were further

investigated as vectors for delivery of immunogenic peptides, namely p53(105) using female C57BL/6 mice. Results indicated that mice immunised with SPIO as a vector showed similar levels of immune response to the p53(105) following immunisation as when incomplete Freund's adjuvant (IFA) was used. However, SPIO immunisations produced a significantly increased specific response compared to the condition using IFA. Results indicate that SPIO could be successful as a vector for cancer vaccines.

Table of Contents

Acknowledgments.....	2
Abstract.....	4
List of Abbreviations	8
Chapter 1.1: Synthesis and functionalization of metal and metal oxide nanoparticles	11
Section 1: Synthesis of Nanoparticles.....	11
Section 2: Coating of Nanoparticles	23
Section 3: Purification of Nanoparticles.....	36
Chapter 1.2: Nanoparticles and Medical Imaging.....	42
Section 1: X-Ray Imaging.....	44
Section 2: Magnetic Resonance Imaging	51
Chapter 1.3: Cancer Immunotherapy	69
Section 1: Cancer	69
Section 2: The immune system and Immunisation.....	80
Section 3: Identifying immunogenic peptides	84
Section 4: P53.....	85
Section 5: Peptide Synthesis	89
Section 6: Vectors	94
Section 7: Adjuvants	99
Section 8: Research Hypothesis, Aims and Objectives	104
Chapter 2: Results and Discussion	105
Section 1: Synthesis and coating of SPIOs	105
Section 2: Medical Imaging.....	141
Section 3: Transdermal drug delivery	148
Section 4: Immunotherapy	155
Chapter 3: Materials and Methodology.....	180
Section 1: General Experimental	180
Section 2: Synthesis, functionalization and purification of iron oxide nanoparticles (SPIOs)	188
Section 3: Synthesis and functionalization of other nanoparticles	210
Section 4: Medical Imaging.....	213
Section 5: Transdermal drug delivery	216
Section 6: Immunotherapy	220
Chapter 4: Conclusion.....	237

Section 1: Synthesis of Particles	237
Section 2: Coating of particles	238
Section 3: Separation and purification of particles	240
Section 4: Medical Imaging.....	242
Section 5: Cell Studies for uptake of coated SPIOs.....	244
Section 6: Mouse Immunisations.....	245
References	246

List of Abbreviations

ACN	Acetonitrile
ATP	Adenosine 5' triphosphate
APC	Antigen Presenting Cell
ATP	Adenosine triphosphate
CD	Cluster of Differentiation
CFA	Complete Freund's Adjuvant
DAPI	4',6-diamidino-2-phenylindole
DCM	Dichloromethane
DIEA	Diisopropylethylamine
DLS	Dynamic Light Scattering
DMF	Dimethylformamide
DNA	Deoxyribose nucleic acid
DODT	3,6-dioxa-1,8-octanedithiol
EDTA	Ethylenediaminetetraacetic acid
EDX	Energy Dispersive X-Ray
FACS	Fluorescence assisted cell sorting
FCS	Foetal Calf Serum
FDA	Food and Drug Agency
FITC	Fluorescein isothiocyanate
Fmoc	Fluorenylmethyloxycarbonyl chloride
GI	Gastrointestinal
GMCSF	Granulocyte macrophage colony-stimulating factor

GNP	Gold Nanoparticle
HBTU	N-[(1H-benzotriazol-1-yl)(dimethylamino)methylene]-N-methylmethan -aminium hexafluorophosphate N-oxide
HCl	Hydrochloric Acid
HEPES	Hydroxyethyl piperazine ethanesulfonic acid
HPLC	High performance liquid chromatography
HSP	Heat shock protein
ICP-AES	Inductively couple plasma – atomic emission spectroscopy
IFA	Incomplete Freund's Adjuvant
IV	Intra venous
KT Cell	Killer T Cell
LPS	Lipopolysaccharide
MACS	Magnetic assisted cell sorting
MHC	Major Histocompatibility Complex
MO	Microorganism
MRI	Magnetic Resonance Imaging
MS	Mass spectrometry
NMP	N-methylpyrrolidone
NMR	Nuclear magnetic resonance
PBS	Phosphate buffered saline
PCR	Polymerase chain reaction
PEG/PEO	Polyethylene glycol/Polyethylene oxide
PET	Positron emission tomography

PGA	Poly glycolic acid
PLA	Poly lactic acid
PVA	Polyvinyl alcohol
RES	Reticuloendothelial system
RI	Refractive Index
RNA	Ribose Nucleic Acid
RPM	Revolutions per minute
SDR	Spinning Disc Reactor
SEC	Size exclusion chromatography
SEREX	Serological Identification of Recombinantly Expressed Clones
SPIO	Superparamagnetic iron oxide
SPPS	Solid Phase Peptide Synthesis
TEG	Triethylene glycol
TEM	Transmission Electron Microscopy
TFA	Trifluoroacetic acid
TGA	Thermogravimetric analysis
TIS	Triisopropyl silane
TOPO	Trioctylphosphine oxide

Chapter 1.1: Synthesis and functionalization of metal and metal oxide nanoparticles

Section 1: Synthesis of Nanoparticles

Nanotechnology is defined as science, engineering and technology conducted at the nanoscale, with nanoparticles being those with at least one dimension being between 1 and 100 nanometres.

In his talk “Plenty of room at the bottom” Richard P. Feynman talks about manipulating and controlling things on a small scale; the underpinning motivation for the field of nanoscience.¹ He talked about rearranging atoms so that we can create substances that are an exact number of atoms high or wide, what we would consider to be nanoscience, although the term was not coined until over a decade after his talk, by Professor Norio Taniguchi.² Although we are not there yet, it points in the direction in which nanotechnology is ultimately travelling. We can now through carefully controlled reactions produce particles of specific sizes and shapes.³

As illustrated in Eric Drexler’s “Engines of creation” he also believes that technology will lead the way to being able to arrange atoms individually, and here he coins the term “molecular technology” which is another way of saying nanotechnology, being slightly more descriptive.⁴ He talks about perfecting the art of building at the molecular level, paying attention to both omission of nucleotides in construction of DNA, and amino acids in construction of proteins, which is of particular relevance to this research.

Above all, both Feynman and Drexler highlighted the abundance of progress that still remains to be made in nanoscience, as well as opening our eyes to all of the potential benefits and applications (as well as dangers) of being able to precisely manipulate things at a molecular level.

Nanoparticles are found in many natural environments, for example they are present in volcanic ash, ocean spray, and even homing pigeons.⁵ Although we are adept at exploiting natural resources, for scientific purposes it is often necessary to artificially synthesise nanoparticles. The main methods that will be discussed herein are: Thermal decomposition,⁶⁻¹² Microemulsion (and reverse

microemulsion),¹³⁻²⁷ Sonochemical,²⁸⁻³⁸ Spinning Disc³⁹⁻⁴¹ and Calcination,^{26, 42-47} although brief mention will be given to other methods.

When discussing each synthesis the merits of the synthetic route, and also the drawbacks with regards to general effectiveness, and in terms of green chemistry will be discussed. As the focus on nanotechnology and producing nanomaterials becomes wider spread, it is important that we not only find effective ways of producing these materials with high purity and even size distribution, but also that we do it in a way that is sustainable.

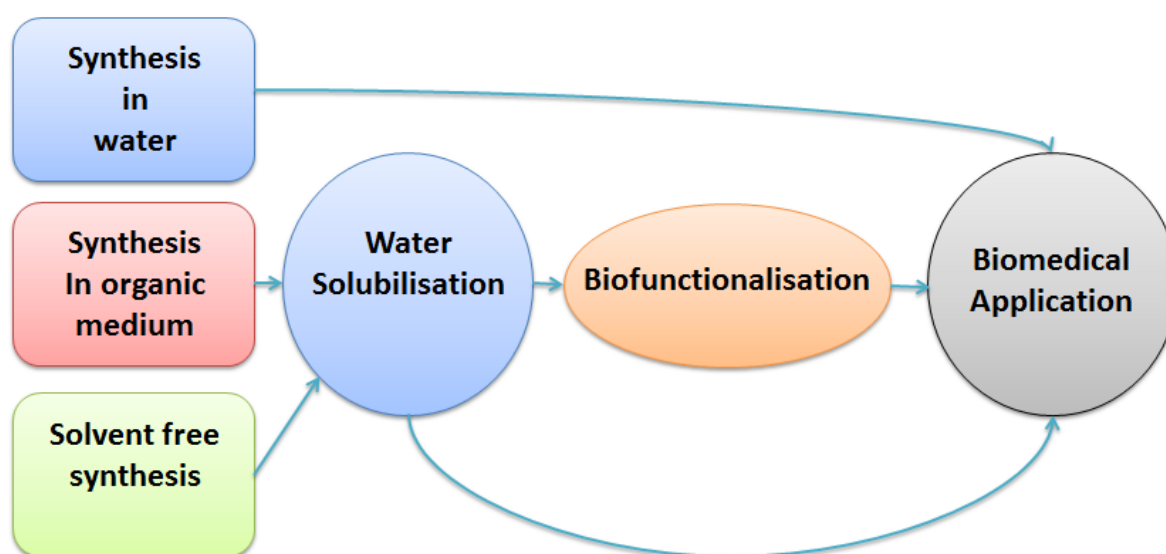


Figure 1. Image showing the basic processes for synthesis of particles for biomedical applications

1.1 Thermal Decomposition, Calcination and Annealing

These three methods all require some degree of heating but are used in different parts of the process. Thermal decomposition is used in the primary synthesis of the particles, whereas calcination and annealing are used to change the particle structure post-formation. During thermal decomposition a precursor material, typically a complex of a metal salt such as copper chloride,⁴⁸ iron carbonyl,⁴⁹ and iron acetyl acetonate¹⁰ is heated until it decomposes to form the nanoparticle. Different decomposition temperatures give rise to nanoparticles of different sizes and so through

controlling the reaction temperature by manipulation of solvents, it is possible to carefully control the size of the materials produced. This occurs because the nucleation rate is affected by temperature, with smaller crystals being formed at higher temperatures due to slower nucleation. One issue with thermal decomposition is that the particles formed are not stable in air and become easily oxidised *e.g.* Iron nanoparticles becoming oxidised to iron oxide and magnetite (Fe_3O_4 containing iron (II) and iron (III) ions) being oxidised to maghemite (Fe_2O_3 containing only iron (III) ions). For this purpose a stabilising agent is added, with oleic acid and various oleate salts being popular (Figure 2).^{10, 48, 50} The oleate ion has a hydrophobic tail and hydrophilic head, allowing it to form a micelle-like structure around the particles. Stabilising agents like this prevent aggregation and Ostwald ripening, as well as protecting the particle from oxidation.⁵⁰

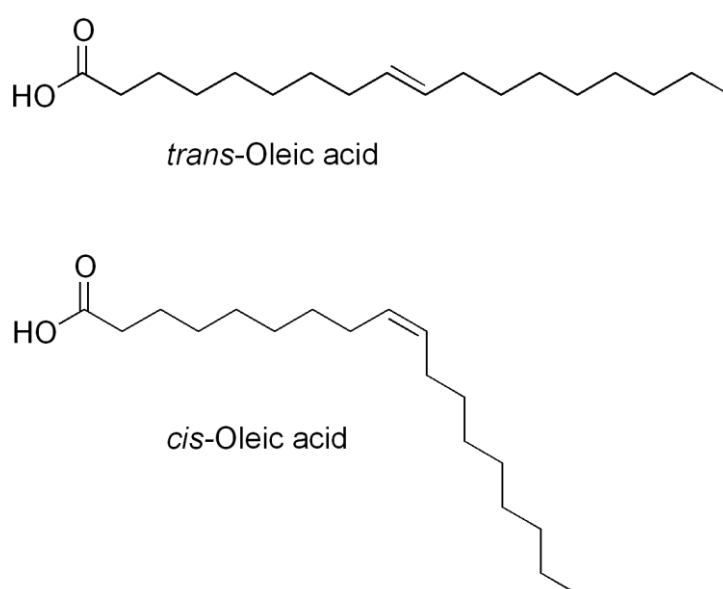


Figure 2. Images of oleic acid, one of the most popular stabilising agents in the formation of nanoparticles.

Although more benign, low energy, methods of synthesis are being explored thermal decomposition remains a popular option for many types of nanoparticle as it can be carried out in organic solvents, which further protect the particle from risk of oxidation.⁵⁰ As has been previously mentioned, use of metal acetyl acetonate precursors containing metals such as copper and iron are commonly used for thermal decomposition (typically in the presence of stabilising materials such as oleyl amine and/or oleic acid)^{10, 48, 50} but other precursors containing ligands such as tetraethoxysilane and tetramethoxysilicate to create silica and silica coated nanoparticles, are also well documented.^{18, 51}

Although organic solvents are the usual choice, decomposition can be achieved in aqueous solvents, using an aqueous soluble precursor. An example of this is the thermal decomposition of a Cu-oleate precursor, formed from CuCl_2 and sodium oleate, to form copper nanoparticles.⁴⁸ In this instance the concentration of the capping agent leads to different sizes of particle. Aqueous soluble magnetite particles have also been produced, by using iron acetyl acetonate in tri ethylene glycol (TEG), with the resultant particles being coated with the TEG.⁵² Aqueous syntheses are preferential as they eliminate the use of organic solvents, and so reduce pollution from the reaction. It also gives rise to aqueous soluble particles, which can lend themselves to biomedical applications.^{53, 54}

In order to overcome the problems associated with using solvents in syntheses, a method has been reported for the solvent free synthesis of magnetite.¹⁰ The experimenters dissolve the iron acetyl acetonate precursor in a mixture of oleic acid and oleylamine, dehydrate the mixture and then heat it to 300 °C (for various times), leading to nanoparticles of different sizes, with size being dependent on the heating time. As could be predicted, longer reaction times lead to larger particles, however the experimenter notes that in the absence of solvent there is also an absence of Ostwald ripening where smaller particles are added to larger particles thus increasing the number of large particles and decreasing the number of small particles. This results indicate that the solvent free methods are a possible solution to this problem.¹⁰ Also of note is that this method overcomes the issue of temperature limitations. Whilst the boiling point of the solvent in traditional thermal decomposition methods limits the reaction temperature, in this solvent free method the temperature can be higher or lower as desired.

Another issue with thermal decomposition is the use of high temperatures to decompose the materials. For example, during the formation of ZnO nanoparticles zinc acetate is used, both because of its high solubility and its "low decomposition temperature".^{7, 55} The reported low temperature is above 200 °C, which is a relatively high temperature, considering other particles can be formed at room temperature.

Annealing is used in conjunction with many synthetic methods, but is a method of changing the particles from one form into another rather than a method of formation itself. Annealing involves heat treating the particles post formation in air or an inert atmosphere, in order to change the microstructure of the particles. For example, during the formation of tungsten nanoparticles from

tungsten hexacarbonyl *via* thermal decomposition, amorphous particles are formed.¹¹ By annealing at temperatures of 600 °C, these amorphous particles all became body centred cubic crystalline.

Calcination, another heating technique, can be used either to decompose the precursor materials, or to affect the particles post formation.⁴² During calcination any salts present which decompose at the temperatures applied, are converted into oxide. Calcining also drives off any water associated to the particles, leading to anhydrous materials. Nickel oxide (NiO) nanoparticles can be formed *via* a calcining procedure during which the precursor material, basic nickel carbonate, is trapped within a gel and dehydrated prior to calcining, leading to uniform particles that do not agglomerate.⁴⁵ This is unusual as typically calcination leads to agglomeration of particles, and in fact this property has been exploited during the formation of TiO₂ particles, to form larger structures with smaller pore size for potential use in photocatalysis and other applications.²⁶ However, the method of forming a gel/sol gel followed by hydration and then calcination has been applied successfully in other cases.⁴⁴

So, whilst these synthetic routes lead to materials with carefully controlled particle sizes, there are disadvantages such as the high reaction temperatures (and energy requirements), and the resultant coating of the particles, which need to be overcome.

1.2 Microemulsion/Reverse Microemulsion

Microemulsions are colloidal 'nano-dispersions' of two immiscible liquids (typically referred to as oil and water) stabilized by a surfactant film. They are thermodynamically stable and can interact to allow chemicals trapped within them to react with each other, as illustrated by the channel between the micelles illustrated in Figure 3.²⁵ In a microemulsion droplet size is typically 6-80 nm and these droplets are often referred to as "nanoreactors".¹⁵ Also documented are "mini-emulsions" with a droplet size of a few hundred nanometres.⁵⁶ The term "microemulsion" refers to emulsions in which the droplets are oil in water and the surfactant has the hydrophilic heads exposed on the outside of the micelle. The term "reverse microemulsion" refers to an emulsion in which water droplets are suspended in oil and the hydrophobic tails of the surfactant are on the outside of the (reverse) micelle.

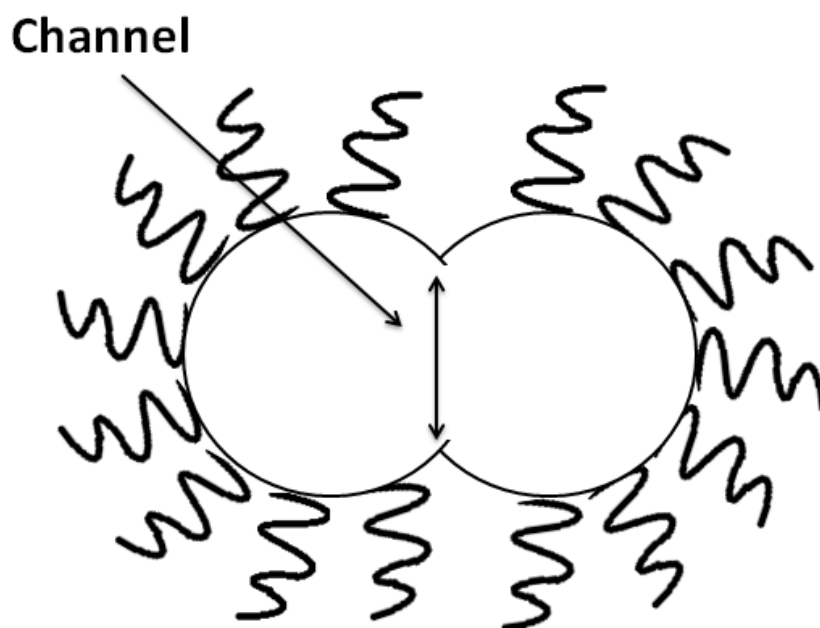


Figure 3. Showing how two micelles can fuse together to form a fused dimer. Note that in the centre the two membrane of the two micelles have formed one large membrane with a channel in the middle through which contents can mix.

The microemulsion can be tailored to both organic and aqueous soluble materials as the colloids can be inverted to have either the hydrophobic or hydrophilic groups on the outside (direct or reverse micelles) as illustrated in Figure 4.²⁵ A typical surfactant is sodium dodecyl sulphate (Figure 5), which has a long chain hydrocarbon tail which can interact with non-polar media, and a hydrophilic head, suitable for interaction with polar (aqueous) media. Microemulsions can be tailored to produce nanoparticles of specific sizes, as the inside of the micelles will limit the nanoparticle growth, particularly if the film is sparingly flexible. This area can also affect other factors such as concentration and ratio of reactants. It is also worth noting that as the particles are formed within a refined space, the possibility of agglomeration (reversible clumping together of particles) and aggregation (irreversible clumping together of particles) is greatly reduced.²⁵

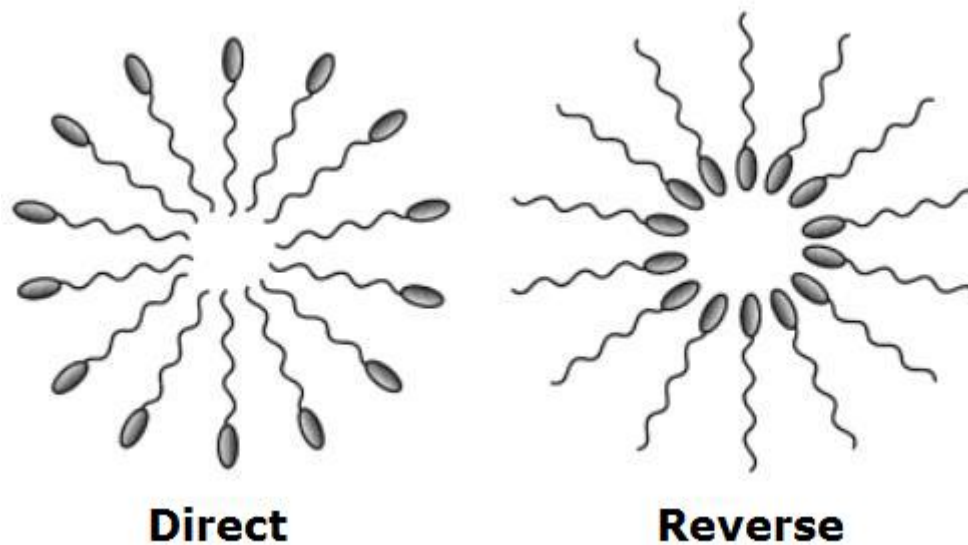


Figure 4. Showing how the hydrophobic ends of the surfactant can point inwards to form a Direct micelle, and outwards to form a Reverse micelle.

Microemulsion techniques are popular for the formation of iron oxide,^{14, 15, 21, 24, 27} silica,¹⁸ silver,²² titanium dioxide,^{19, 26} and zinc oxide nanoparticles,¹⁷ amongst other applications which include the formation of hydroxyapatite, a calcium containing compound widely used to coat prostheses due to its high biocompatibility.⁵⁷

A typical example of the microemulsion technique is the *in situ* formation of chitosan coated iron oxide nanoparticles, which are currently desirable for biological applications such as controlled drug release and enzyme immobilization.⁵⁸ For this reaction the well documented surfactant Triton X-100 (Figure 5) is used to form a water in oil emulsion.^{15, 17, 19, 56} In this example the resultant particles are square, with a spherical coating of chitosan. This method is in contrast to the traditional method of chitosan magnetite particles, suspension cross-linking, during which a suspension of the polymer is created in an immiscible liquid and then hardened to form solid capsules *via* covalent cross-linking.

1.4 Sonochemical Methods

Sonochemistry / Ultrasound have been applied to the fabrication of many types of nanoparticle, including zinc oxide nanocups, nanorods and nanoflowers.³ It has also been used to improve the “greenness” of reactions, including the formation of silver nanoparticles using gelatin as a stabiliser and glucose to replace NaBH_4 as the reducing agent.³⁰ Other examples of synthesis using ultrasound include magnetite nanoparticles,^{31, 32, 37} gold-ruthenium nanoparticles,³⁴ and gold nanoparticles synthesised on the surface of chitosan.³⁶

At frequencies of 20 kHz to 1 MHz sonochemistry can be performed, which involves acoustic cavitation, illustrated in Figure 6. The sound waves create bubbles in the solvent in which reactants can be trapped. The bubble, through a series of compressions and rarefactions, expand and contract, until it reaches an unstable size at which it collapses, creating temperatures reported as high as 5000 °C and pressures of up to 2000 atm.⁶⁶ The cooling rates in these systems are also extraordinary, at 10^{10} K.s^{-1} . For the formation of HfO_2 nanoparticles, enhanced reaction rates and smaller particles were formed using sonochemistry as opposed to other reaction routes.³⁸ The precursor materials used in ultrasound reactions are the same as those used for other methods, such as a metal chloride, a base to reduce it, and a stabilising agent. For example, CuO nanoparticles have been fabricated from CuNO_3 in the presence of NaOH, using PVA (poly vinyl alcohol) as a stabiliser.³³

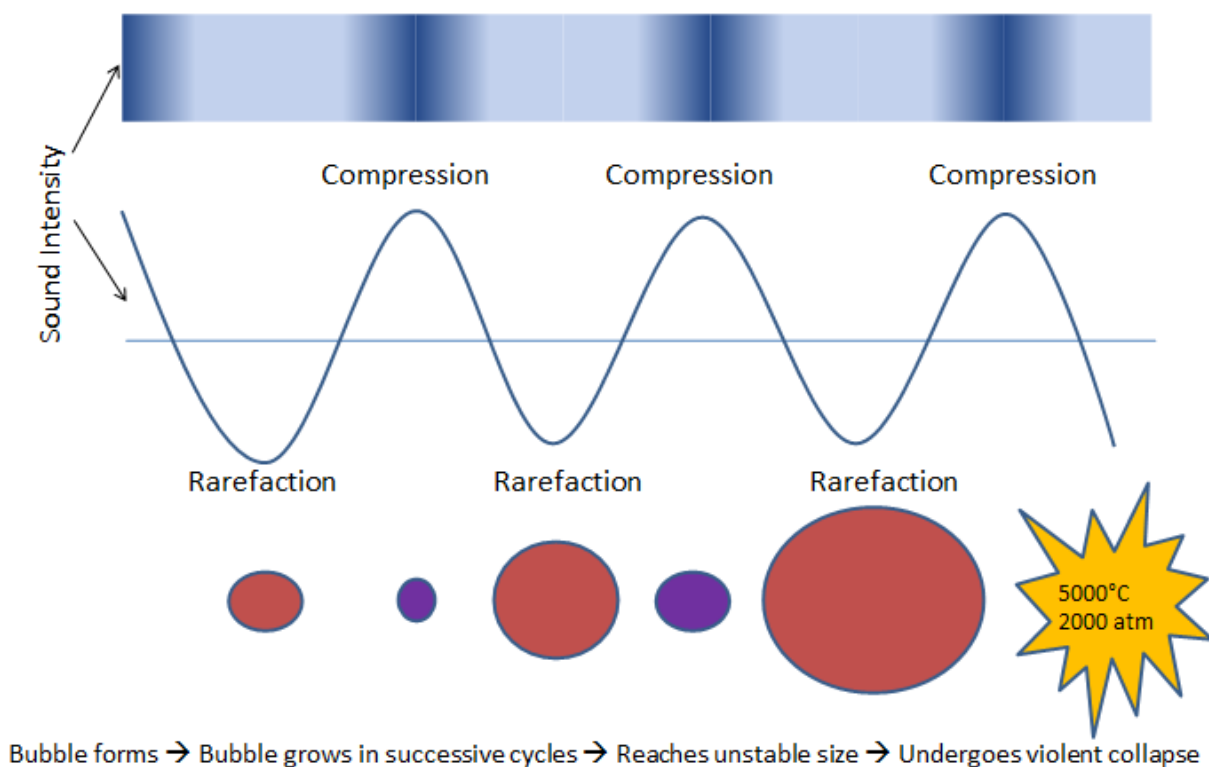


Figure 6. Showing how cavitation bubbles can form using ultrasound

Ultrasound is reported as being a green alternative to other reaction routes, in that it can be carried out at ambient temperatures, has short reaction times, and overall lower energy requirements.³⁰ However, as with other methods, it may be necessary to perform a calcining/annealing step following the initial ultrasound reaction. This reduces how green the reaction is, as the high temperatures used require a large amount of energy. This is a common requirement for nanoparticles formed from ultrasound as the rapid cooling rates prevent the formation of highly crystalline particles (the resultant particles are more like a powder).

1.5 Spinning Disc Reactor

To synthesise nanoparticles on a spinning disc reactor, the reagents are fed into the reactor at specific rates, as controlled by a mechanical pump (Figure 7). It is possible to use both liquids and gases in the reactor, as in the case of synthesis of superparamagnetic iron oxide particles.³⁹ In this case ferrous and ferric chloride solutions of varying concentrations are fed onto the reactor at a controlled rate (1 ml s^{-1}) and NH_3 gas is introduced. This can also be carried out using NH_4OH solution *via* a separate feed. The disc of the reactor, on which the reaction occurs, contains many grooves of a specific size, and as the reactants are introduced to the spinning disc *micro-mixing* occurs, which can affect particle size.⁶⁷ A combination of the movement of the fluid caused by the spinning effect pushing the fluid towards the edge of the disc, and the friction created by the surface of the disc, lead to turbulent areas in the fluid. These “turbulent waves” travel in two directions: circumferentially and helically. The circumferential waves travel from the centre of the disc to the discs edge, and the helical waves are observed in zones. Both of these waves can be tailored by varying feed rates and spin speeds to control mixing and transport rates and thus control particle size. It is also possible to heat the disc, which can affect particle size as crystallisation will be affected by temperature (more crystalline materials will be formed at higher temperatures).⁶⁷

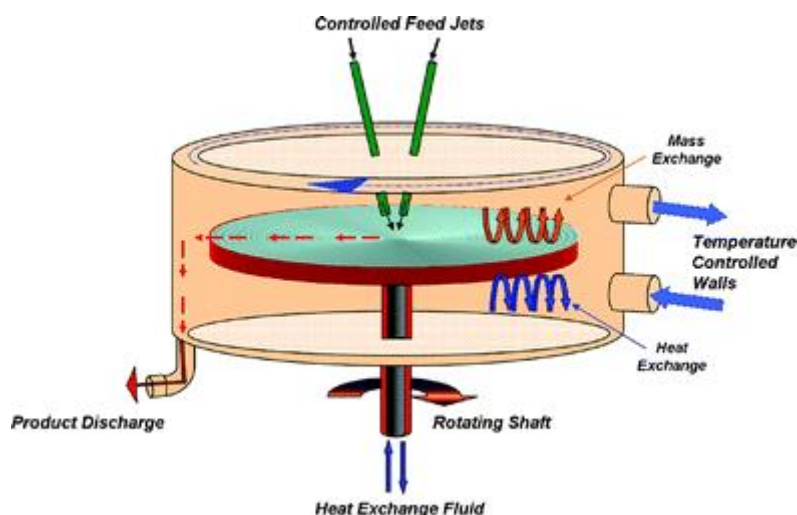


Figure 7. Showing the components of a spinning disc reactor⁶⁷

Other particles have been synthesised using this technology including MgO ,⁶⁸ Ag ,⁴¹ and hydroxyapatite.³⁹ During manipulation of disc speed it was found that as the rotational speed of the disc increased, the size of the particles generally decreased, although in the case of iron oxide

nanoparticles the reaction occurs spontaneously i.e. before micromixing, so altering disc speed is thought to be unlikely to affect nanoparticle size, although it may reduce agglomeration and limit Ostwald ripening.

It is possible to coat the particles *in situ* by adding the coating material to one of the feeds, usually the one containing the metal precursor. In this way Fe₃O₄ nanoparticles have been coated with alginic acid and Ag nanoparticles with starch.⁴¹ The latter example can be used to illustrate how benign reaction materials can be used to replace hazardous chemicals. In this example the starch replaces many alternative coating materials and glucose is used as the reducing agent. As explained previously, benign chemistry is becoming more popular and so technologies that allow green principles to be applied are preferable. The spinning disc system also allows recycling of unused materials and can be used as a continuous reactor, creating less waste and reducing the start-up costs associated with batch processes. Of particular significance is the fact that spinning disc technologies allow scale up of this process, which means that large quantities of the desired material can be made, and thus commercialised.⁶⁹

Section 2: Coating of Nanoparticles

Nanoparticles can be formed pre-coated⁷⁰⁻⁷² or can be coated after formation in various ways that will be discussed, with the coating material carefully chosen so as to suit a specific function. Whilst some nanoparticles may remain stable without a coating agent, it is more often the case that the coating is essential for stabilisation of the particle, as well as biocompatibility and biodistribution in biological applications.⁷³⁻⁷⁶ In some cases the coating agent is added *in situ* to ensure that the particle only grows to a particular size. Restriction of size based on formation inside micelles or in the presence of surfactants is discussed in detail in Section 1. In these cases, were the coating agent removed, the particles would undergo Ostwald ripening to become much larger particles (Figure 8), thus affecting their physical and chemical properties and possibly rendering them useless for certain applications, particularly those that require a specific size. For example, the magnetic properties of iron oxide (magnetite) nanoparticles can differ greatly depending on their size, and so larger particles would be useless for certain magnetism based applications.^{37, 77-79} For delivering substances into cells, particles of 40-60 nm are optimal, and particles larger than 500 nm are not able to enter cells.⁸⁰ Ostwald ripening works on the principle that although smaller crystals are kinetically favoured and will form quicker than larger crystals, larger crystals are thermodynamically favoured and if left in solution for too long, or in the absence of an agent to control growth (microemulsions, capping agents etc.) the particles will grow. If the particle is capped post-formation, then typically the coating agent is required to stop the particles from sticking together to form larger particles through aggregation or agglomeration.

Different functional groups are required for interaction of a molecule with particular nanoparticles. For example, thiols are typically used for gold nanoparticles,^{81, 82} and silane groups for modification of silica surfaces.^{83, 84} Other nanoparticles are more versatile, having a selection of moieties that will form an interaction with their surfaces. These will be discussed in further detail throughout this section.

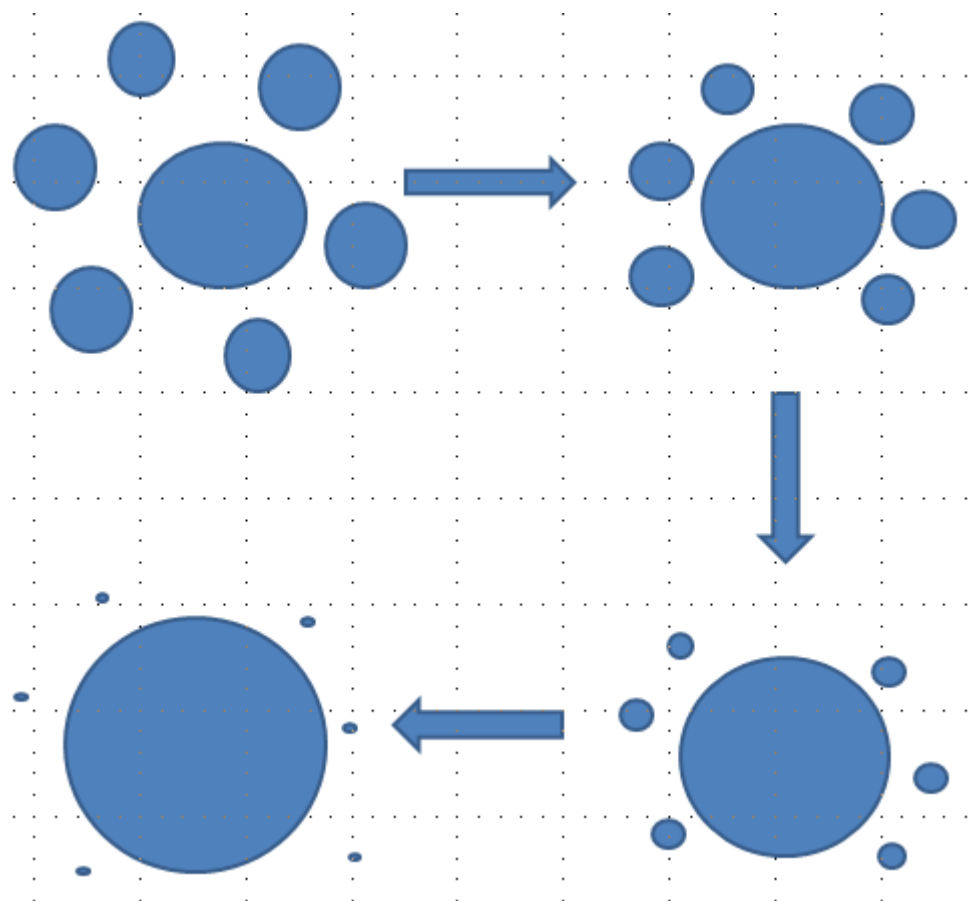


Figure 8. A schematic of Ostwald ripening showing how the smaller particles “feed” the larger particle, leading to one very large particle and a few very small particles.

Coating of particles is also essential if the particle is required to be soluble in either polar or non-polar solvents, as the metallic and metal oxide nanoparticles are essentially insoluble. This is particularly important for biological applications, as particles are required to be aqueous soluble for the majority of these applications. Finally, the coating may functionalise the particles for a more specific application, such as targeting cancer cells with antibodies.⁸⁵

The principle behind coating nanoparticles is that there will be an interaction between part of the coating molecule and the surface of the particle, although polymers such as chitosan and dextran rely on crosslinking around the surface.^{58, 74, 86, 87} Typically linkage groups include carboxylic acids, alkane thiols, alcohols, amines, organosilicon derivatives, and dialkylsulphides.⁸⁸ Each of these is able to adopt a charge either through acidic or basic dissociation or through conjugation, which allows an electrostatic interaction between the molecule and the charged surface of the particle. The “tail” end of the molecule is of equal importance, as this will allow the particle to be soluble in

the reaction medium, or alternatively leave it free to interact with a target. A typical example of this is the frequently applied oleic acid, which has a long hydrocarbon tail, meaning that when the acid head group attaches to the particle, the hydrophobic tail group renders the particle soluble in non-polar (organic) solvents.^{10, 50}

2.1 *In situ* coating

As mentioned previously, some particles are coated during their formation, so that they are soluble in particular media. Iron oxide particles capped with PEG, PVP and PEI are typical of this type of reaction, and in this case a combination of the coating agent and reaction temperature are used to limit the size of crystal growth to 4-14.9 nm.⁸⁹ During this thermal decomposition reaction the long organic chains of the oleic acid molecules form a micelle type structure around the particle as it forms, with the thermal decomposition reaction occurring in the centre of the *micelle*. At the end the nanoparticles are coated with the oleic acid, thus rendering the particles hydrophobic. It is possible to perform a ligand exchange on these particles, which will be discussed later on.

In contrast to the production of these hydrophobic particles, it is possible to cap the particles with a hydrophilic coating. A popular example of this is coating with the sugars dextran or chitosan.^{74, 86, 87, 90} In these cases the coating materials are added at various concentrations with the aqueous ferrous and ferric chlorides prior to reduction under basic conditions. Thus, as the particles are formed the coating agents form electrostatic associations with the particles and so coat them. The size of the particles in this case is controlled by the reducing agent rather than the coating material, and the reaction is carried out at ambient temperatures. The majority of commercially available SPIOs are coated with dextran type materials.⁹¹ Research has shown that dextran coatings on iron oxide nanoparticles are not strongly bound and so there is a problem with precipitation at some concentrations.⁸⁷ As such, a facile method for coating SPIOs, and indeed other metal oxides, rendering them stable for longer periods of time would be advantageous.

2.2 Ligand Exchange

Many metal oxide particles that are coated *in situ* are often hydrophobic due to synthesis in organic solvents, although aqueous synthesis to form water soluble NPs is becoming more common. Hydrophobicity severely limits their biological applications, and so further reaction is required in order to make them suitable. In addition to this, if the particle is to be functionalised for a particular purpose, a different functional material may be required and often this cannot be used to cap the particle during formation due to incompatibility with reaction conditions or the reactants themselves. For example, peptides would be susceptible to cleavage of amide bonds by ammonia or sodium hydroxide during SPIO formation, and would degrade at the high temperatures required for thermal decomposition (245 °C for thermal decomposition of acetyl acetonate). Whilst a ligand can be altered very simply by, for example, an oxidation reaction, this is sometimes not sufficient for the desired purpose. A popular option for changing the coating material is ligand exchange which works on the principle of swapping the coating ligand with another ligand, having a higher affinity for the nanoparticle (Figure 9).⁹²

There are various methods of ligand exchange including heating, stirring and manipulating ligands through changes in pH.^{50, 70, 72, 77, 93-96} Initial attempts at ligand exchange involved heating the particles to a high temperature in a suitable solvent. More recently the ligand exchange has been effected at ambient temperatures by stirring with the replacing ligand. Investigations into coating iron oxide nanoparticles with dopamine have led to much faster methods of ligand exchange, during which oleic acid coated particles were prepared and isolated, and dopamine hydrochloride solution at pH4 added and stirred (for only two minutes) to yield dopamine functionalised particles.⁹³ This is a much improved method to the previous ones involving long reaction times and emulsification, leading to complicated and time consuming isolation steps, not to mention large amounts of waste.

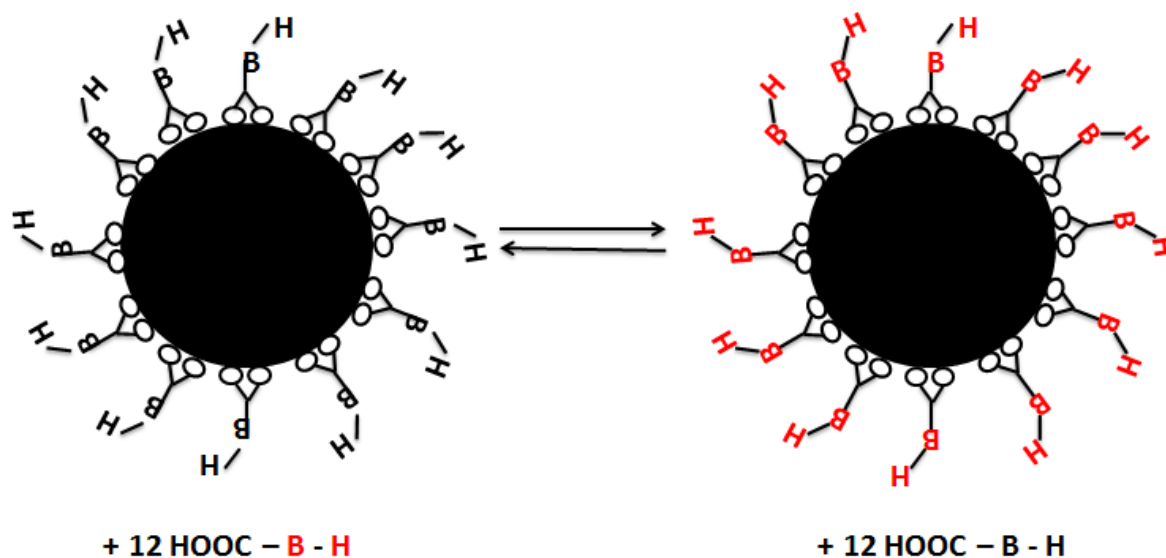


Figure 9. Showing how the ligands on an iron oxide nanoparticle can be changed via ligand exchange.

2.3 Further Reaction

As mentioned, one way in which to alter the functionality of the coating agent is to further react it by, for example, oxidation or reduction.⁹² Another method, is to add another molecule to the coating agent *via* a covalent bond.⁹⁷ An example of how this can be done is illustrated by the commercially available "Molday ION Carboxyl Terminated" (BioPal), a SPIO with a coating agent containing terminal carboxyl groups (also available with terminal amines that can be further reacted). The principle behind these particles is that they can be covalently linked to another molecule, providing it has a terminal amine (or alternate functional group for alternate terminating groups) *via* a simple coupling reaction usually involving a carbodiimide. A linking of these particles with spermidine has been reported, but its applications potentially extend to many different molecules.⁹⁸

Another example of further reaction, is the addition of folic acid to the glutathione coating of gold nanoparticles. In this instance the sulfur-containing cysteine in the centre of the glutathione (Glu-Cys-Gly) forms an electrostatic interaction with the gold nanoparticle which is strong enough to withstand the coupling conditions required to covalently link the carboxylic acid or amine groups located at the ends of the polypeptide, to the folic acid molecule (Figure 10).⁹⁷ This particular

example has clinical applications as the folic acid is used to target and detect cancer cells *via* linkage with the folate receptor which is overexpressed in cancerous cells.

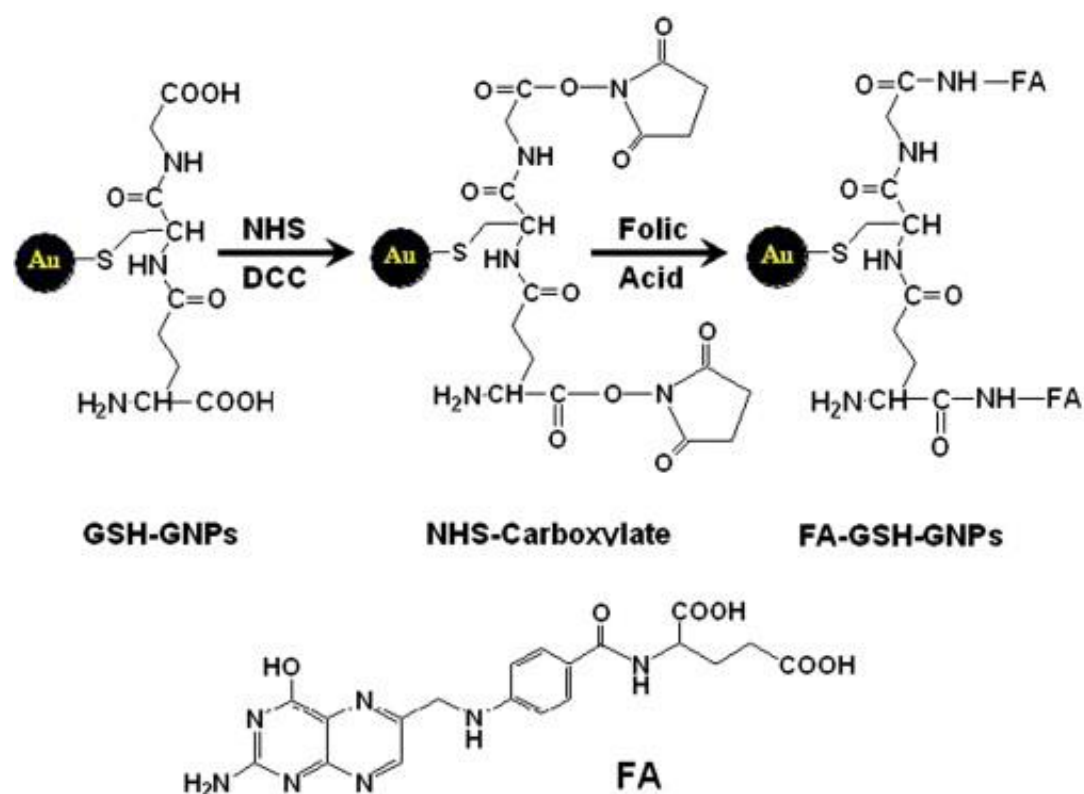


Figure 10. Reaction scheme showing the sequence of reactions for forming the folic acid conjugated gold nanoparticles.

2.4 Self-Assembled Monolayers

Self-assembled monolayers are a single layer of a coating molecule which arranges itself spontaneously on the surface of the particle. The mechanism behind this spontaneous process is that the head group of the coating molecule is attracted to the nanoparticle (typically a metal or metal oxide) leading to an electrostatic interaction, and the other end of the molecule will be either polar or non-polar depending on the solvent in which the nanoparticle is to be dissolved or

suspended (Figure 11). Of equal importance is the interaction between the coating molecules themselves, as van der Waals interactions between the molecules help to stabilise the particle. However, interactions between coating molecules on separate particles can cause problems, if they interact with each other this may cause agglomeration or aggregation of particles.⁹⁹

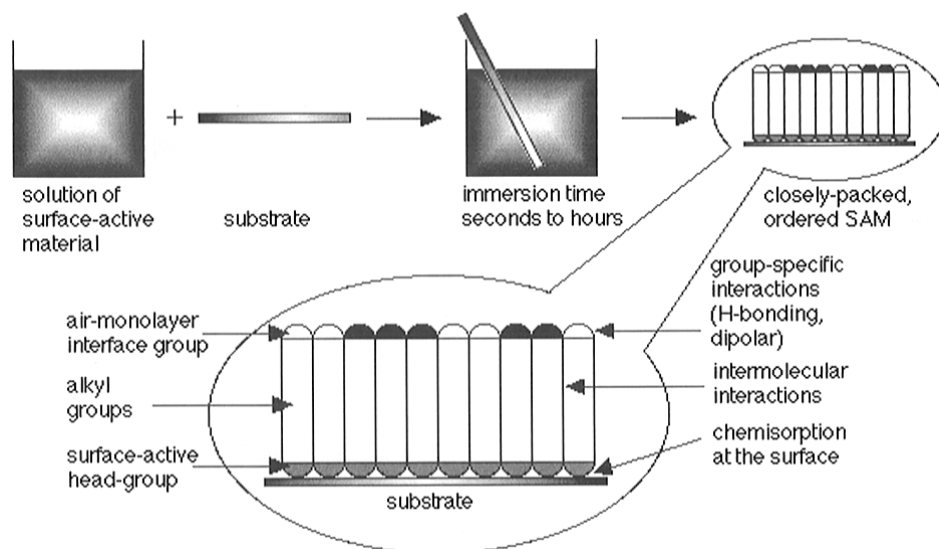


Figure 11. Showing how the head group of the coating molecule, referred to as the surface active head group, adsorbs to the surface, leaving the alky chain to interact with the solution. The coating molecules are attracted to each other via intermolecular interactions⁹⁹

Organothiols such as *n*-dodecanethiol (Figure 12), have been reported to form SAM's on the surfaces of many metal nanoparticles including Au, Ag, Fe and Ni.⁹⁹⁻¹⁰¹ The thiol group is able to form an interaction with the particle, with the hydrocarbon chain forming a spacer, and the tail group interacting with the surrounding solvent. There have also been extensive studies into the application of carboxylate anions, particularly on the surface of Al₂O₃ and AgO surfaces.⁹⁹



Figure 12. *n*-dodecanethiol

Self-assembled monolayer formation is a desirable option for coating particles as it requires no auxiliaries, heating or other complicated steps. However, it is not suitable for all coating materials on all substances, and in the event that a complete monolayer does not form, other components of the reaction mixture such as the solvent, can form an interaction with the particles, leading to an impure product. In terms of scale-up this is undesirable as extraction/separation steps, usually requiring solvents, are necessary to obtain a pure product. For biomedical applications purity and quality control are essential due to FDA regulations and the monitoring of both effectiveness and side effects. It is also possible that a bilayer, or several layers, will form on the particle, which will increase the size of the particles possibly to a size that renders them unsuitable for certain applications.

2.4 Determining Effectiveness of Coating

There are several ways in which the effectiveness of a coating method can be measured. Powder diffraction methods may show the coating if the capping agent remains crystalline. If the coating material contains a particular functional group then IR spectroscopy could be used, and EDX can be used to determine if particular elements only present in the coating material can be identified around the particle. TEM images may show an area around each individual particle which corresponds to the coating material and DLS will show an increase in particle size that may be dependent upon the coating. Although the particles will not go into solution unless they are coated, UV-vis is another technique that allows for confirmation of the presence of coating materials.¹⁰²

TGA can be used to determine the mass of coating material present on the surface of a known mass of nanoparticles. This involves heating a known mass of nanoparticles in an inert atmosphere by increasing the temperature in increments over a period of time and weighing the sample throughout to create a graph. This shows a decrease in mass corresponding to the coating material alone being removed, followed by a second dip corresponding to the breakdown of the particle itself. Typically the temperature is increased to 600 °C over a period of four hours.¹⁰³

Where the coating material is chiral a technique known as circular dichroism can be also be used, and would be particularly useful where larger polypeptides are used as the functionalising material.

¹⁰⁴ Realistically these analysis tools must be used in conjunction with each other for a definite characterisation.

An important factor to consider when looking at either charge or size of the particles is the interaction of the particles with each other, as illustrated in Figure 13. ¹⁰⁵ The coating materials will lead to repulsion between particles and so a reduced likelihood of aggregation. However, if the particles get closer together then due to their high surface energy, a consequence of their small size and large surface area, the van der Waals interactions between the particles increase leading to increased aggregation. For this reason many particles are synthesised in very dilute concentrations, and a stabilizing/coating agent may be selected which sterically hinders particle interaction. For example, citrate capped gold nanoparticles are synthesised using a gold solution of 0.01% (w/v) in water. ⁷²

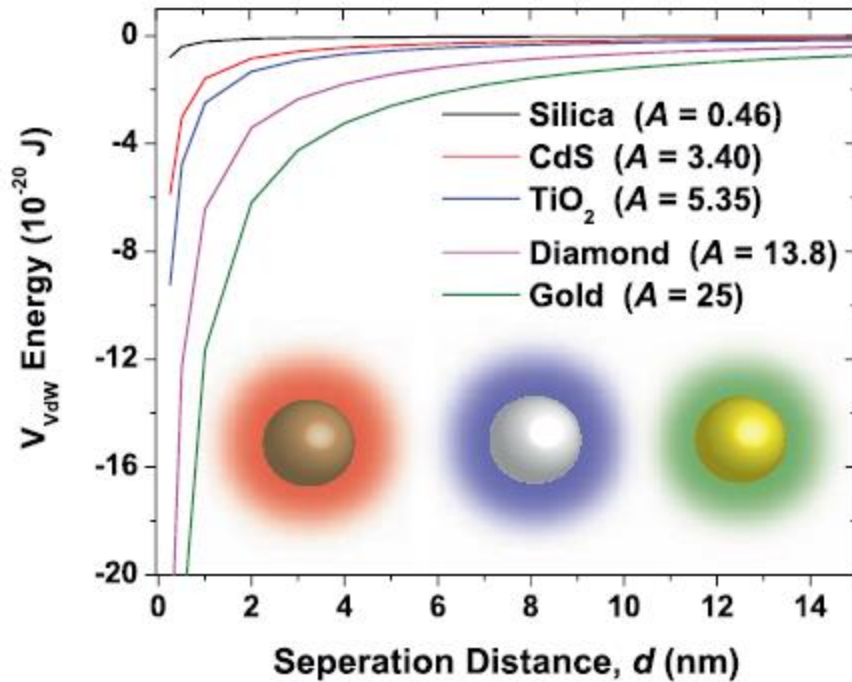


Figure 13. Showing how van der waals energy changes with separation distance for different nanoparticles.

Zeta potential is another useful tool in determining the nature of coatings. It measures the charge of the area surrounding the nanoparticle rather than the nanoparticle itself. This is illustrated in Figure 14.

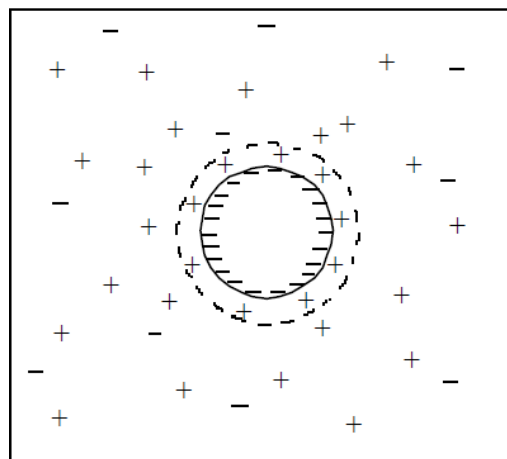


Figure 14. The diagram shows that the particle itself is negative, the particles bound directly to it are positive and the particles attracted to these negative again. This leads to an overall negative charge over the particle and thus a negative zeta potential.

The zeta potential of the particle plays an important role when it is to be used for biomedical applications in which it is required to deliver substances into cells.⁷⁶ As shown in Figure 15, when the particle is taken into the cell *via* pinocytosis it is encapsulated in a lysosome/endosome with an internal environment that is capable of degrading certain particles, for example SPIOs which will degrade at *ca.* pH 4.5 - 5.0. However, if the particle is cationic, then it will interfere with the proton pump, causing an influx of protons into the endosome. This is known as the proton sponge effect.¹⁰⁶ As a result of this, a large quantity of chloride ions will enter and remain in the cell, thus causing water to enter leading to swelling and bursting of the lysosome and release the particle along with the coating, possibly an active agent, into the cytosol (Figure 16).

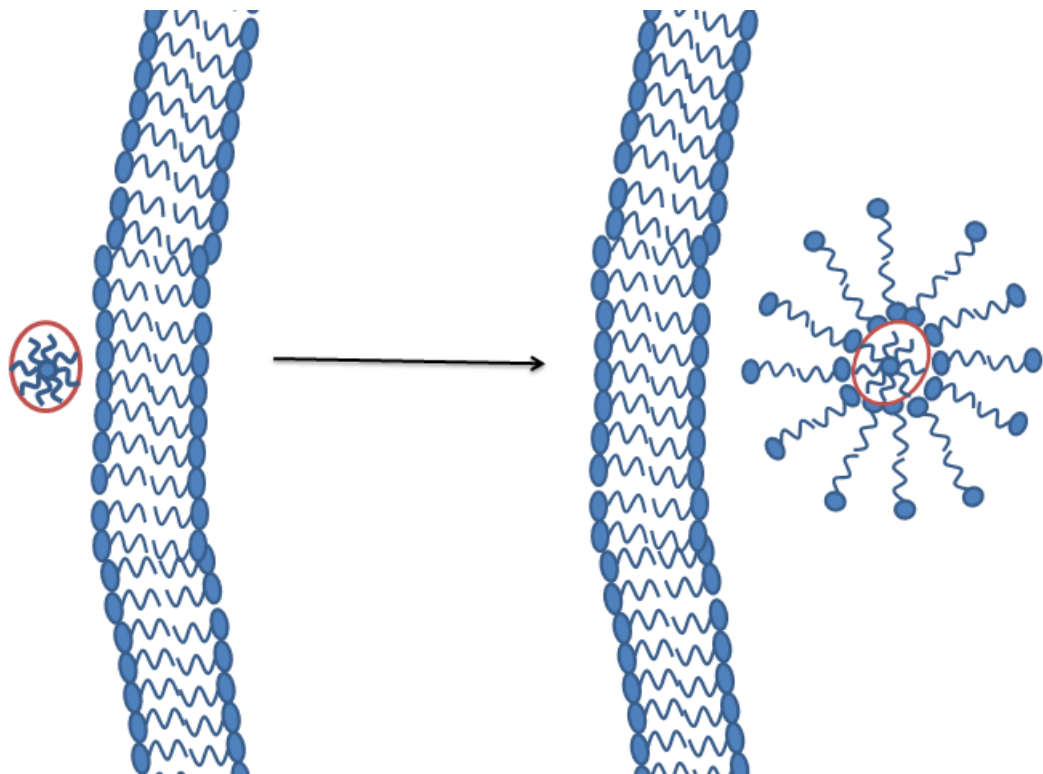


Figure 15. Image shows a nanoparticle approaching the cell and interacting with the cell wall. The cell forms a vesicle known as a lysosome around the nanoparticle as it enters the cell.⁷⁶

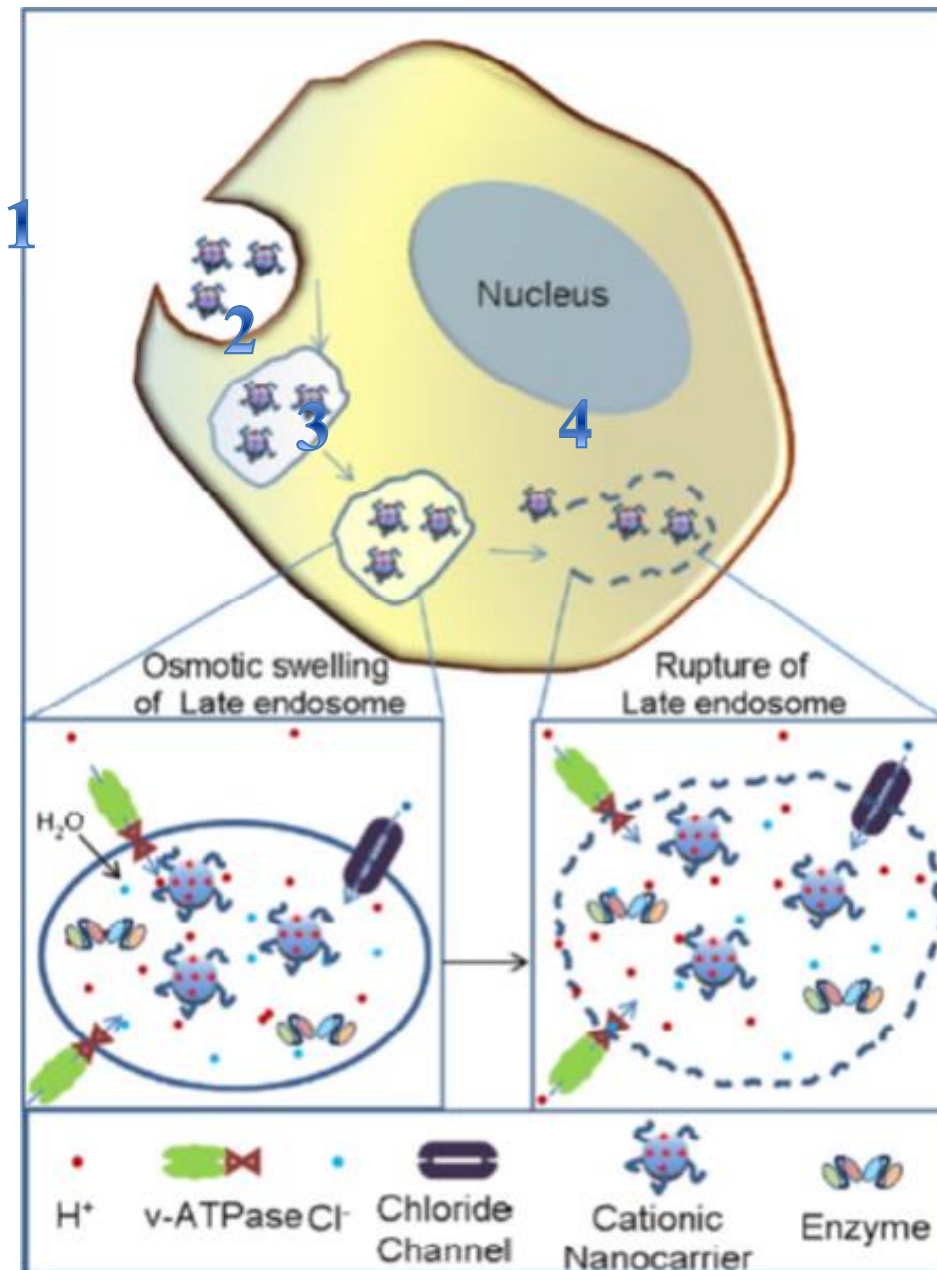


Figure 16. Schematic showing how cationic nanocarriers are able to induce osmosis into the cell, resulting in endosome rupture and release of the particle into the cell.¹⁰⁶

The example of endosome rupture is useful in showing the importance of charge on the particles. However, it has been discovered that if a particle is too charged then it may not interact with the cell in the desired way.⁷⁶ The charged particle is able to interact with the cell wall (positively charged particles are taken up better than neutral or negative as the cell wall has a slight negative charge), but if the charge on the particle is high then it will be accelerated towards to the cell by electrostatic interactions. This does not leave time for the particle to recognise specific domains on the cell, and it can end up binding to an irrelevant part and so not have the desired effect, such as binding to

receptors. In contrast, if the charge on the particle is too low then the electrostatic interaction between the particle and the cell may not be sufficient to pull the particle in the desired direction and so it will move away from the target by means of thermal diffusion and Brownian motion, and also not have the desired effect. So, the zeta potential of the particle must be tailored for biomedical applications because as discussed, it is essential for interaction between the nanoparticle and its target.⁷⁶

Section 3: Purification of Nanoparticles

There are several different ways of isolating these particles and separating them from any unreacted material or free coating. This is essential when the particles are being used for applications as any free material may cause anomalies or incorrect conclusions to be drawn. The methods most frequently highlighted in the literature include; use of antisolvents and washing, magnetic separation, size exclusion chromatography, dialysis, and centrifugation.^{16, 107-114}

3.1 Antisolvent Precipitation and Selective Precipitation

As with organic synthesis, it is possible to purify and isolate the product (in this case the coated nanoparticles) by selecting a suitable anti-solvent, in which the coating material is insoluble.⁹² On addition of this solvent the coated particles should precipitate out first, as energetically, it is more unfavourable to keep these particles suspended in the anti-solvent than the free coating material. An example of this method can be found in the formation of CdSe nanoparticles coated with TOPO (trioctylphosphine oxide), where hexane is used to precipitate the TOPO-CdSe particles out of solution.¹¹⁵ In all cases in which this method is employed, it is essential that the primary solvent (that in which the particles are dissolved) and the anti-solvent are miscible.

3.2 Size Exclusion

Size exclusion chromatography is a viable method of separation if the size of the coated particles and the size of the free coating material are very different. For example, the size of the largest amino acid (tryptophan) is in the region of 1.5 nm, whereas the size of an iron oxide nanoparticle prepared *via* the microemulsion method is around 10-15 nm.

The technique, also known as *gel filtration* uses specialised beads with pores of different sizes, controlled by the cross-linking of the substance from which they are made. SEPHADEX (SEparation PHarmacia DEXtran) for example, is made of cross-linked dextran and comes in many different bead sizes ranging from "10" which separates peptides and small biomolecules with a molecular weight > 700, to "75" which is used for large biomolecules with a molecular weight > 80 000.

In brief, the beads are swelled in an appropriate buffer or solution and packed into a separating column. The components to be separated are dissolved in the buffer and added to the top of the column, and washed through the column using a continuous flow of buffer. The fractions are collected, each containing different molecules depending on the retention time of each component. The larger molecules will move around the beads, and so will move through the column quicker and elute in the earlier fractions, whereas the smaller molecules will fall through the pores in the beads and so their path through the column will entail moving through each individual bead that they come into contact with, meaning that they will be retained on the column for longer, and so will elute in the later fractions (Figure 17). The length of the column, the size/type of beads, and flow rate can be tailored for optimal separation.

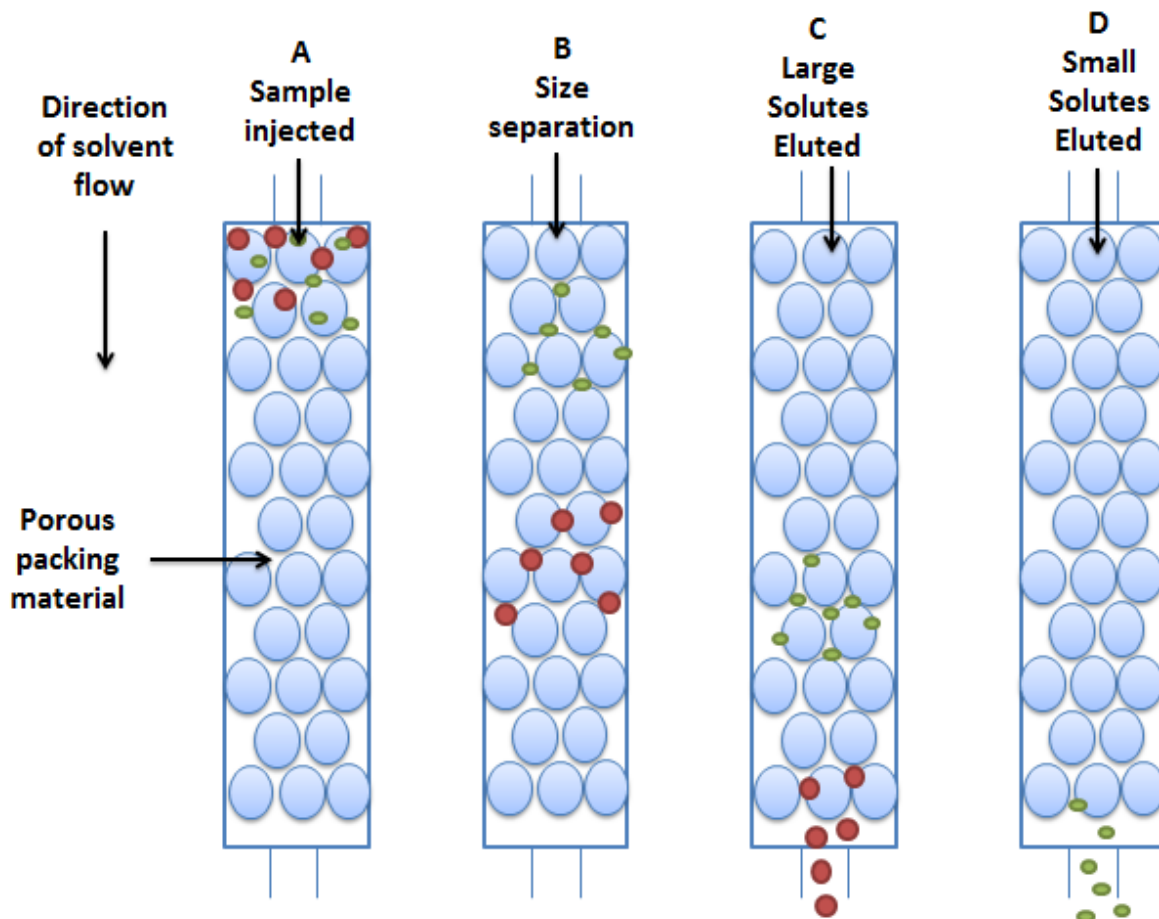


Figure 17. Showing the movement of small and large molecules through a size exclusion column packed with porous beads.

3.3 Magnetic Separation

Magnetic separation is carried out by using a rare earth magnet with a very strong magnetic field, and is only suitable for magnetic nanoparticles such as iron and nickel metals and oxides. Whilst gravity cannot act on the particles strongly enough to pull them out of the solution, the magnet is sufficiently strong so as to be able to pull the solvated particles out of solution.

The magnetic force which acts on a particle is given by:

$$F_M = \mu_0 \chi V_p \nabla H,$$

where H is an external magnetic field, χ is the magnetic susceptibility, and V_p is particle's volume.⁹²

Theoretically, this method will only work for particles of 50 nm or more in solution/ as for smaller particles the combined energy of thermal diffusion and Brownian motion overcome the force imposed by the magnetic field, and so the particles remain stable in solution.⁹²

During synthesis of hydrophobic coated iron oxide nanoparticles, a rare earth metal magnet such as neodymium, is typically used to settle the particles when they are suspended in solvent. This is repeated several times with the solvent being decanted off and the resulting product washed with fresh solvent until a pure product is obtained. This settling technique is frequently used during the formation of coated nanoparticles.¹⁰⁸ However, in these cases the particles tend to be aggregated, due to insolubility in the reaction media, and so do not fit the theoretical values. In fact it has been found that even in solutions the calculated properties can be inaccurate as they are extrapolated from data on the bulk material, ignoring the changes in properties observed at the nanoscale such as dipole-dipole interactions and magnetic properties, which will be discussed further in Section 2.

Magnetic separation is considered to be superior to size exclusion techniques as it is quicker and does not suffer from some of the limitations of SEC, such as incompatible materials and limitations with bead and pore size.¹⁰⁸ From a green chemistry perspective, it is superior as it does not require excessive solvents and reduces the need for an extraction step at the end of the separation.

3.4 Dialysis

Dialysis, like size exclusion, works on the principle that the coating agent is much smaller than the coated nanoparticles. In this case rather than using porous beads, semi-permeable tubing with a pore size to match the application, is used.^{110, 113} The solution containing the coated nanoparticles and the free material is sealed into the tubing and the tubing placed into a beaker of buffer which is gently agitated (usually through stirring) and can be heated if required. The free coating material will diffuse out of the tubing into the surrounding buffer until equilibrium is achieved. By replacing the buffer with fresh buffer at intervals, the equilibrium can be shifted so that virtually all of the free coating material diffuses out of the tubing and the resultant nanoparticle solution contains only the coated particles. This process is illustrated in Figure 18,¹¹⁶ which shows the dialysis technique being used to separate antibodies from other components in a mixture of proteins. In this instance pores of $\sim 24 \text{ \AA}$ are used although other tubing with different pore sizes are available.¹¹⁶

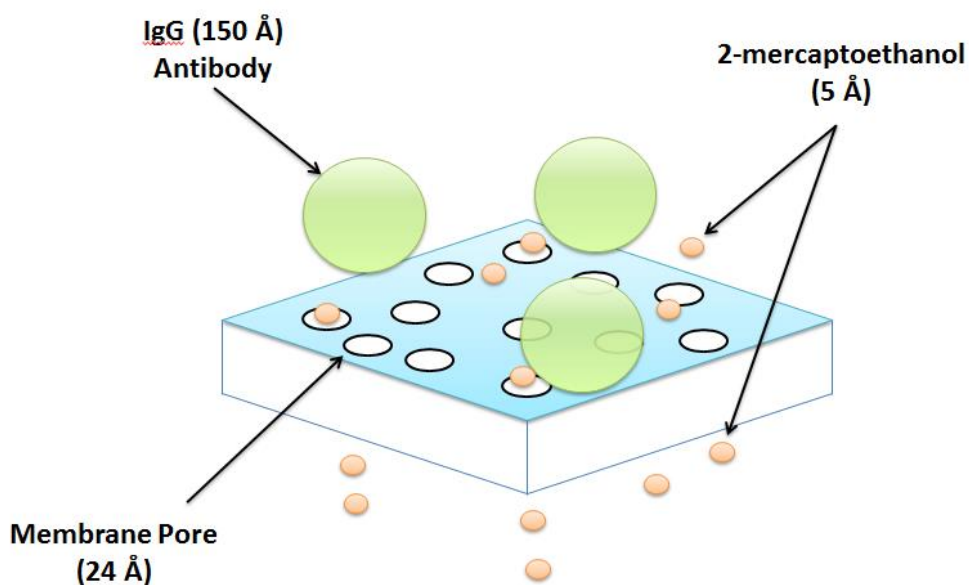


Figure 18. A membrane with pores of 24 \AA is being used to separate antibodies of 150 \AA which are desired, from undesired components such as 2-mercaptoethanol which is 5 \AA . Tubing with smaller pore sizes is available commercially.

3.5 Centrifugation

It has been previously mentioned that the gravitational force that acts on the nanoparticles in solution is not sufficient to force them to sediment. The force of Brownian motion and thermal diffusion on these small particles is larger than the force of gravity on them and so they are able to remain suspended. However, it is possible to increase the gravitational force on these particles and so force them to sediment out. During centrifugation the gravitational force increases dramatically, for example at a speed of 60 000 rpm, the gravitational force is 200, 000 times greater. By tailoring the centrifugal force and the time it acts on the particles, and working on the principle that the larger particles will sediment out first, it may be possible to draw the coated particles, but not the free material, out of solution. It is also possible to create a density gradient within the centrifuge tube which can help to separate out particles of different sizes (Figure 19).^{110, 113}

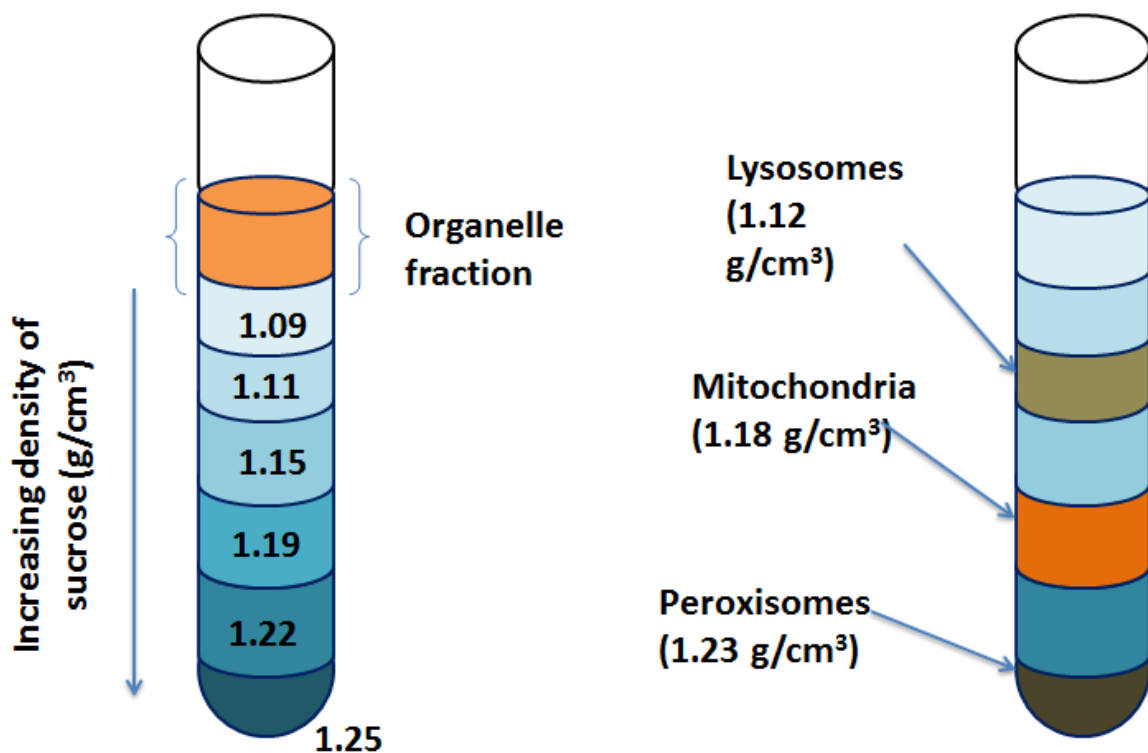


Figure 19. Image showing how solvents of different densities can be exploited to create a gradient within the centrifuge tube. This example shows separation of organelles.

3.6 Alternatives

In addition to these techniques it is worth noting that electrophoresis can also be exploited for the separation of particles, discriminating not only size but shape. ¹¹² Electrophoresis can be used to separate gold and silver nanoparticles of varying shapes and sizes by coating them with PEG terminated in COOH groups and passing them through an electrophoresis gel by tailoring the pH and gel type (Figure 20). ¹¹¹ This has proved useful as for certain applications, particularly catalysis, where the shape of the particle is essential to its function. Other methods of separation tend to discriminate solely by size. During this project, the aim was to separate the free coating material rather than from other particles, and so this type of method will not be discussed in further detail.

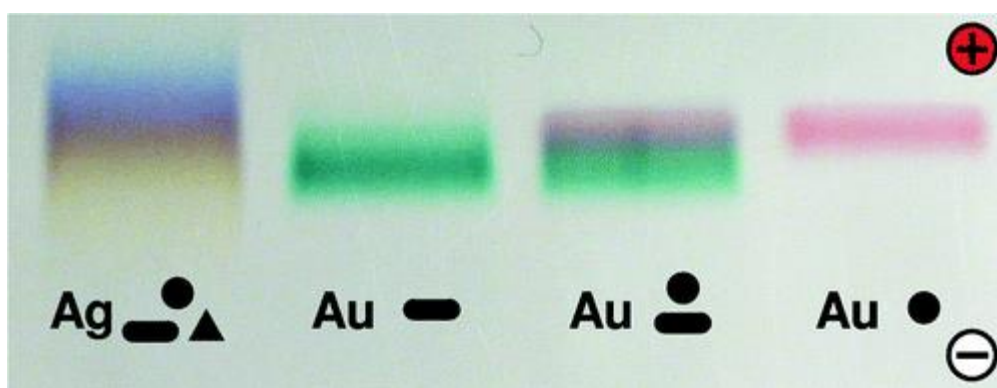


Figure 20. Gel electrophoresis for separation of nanoparticles¹⁰⁸

Chapter 1.2: Nanoparticles and Medical Imaging

Medical imaging is essential for the detection, diagnosis and treatment of disease. There are several imaging techniques commonly used in hospitals for these three functions including Ultrasound, X-Ray computed tomography (CT), magnetic resonance imaging (MRI) and positron emission tomography (PET). Imaging can be defined using Equation 1, where in order to make an image mass and energy are measured as a function of their three-dimensional location and time, although generally images are based on energy rather than mass as is the case with many types of medical imaging.¹¹⁷

$$U = (m,E)(x,y,z)(t)$$

Equation 1. Definition of an image (U), where m = mass, E = energy, (x,y,z) are the three dimensions in space, and t = time.

Ultrasound exploits high frequency sound waves that are detected as they are reflected from various structures within the body. It is commonly used for diagnosis of heart diseases,¹¹⁷⁻¹¹⁹ various ailments of the gastrointestinal (GI) tract,¹²⁰ and for dating and monitoring pregnancy.^{121, 122} CT (computed tomography) makes use of X-rays generated at the time of imaging and is most commonly used as a modality for detecting broken bones and infections such as pneumonia as well as for angiography which is essential for treatment of aneurysms.¹²³ MRI (magnetic resonance imaging) exploits the magnetic susceptibility of tissues within the body. Whilst commonly used for detecting cancer and soft tissue damage, with the addition of an imaging agent such as a barium meal, it can aid in the diagnosis of obstructions to or within various organs.¹²⁴ PET (positron emission tomography) is the only one of these techniques that relies on the introduction of an imaging molecule in order to build an image, as it requires a signal that body tissues alone cannot produce. A radioactive tracer is introduced to the body, usually bound to a molecule that will bind to a specific target.¹²⁴⁻¹²⁷ The tracer will bind to the target tissue and when the body is scanned the radioactive label is detected and an image built based on the prevalence of the radioactivity across

the body. This has proved particularly useful in the detection of diseases such as Alzheimer, where Pittsburgh Compound B binds specifically to beta amyloid plaques.^{127, 128}

Whilst contrast agents are necessary for PET imaging they are not essential for either CT or MRI, but under certain circumstances they are useful: The natural contrast of bodily tissues is exploited as much as possible but when two tissues show very similar contrast it may be necessary to introduce a contrast agent to create a difference in contrast (by affecting the relaxation of protons within one of the tissues) and obtain a better image of the tissue or organ in question. A typical example of this would be the similarities between blood vessels and kidney tissue.¹²⁹ In addition to this, contrast agents can be doctored so that they bind specifically to certain types of tissue or molecules, for instance by adding an antibody for a tissue-specific antigen, leading to further advances in diagnosis and molecular imaging.¹³⁰⁻¹³² By making imaging agents tissue specific it is possible to track the delivery of drugs and movement of immune cells such as T cells *in vivo*. T cells can be tracked using high field MRI (around 10 T).¹³² Thus the fields of nanomedicine, molecular imaging and immunotherapy can be joined together to form a system analogous with Ehrlich's magic bullet.¹³³

The science of designing and making imaging agents comes under the term "Nanotechnology". A more in depth definition of this is as the synthesis, application and study of materials of 1-100 nm in at least one dimension, that also exhibit some form of novel or enhanced characteristic that is not observed at either the quantum or macromolecular level. The only properties that have demonstrated a clear difference between the nanoscale and these other scales are either magnetic or optical,¹³⁴ although nano-gold exhibits physiological inertness compared with bulk gold, a useful property when developing contrast agents or delivery systems.⁸¹

Section 1: X-Ray Imaging

1.1 Background

X-rays were first discovered by Wilhelm Conrad Roentgen during experiments on vacuum tubes. ¹³⁵

Figure 21 shows the first X-ray image that Roentgen took of his wife's hand.



Figure 21. An image of Roentgen's wife's hand, taken days after the discovery of X-rays. ¹³⁶

In medical imaging, X-rays are generally produced with an X-ray tube powered by an X-ray generator which produces a high voltage to accelerate electrons from the cathode to the anode in the tube. The resulting high-energy electrons produce X-rays when they strike the anode.

X-rays interact with matter in accordance with Beer's law (Equation 2).¹¹⁷

$$I = I_0 e^{-\mu t}$$

Equation 2. Beer's law where I_0 is the number of X-rays entering an object, I is the number of X-rays exiting an object, t is the thickness of an object and μ is an intrinsic property of the material called the linear X-ray attenuation coefficient.

Attenuation (μ) is proportional to the atomic number cubed (z^3) and so for materials with high atomic number the X-rays will interact more strongly, leading to a greater loss of energy for X-rays passing through the material. X-ray interactions are primarily involved with exciting the inner electrons of a material to a higher energy level and in some cases this can lead to production of further X-rays, known as *Auger electrons*, which will interact with tissue and interfere with the images produced unless they are captured. For this reason the energy of electrons and concentration of imaging agent must be carefully selected to avoid this effect as much as possible.

As an X-ray beam passes through a body it undergoes changes with some of the X-rays being scattered and others being absorbed by the body tissues. The absorption is attenuation as described in Beer's Law. So, the beam exiting the body differs from the beam that enters the body in that it has varying intensities at various points depending on the tissue that it has passed through, and so contains information that can be recorded and then transformed into a visual display.

Historically X-ray detection has been by means of photographic film where the high or low energy of the X-ray beam develops the film or leaves it untouched, leading to a negative print.¹¹⁷ However nowadays detectors typically consist of an X-ray attenuator that turns the X-ray signal into either an optical or electronic signal which can then be processed, and a device for recording the light or electrons. Digital detectors are now used and imaging conducted using digital detectors is referred to as *computed tomography (CT)* or *digital radiography*.

1.2 Contrast Agents

Bone and soft tissues are easily distinguishable by X-ray imaging due to their difference in composition. Soft tissue contains low atomic number atoms such as carbon and bone contains higher number atoms such as calcium. However, many tissues in the body have very similar composition making it difficult to tell them apart on an X-ray image, and for this reason, imaging media need to be introduced in order to clarify the image. These can work in two possible modes; as a positive contrast agent, whereby the agent reduces interaction of the X-rays in the tissue by means of lowering attenuation leading to more energy from X-rays reaching the detector, or as a negative contrast agent which increases the interaction of the tissue or area with the X-rays by increasing attenuation, thus leading to less energy from the X-rays reaching the detector.¹¹⁷

1.2.1 Positive Contrast

Carbon dioxide, containing atoms with low atomic numbers, is often used as a positive contrast agent for imaging of the gastrointestinal (GI) tract, with some patients being given carbonated drinks prior to X-ray.¹³⁷⁻¹⁴⁰ Areas where the positive contrast agent is present appear lighter on images as the gases used do not interact strongly with the X-rays and so it is easier for the X-rays to pass straight through that area to the detector without any significant loss of energy. One widely used positive contrast agent is barium sulphate, otherwise known as *barium meal*, which is also used for imaging of the upper GI tract.

1.2.2 Negative Contrast

Typically these contain high atomic number atoms, with iodinated agents being commonly used, as iodine has an atomic number of 53, making it significantly different from the atoms found in tissues (Carbon $z=6$, Oxygen $z=8$, Nitrogen $z=7$). Iodipamide[®] and Iohexol[®] are two popular contrast agents

(Figure 22) that can be administered intravenously to aid diagnosis and treatment, particularly for problems with blood vessels such as obstructions and haemorrhages.^{141, 142}

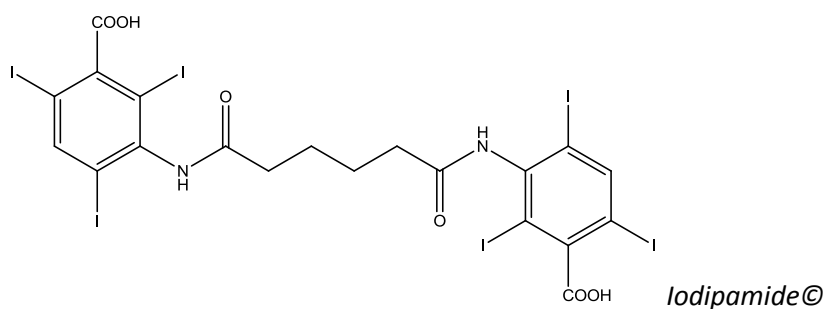
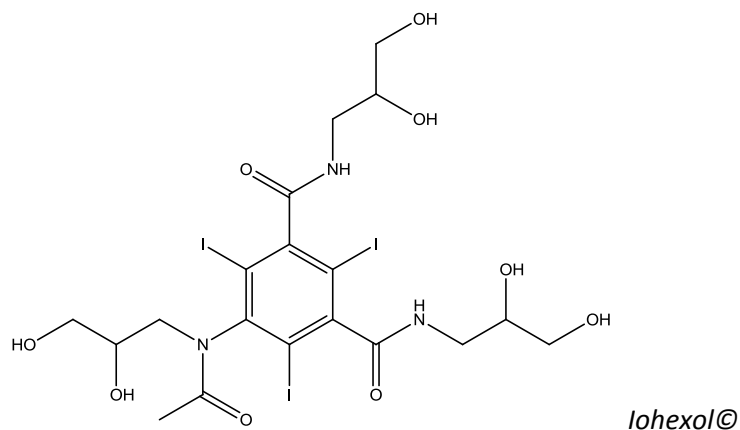
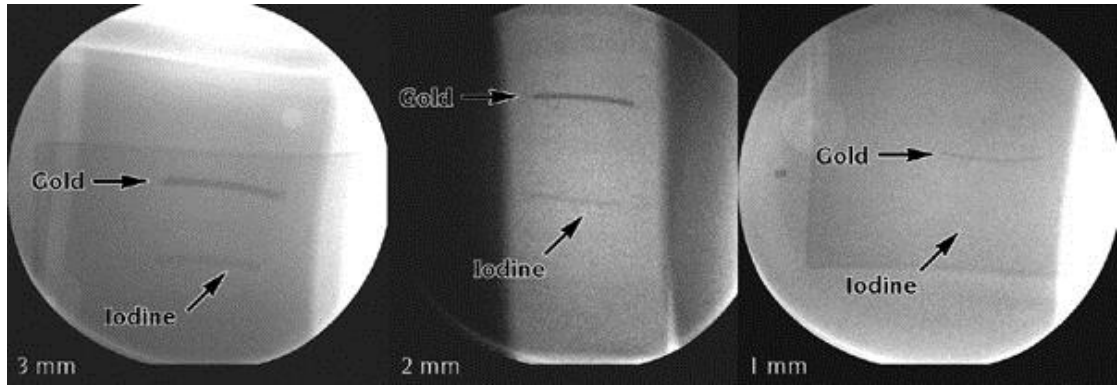


Figure 22. Commonly used X-Ray imaging agents

In recent years gold has been investigated for use in X-ray contrast, having an atomic number of 79. Gold nanoparticles (GNPs) have been suggested as an alternative to iodinated media due to their increased contrast, residence time, and inertness. Figure 23 shows that gold is superior to iodine in terms of contrast.¹⁴³



a) Imaging of iodinated contrast agent vs. gold nanoparticle contrast agent performed using X-ray phantom



b) Image of rat kidneys using intravenous iodinated imaging media



c) Image of rat kidneys using intravenous gold imaging media

Figure 23. Images showing the contrast between iodine and gold as X-Ray imaging agents. ¹⁴⁴

Whilst GNPs may seem like an ideal replacement for iodinated media, particularly due to the side effects and risks involved in using them, they also have their problems. In preliminary studies it has been shown that far from being cleared by the renal system as is the case with media such as Iodipamide[®], GNPs are too small to be cleared by the reticuloendothelial system (RES) and so accumulate in the liver causing liver damage.^{71, 145} This is a problem that needs to be overcome if GNPs are to be successful in making it to the market as an *in vivo* imaging agent.

1.3 Applications

Iodine occurs naturally in the body in many forms including that of the hormone thyroxine, so it is important that when the contrast media is administered to the body it has levels of iodine that far exceed those naturally present. A single dose of X-ray contrast medium commonly contains around 2000 times more iodine than the body and so overcomes this problem. In addition to this, it is efficiently cleared from the body with low incidence of side effects, although side effects such as skin irritation, kidney damage and anaphylactic shock can occur.¹⁴⁶

Iodinated contrast media are commonly used for angiography.^{138, 147} The media is injected intravenously and blood flow can be monitored as it pumps the media around the body. This can highlight any blockages in blood vessels and is also useful for diagnosis and treatment of aneurysms where contrast agent is used to help to guide the surgeon during the procedure to fill the aneurysm (Figure 24).¹²³

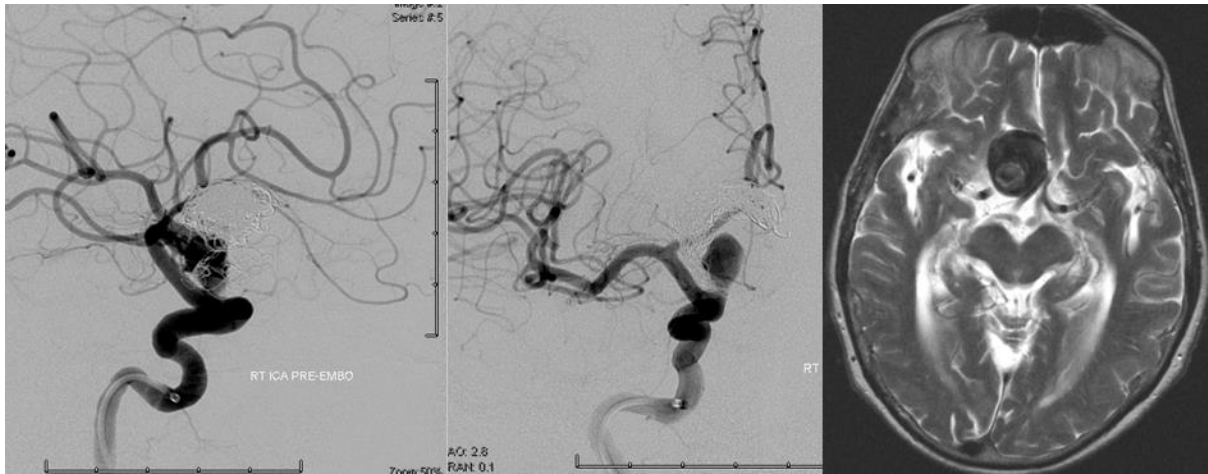


Figure 24. Image showing how blood vessels can be imaged via CT angiography. The first and second images show the blood vessels in the brain as they are flushed with Iodipamide® and imaged by CT. The final image shows a large dark area, which is the aneurysm picked out, again using Iodipamide® contrast agent.

Another important application of X-Ray contrast media is for imaging of the gastrointestinal (GI) tract. A *barium meal* (barium having a high atomic number of 56) which is essentially barium sulphate, is taken orally and its passage through the GI tract monitored by X-Ray. It is also possible to use carbon dioxide gas in addition to the barium meal for a double-contrast analysis.¹⁴⁸ Other applications include urography,^{149, 150} myelography^{151, 152} and arthrography.¹⁵³

Section 2: Magnetic Resonance Imaging

2.1 How MRI works

Hydrogen nuclei (protons) possess a natural magnetization and so, when placed in a magnetic field, will align themselves with that field. MRI works on the basis that protons in different environments will behave in different ways when the magnetic field is manipulated.

Medical MRI works in the following way: an initial magnetic field is applied and so the protons in body tissues in the form of water or fat, will align themselves with this field. When a radio frequency pulse is applied the nuclei rotate by 90° so that they are at a right angle to the original magnetic field (B_0). When aligned in this way the nuclei precess in phase with each other. Following the Rf pulse two things happen, both of which can be measured. The nuclei flip back from the 90° rotation to realign with the original magnetic field, known as longitudinal relaxation, or *spin-lattice* relaxation (T_1), characterised as an increase in signal as they return to their original position. The longer it takes for the protons to return to alignment with the magnetic field the smaller the signal received. The nuclei also begin to precess out of phase with each other, with some precessing faster and some falling behind, known as spin-spin relaxation (T_2) due to the fact that in this case the nuclei transfer energy to each other as they spin. In this case the signal is lost as the net precession adds up to a total loss of phase (Figure 25).^{129, 154} These values are often reported as R values, where $R_1 = 1/T_1$ and $R_2 = 1/T_2$. This calculation makes the small numbers for T_1 and T_2 more manageable and shows a quicker relaxation time as a more positive number.¹²⁹

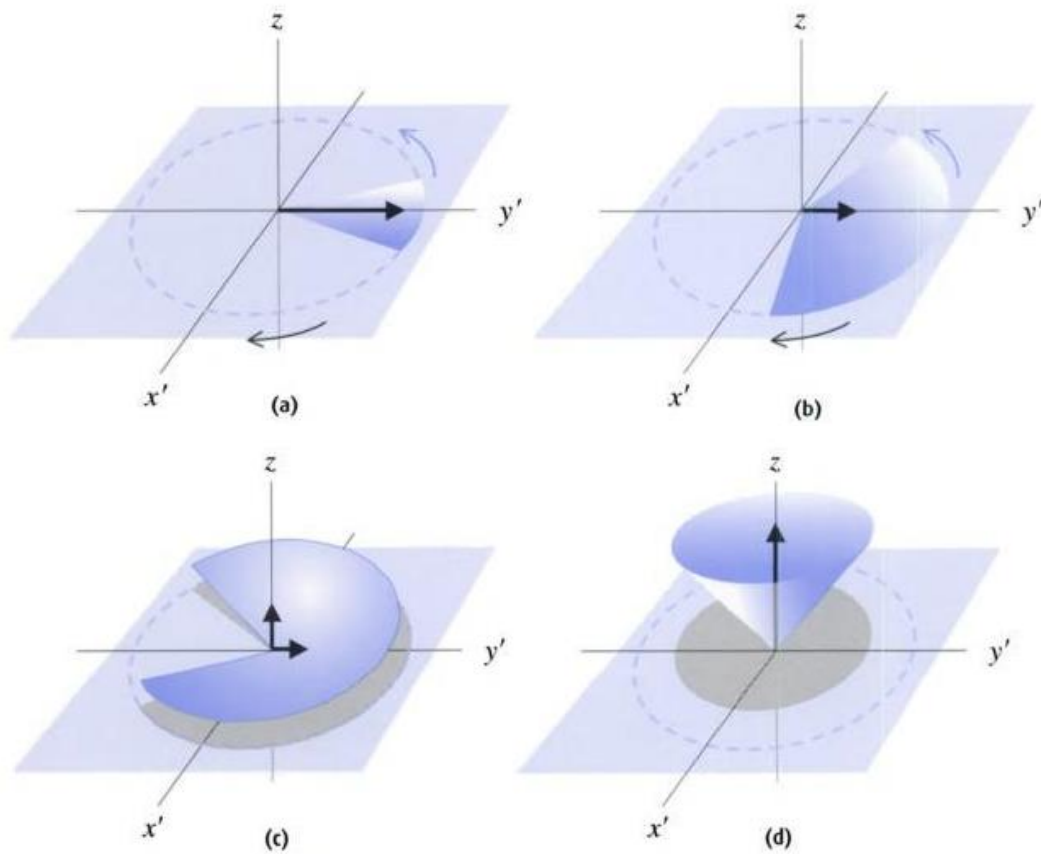


Figure 25. a) b) Spin-lattice relaxation (T_1); c) d) Spin-spin relaxation (T_2)¹⁵⁴

T_2^* is similar to T_2 in that it involves the nuclei precessing out of phase, but whilst T_2 comes about purely through spin-spin relaxation, T_2^* occurs faster because it also involves inhomogeneities in the magnetic field and can be affected by the magnetization of the material itself. T_2 and T_2^* are related by the equation in Equation 3 where γ is the gyromagnetic ratio and ΔB is the variation in magnetic field.¹²⁹

$$\boxed{1/T_2^* = 1/T_2 + \frac{1}{2} \gamma \Delta B}$$

Equation 3. Equation showing the relationship between T_2 and T_2^*

Once these relaxation times have been measured the signal, which will be large for long relaxation times and small for short relaxation times, is converted into an image, with the larger signal

translating as a white area, ranging through shades of grey, to the smallest signal for the shortest relaxation times translating as a dark or black area. Differences in proton density and relaxation times between tissues lead to natural contrast in MRI images, but in some instances the proton environments are so similar that further contrast needs to be created.¹²⁹

2.2 Contrast Agents

Different bodily tissues have different relaxation times and thus appear differently on images, depending on the hydrogen density of the tissue (Table 1.)

Tissue	T ₁ -weighted image	T ₂ -weighted image
Fat	Bright	Bright
Aqueous liquid	Dark	Bright
Tumour	Dark	Bright
Inflammatory tissue	Dark	Bright
Muscle	Dark	Dark
Connective tissue	Dark	Dark
Hematoma, acute	Dark	Dark
Hematoma, subacute	Bright	Bright
Flowing blood	No signal	No signal
Fibrous cartilage	Dark	Dark
Hyaline cartilage	Bright	Bright
Compact bone	Dark	Dark
Air	No signal	No signal

Table 1. Indicating the MRI similarities and differences between tissues in the absence of contrast agent.¹²⁹

Some tissues have very similar relaxation times, such as tumour and inflammatory tissue.^{129, 154} As a result it is necessary for contrast agents to be introduced. To reduce the T₁ relaxation times which

leads to an increased signal intensity on T_1 weighted images (positive contrast agents) or decrease the T_2 relaxation times leading to a decrease in signal (negative contrast agents). Thus the contrast of tissues is altered so that they can be differentiated from each other with greater ease on the resultant image. These agents will work either by altering T_1 leading to T_1 weighted images, by altering T_2 leading to T_2 weighted images, or in some instances the contrast agent is capable of altering both T_1 and T_2 significantly and so either can be exploited.¹²⁹

2.2.1 Positive Contrast Agents

The first positive contrast agent to be produced was Gd-DTPA (Magnevist, Schering AG), in 1988.¹⁵⁵ Gd itself has seven unpaired 4f electrons and the largest spin moment ($S= 7/2$) of all of the rare earth metals meaning that it has a strong magnetic effect making it suitable for MRI contrast. However, Gd^{3+} is highly toxic and so has to be heavily chelated before it can be administered into the body.¹⁵⁵⁻¹⁵⁹ Chelating has the effect of reducing the proton relaxivity of Gd, meaning that although alone it has a very strong relaxation effect in low doses, it must be administered in large doses in the chelated form leading to some severe side effects such as nephrogenic systemic fibrosis, which increased in incidence as the use of Gd chelates for MRI increased.¹⁶⁰ It is thought that the disorder occurs when other metal ions such as Zn, Cu or Fe replace the Gd, leading to dissociation of free Gd^{3+} into the body. Due to this problem there is continuous research into the development of suitable chelating agents which do not allow this to occur, such as the ligands offering eight coordination sites (Figure 26).¹⁵⁶ In addition to this, compounds containing other elements have been explored such as manganese^{161, 162} and iron¹⁶³ both producing T_1 weighted images where the tissue surrounding the imaging agent appears lighter than other tissues (Figure 27).

The type of image produced is affected not only by the nature of the tissue surrounding the contrast agent but also by the rate at which any water associated with the Gd chelate exchanges with water in the nearby tissues. This can be affected by the number of water molecules present and the nature of the chelating agent, and so the chelating agent should be carefully chosen.

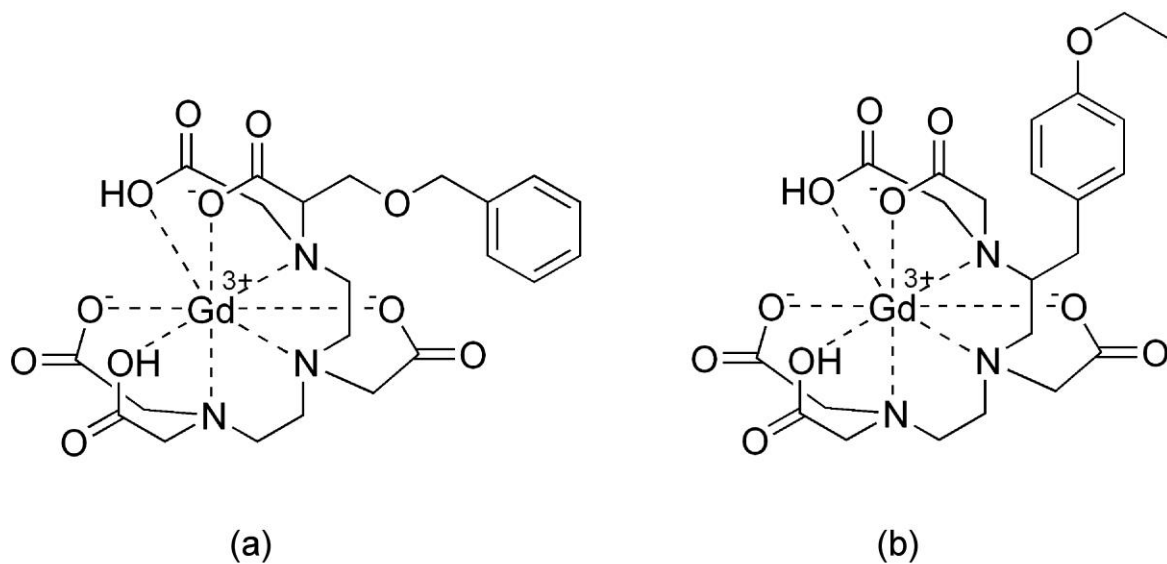


Figure 26. Structural formula of common Gd chelates. Note that there are eight coordination sites making this a very stable chelating agent (A-D). Lower image shows the structures of two representative commercial gadolinium MRI contrast agents; (a) gadobenic acid and (b) gadoxetic acid with optimum doses of these agents being 1 mmol kg^{-1} in adults.¹⁵⁶

Areas in the rat brain where imaging agent has accumulated leading to lighter contrast.

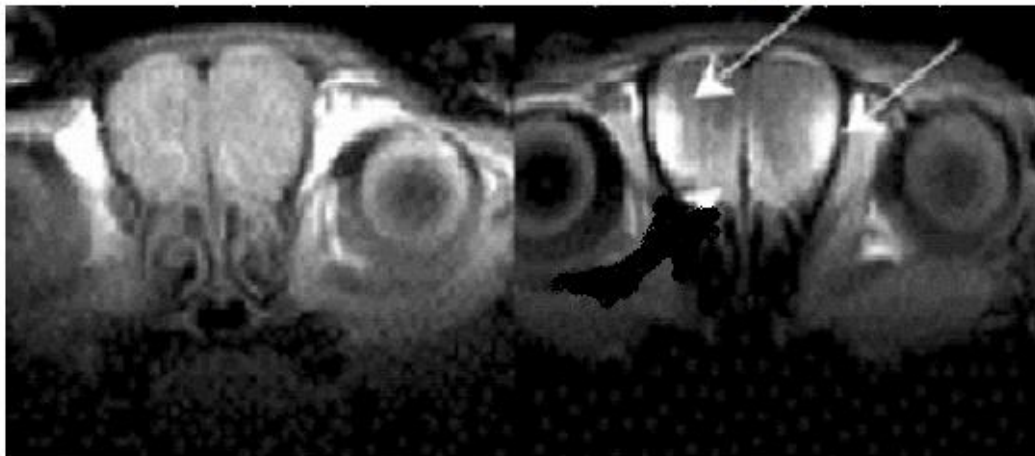


Figure 27. The left hand image shows an image of a rat brain and eye sockets before addition of a contrast agent. The right hand image shows white enhanced areas where the positive contrast agent, in this case Mn^{2+} has accumulated in the tissue.¹⁶⁴

Whilst Gd is typically used to image organs, blood vessels, intestines and occasionally the brain, through its formation of protein adducts the possibility of using Gd to image proteins (specifically human serum albumin (HSA)) has been explored. The *in vivo* imaging of proteins would be beneficial for identifying the presence of disease related proteins and the presence of certain cell types.

Whilst these Gd complexes themselves cannot cross the blood-brain barrier, they can slowly leak across and accumulate in lesions where the blood-brain barrier has been disrupted.^{161, 165, 166}

2.2.2 Negative Contrast Agents

Recently superparamagnetic iron oxide (SPIO) nanoparticles have been used as negative contrast agents.¹⁶⁷⁻¹⁷¹ The iron oxide structure contains both Fe^{2+} and Fe^{3+} ions which have unpaired electrons within the lattice that are able to align with the magnetic field leading to the paramagnetic

effect. When the SPIOs, such as Endorem[®], which was recently removed from the market due to safety issues, are used for imaging of the GI tract they are introduced to a particular part of the body and a magnetic field applied, the magnetic effect of the SPIOs greatly reduces the relaxation time of the protons in the surrounding tissues, thus making them appear dark on the image. In particular, SPIOs are useful for imaging of the liver, as SPIOs are taken up by Kupffer cells, which are specialized macrophages found in the liver lining (Table 2).¹⁷²

Class	Agent	Trade Name	Status	Mean Particle Size
Oral SPIO	AMI-121 (Ferumoxsil)	Lumirem, Gastromark	Approved	> 300 nm
	OMP	Abdoscan	Approved	3.5 μ m
SSPIO (Small superparamagnetic iron oxide)	AMI-25 (Ferumoxide)	Endorem, Feridex	Approved	80 - 150 nm
	SHU555A (Ferucarbotran or Ferrixan)	Resovist	Phase III complete	62 nm
USPIO (Ultrasmall superparamagnetic iron oxide)	AMI-227 (Ferumoxtran)	Sinirem, Combidex	Phase III	20 - 40 nm
	NC100150	Clariscan	Phase III	20 nm
	CODE 7228	Advanced Magnetics	Phase II	18-20 nm

Table 2. Examples and properties of Commercial SPIO Agents⁹¹

Whilst it is beneficial to have an effective imaging agent, the doses cannot be too high as they shorten the T_2 to such a degree that it is too short to provide a signal. Optimal doses are typically 8-16 μ mol of Fe per kg.⁹¹ The problem with this approach is that it does not take into account the effect that any coating agent or solvent-solvent interactions, which may alter relaxation times.

2.3 Detection, Diagnosis and Treatment

MRI and the various contrast agents associated with it have been used in various areas of research into both diagnosis and treatment of disease.^{134, 167, 173-178} The high resolution of MRI allows for very precise detection of diseases such as cancer, and so is an invaluable tool in its diagnosis. In addition to this it is possible to functionalise the contrast agents that are used in order to treat the disease, monitoring it by MRI as treatment progresses.¹⁷⁶

2.3.1 Hyperthermia

The National Cancer Institute defines hyperthermia in terms of a cancer treatment in which body tissue is exposed to high temperatures (113° F) to damage and kill cancer cells.¹⁷⁹ 113 °F is roughly 45 °C so the research shows that the SPIOs are able to induce sufficient temperatures for hyperthermia treatments.

Hyperthermia is a rise in normal body temperature caused when the body absorbs more heat energy than it can dissipate; this can be local or systematic. The use of hyperthermia in the treatment of diseases, specifically cancers, dates back to the time of Hippocrates who used hot iron to cauterize surface tumours. In more recent years this technology has been brought up to date with the use of pyrogens (such as bacterial toxins), high frequency radiation and magnetic fluid hyperthermia.^{73, 78, 178, 180-184}

Hyperthermia is emerging as a promising application of SPIOs for treating cancer. Due to their superparamagnetic nature SPIOs, when placed in a rapidly oscillating magnetic field, are able to flip rapidly leading to localised heating effects. Work carried out on Ehrlich carcinoma's in mice indicated that the SPIOs could induce a maximum temperature of 47 °C in the centre of a tumour measuring $78.2 \pm 3.5 \text{ mm}^3$. These elevated temperatures led to restriction of blood vessels around the tumour and thus hypoxic conditions, leading to apoptosis and a subsequent slowing in tumour growth.¹⁷⁸

Hyperthermia works by damaging cancerous cells and proteins associated with those cells so that either the cells die or they are more susceptible to radiation (radiotherapy). So, hyperthermia can

be used either on its own as a localised, regional or whole body therapy, or in conjunction with the more commonly used radiotherapy and chemotherapy.¹⁷⁹

The possible side effects of traditional hyperthermia techniques, in which probes or directed microwave or radio-waves are used to create a rise in temperature, include burns, blisters and general discomfort as well as possible bleeding and blood clots.¹⁷⁹ This is because these methods are not specific enough and may damage healthy tissues. By using nanoparticles to direct the heating effect to certain areas only, it is possible that the heating effect could be mainly contained to the tumour area only (although whole body hyperthermia for treating metastatic cancers would not benefit), thus reducing side effects.¹⁷⁹

A specific method has been to use modified aminosilane magnetite nanoparticles which have a 10-fold higher uptake by malignant prostate cells than by normal prostate cells, making it easier to facilitate a specific hyperthermia treatment.¹⁸⁵ If this contrast can be repeated in other types of cancerous cells, it would give a much more specific response to the effects of hyperthermia than other methods.¹⁸⁶ Another example of the success of using magnetite nanoparticles for hyperthermia is the use of dextran magnetite for oral cancer hyperthermia¹⁸⁶ In this study the particles were injected into the tumour directly and the hyperthermia group showed a significant reduction in tumour growth and a significant increase in survival rates when compared with the control group.

Hyperthermia has also been used for inducing production of heat stress/heat shock proteins which have will be explored in Ch. 1.3, Section 7.4.

Currently the main method for delivering SPIOs to the desired area for hyperthermia is through injection directly at the site, although it is possible that other methods could be used.

2.3.2 Transdermal drug delivery

In 1995 transdermal drug delivery was hailed as “a breakthrough in the field of controlled drug delivery systems”.¹⁸⁷ Oral drug delivery routes are problematic as the drug must pass through the digestive system where it is subject to enzymatic attack and degradation by pH, and then must also evade breakdown by the liver *via* the first pass effect. For many therapeutics, such as insulin, the conditions in the GI tract render them useless. Bearing this in mind it is obvious that the

transdermal route, bypassing all of these problems, would be more desirable. However, the transdermal route is not without its own complications.

The skin is designed to prevent the passage of many substances, and so is a barrier for the delivery of drugs. Therefore, most drugs are unable to pass through the skin at a rate that is beneficial therapeutically, with rates being reported as being between 500 and 10, 000 times slower in the stratum corneum than in the dermis or sub-cutaneous tissue.¹⁸⁸ When determining the dosage of a drug required the actual amount of drug that must be applied in order for an effective amount to enter blood circulation must be considered. As the rate of passage is so low a vast amount of the drug will be wasted, and only very potent drugs are usually effective. In addition to this, the stratum corneum (Figure 28) only allows the passage of small, lipophilic molecules of $< 400 \text{ Da}$ ($400 \text{ g}\cdot\text{mol}^{-1}$), which further reduced the number of different drugs for which this technique is useful.¹⁸⁸

To increase the permeability of the stratum corneum a process known as *electroporation* can be carried out.¹⁸⁹ This involves applying short, high-voltage pulses to the skin which create pathways in the pores through which aqueous medium, or indeed hydrophilic drug molecules, can pass.¹⁸⁹ Other methods for increasing permeability include *pressure waves*,¹⁹⁰ *thermal ablation*,¹⁹¹ and *ultrasound*.¹⁹²

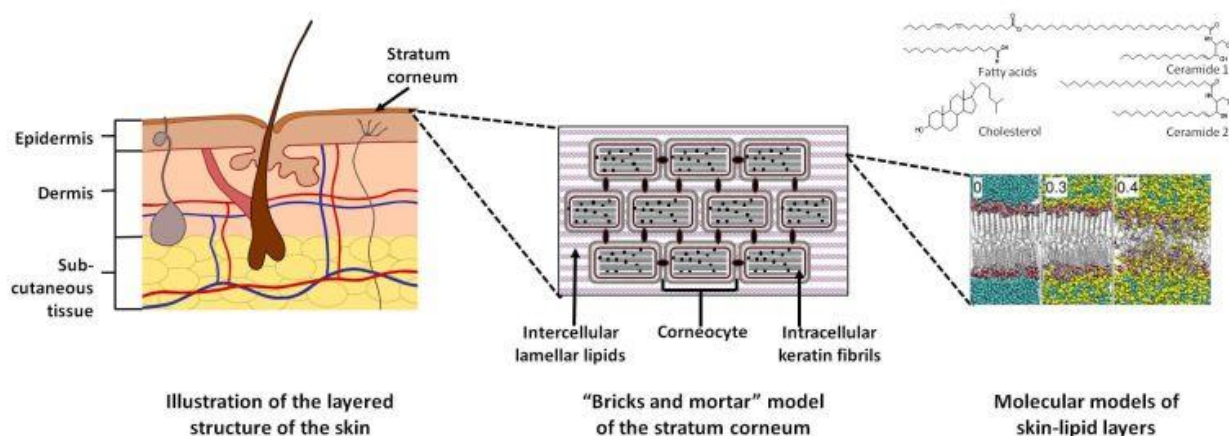


Figure 28. Images of the skin in different formats. The first image shows the structure of the skins with the second image being a schematic showing the building blocks of the skin. The right hand image shows the molecules that make up the various areas of the skin.

Patches have previously been favoured, with the first patches being developed by Tojo in 1987 for the treatment of motion sickness. Since then many other applications have been trialled which include the popular nicotine patches, hormone replacement therapy (HRT) and pain relief.¹⁸⁸

For these reasons hypodermic injections have been favoured for delivery of therapeutics, and recent efforts have been focused on synthesis and trialling of microneedles. These needles are able to bypass the stratum corneum and so allow delivery of large macromolecules that would not otherwise be able to pass the top layer of skin.¹⁸⁸ One study reports using materials such as polyglycolic acid (PGA) and polylactic acid (PLA) and their copolymers. These needles were synthesised with a diameter of $\sim 100 \mu\text{m}$ at the base and $\sim 10 \mu\text{m}$ at their tips, and were plated at 300 needles per cm^3 , and were found to be successful in piercing the stratum corneum.¹⁹³ However, these techniques are limited in that they require a professional to administer the injection, in contrast to creams and patches that can be administered by the patients themselves.

Microemulsions have also been explored as an alternative to traditional gel preparations and have been found to enhance the delivery of both lidocaine and acetaminophen.²³ A more recent study (2006) into the effectiveness of microemulsions in improving passage of diclofenac through the stratum corneum, showed an 8-fold increase in the concentration of diclofenac passing into blood circulation in rats.

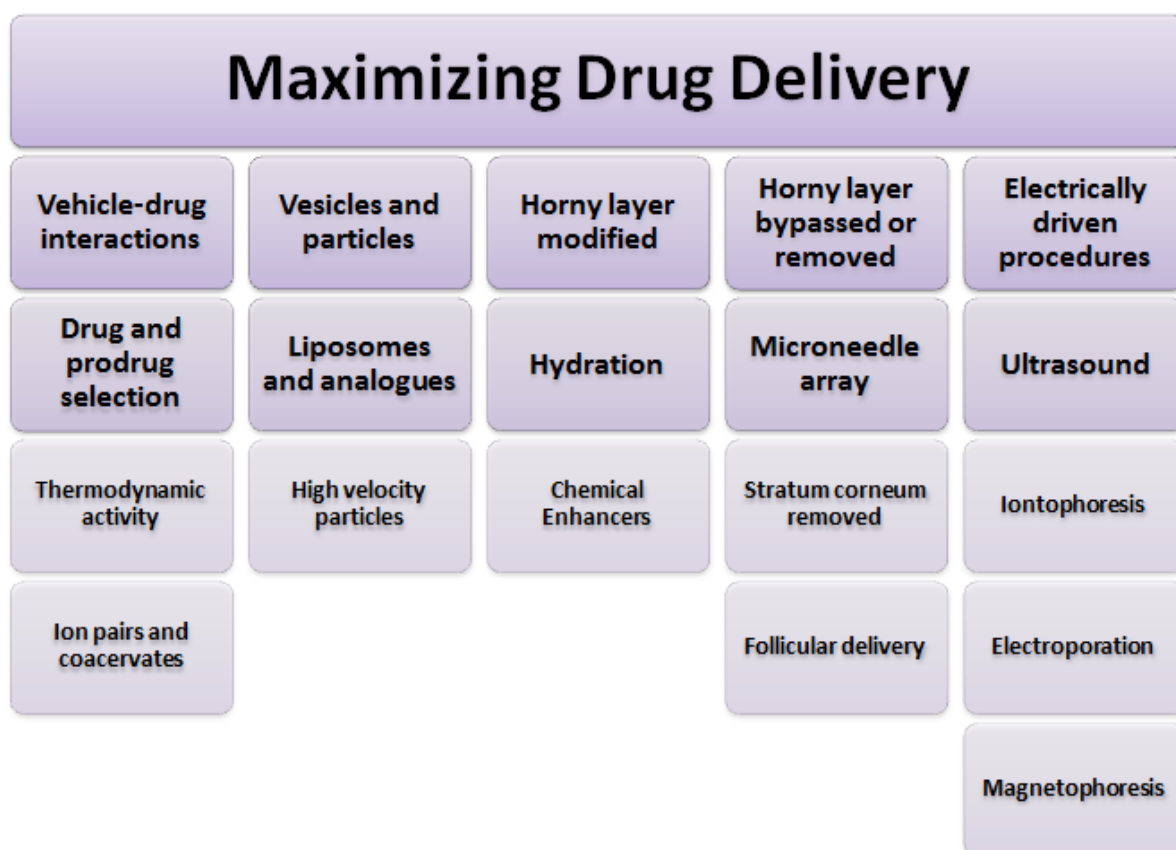


Figure 29. Showing the possibilities for maximising drug delivery¹⁹⁴

Whilst all of these are good options for improving passage of drugs across the stratum corneum, they are all limited by both the solubility and size of the drugs, and means that delivery of peptides and DNA/RNA is not possible *via* transdermal routes. One research group reported using a cell-penetrating peptide to modify iron oxide nanoparticles in order to carry siRNA to cancer cells. The results of the study showed an enhanced permeability and retention effect which has the possibility to be useful for MRI and other drug delivery applications.¹⁹⁵

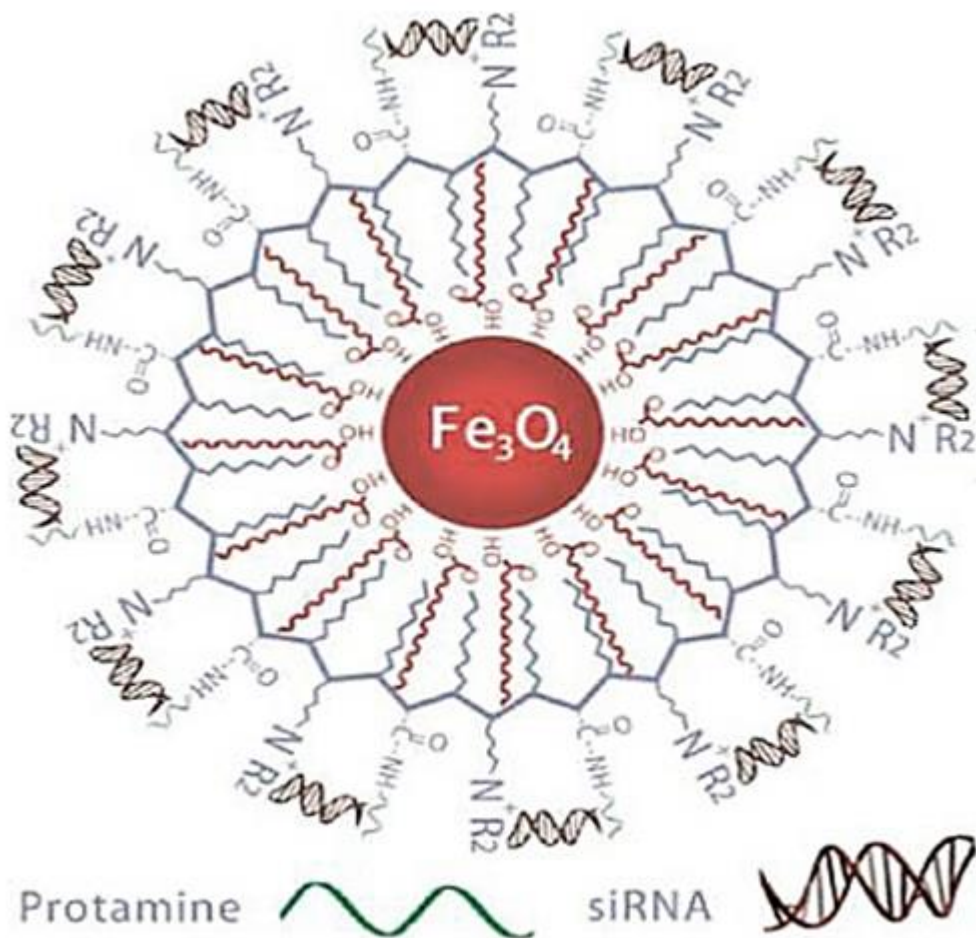


Figure 30. Showing an iron oxide nanoparticle coated with a cell penetrating peptide, with siRNA held between the amine moieties at the terminal end of the peptide.¹⁹⁵

2.3.3 Anaemia

Iron oxide was used for years in the treatment of Anaemia with various preparations being used to overcome problems with toxicity and bioavailability.¹⁹⁶ Studies into bioavailability have used ⁵⁹Fe for radioactive tracing of iron from IV preparations (⁵⁹Fe AMI-25), through the liver and its subsequent incorporation into haemoglobin. Studies on rats showed that 1 % of the ⁵⁹Fe had been incorporated into erythrocytes after 2 days, rising to 20 % by day 49 with similar rates being observed for haemoglobin.¹⁹⁷ More recently studies into using iron oxide nanoparticles coated with ascorbic acid (vitamin C) have been carried out which indicate that the two substances combined lead to an overall increase in the bioavailability of iron to the body.¹⁹⁶ In their patent Salah El-Din et

al describe using ascorbic acid coated SPIOs to treat anaemia orally, and claim that this single dose preparation is able to increase iron levels back to normal within 10 days.¹⁹⁶

As well as being used for detection or diagnosis of disease SPIOs can be used for the treatment of disease. The particles can be conjugated to drug molecules and used as a delivery system,¹⁹⁸ or can be used to stimulate hyperthermia so that cancer cells can be specifically killed through heating.^{182,}¹⁹⁹ In a very different application, SPIOs have previously been used in the treatment of anaemia as the body can process the SPIOs, using the iron for making haemoglobin.²⁰⁰

2.4 Structure of iron oxide

The atoms in the iron oxide bulk material are arranged in what is referred to as an *inverse spinel* structure. What this means is that there are two types of metal coordination site, one being octahedral (2/3) and the other being tetrahedral.²⁰¹ In a regular spinel structure the general formula is AB_2X_4 where A is usually M^{2+} , B is M^{3+} and X is generally oxygen. However, in an inverse spinel half of the sites occupied by M^{2+} ions are generally swapped for M^{3+} ions as illustrated in Figure 31.

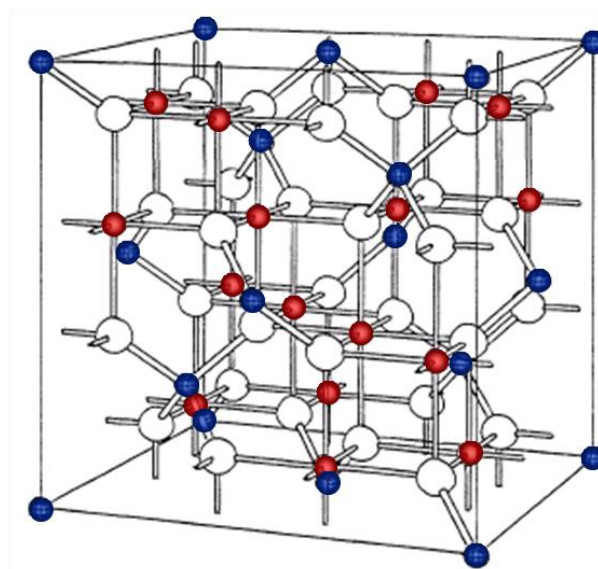


Figure 31. Crystal structure of magnetite with blue atoms representing tetrahedrally coordinated Fe^{2+} ; red atoms representing octahedrally coordinated 50/50 Fe^{2+}/Fe^{3+} ; white atoms are oxygen.

This structure explains why during synthesis of Fe_3O_4 the molar ratios of the Fe^{2+} and Fe^{3+} are 2:3 respectively.

What is also clear from this structure is that at the surface of any material made from iron ^{II, III} oxide is that there will be Fe^{2+} and Fe^{3+} ions exposed at the surface. This gives the material a positive charge which makes it able to interact with any solvents of coating materials nearby. There will also be O^{2-} ions present at the surface which under certain conditions allow the substances to interact electrostatically with positively charged materials.

2.5 Magnetic properties of bulk iron oxide

Iron oxide as mentioned consists of Fe^{2+} and Fe^{3+} ions which contain electrons with unpaired spins which make the material paramagnetic, meaning that these unpaired spins will align with a magnetic field when exposed to it but return to their original unaligned state when the magnetic stimulus is removed. In the bulk material the electrons are arranged in magnetic domains, known as *Weiss* domains that are separated by an area called a *Bloch wall*. The alignment of spins with the magnetic field can be parallel or anti-parallel depending on the direction of the electron's spin.⁹²

2.6 Magnetic properties of iron oxide at the nano scale

The magnetic properties of magnetite in its nano form differs from magnetite in its bulk form primarily due to the fact that in the nano form the particles become so small that the formation of Bloch walls becomes energetically unfavourable, leading to the formation of crystals that have a single Weiss domain (single-domain crystals) as depicted in Figure 32. These single domain crystals have a much higher saturation magnetization as the whole crystal is able to align itself within the magnetic field.⁹² Iron oxide nanoparticles therefore exhibit stronger paramagnetism than ordinary iron oxide and so are given the term *superparamagnetic*. Despite this large magnetism SPIOs do not retain any magnetization when the magnetic field is removed, as thermal energy is strong enough to randomize the orientations of the SPIOs leading to disorder of the electron spins.

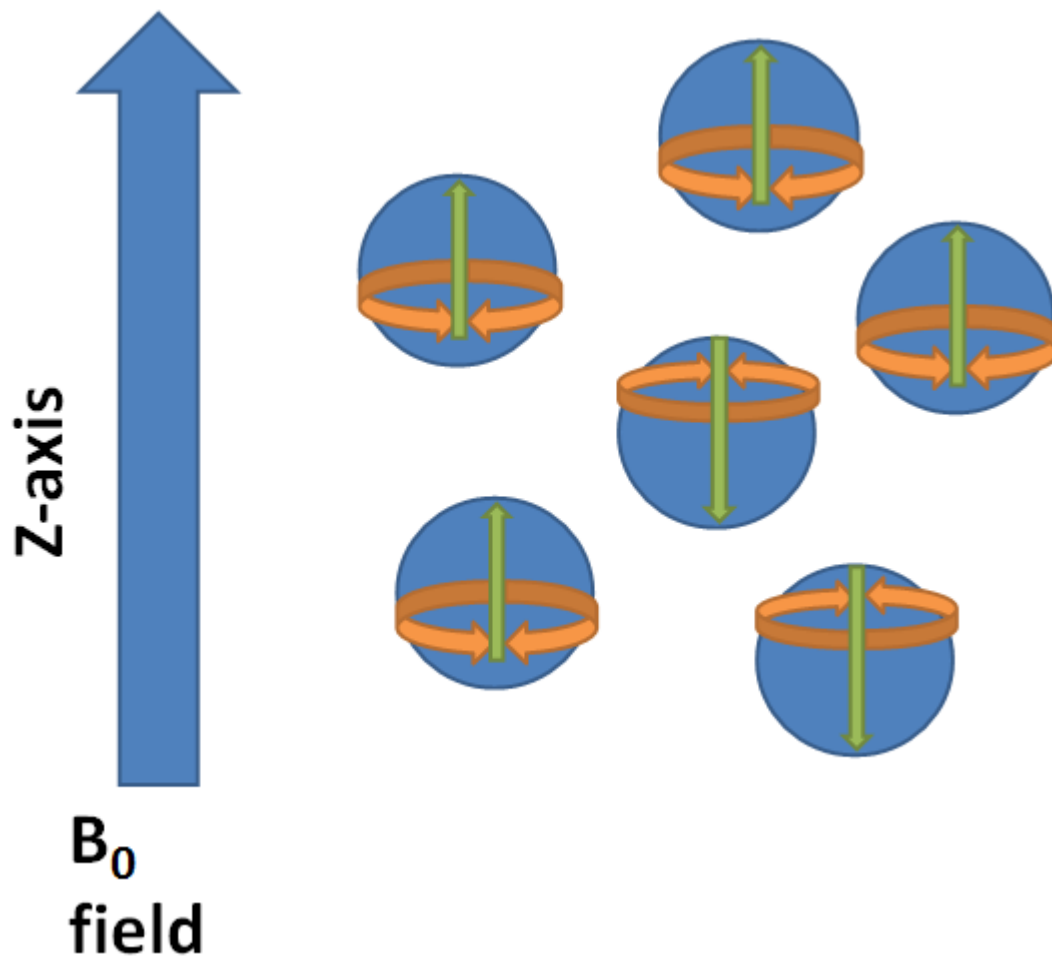


Figure 33. Showing how protons or electrons align with the magnetic field depending on their spin (opposite spin leads to alignment in opposite directions to the magnetic field).

2.7 Current status of clinical application

Of the numerous iron oxide nanoparticles produced so far only two of these have been approved for clinical use, and more recently these have been removed due to bioaccumulation to toxic levels in some long lived cells leading to side effects. These fall under the categories of ferumoxides (including Endorem®) and ferucarbotran.

Ferumoxides are SPIOs coated with a low molecular weight dextran. As has been mentioned previously, polymers such as dextran make the particles water soluble and increase biocompatibility. The particle size is 120-180 nm which is large enough that the particles will be picked up by the RES. Side effects from these preparations include low blood pressure and back pain, although side effects

are only severe enough to stop diagnosis in 2.5 % of patients. The optimal dose is set at 0.56 mg (0.01 mmol) of iron per kg of body weight.²⁰²⁻²⁰⁵

Ferucarbotran[®], also known as Resovist[®], is a carboxydextrane coated SPIO with a particles size of 45-60 nm. It has a similar mode of action to the ferumoxides but has significantly lower incidences of side effects and can be delivered in much larger doses over a short period of time with no ill effect. The application of a bolus injection technique to this drug is very different to the delivery of ferumoxides which need to be injected slowly over the period of up to half an hour, as oppose to the bolus which can be delivery is 20 – 30 seconds.²⁰⁶ The optimal dose for Resovist[®] is set at 0.45 mmol of iron per patient for patients < 60 kg, and 0.7 mmol of iron for patients > 60 kg. Vasodilation (possibly due to the bolus technique) and paraesthesia are the most common side effects for this imaging agent²⁰⁶

Both of these are used for liver imaging as upon clearance by the RES the SPIOs are transported to the liver (if it is functioning normally), spleen, bone marrow and lymph nodes. These iron compounds are degraded in lysosomes (~ pH 4.5) and the resultant iron ions are used to form iron compounds in the body such as haemoglobin, or else are cleared from the body.

Other potential imaging agents such as Clariscan[®], a PEG coated SPIO formulation and Ferumoxtran-10 for diagnosis or prostate cancer have been unsuccessful in gaining FDA approval. Clariscan[®] led to severe side effects and Ferumoxtran-10 led to false positives in too many cases. Recently Resovist[®] has been taken off the market due to concerns over safety and it looks likely that ferumoxides will also be removed from clinical application for similar reasons.²⁰⁷

Although SPIO preparations have proved to be non-toxic in an *in vitro* setting, when administered *in vivo* they have a negative effect on cell homeostasis and are able to bioaccumulate in cells. In high concentrations SPIOs can hinder cell proliferation by altering the cytoskeleton.²⁰⁸ If targeted to the correct cell this could be exploited to hinder cancerous cell growth, but in a normal setting it is detrimental to the patient.

Although SPIOs are so far unfavourable as IV agents, the oral agents for GI imaging such as Ferumoxsil[®] and Lumirem[®] are still available on the market although there is very little demand for these as other preparations such as barium sulfate and Gd chelates are already well established.^{124,}

148, 156, 209

Chapter 1.3: Cancer Immunotherapy

Section 1: Cancer

1.1 Background

Cancer is a multifaceted disease that is characterised by unlimited replication of cells and other attributes which will be discussed in detail later on. One definition of cancer cells is that they are altered self-cells that have escaped normal growth-regulating mechanisms.²¹⁰

It has been reported that in 2008, 12.66 million people were diagnosed with cancer worldwide, and 7.56 million people died from cancer.²¹¹ The statistics reflect both developed and developing countries, although incidence and deaths from cancer are generally higher in developing countries. The same data indicates that men are at an increased risk of developing cancer, with 204 men per 100,000 in the UK being diagnosed, as opposed to 165 per 100,000 women. These statistics show that lung, breast, colorectal and prostate cancers are the most prevalent in the UK, accounting for 54% of cancer diagnoses (Figure 34).²¹¹

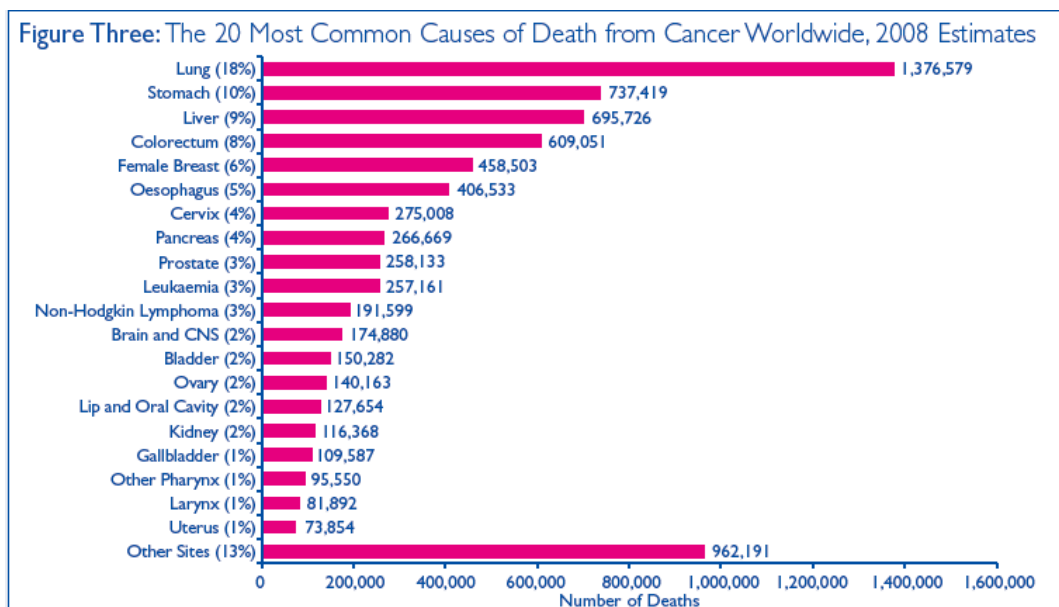


Figure 34. Bar chart showing the number of deaths from different types of cancer worldwide in 2008

As mentioned, cancer is a disease defined by several characteristics, each of which must be acquired during the development of the disease in order for a successful tumour to develop. The key characteristics are referred to as the *Hallmarks of Cancer* (Figure 35) ²¹⁰ and include: limitless replicative potential, sustained angiogenesis, evading apoptosis, self-sufficiency in growth signals, insensitivity to anti-growth signals, and tissue invasion and metastasis. ²¹⁰

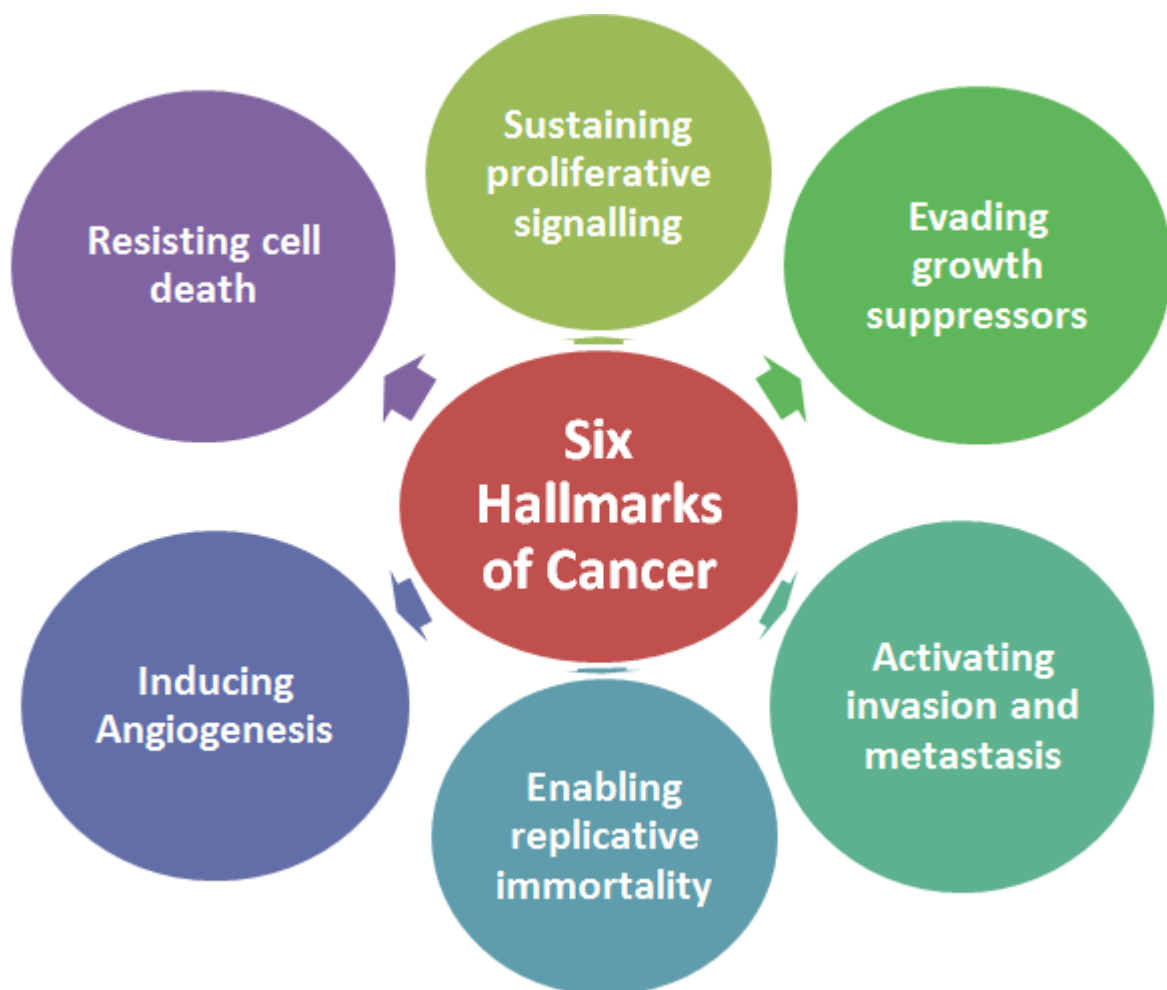


Figure 35. Diagram naming the six hallmarks of cancer

More recently two other hallmarks have been discovered, although these have not yet been confirmed. They are; Reprogramming of energy metabolism, and Evading immune destruction. ^{212,}

²¹³ By looking at the different hallmarks together and understanding that in order to become successfully established the cells must undergo multiple mutations to develop each of these hallmarks, it is clear to see that cancer is a very complex disease, and so must be better understood in order for simple treatments to be developed.

1.2 The hallmarks of cancer

Tumorigenesis is a multistep process that is thought to involve six key processes, revealing cancer to be a disease involving dynamic changes in the genome. This process is analogous with Darwinian evolution where, through a series of mutations in the genome, normal cells are transformed into cancerous cells, adapted to survive and thrive in their environment. These genetic mutations are involved primarily in disruption of the cell's normal relationship and response to surrounding cells and the body's defence mechanisms, including recruiting normal cells to assist their survival. These *acquired capabilities* of cancer are referred to as the six hallmarks of cancer (Figure 35).²¹⁰ With the addition of two possible new hallmarks this number could increase to eight.

1.2.1 Self-sufficiency in Growth Signals

Our body cells are designed so that they are carefully controlled in terms of growth, proliferation and senescence. This is essential for the growth of normal tissues, as without these controls tissues will not function properly and will not form the correct shapes and arrangements needed to make up working organs. Whilst normal cells rely on neighbouring cells to signal for them to proliferate, known as heterotypic signalling, cancer cells are able to stimulate or regulate their own proliferation.²¹⁴ The three main ways in which they achieve this are herein described.

Cells are able to produce their own growth signal ligands and the receptors needed in order to respond to them. This is known as autocrine stimulation.²¹⁵ When this occurs the cell is no longer dependent on other cells within the tissue for proliferation, and so an element of the regulation is no longer controlled.

Neighbouring cells release small levels of growth factors that cancer cells would not usually respond to, but overexpression of growth factor (GF) receptors can make the cell hyperresponsive to these

low levels. One example of this type of cancer adaptation is in the overexpression of the HER2/neu receptor in stomach and mammary carcinomas.²¹⁶

Alternatively, the same types of receptors may be mutated so that they are able to fire independent of the ligand they come into contact with. As has been mentioned, in order to successfully become a tumour, normal functioning neighbouring cells are often co-opted into supporting the growth in some way. It is possible for cancer cells to produce signals (proteins) that will induce the surrounding cells to produce growth signals.²¹⁷

1.2.2 Insensitivity to Antigrowth Signals

Normal cells are subject to control of proliferation by antigrowth signals that either force the cell to stay in the growth phase (G_0 phase) as oppose to the active proliferation stage, or that induce the cell to enter a postmitotic state associated with terminal cell differentiation, after which the cell can no longer proliferate.²¹⁴ Nearly all antiproliferative signals are directed through the retinoblastoma protein (pRb) which, when hypophosphorylated, will block proliferation by altering the function of certain transcription factors (E2Fs) involved in progression from the growth phase to a stage of active cell division. One of the most well documented antigrowth factors, TGF β , works by preventing phosphorylation and thus inactivation of pRb in various ways including by synthesis of proteins that are able to block complexes responsible for phosphorylation.²¹⁸ One of the ways that cancer cells lose their responsiveness to antigrowth signals is by down-regulation of TGF β receptors or by producing mutant receptors. If receptors do not work then pRb can become hyperphosphorylated, inactivated, and so E2Fs are free to signal to the cell to enter a state of active proliferation. It is also possible for the pRb gene itself to become mutated leading to a non-functional protein, or as in the case of human papillomavirus, the pRb function is eliminated as viral oncoproteins hijack cell machinery.^{210, 212, 213}

In addition to these mechanisms, cancer cells are also able to switch off expression of integrins and other molecules that send antigrowth signals to the ECM. This means that progrowth signalling molecules are favoured, and the cell can avoid terminal differentiation by shifting the balance of molecules that lead to differentiation back to favour growth and proliferation.²¹⁰

1.2.3 Evading apoptosis

If a tumour cell population is to prosper then it must increase levels of proliferation (as detailed previously) and decrease cell attrition (reduction in numbers/size), the main source of which is breakdown due to apoptosis or programmed cell death. The idea that apoptosis was a barrier to cancer was first suggested in 1972 by Kerr *et al.* when it was noted that when hormones were removed from rapidly growing hormone-dependent tumours there was mass apoptosis.²¹⁹ Since this time anti-apoptotic oncogenes have been discovered which support the theory. Studies indicate that apoptosis is triggered by overexpression of certain oncogenes, supporting the theory that apoptosis is a defence mechanism against cancer.

Resistance to apoptosis can be acquired through many different routes, with the most commonly occurring mutation involving the p53 tumour suppressor gene. Non-functional p53 proteins are prevalent in over 50% of human cancers.²²⁰ Loss of this protein leads to less detection and thus removal of damaged DNA. The p53 protein will be discussed in more detail in Ch. 2; Section 4.

1.2.4 Limitless Replicative Potential

Research over the past 40 years has indicated that even with the cancer cells being completely independent of their environment in terms of regulatory and growth signals, this is still not sufficient for the cell to prosper and form a tumour. Normal cells in culture are found to have a finite replicative potential, termed senescence, being able to replicate only a certain number of times before further proliferation leads to them going into a crisis state as faults within the cell, including fusion of chromosomes to each other, stop it from further replicating and induce mass apoptosis.²²¹

However, if a cell is able to multiply successfully without limit then it is said to have been immortalized, and this is what is observed with most cancer cells in culture.²¹⁴ Normal cells can double 60-70 times, but as cancer cells suffer very high rates of attrition, this replication barrier becomes a problem if they are to amass enough cells to successfully form a tumour.

The main defence mechanism against immortalization is the presence of telomeres on each chromosome. These act as a barrier to chromosomes fusing together which leads to karyotypic disarray (a characteristic of the crisis state that leads to cell death). However, there are a limited number of these and at each replication one of the telomeres is removed. Once every telomere has been removed the cell will eventually die. What is noticed in cancer cells is that the telomeres are maintained.²²² The most commonly reported reason for this is the upregulation of the telomerase enzyme which adds hexanucleotide repeats onto the ends of telomeric DNA, thus preventing the chromosomes from fusing together and increasing the cancer cells replicative potential.²²³ This property of cancer cells is exploited for the synthesis of monoclonal antibodies. A plasma cell producing a specific type of antibody can be fused with a cancer cell and thus become immortalised, leading to an immortal cell which can replicate and produce masses of a particular antibody.²¹⁴

1.2.5 Sustained Angiogenesis

Virtually all cells in a tissue need to be within 100 μm of a capillary in order to receive the oxygen and nutrients that they need, so in order for the tumour cells to survive they must develop an angiogenic ability so that new blood vessels can be grown in the proliferating tissues. Proliferating tissues do not naturally have angiogenic ability, this is developed *via* a series of signals and interactions with over two dozen angiogenic inducer factors and endogenous inhibitor proteins currently known.²¹⁴ Vascular endothelial growth factor (VEGF) plays an important role in the control of angiogenesis and experiments have shown that in the presence of anti-VEGF antibodies neovascularisation is impaired.²²⁴ In this study it was shown that subcutaneous tumours were unable to exhibit rapid growth when the antibodies were introduced, further proving that angiogenesis is important in the formation and expansion of tumours.²²⁵

It is thought that tumours activate the “angiogenic switch” by altering levels of angiogenesis inducers through increasing gene transcription leading to increased expression of growth factors such as VEGF and decreased expression of inhibitors such as β -interferon.^{226, 227} It is also possible that changes in expression are a result of loss of function of other proteins such as the p53 tumour suppressor which regulates the anti-angiogenic regulator thrombospondin-1. When p53 becomes

non-functional the levels of thrombospondin-1 decrease and so angiogenesis can occur.²²⁸ However, the mechanisms by which the balance of various angiogenic factors is changed is little understood and much further research will need to be carried out before it will be possible to fully understand the ways in which cancer cells induce vascular formation.

1.2.6 Tissue Invasion and Metastasis

Metastases are the cause of 90 % of human cancer deaths, and so understanding the way in which cancers invade tissues and metastasise is of the utmost importance.²²⁹ The reason that some cancer cells break off and form new “colonies” is thought to be because in the new area of the body there is more nutrients and space, but it is a very complex process that is at present not sufficiently understood. One key factor that seems to lead to metastasis in particular is the malfunction of proteins known as cell-cell adhesion molecules (CAMs). In one case it was found that in cancer the N-CAM molecule undergoes a switch in expression from a highly adhesive form to a weakly adhesive or repulsive form. It seems that this lack of adhesion is what leads to cells breaking away from the mass and relocating in other parts of the body.

In terms of tissue invasion proteases that can facilitate invasion of cancer cells across blood vessel walls and through normal epithelial cell layers play a large part although this is also poorly understood.^{230, 231}

1.2.7 Two New Hallmarks?

Although there is currently not enough evidence to justify calling the following two characteristics new hallmarks, there is an increasing body of evidence to suggest that the reprogramming of energy metabolism and evading immune destruction are likely to be characteristics that are essential to the formation of successful tumours.²¹³

1.2.7.1 Reprogramming of energy metabolism

The uncontrolled and rapid cell proliferation associated with cancer requires a huge amount of energy, and so respiration in these cells is of utmost importance.

Normal body cells respire aerobically, starting with glycolysis during which glucose is broken down to pyruvate in the cytosol. Following this the pyruvate is, for the majority, taken up into the mitochondria where it undergoes a series of reactions forming adenosine 5'- triphosphate (ATP) energy and consuming oxygen. Under anaerobic conditions this pathway is changed and the pyruvate is diverted through a different series of reactions.²¹³ Typically the cells in an environment with plentiful oxygen will respire aerobically, and those in a hypoxic environment will respire anaerobically. However, it has been observed that many cancer cells are able to reprogram themselves to favour glycolysis even when the concentration of oxygen is high. This seems counterproductive as there is an 18-fold lower efficiency when compared to anaerobic respiration.²¹³ So, what is the reason for this adaptation if not for more energy?

The answer is that we do not really know, hence why this hallmark of cancer has not been accepted officially. A theory was first proposed by Potter in 1958, and further improved by Vander Heiden *et al.* in 2009.²³² They suggest that when the pyruvate from glycolysis is not passed on to the mitochondria, this allows diversion of the glycolytic intermediates to other processes. These might include synthesis of macromolecules and organelles that are essential to the production of new cells. So, whilst the energy produced from respiration might be less, the materials available for synthesising new cells increases. In addition to this, the cancerous cells up-regulate glucose receptors, and so increase the overall amount of glucose entering the cell, thus providing more materials and so more energy.²³²

This theory has not gained sufficient evidence, however it has been noted that embryonic tissues behave in a similar way. Embryonic cells have to proliferate at a rapid rate, and so would also be relying on a supply of materials for making new organelles and such like.²¹³ Bringing these two types of tissues together, it is a logical assumption that the reasons for the two different cells to have this anaerobic glycolysis adaptation are the same, and the idea of having a large supply of materials for organelle synthesis is a sensible suggestion. However, as with any theory there must be more evidence before this can be fully understood, and accepted as a true hallmark.

1.2.7.2 Evading immune destruction.

Whilst there is little evidence to support *reprogramming of energy metabolism* as a true hallmark, there is even less evidence for *evading immune destruction*. However, it does pose some interesting questions. The immune system, as will be discussed later on, is designed to eradicate cells displaying foreign antigens, which includes cancerous cells with gene mutations. In fact it has been shown that when cancerous tissue from an immune deprived individual is implanted into another individual with a fully functional immune system, the cancer is not able to establish a tumour.^{233, 234} So, the question posed is how do cancers adapt to evade eradication by the immune system?

There are several theories in development with one of the most prevalent being coercion of immune cells. As cancers recruit cells of neighbouring tissues it is also possible that they recruit immune cells and in doing so are capable of evading immunosurveillance. This in addition to immune tolerance will stop the immune system from recognising the cancer cells and their antigens as foreign and so reduce the chance of the immune system eliminating potential cancer cells.²¹³

1.3 Treatment

The original treatment for cancer was surgery.²¹⁴ Through history there have been reports of tumours being removed through surgical processes. This is a very effective method of treatment, but only as long as the whole tumour is removed and no metastasis has occurred. Whilst surgery can remove any affected localised tissue, if the disease has spread or has entered the blood or lymph, then surgery is useless in its general treatment and so other methods of treatment need to be adopted.²¹⁴

Radiotherapy was the next method to be discovered. It works on the principle that radiotherapy damages DNA, and cancer cells are more susceptible to death from DNA damage as their DNA is already mutated and so does not have the capability to repair itself, meaning that the cell will die. However, Radiotherapy can cause cancer in unaffected cells due to DNA damage, as it does not

specifically target cancerous cells, hence side effects such as sickness and hair loss. These therapies typically target fast growing cells as cancer is fast growing, but both hair follicles and epithelial cells in the lumen of the small intestines are fast growing and so are targeted due to lack of specificity.²¹⁴

Chemotherapy is the most recent treatment to be trialled, and there is a wide variety of anti-cancer drugs currently on the market including Docetaxel, Paclitaxel and Doxorubicin. These work by disrupting the cell cycle (essential for tumour formation) in a variety of ways which include the prevention of microtubule disassembly which stops the spindle required for metaphase from forming (Paclitaxel). Alternatively Doxorubicin prevents the DNA double helix from being resealed following DNA replication, and so stops the cell cycle at an even earlier phase.²³⁵

An example of another drug trialled for use in chemotherapy was Motexafin Gadolinium (MGd).²³⁶ This drug is an inhibitor of ribonucleotide reductase, and works by halting the synthesis of deoxyribose nucleotides which are essential for the synthesis (replication) of DNA. However one year on from the original trials with this drug the FDA deemed it unsafe and so it is no longer in use.²³⁶ However, another motexafin derivative, Motexafin Lutetium, is currently used for the treatment of superficial cancers. Although similar in name it has a completely different mode of action. This derivative preferentially accumulates in tumour cells, thus making it specific, and causes local cytotoxic effects through production of singlet oxygen.

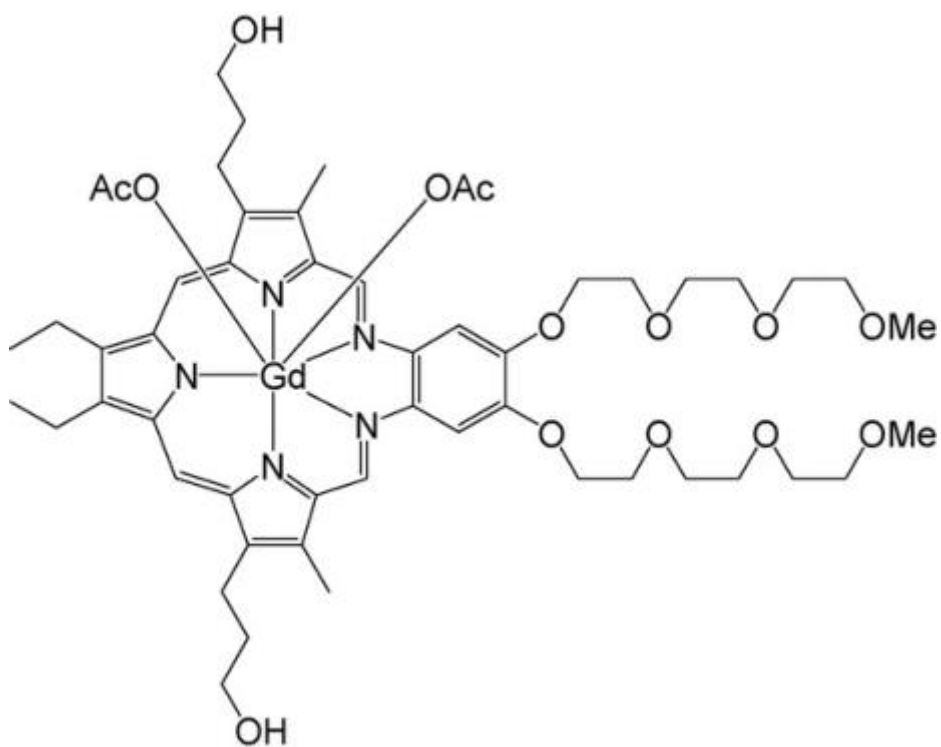


Figure 36. Motexafin Gadolinium complex with the Gd ion being coordinated to five nitrogen atoms and two acetate ions.²³⁶

Section 2: The immune system and Immunisation

The word *immunity* comes from the Latin *immunitas*, which was a word for the special protection or exemption from tax offered to Roman soldiers by their emperors. The development of successful vaccines to provide immunity has been historic, starting with Edward Jenner's smallpox vaccination in 1776 the field of vaccination/immunisation has since been growing.²³⁷ Whilst Jenner used a different strain to vaccinate against smallpox (he took puss from cowpox sores and injected these into patients, which created immunity against smallpox), Pasteur carried on this work but using weakened forms of a pathogen to create an immune response and thus immune memory.²³⁸ His most notable work was using weakened cholera to immunise chickens against cholera. A twist on this was the use of weakened toxins by Emil von Behring, which is widely used as the Diphtheria vaccine and is also the method behind the creation of antivenom.²³⁷

Nowadays, vaccines are created using weakened forms of a virus or disease, or more simply by administering pathogen specific antigens. Over the past two decades we have developed a comprehensive understanding of how the immune system works to create an immune response and subsequently immune memory.

Niels Jerne was the first immunologist to correctly hypothesise that we are born with a set of antibodies that are able to complement any antigen that we can possibly encounter. This contradicted previous beliefs that the body produced antibodies to fit the antigens it had encountered.²³⁸

The immune system works following the series of events described in the following paragraphs:

The immune system is divided into the innate immune and adaptive systems. The passive immune system is not antigen specific, and is more of a general barrier to infection, where the immune cells involved such as macrophages, engulf and destroy pathogens indiscriminantly. As well as these indiscriminant immune cells, the innate immune system includes physical barriers to infection such as skin, hair, and mucous.²³⁸

The adaptive immune system consists of a variety of cells that work together to recognise, respond to, and remember foreign antigens.²³⁹ This system begins with a number of proteins that circulate

in the blood referred to as complement which alert the immune system is a foreign microorganism/pathogen is encountered. This is known as *opsonisation*.²³⁸ Although complement is involved in other processes in the immune response such as disabling MO's only its role in alerting the immune system will be mentioned here. Due to signalling involving these proteins other components of the innate immune system such as macrophages are drawn to the site of infections. Macrophages such as dendritic cells are able to engulf pathogens, cut up their antigens (polypeptides) and then present parts of these antigens on their surfaces. From this point onwards these cells are referred to as antigen presenting cells (APC). The APC's then take the antigens to the lymph nodes where they encounter T lymphocytes, also known as helper T cells. There are many variants of these cells, each with a different antibody on their surface. This variation is brought about by gene shuffling in a variable region of the DNA which can produce enough different combinations so as to lead to antibodies able to recognise a very large number of different antigens.

240

When the APC finds a T lymphocyte with a complimentary antibody it binds to it and thus activates it to replicate and produce proteins that are able to activate both B lymphocytes and killer T cells (KT).^{238, 239} The B lymphocytes produce large numbers of genetically identical cells, known as plasma cells, that can produce antibodies of one specific shape identical to that present on the surface of the activated T cell. These are able to bind to the antigen that has been encountered. Antibodies are able to bind to two antigens at a time as they have two identical variable regions (Figure 37). This means they are capable of "clumping" pathogens together, marking them out for phagocytosis and in some cases completely disabling them. In addition to this, antibodies are able to neutralise toxins, in which case they are more commonly referred to as antitoxins.²³⁸

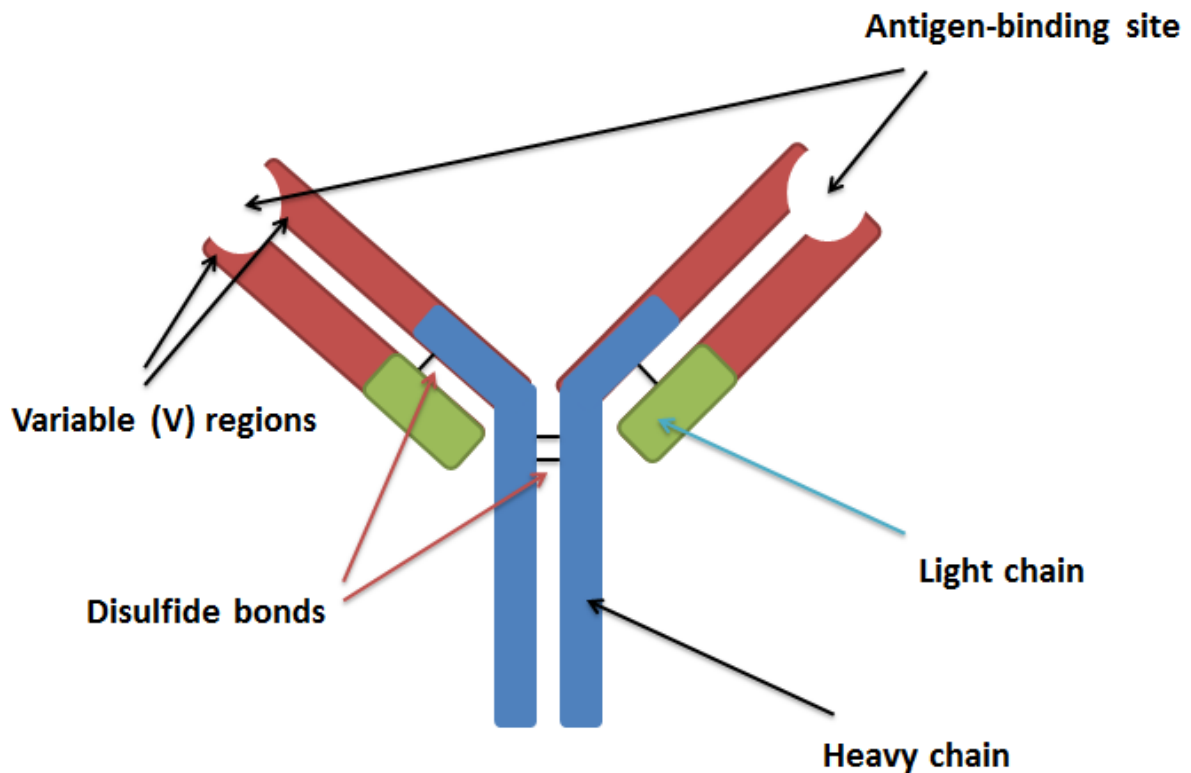


Figure 37. Image showing the structure of an antibody. The variable regions make up the antigen binding sites which are identical on a specific antibody. The disulphide bonds hold the light chains and heavy chains together to maintain the antibody structure.

As well as producing plasma cells that are capable of producing specific antibodies known as monoclonal antibodies for one type of plasma cell, B lymphocytes also divide to produce long-lived memory cells. The benefit of this is that, should the same pathogen invade again, the B memory cells are able to mount a much faster immune response and hopefully lead to eradication of the disease before symptoms are observed. When booster vaccines are given it is with the aim of producing sufficient long lived memory cells so that some form of remembered immunity is present. The mechanism behind forming long-lived memory cells is currently ill understood.²³⁸

Killer T (KT) cells are different to the antibody producing B lymphocytes in that they kill infected cells directly themselves. KT cells have antibodies that are again identical to the originally activated T lymphocyte but in this instance they are able to recognise which cells are infected with the pathogen and kill them using enzymes and cell signals. KT cells are able to tell if a pathogen has entered a cell as we have specific antigens/proteins on the surface of our cells that help our immune cells to recognise them as self-cells. This is referred to as self-recognition and is essential to avoid

autoimmune diseases. These proteins, referred to as major histocompatibility complex (MHC), become damaged when the pathogen enters the cell. When the KT cell approaches it is able to recognise that the cell is a self-cell, that is has been damaged, and will also recognise antigens left on the surface of the cell by the invading pathogen.²³⁸

KT cells are also able to recognise if proteins expressed by a cell have been altered for example by mutations. In this way KT cells are able to not only recognise and kill infected cells but also potentially cancerous cells that have produced incorrect proteins through gene mutation.^{214, 238, 239}

Section 3: Identifying immunogenic peptides

Tumour specific antigens include those encoded by genes that are only expressed in cancer (tumour) cells, including those expressed as a result of gene alteration by mutation and those that are overexpressed by tumours, for example the folate receptor which is often used to target cancerous cells.

In order to create cancer vaccines it is essential to search for antigens that distinguish cancer cells from normal cells. The main method for this is SEREX (Serological Identification of Recombinantly Expressed Clones),²⁴¹ the procedure for which is outlined in Figure 38.²⁴¹

It is essential to identify antigens that are expressed mainly or solely in cancers, and more specifically those that can elicit immune responses in the host, and as of 2007 over 2,500 tumour antigens had been identified using SEREX including those for prostate cancer.^{242, 243} It is hoped that it will eventually be possible to produce a multivalent vaccine that is able to target several antigens displayed by a particular tumour.

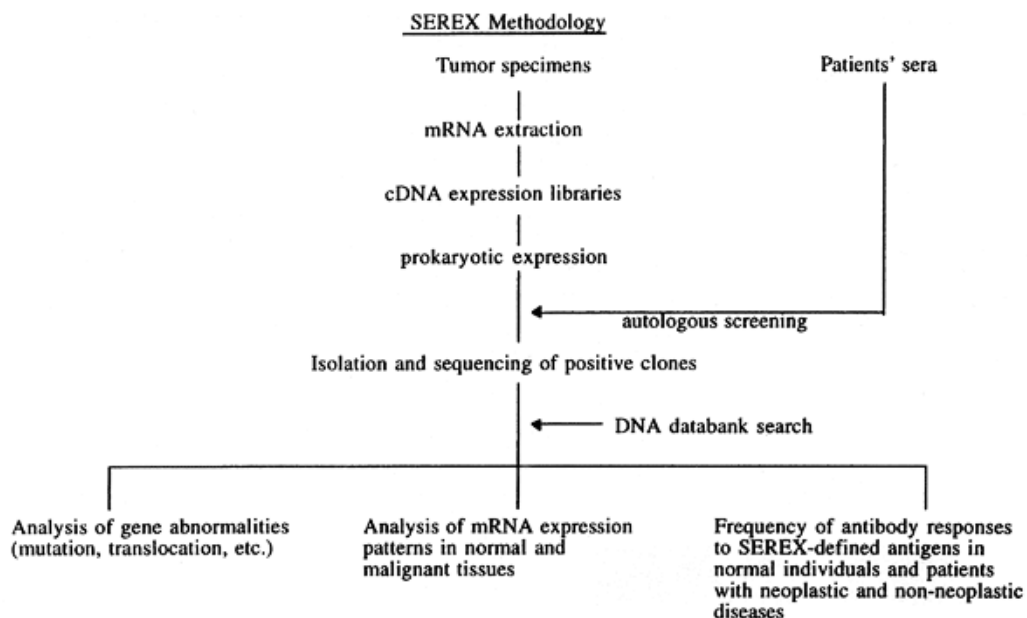


Figure 38. Flow chart describing the steps undertaken during SEREX screening.

Section 4: P53

The immunology section of this project focuses on the tumour suppressor protein p53 (encoded by the TP53 gene), or rather the mutated analogues of the protein that are strongly associated with certain types of cancer. The rationale behind this choice was that the collaborating research group (working at the John van Geest cancer research centre under the leadership of Professor Robert Rees) were at the time of this research, focussing heavily on this peptide; they were currently trialling immunisation methods with this peptide and were in the process of synthesising a tumour model.

The role of p53 is complex and is summarised in Figure 39.^{220, 244-246} Mutated p53 is unable to block growth of damaged cells which may lead to cancer if other mutations initiate rapid cell growth.

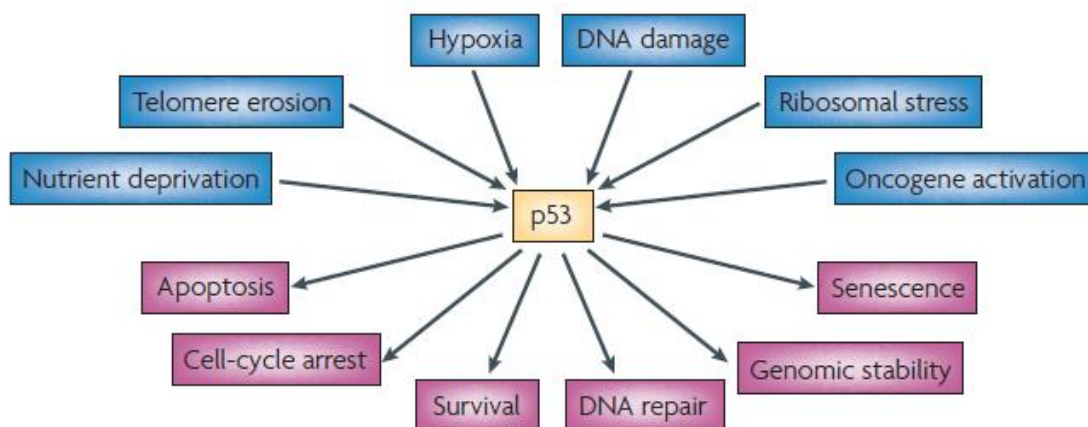


Figure 39. Diagram illustrating p53 role in the body. Blue boxes indicate ways in which p53 can be activated, and purple boxes show the roles of p53 in protecting the body.

Typically if a cell becomes damaged, by radiation for example, then p53 halts cell production until DNA damage can be repaired. If repair is not possible it will initiate apoptosis. p53 is found in low levels in cells all the time but when DNA is damaged it is expressed at high levels, the reasons for which are explained below.

Figure 40 shows that when the damage to a cell is significant the p53 acts to induce apoptosis in the cell. During radiotherapy and chemotherapy cells can become badly damaged and in this case the p53 initiates apoptosis, which leads to the symptoms of radiation sickness as well as those associated with chemotherapy. Whilst p53 essentially stops damaged cells from replicating, and can induce apoptosis of these damaged cells, it can also help to rehabilitate damaged cells, so that once their DNA is repaired they can re-enter the normal cell environment. When damage is observed, p53 induces cell-cycle arrest and the cell is not able to replicate until the DNA is repaired and the p53 leaves the cell. P53 is a transcription factor, and works by binding to the DNA in a claw-type action, thus hindering RNA polymerase and preventing transcription and thus translation. The key amino acid involved in binding to the DNA is arginine. In the p53(105) used in this research the mutated gene leads to the substitution of an arginine group, which will essentially reduce the ability of the peptide to bind to the DNA, thus leading to a peptide with impaired function.^{220, 244-246} A typical mutation is illustrated in Figure 41.²⁴⁶

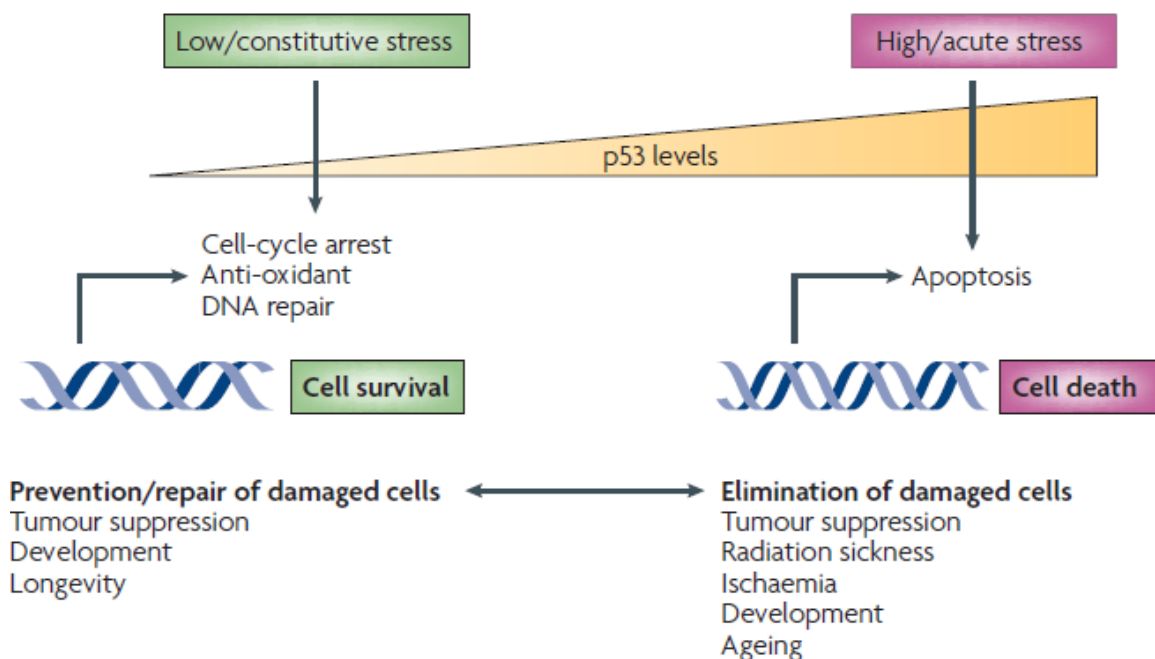


Figure 40. Diagram showing the way in which fully functional p53 regulates cell growth/repair/death following DNA damage.

Structure of p53 region we are interested in : GFRLGFLHSGTAKSV

Structure of mutated p53(105) : GFHLGFLQSGTAKSV

Figure 41. Part of the sequence of functional p53, and the same sequence with a common mutation

Although 95 % of p53 mutations occur in the DNA binding region,²⁴⁶ other mutations occur in places involved in positioning other amino acids in a suitable position for DNA binding, and so even if all arginine residues are present, it may be impossible for them to get into a position in which they can bind to the DNA. In addition to this, mutated p53 is capable of acting as a negative inhibitor. Its shape has changed enough that it can no longer serve its intended function, but not so much that it is not capable of blocking an enzymes active site, thus preventing functioning p53 from binding and increasing the likelihood that a damaged cell will escape apoptosis and divide, leading to a possible tumour.^{220, 228, 244}

One angle for treatment has been to exploit viral vectors and try to insert the gene for functional p53 into the host DNA. This method is problematic as the side effects from using this type of vector are significant, and the body quickly becomes tolerant to the treatment and stops responding. Vectors are discussed in more detail in Ch. 1.3; Section 6.

By a series of gene switching experiments it has been possible to show that when the p53 gene is switched off, equating to a non-functional protein, when exposed to radiation levels known to cause a significant amount of DNA damage mice that have the p53 gene switched on would die. In contrast, those mice with the p53 gene switched off were able to survive. In a second step the mice whose p53 gene remained “off” developed tumours whereas those who had the gene switched back on again did not. This is an illustration of how p53 is useful for preventing tumours, but could in some ways hinder the recovery process.^{244, 245}

P53 causes a response that will kill damaged cells - this is why radiation sickness occurs, and also why during chemotherapy cells die and the symptoms such as sickness and hair loss occur. However, it should be noted that with p53 turned off, although the mouse does not show any short-

term toxicity in the long term the mouse is unable to react to mutated DNA and so cancer occurs. ^{244,}
245

Section 5: Peptide Synthesis

Whilst antigens can be extracted from cultures or the genes spliced into bacteria and produced in large quantities it is easier to control the quality of peptide produced synthetically, and recent advances in solid phase, and microwave chemistry in this area now allow us to synthesise peptide whether antigenic or not in nature, quickly and easily.

In nature polypeptides are made *via* a condensation reaction that links amino acids together to form an amide bond. This task is carried out by ribosomes. In order to mimic nature and synthesise peptides in laboratory conditions, initially solution phase synthesis was carried out using coupling agents such as Dicyclohexylcarbodiimide (DCC) or diisopropylcarbodiimide (DIC) which work by activating the carboxylic acid ready for addition. In order to prevent side reactions to give unwanted peptide products, the carboxylic acid terminal of one amino acid must be protected, for example by reaction with ethanol and thionyl chloride to yield the ester. The amine group of the other amino acid must also be protected, typically done using protecting groups such as tert-butoxycarbonyl (BOC), and fluorenylmethyloxycarbonyl chloride (Fmoc).²⁴⁷ This means the reaction can be carried out to selectively yield only the desired peptide. However, there are many drawbacks to the solution phase route such as the formation of DCC-urea, an insoluble by-product that is very difficult to remove from the products. These methods also suffer from low yields (< 10 %) due to the protection and deprotection steps that accompany the addition of each amino acid onto the chain, as well as the conditions for these steps being so harsh that they can damage the peptide by cleavage of amide bonds, or oxazolone formation which can lead to racemization.²⁴⁸

So, in 1963 Bruce Merrifield pioneered work into solid phase peptide synthesis, which has dramatically improved both the process and the yield.²⁴⁹ The principle behind this process is that the peptide is built onto a solid support, meaning that the product, on the insoluble support, can easily be separated from excess reagents and soluble by-products by simple filtration and washing. The most commonly used support is the cross-linked polystyrene (PS) based support although others are available.²⁴⁷ Key features of the support include the ability of it to swell when put into a solvent as 99 % of the coupling sites are not at the surface of the bead but inside it, and so it must increase in size to allow reagents to diffuse to the coupling site.

The first amino acid is linked to the support by a linking group such as the linker designed by Wang.^{250, 251} Examples of linkers are shown in Figure 43, with the ball depicting the various matrices that can be used for the solid support.

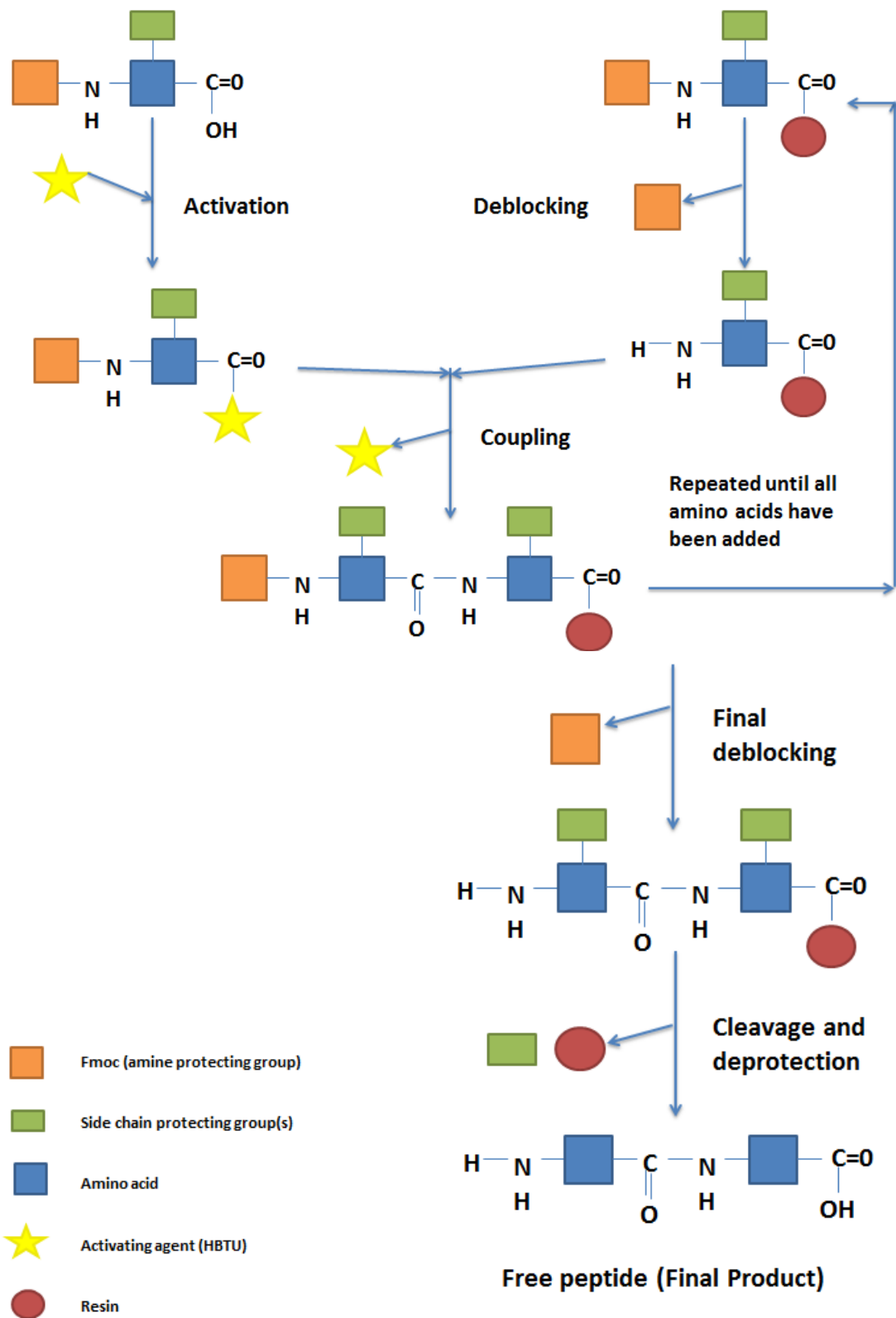


Figure 42. Schematic to indicate how peptide formation takes place during solid phase peptide synthesis

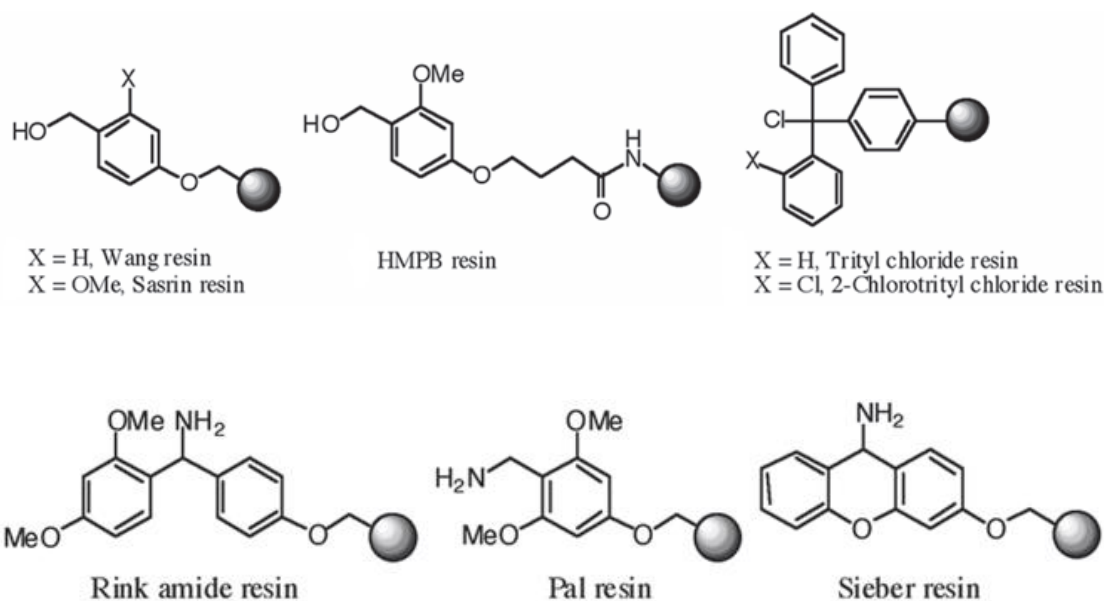


Figure 43. Linkers commonly used for SPPS. These resins are compatible with Fmoc chemistry and TFA cleavage.²⁴⁷

The amino acid linked to the support is generally linked *via* the carboxylic acid group and has a protecting group on the amine to allow a selective reaction. Amino acids to be added onto this are also protected on the amino group and a deprotection step must be carried out before the coupling can take place. Whilst both of the commonly used protecting groups (BOC and Fmoc) are effective in protecting the amine functionality harsh conditions are needed to remove the BOC group, namely strongly acidic conditions, which may either cleave the resin or lead to damage of fragile sequences in the peptide. Fmoc on the other hand, is removed under very mildly basic conditions which do not put the peptide at risk of damage, and for this reason it is generally preferred for SPPS.²⁵²

Whilst protection of the amino group during coupling is important, of equal importance is protection of side groups. Some amino acids contain amino, carboxylic acid, thiol or hydroxyl side groups that could react during coupling and each of these needs to be rendered inactive in order for the reaction to proceed with the desired selectivity.²⁴⁸ The protecting groups need to be able to remain attached during the deprotection step but be cleaved in the final cleavage step under conditions that do not damage the peptide. Typically TFA-labile protecting groups are used.

The coupling step itself can be carried out using a multitude of reagents that activate the carboxylic acid group by turning it into a carboxylate with diisopropylethylamine (DIEA) being the most commonly utilised reagent for this step. As previously mentioned, in solution phase synthesis the coupling reagents most often employed were dicyclohexylcarbodiimide (DCC) or diisopropylcarbodiimide (DIC), but in SPPS the most commonly used reagents are O-(benzotriazol-1-yl)-1,1,3,3-tetramethyluronium tetrafluoroborate (TBTU) or *N*-[(1H-benzotriazol-1-yl)(dimethylamino)methylene]-*N*-methylmethan-aminium hexafluorophosphate *N*-oxide (HBTU).

During the final cleavage step trifluoroacetic acid (TFA) will remove the polymer support and the protecting groups, but it also leads to the formation of carbocations that will react with the electron rich side chains of amino acids (Cys, Met, Tyr, Thr, Ser, Trp) to form unwanted products. This can be prevented by the addition of scavengers including silane containing molecules such as triisopropylsilane (TIS). Thiol cocktails can also be used although these are toxic and have a bad odour, reducing suitability for synthesis of peptide for biomedical applications.²⁴⁷

Overall, procedures in SPPS are able to overcome many of the problems originally encountered in the synthesis of peptides, and so the technique can be easily utilised to make a wide array of different peptides.

Section 6: Vectors

In order to effectively target and deliver immunogenic peptides to cells it must be possible for the nanoparticle to avoid clearance by the reticuloendothelial system, and possibly to bind to the cell in order to aid endocytosis. For instance, it is essential that peptides are taken up by dendritic cells if they are to illicit an immune response.²⁵³⁻²⁵⁵ This can be achieved in a number of ways which include adding biomarkers such as antibodies recognising specific CD molecules, onto the surface of the nanoparticle and more simply, ensuring the nanoparticle is a suitable size for uptake. Dendritic cells will not take peptides up on their own as it is energetically unfavourable to do so, and so delivery agents, known as vectors, are used to increase the size and make the energetic conditions more favourable.⁸⁰

6.1 Viruses

Viruses are designed to invade cells and this can be exploited in order to get other substances into the cell. Viruses are also able to insert their own DNA into the host DNA and thereby hijack host machinery to enable virus replication. As viruses have their own DNA it is possible to replace viral genes with desired genes, such as functional p53, and so deliver a working gene into the cell. This type of gene therapy has been used in the treatment of cystic fibrosis and other genetic disorders.²⁵⁶

Viruses can also be exploited to deliver drug molecules and immunogenic antigens into cells.^{76, 257}

The shigella virus has recently been used to target dendritic cells as it has a surface receptor that binds specifically to antigens on the surface of dendritic cells.²⁵⁸ Due to this interaction endocytosis can be facilitated and molecules can be delivered into the cells, leading to maturation into APC's. As dendritic cells are key to promoting an immune response these are very promising peptide delivery agents.

Whilst viruses are very effective as vectors they can also produce severe side effects such as intense immune responses and insertional mutagenesis. In addition to this, whilst the body might allow the virus to infect cells a first time, it can form a type of immune memory that makes it impossible to use this type of therapy repeatedly.²⁵⁹

6.2 Recombinant proteins

Recombinant proteins are receiving much attention as they offer the same benefits as viral vectors but are less likely to lead to the side effects associated with viruses. Recombinant proteins contain peptide sections present on viral particles that are essential for delivery of genes into a cell.²⁶⁰ Protein sections involved in gene delivery are selected and engineered into a single molecule, including polylysine containing segments involved in increased uptake into the cell, cationic peptides that are able to bind DNA, and antibodies for targeted delivery. Typically recombinant proteins are designed with gene delivery in mind, but could be engineered to deliver other molecules into the cell. These proteins have the advantage of being more biocompatible than other methods of gene delivery such as cationic compounds, but are complicated to synthesise. The use of recombinant proteins to illicit an immune response against is illustrated in Figure 44.²⁶⁰

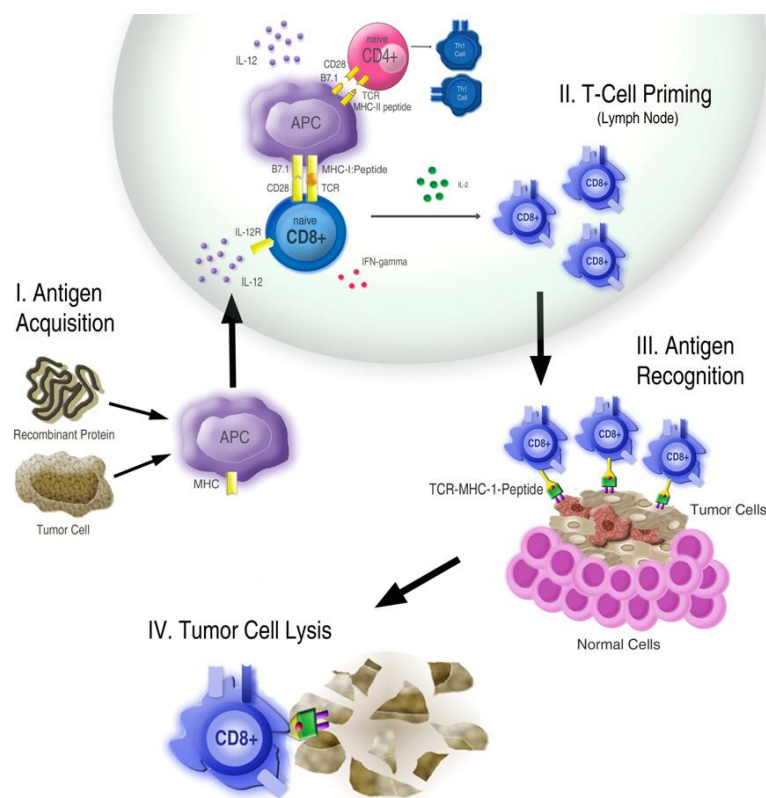


Figure 44. Schematic showing how by combining recombinant proteins with tumour cells it is possible to mount an immune response against tumour cells.

6.3 Organic cationic compounds

Cationic polymers, being positive, are able to bind to the negatively charged DNA and form a type of micelle around the DNA leading to a complex known as a polyplex. The positive charge on the particles also allows them to interact with the cell membrane and thus facilitates endocytosis. Block copolymers including PEO blocks have been formulated and made into polyplexes with DNA. As has been mentioned the toxicity of any substance must be assessed before it can be approved for human use. The advantage of using these copolymers is that by altering the length of each block the toxicity could be greatly reduced, thus tailoring the vectors to their use.²⁶¹

Liposomes, when made from cationic lipids, are classified under the *organic cationic compounds* title.²⁶¹⁻²⁶⁶ Liposomes have been used extensively to deliver drugs to target molecules and have a membrane in which targeting molecule such as antibodies and peptides can be embedded (Figure 45). The inner space of the membrane can carry drug molecules or ferrofluids enabling a further drug payload or alternatively a method for tracking. Antibodies used on the surface would ensure that the liposome will preferentially bind to a particular type of cell, hopefully inducing endocytosis. The size of the liposome is of key importance, as small molecules will not be taken up by the cell as they are energetically unfavourable, and large molecules will be too big for the cell to engulf. Typically liposomes of 50-100 nm are considered thermodynamically optimal although much of the literature suggests 200 nm liposomes have better uptake.^{235, 267}

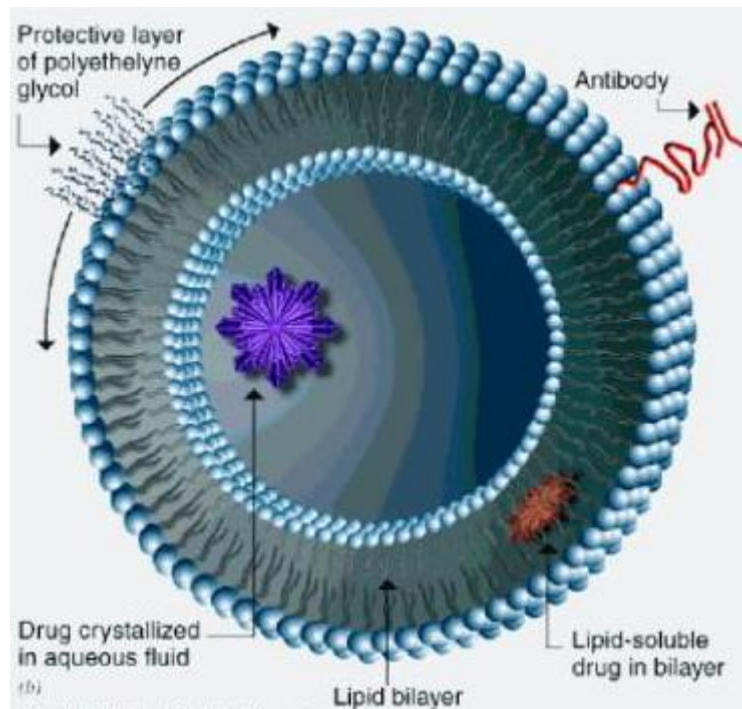


Figure 45. Showing a liposome with an antibody embedded into the membrane for targeting, a PEG protective layer with hydrophobic tails embedded in the membrane, a lipid soluble drug on the hydrophobic inside of the bilayer and a drug in aqueous fluid on the inside

6.4 Other Nanoparticles

Other types of particles, including SPIOs and GNPs can be functionalised to bind to specific cells using the antibody method. This targeting has been exploited for imaging of tumours,^{85, 268-270} hyperthermia to kill cancer cells,^{175, 182, 183, 199, 271} and drug delivery to specific cells.^{97, 272} Folic acid is frequently reported as being a good functionalising molecule for increasing cellular uptake and is in fact five times more effective than PEG alone, although PEG is more commonly utilised.²⁷²

Nanoparticles are particularly efficient for reducing the enzymatic attack of nucleic acids. The nanoparticle will physically hinder the enzyme from interacting with the DNA, although it may still be able to attack the exposed end of the DNA. In addition to this, the positively charged particle may repel the enzyme and thus reduce the likelihood of attack.^{261, 264, 266}

Molecular imaging is of key importance in the tracking and treatment of disease and has been defined as a non-invasive, quantitative procedure during which imaging of biomolecules or biological

process is repeated. This must be occurring within a living organism. SPIOs can act as both a passive and an active targeting imaging agent which makes them ideal for molecular imaging. By coating with dextran it is possible to attach magnetite nanoparticles to the surface of the cell, although this leads to a decreased likelihood of nanoparticle uptake.²⁷³ However, in this instance the binding of the particles to the outside of the cell leads to cell death which can be exploited for use in cancer therapy.^{178, 181, 199} SPIOs also lend themselves to theranostic applications as they can be attached to drug molecules and so be used both for treatment and diagnosis purposes. Additionally, due to their superparamagnetic properties they can be directed to a specific target by using a magnetic field gradient, and manipulated to produce hyperthermia in a specific region, such as a melanoma.^{178, 181, 199}

Gold nanoparticles can also be functionalised with a wide variety of molecules, with binding typically being through electrostatic interaction with amine and carboxyl groups, and more importantly through interaction with thiols.^{82, 97, 175} Gold nanoparticles are also traceable as they have unique optical properties. It is possible to trace GNP's using optical coherence tomography (OCT) and to activate them using infra-red (IR).¹⁷⁵ It is also simple to make GNP's of various sizes and shapes with a high degree of control, and so they lend themselves well to biomedical applications where quality control is of huge importance.^{82, 274}

Section 7: Adjuvants

As cancer antigens are essentially “self” antigens and the immune system is carefully designed and trained to not react to these antigens, it is difficult to produce an immune response by means of vaccination.²¹⁴ As we develop in utero we develop immune tolerance to certain antigens, such as those associated with ourselves, and also those crossing the placenta due to infections in the mother. In addition to this, cancer cells also undergo immunoediting, with each repeated evasion of destruction by the immune system the cancer becomes more and more ‘invisible’ to the immune system until it does not illicit any immune response. Another possibility being explored is that the cancerous cells are able to influence regulatory T cells, in a similar way in which they influence neighbouring cells to support them, to ignore their antigens and thus induce immune tolerance. However, there is evidence to suggest that by continually prolonging toll like receptor (TLR) signalling, it is possible to reverse immune tolerance to tumours and TSA’s but first the technology for carrying out this signalling must be devised and refined.²¹⁴

Adjuvants come in different forms but they all have the general purpose of increasing or enhancing the immune response to weak antigens, and are subdivided into vehicles (vectors which have been previously described in Ch.1.3; Section 6) and immunostimulants.^{257, 275-278} Vehicles present the relevant antigen to the immune system in what is described as an ‘optimal manner’, which can include controlled release of the antigen including depot delivery systems. It is possible that the continual release of the antigen over time serves to stimulate the TLR’s, which was one of the aims set out for reversal of immune tolerance. Viruses which are able to infect APCs are classed as vehicle type adjuvants.^{257, 279, 280}

In addition to the delivery of the antigens the vehicle can also deliver immunostimulants and so further increase the immune response. Immunostimulants engage the innate immune system by direct stimulation. Species such as those in the mycobacteria family are used as adjuvants.^{281, 282} Biomolecules in the bacterial cell wall can stimulate an immune response, and with the relevant antigen being present this immune response can be directed against that antigen.

The first instance of a type of adjuvant was designed by William Coley in 1891.²⁸³ He noticed regression of tumours that were injected with weakened strains of bacteria, and spontaneous regression in some patients who had bacterial infections. We now know that this system, known as

“Coley’s toxin” worked because it stimulated the immune system to react in that area, thus leading it to the site of the damaged cells. It is also possible that the fever associated with the bacterial infection led to the formation of heat shock proteins which themselves lead to an increased immune response, as heat shock proteins are immunodominant antigens (strong antigens).²⁸⁴ In addition to this use of bacteria, it has been found that children exposed to a wide range of pathogens are less likely to develop certain childhood leukaemia’s, which supports the theory that by reacting to other strong antigens we stimulate the immune system to react to weaker antigens.²⁸⁴

Whilst Coley’s toxin was successful in treating cancer for a time, the creation of a vaccine that leads to immunity against cells expressing tumour specific antigens (TSA) is preferable as it is specific to the cancer cells only and provides memory cells in case of recurrence of the cancer.

According to Debensky Jr and Reed the idea adjuvant will be stable, safe, and easily biodegradable as well as being eliminated from the body without problems.²⁷⁷ It will also be able to promote an antigen-specific immune response. This is one of the aims of the research carried out within the scope of thesis.

7.1 Freund’s Adjuvant

As previously mentioned mycobacteria are used in preparations including *Complete Freund’s Adjuvant* (CFA) which contains either components of the bacterial cell wall or heat treated bacteria. CFA has been used in clinical trials such as a study on squamous cell carcinoma tumours, with positive effect.^{277, 285} However, the use of these bacterium and their components leads to problems due to the large inflammatory response produced. The response to this problem has been to remove the mycobacteria components to create *Incomplete Freund’s Adjuvant* (IFA) and so reduce the inflammatory response, but this could in turn reduce the effectiveness of the vaccine and so other adjuvants have been investigated.^{277, 278, 280}

Whilst there are adjuvants such as CFA which are very effective there are concerns over the safety of adjuvants in vaccines. This has arisen due to incidents such as withdrawal of the rotavirus vaccine due to cases where patients who had received the vaccine suffered from intussusception of the intestines. Another notable incident was an increase in the incidence of Guillain Barre Syndrome which was linked with a swine flu vaccination in 1976.²⁸⁶

7.2 Alum

Alum and other aluminium compounds are popular as adjuvants and some of these have been FDA approved.^{275, 278, 287} Alum works by interacting directly with the cell membrane of dendritic cells, thus triggering an immune response terminating in activation of CD4+ T cell activation. Alum is currently used in the vaccinations for many infectious diseases such as diphtheria and tetanus. It has the advantage of being suitable for large scale production and being relatively safe compared with many of the adjuvants that have been trialled, and the mercury that it has replaced. However, it is only suitable for simple immune responses and is not useful for pathogens such as HIV and malaria that remain in the body for a prolonged period of time. In addition to this Alum is known to create granulomas at the injection site which can lead to problems when booster injections are required, as would be the case with cancer vaccines. There are also concerns that because aluminium is a neurotoxin it could be linked with autism although these claims are as yet unfounded.^{275, 278, 287}

7.3 Oil in Water Emulsions

Oil in water emulsions are a popular choice for adjuvants, as the antigen is released slowly from the mixture over a period of time, and in fact some of these emulsions have been FDA approved.^{275, 278} Squalene and squalane have recently been used to replace some of the more popular mineral oils traditionally used in these preparations.^{275, 278} These oils have been chosen as they are easy for the body to metabolize and so are less likely to cause side effects and granulomas. At present these new studies aim to reduce the oil content in each emulsion to < 5%. Monophosphoryl Lipid A (MF59®) is a TLR-4 targeted adjuvant containing squalene, that is safe for use, but has a reduced effect when compared to CFA. Another drawback of this particular adjuvant is that one of the key ingredients is shark oil, and as one of the aims for production of a successful adjuvant is that it is inexpensive to produce, shark oil is not ideal. In addition to this, shark oil is not a sustainable resource and must first be extracted. For these reasons a more efficient adjuvant that can be created on a large sustainable scale must be produced.

3-O-desacyl-4'-monophosphoryl Lipid A (MPL) is a similar adjuvant which was recently approved, and is present in the HPV vaccine Cervrix®.²⁸⁸ This is an effective adjuvant but comes with the

added drawback that part of its manufacturing process requires a 20- year batch fermenting process. This is both expensive and time consuming, and has high energy requirements. It has also been pointed out that in order to meet worldwide demand a batch process which occasionally leads to failure due to the complex components of the mixture, and which takes 20 years, would be insufficient.^{275, 278}

7.4 Heat Shock Proteins

The primary function of *heat shock proteins* (HSPs) is to maintain cell homeostasis under stress or heat conditions.²⁸⁴ They have previously been mentioned in relation to the fevers produced as a result of bacterial infection, and have received much attention recently due to their use as non-specific adjuvants.²⁸⁹ These special proteins interact with surface receptors on APCs such as dendritic cells and through cell signalling this leads to a cascade immune responses which includes activating NK cells. When used in combination with antigens, HSPs can increase the presentation of that antigen on the DC surface and so possibly lead to an increased immune response to that antigen. Figure 46 illustrates how heat shock proteins and antigens can interact to form the complex used for immunisation. Again, mycobacteria have been used in the production of heat shock proteins, namely mycobacterium tuberculosis HSP70 for the treatment of porcine circovirus type 2.²⁸² All organisms studied to date produce a heat shock protein encoded by the HSP70 gene family when temperatures become elevated, and it is possible to produce these proteins in large quantities by isolating, for example, the murine gene, replicating it by PCR, and then using a gene transfection agent to splice this into bacterial cells such as *Escherichia coli*. which will replicate and express the gene.²⁸²

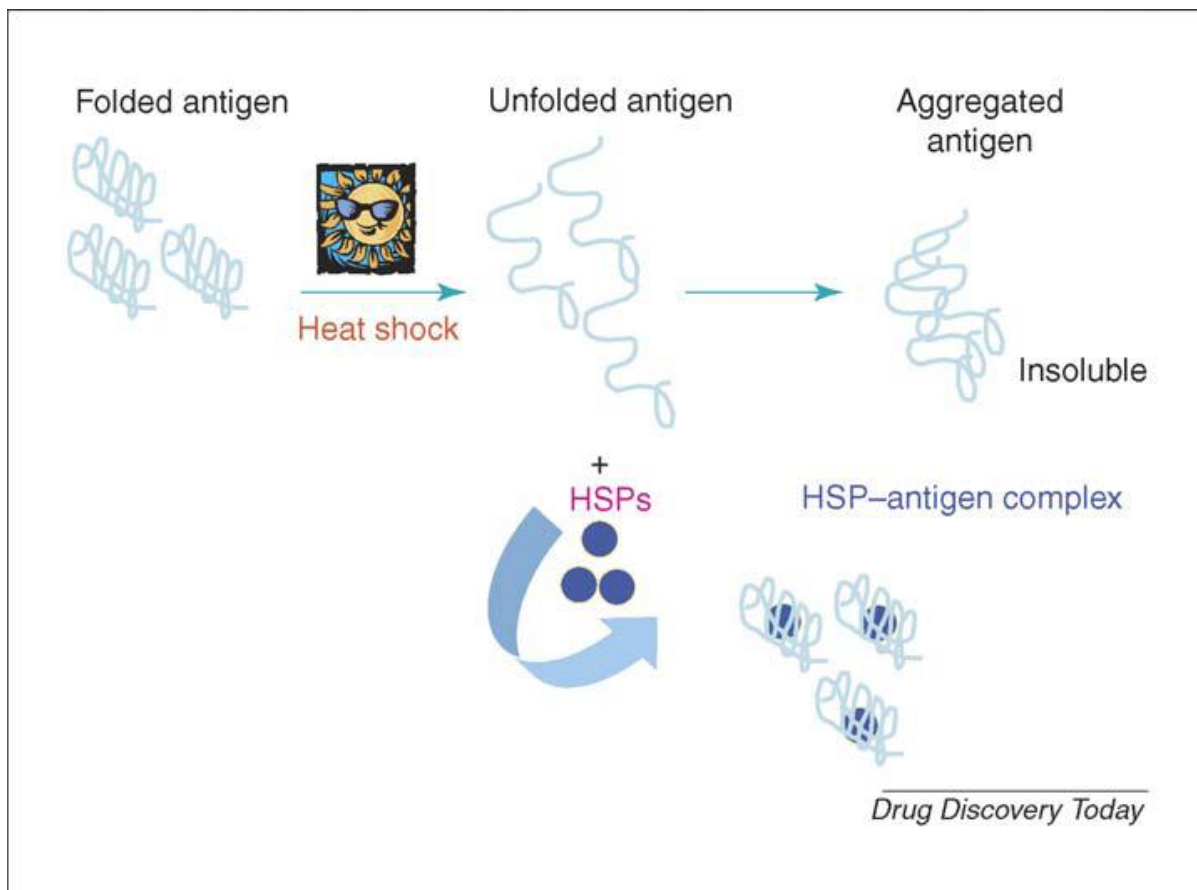


Figure 46. Illustration of the formation of an HSP-antigen complex

Section 8: Research Hypothesis, Aims and Objectives

The research hypothesis for this thesis was that functionalised metal and metal oxide nanoparticles could be synthesised *via* a novel route, and then used for a variety of biomedical applications.

The aim of the research was to synthesise a variety of metal and metal oxide nanoparticles; to functionalise and purify the particles; and to use these particles for NMR contrast, cancer immunotherapy, and transdermal drug delivery.

The individual objectives were as follows:

- To synthesis metal and metal oxide nanoparticles *via* well documented methods
 - Synthesis of gold nanoparticles using a citrate capped method
 - Synthesis of iron oxide nanoparticles *via* co-precipitation and spinning disc methods
 - Synthesis of calcium oxide nanoparticles *via* spinning disc methods
 - Characterisation of particles *via* ICP-AES and TEM
- To synthesise biologically active peptides using solid-phase peptide synthesis
 - P53 variants for cancer immunotherapy
 - Cell penetrating peptide for transdermal drug delivery
- To functionalise nanoparticles *via* a novel solvent-free route
 - Develop a method for solvent free coating of nanoparticles with simple organic molecules and peptides by trialling incubation, heating and solid state methods
 - Characterisation of functionalised particles *via* TEM, ICP-AES, DLS and TGA
- Develop a method functionalised particles
 - Develop a method for purification of 10-15 nm magnetic and non-magnetic nanoparticles
 - Trial size exclusion, dialysis, magnetic separation and centrifugation
- To determine suitability of newly functionalised nanoparticles in biomedical applications; medical NMR, transdermal drug delivery, and as cancer adjuvants
 - Measure NMR relaxation of solutions containing functionalised SPIOs both with and without buffers to determine suitability as a CT contrast agent
 - Use mice for immunisation using particles functionalised with p53 variant as an adjuvant
 - Use an NMR MOUSE to track SPIOs functionalised with cell-penetrating peptide penetrating pig skin

Chapter 2: Results and Discussion

Section 1: Synthesis and coating of SPIOs

1.1 Size, Morphology and Distribution

The primary aim of the experiment was to synthesise metal and metal oxide nanoparticles *via* well documented methods. These particles, synthesised as detailed in Ch.2. 2.1, were analysed by transmission electron microscopy (Figure 47) at a magnification of 100 K and were found to be spherical, indicative of the desired SPIOs, and fairly uniform in diameter with a size range of 8-12 nm. This shows that for these particular metal oxide nanoparticles the primary aim has been successfully met.

The secondary aim of the research was to functionalise nanoparticles with the desired coating material. The images show that there is a clear area surrounding each particle, indicative of the coating agent. EDX confirmed that the particles contained iron and had coatings containing carbon, oxygen and nitrogen which confirms that the dark spherical areas relates to SPIOs and the aforementioned clear area is the organic coating material (Figure 48). This data combined with the fact that the particles had become soluble following the coating method, indicates that the secondary aim has also been met.

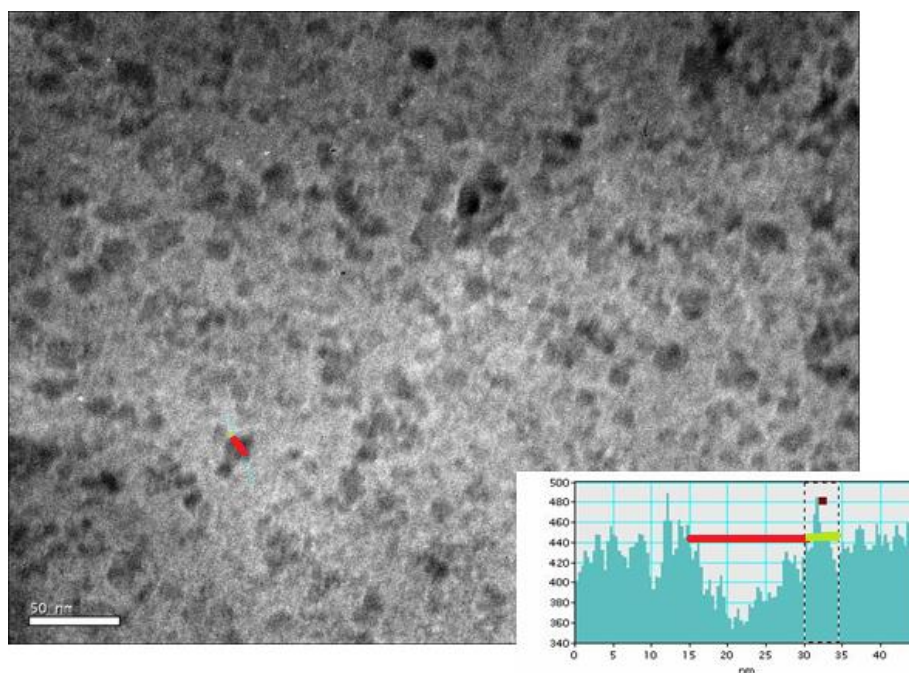


Figure 47. TEM image showing p53(108) coated SPIOs. The red line indicates the SPIO itself which is around 15 nm and the green line shows the peptide coating at around 2 – 4 nm. The scale for the bottom right hand image shows the amount of transmission of electrons through the sample and is in arbitrary units. *Poor image resolution is due to limitations of the available transmission electron microscope.

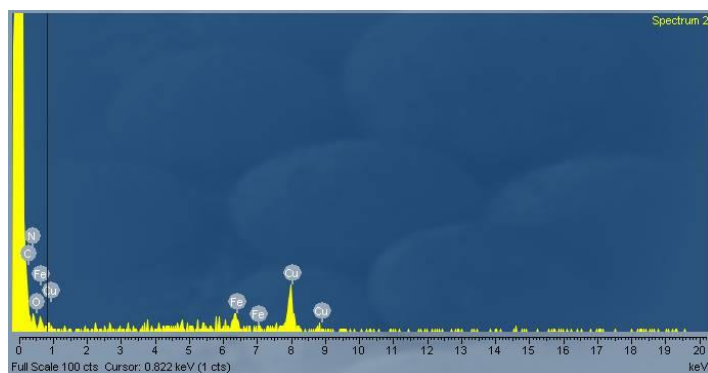
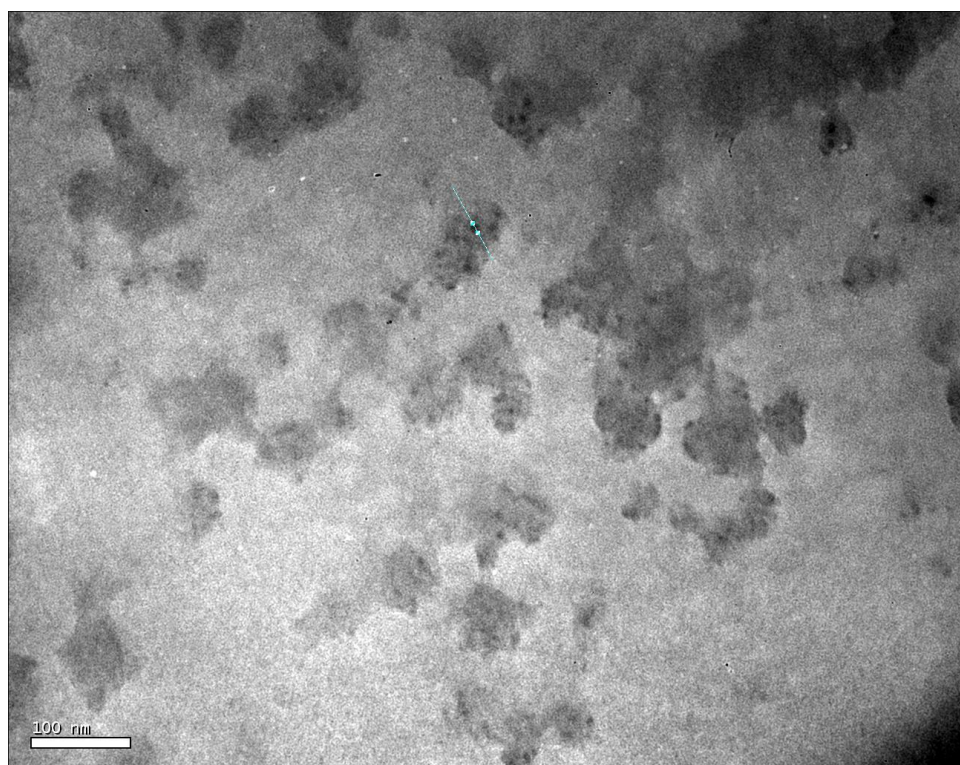


Figure 48. EDX of p53(108) coated SPIOs showing Cu (the TEM grid), Fe (iron oxide nanoparticle), O (oxygen from peptide) N, and C (both from the peptide).

Whilst the primary aim has already been met, spinning disc synthesis was trialled to determine if this was a better way to synthesis superparamagnetic iron oxide nanoparticles in terms of size and morphology. This was also carried out with a view to scale up the reaction for commercial application. The SPIOs synthesised using the SDR were found to be less uniform in size with ranges

of 7-40 nm for ammonia liquid and 15-42 nm for gaseous ammonia as illustrated in Figure 49 and 50. Literature suggests that the particles should be more uniform in size due to the micro-mixing effect. Additionally, there were some rod shaped structures present in the sample which on investigation turned out to be made of iron oxide (not excess iron chloride as had been previously assumed). Both of these findings lead to the question of why the SDR was not producing uniform particles. One suggestion is that the fast spin speeds whilst leading to formation of smaller particles, will also mean that excess iron chloride solution will be spun onto the sides of the reaction vessel. It is possible that in this case the smaller particles then act as a nucleation site as the remaining reactants carry on reaction on leaving the disc, leading to formation of larger nanoparticles, and the additional nanorods. This theory was further supported by the absence of nanorods in the samples synthesised using gaseous ammonia. In these samples the particles also showed much less aggregation/agglomeration, providing further evidence that in the absence of ammonia in the liquid and precipitate collected, the particles could not carry on reacting and so nucleate bigger particles.



*Figure 4947. TEM image of SPIOs synthesised using SDR. Blue line indicates particles measured in Fig 61. *Poor image resolution is due to limitations of the available transmission electron microscope.*

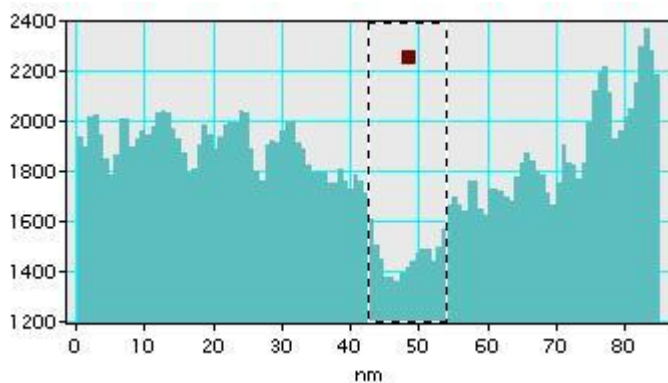


Figure 5048. Depth profile showing particle highlighted in Fig. 60 to be 10 nm

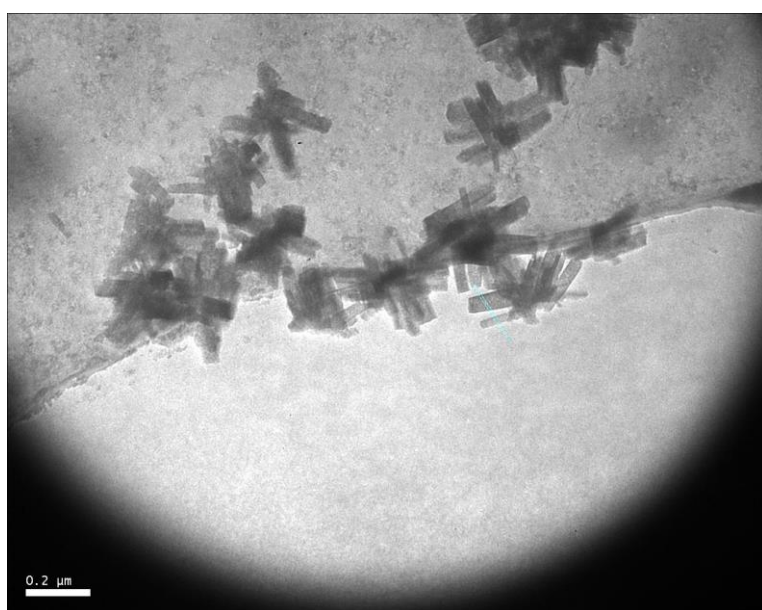


Figure 51. TEM image showing rod/crystal type structures in the SDR SPIO sample. *Poor image resolution is due to limitations of the available transmission electron microscope.

1.2 Coating Methods

Going back to the secondary aim, of functionalising the nanoparticles, the following methods were trialled: Incubation, sonication, heating, ball mill, pestle and mortar, and coffee grinder. These showed varying rates of success, with the pestle and mortar and coffee grinder being deemed the most successful; all 20 amino acids and various other organic substances could be attached to the SPIOs using these methods.

For each methods, the products when solubilised were analysed by DLS, TEM, ICP, and NMR MOUSE®. Methods were considered successful if the solutions contained particles of 10-20 nm with a clear coating, contained iron and were successful in inducing shorter relaxation times for water by NMR.

The incubation method brought about some difficulties as many of the amino acids were only sparingly soluble in distilled water; however, it was assumed that as a small amount of coating material bound to the SPIOs this would shift the equilibrium and so a further small amount of amino acid would dissolve in the water. However, the results indicated that only one amino acid, threonine, successfully bound to the SPIOs to yield a pale brown solution containing particles of 10-20 nm with a clear area around them, again corresponding to the coating material. Bearing this in mind it is very likely that it is the solubility issues that have prevented this method from being successful.

Sonication proved to be completely unsuccessful. Whilst sonication aided synthesis of the particles themselves, every sample analysed was devoid of iron. This could be attributed to the energy from sonication being directed to break the electrostatic forces of attraction, and thus removing any bound coating material rather than helping to attach it. It has been concluded that regardless of any adjustments made sonication will not be a viable coating method.

Amino acids tend to degrade rather than having melting points and so it was essential when attempting to use heat to attach them to SPIOs that this point was not exceeded. Both Bunsen burners and heat guns were trialled but these proved to be too efficient at heating, often leading to decomposition. Following these attempts SPIOs were heated using a hot plate with careful temperature control. For every sample a dark brown solution was produced containing iron although none of these were able to alter NMR relaxation times. When viewed under the electron microscope it was clear to see that the particles, rather than being single particles with a clear area surrounding them, were clumped together into large aggregates of several μm . DLS confirmed aggregates of *ca.* 1000 nm at least. These results indicate that the heating method is not able to produce coated particles that are separate from one another, but rather it partially decomposes the coating, causing the particles and coating to stick together in a large mass which is no longer able to move. This aggregation of particles renders the particles unable to move in solution and so they cannot align with the magnetic field as single particles or smaller aggregates are able to. So, it can be concluded that the heating method is not suitable for producing coated SPIOs that can be used as NMR imaging agents.

What is of note, as illustrated in Figure 52, is that the heating method led to the greatest amount of coating of iron oxide, with iron concentrations being in excess of 1000 mg.l⁻¹ vs. incubation and sonication which both resulted in concentrations below 100 mg.l⁻¹. So although the particles were not MRI active, they did have a high iron content, and this could be exploited for other applications such as treatment of anaemia or doping of other substances with iron.

In order to keep the particles separate during coating and avoid the negative effects associated with aggregation, it was decided that a ball mill would be used. It was possible to heat the ball mill and so agitation and heating were combined in the next method. The ball mill on its own was unable to produce coated particles, with any samples giving rise to solutions devoid of iron. The heating method was successful in producing solution containing iron. However, these were similar to the sample observed in the heating method, giving large aggregates which were not MRI active.

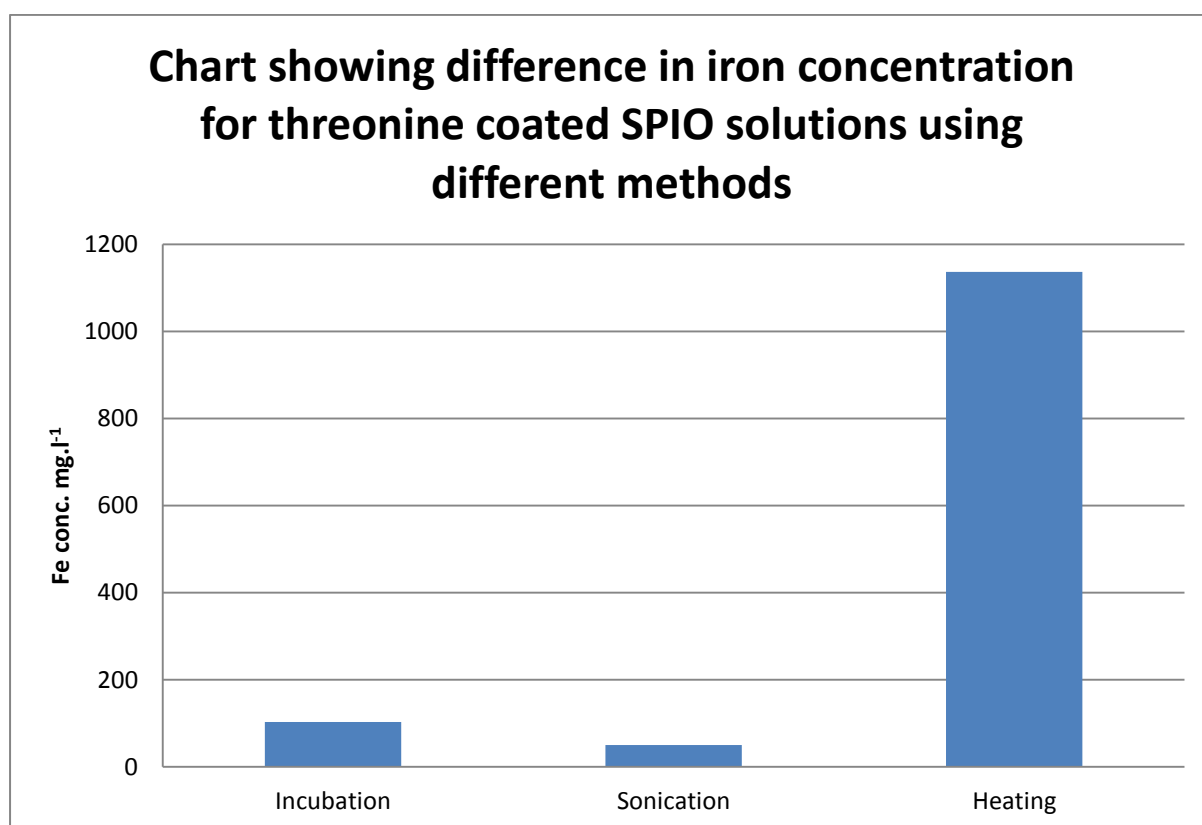


Figure 52. ICP results for alternative methods of coating SPIOs with threonine.

In keeping with the agitation theme the ball mill was replaced with a pestle and mortar. The mixtures were energetically agitated for a minimum of 5 min and the resultant powders once take

up into solution were found to contain iron, be MRI active, and contain evenly coated particles of 10-20 nm. This method was successful for all compounds trialled that contained the following functional groups: -OH, -COOH, -NH₂. It was also important that the correct solvent was used to ensure maximum uptake into solution, as the solubility of the coated SPIO was less than the coating material itself.

When considering taking this method and applying it on a larger industrial scale it quickly became clear that it would not work on a larger scale due to mixing effects. As shown in the use of the ball mill, the mixtures require close contact and a higher pressure for successful binding. The coffee grinder was trialled as the burrs would provide the close contact and grinding action that was found to be successful in the pestle and mortar method, with the material needing to be passed through the grinder a minimum of four times. Further passes through the grinder resulted in a further loss of product, with some of the material becoming stuck inside the grinder on each pass.

The method was found to be successful for all samples that were able to attach *via* pestle and mortar. However, the method led to a lower yield and was not as effective as the pestle and mortar, in terms of the amount of iron taken up into solution following processing. This method is limited by the limited positions in which the burrs can be placed, and by the large size of the grooves within the burrs themselves. In order to process materials on the nanoscale the burrs needed both to have smaller grooves, and to be closer together. Despite this, this method is effective and provides the most promising method for scaling up. Whilst this was not one of the aims of the research project, it does lead well into future research.

1.3 Further Coffee Grinder Experiments

It has already been mentioned that the secondary aim of functionalization was met through the pestle and mortar method, but as with the use of the spinning disc reactor, a method needed to be developed that could be scaled up for commercial application. For this reason a coffee grinder was used, which allowed more material to be ground together at any one time than the pestle and mortar method. The results in Table 18 show that the coffee grinder is a suitable alternative to the pestle and mortar for attaching the coating material to the SPIOs *via* a solvent free grinding method. What is also clear from the table is that the number of times that the material passes through the grinder will affect how much of the iron ends up in the solution, which indicates the amount of SPIO successfully coated. This could be due to the following reasons:

1. The powder produced from grinding several times as opposed to just one is much finer than if only one grind is applied. This will mean that the finer powder will be more soluble in water due to its larger surface area.
2. With each successive grind, more of the particles are successfully coated, due to more of the coating particles and SPIOs being forced close together and thus forming electrostatic interactions.
3. The heat from the friction of the burrs could be causing some of the coating material to be melted onto the SPIOs. Whilst in the heating method this led to a large degree of aggregation, in this method the action of the burrs would keep the particles apart and reduce aggregation.

Any of these possibilities is likely but further investigation would be required to determine which of these is occurring, if not something else entirely.

As mentioned, the grinding process provides energy in the form of heat from friction. This will possibly help to overcome electrostatic repulsion between particles, and break intermolecular forces between them, thus forcing the particles closer together. When they are close to each other they will have more chance to interact with each other and so form an electrostatic interaction. In solution the particles and molecules are able to diffuse randomly and so there is a chance that they will bump into each other or come close enough for an electrostatic interaction to occur. In solid state the grinding action first makes the particles and coating agent into a fine powder. This increases the surface area of both agents and so increases the likelihood of the coating agent and particle coming into close contact with each other.

Solubility was found to be the biggest issue during this method, which was overcome by forming the HCl salt of any difficult materials. Once solubility was not an issue these materials could be coated onto the SPIOs *via* the solvent free grinding method (typically the pestle and mortar method) as described. These salts coated SPIOs to form particles of 10-20 nm with a clear area surrounding them, as observed using TEM. This led to exploration of salts, namely ammonium chloride, and sodium chloride, as coatings. Neither of these were successful coating materials, further supporting the theory that $-OH$, $-COOH$ or $-NH_2$ are needed in order for sufficient electrostatic interactions to occur.

1.4 Suggestion for mode of action of solvent free grinding method

Now that we know that it is possible to functionalise the particles *via* a novel solvent free method, it is important to be able to understand how this is happening. As previously mentioned, the coating of nanoparticles relies on electrostatic interactions between the particle and a functional group on the coating agent. It could be suggested that with the hydrated form of the SPIOs there are hydrogen bonds between the Fe-OH functionality and the coating materials, however the IR data for the SPIOs has proved that we do not have this form, so this form of bonding can be ruled out.

The particles themselves have both Fe³⁺ and Fe²⁺ ions at the surface of the particle. This gives the surface a positive charge, and so it can interact with any materials with functional groups that are negatively charged. In solution the particles and molecules are able to diffuse randomly and so there is a chance that they will bump into each other or come close enough for this type of electrostatic interaction to occur. In solid state the grinding action first makes the particles and coating agent into a fine powder. This increases the surface area of both agents and so increases the likelihood of the coating agent and particle coming into close contact with each other.

The grinding process also provides energy in the form of kinetic energy and a small amount of heat. This will possibly help to overcome electrostatic repulsion between particles, and break intermolecular forces between them, thus forcing the particles closer together. When they are close to each other they will have more chance to interact with each other and so form an electrostatic interaction.

In order to test the theory that all coating materials could be attached to SPIOs *via* the solvent-free grinding method all 20 naturally occurring amino acids were attempted. Whilst every amino acid could be successfully bound to the SPIOs the effectiveness of this differed between amino acids.

1.5 Coating of SPIOs with all 20 naturally occurring amino acids

For the research hypothesis to be successfully met, it was important for the nanoparticles to be coated with a plethora of molecules. As we were extending to peptides later in the project, amino acids seemed like the perfect starting point. They are also very varied so if successful, would prove that the method was viable for many different coatings.

As can be seen from Figure 53, the properties of amino acid side chains differ significantly, and it is possible that it is the properties of these side chains that gives rise to the differences in binding to the SPIOs. For example, in the preliminary experiments it was noted that threonine had a very high binding capacity without recrystallization. By looking at the structures depicted in Figure 53, it can be seen that this particular amino acid is nucleophilic. It also contains an alcohol, amine and carboxylic acid group, all three of which have been shown to bind to the particles. It is possible then that the ease with which threonine binds to the SPIOs is due to the nucleophilic nature of all three functional groups. However, it was decided that the good solubility of this particular amino acid in water was the biggest factor in it being able to bind. In contrast to this glycine contains the least electron donating groups, and contains only one amino, and one carboxylic acid moiety. However, the results clearly show that for glycine there is not much difference so other factors must be involved such as interaction with the solvent or steric hindrance.

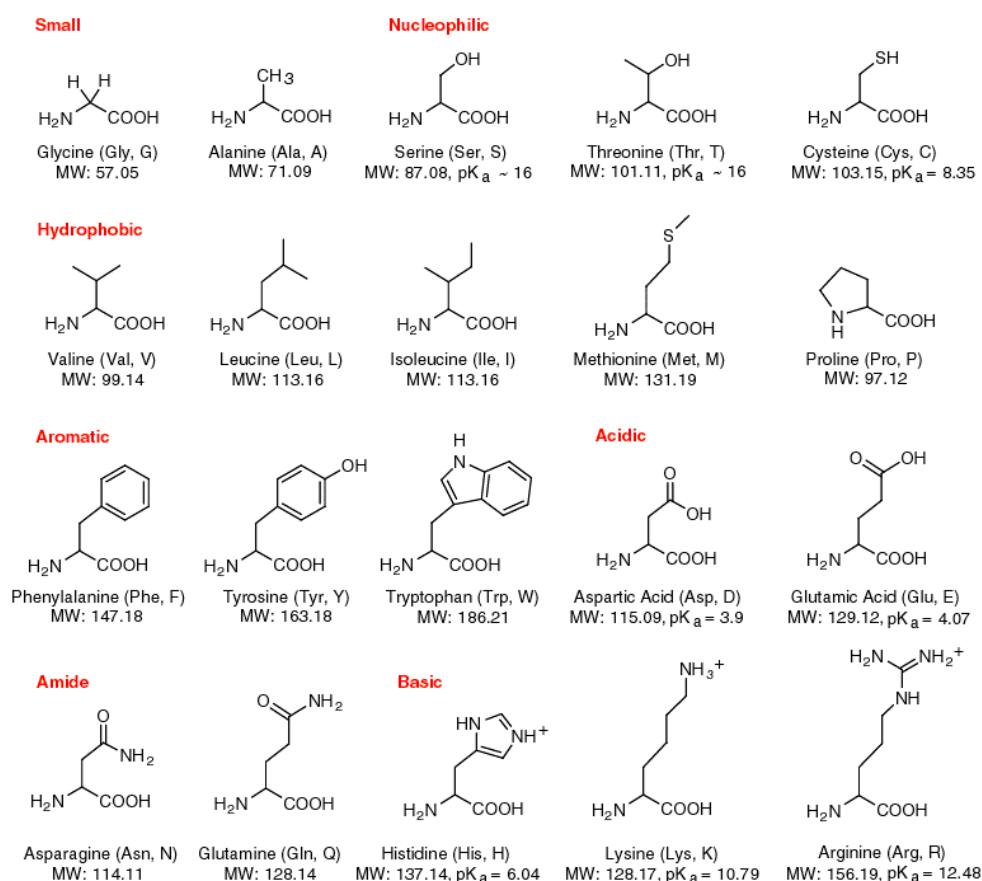


Figure 53. Showing all 20 naturally occurring amino acids

Amino Acid	Iron concentration (mg/L)	Average Size by DLS (nm)	T1 (ms)	T2 (ms)
Hydrophobic Non-polar				
Alanine	1638	36.6 d.nm 81.4 %, 1379 nm 18.6 %	62.00 ± 0.98	9.50 ± 0.24
Valine	219.1	23.2 d.nm 62 %, 723 d.nm 38 %	15.67 ± 0.88	3.14 ± 0.13
Leucine	2376	8.72 d.nm 14.2 %, 116 d.nm 85.8 %	72.36 ± 1.42	7.93 ± 0.39
Isoleucine	2288	8.60 d.nm 25.5 %, 234 d.nm 74.5 %	56.92 ± 1.86	8.26 ± 0.33
Proline	976.4	27.5 d.nm 97.1 %, 3790 d.nm 2.9 %	16.45 ± 0.71	3.72 ± 0.13
Methionine	1178	27.3 d.nm 96.9 %, 4100 d.nm 3.1 %	1.86 ± 0.98	1.04 ± 0.02
Phenylalanine	56.87	14.2 d.nm 58.2 %, 433 d.nm 41.8 %	75.05 ± 2.07	7.86 ± 0.44
Tryptophan	61.27	0.705 d.nm 66.6 %, 67.4 d.nm 33.4 %	180.29	5.25
Hydrophilic Polar				
Threonine	666.6	58.9 d.nm 94.9 %, 3570 d.nm 5.1 %	31.00 ± 2.94	7.03 ± 0.10
Cysteine	2029	22.7 d.nm 50.6 %, 893 d.nm 44.1 %, 134 d.nm 5.2 %	1870.97 ± 1.05E+1	1954.63 ± 0.51
Asparagine	51.67	273 d.nm 100%	124.66 ± 4.68	7.30 ± 1.11
Glycine	480.2	14.6 d.nm 33.6 %, 714 d.nm 66.4 %	92.93 ± 1.64	7.40 ± 0.79
Serine	802.3	35.0 d.nm 94.6 %, 2400 d.nm 5.4 %	52.34 ± 4.10	8.82 ± 0.19
Glutamine	1945	12.2 d.nm 19.4 %, 331 d.nm 80.6 %	51.47 ± 1.97	8.40 ± 0.34
Tyrosine	101.3	4.01 d.nm 10.4 %, 114 d.nm 89.6 %	65.92 ± 3.13	4.48 ± 0.54
Acidic				
Aspartic Acid	592.3	37.7 d.nm 72.3 %, 656 d.nm 24.5 %, 5040 d.nm 3.2 %	35.84 ± 0.39	5.53 ± 0.33
Glutamic Acid	169.6	21.9 d.nm 86.8 %, 318 d.nm 9.7 %, 4350 d.nm 3.5 %	18.19 ± 1.24	3.92 ± 0.12
Basic				
Lysine	1560	102 d.nm 100%*	58.85 ± 3.75	8.53 ± 0.10
Arginine	203.5	25.3 d.nm 98.3 %, 4410 d.nm 1.7 %	12.58 ± 7.92	3.35 ± 0.52
Histidine	291.6	14.6 d.nm 98.4 %, 4950 d.nm 1.6 %	11.02	3.71

Table 3. Results for coating of SPIOs with HCl salts of each of the 20 naturally occurring amino acids.

This finding has potential applications when attempting to attach active pharmaceutical ingredients or peptides to the particles, as it may be possible to modify the coatings slightly to increase the

attachment, or it may simply make it easier to identify which potential coating agents are likely to bind, which goes some way to meeting the aim of using these particles for biomedical applications.

1.6 Determination of mode of binding to SPIOs

Whilst the literature states that it is the carboxylic acid groups of the coating materials that bind to the SPIOs, the salts of the amino acids were used which may have altered their binding.

The initial experiments with amino acids indicated that the coating materials that will bind to the nanoparticles with the highest affinity would be those with charged groups. It appears that those groups containing lone electron pairs are able to coordinate to the particle with the most ease. As we are relying on electrostatic type interaction, the increased binding exhibited by the salts of various coating agents could be attributed to an increased electrostatic interaction between the coating and the particle. Amino acids are amphoteric and in making them into salts the potential to have charge and dissociate turns into the actual dissociation of the particle to form a charged species. As with any electrostatic interaction, an increase in charge leads stronger interactions and so the binding becomes more favourable in accordance with Coulomb's Law.

However, it should be noted that salts on their own do not bind to the SPIOs. When NaCl and NH₄Cl were trialled using the solvent free grinding method, the resultant solutions contained no iron, suggesting that they did not bind to the SPIOs. So, it can be suggested that the binding relies primarily on the presence of the nucleophilic groups (COOH, NH₂, OH, PO₄ etc.) but can be enhanced by presenting these in the salt form.

These finding could also help to increase binding of substances that will only sparingly bind. It may be that by turning the compound into a salt it will increase the likelihood of an electrostatic interaction.

1.7 Assessing if the salt form of the coating affects degradation of the particle

If particles are to be used in biomedical applications it is essential that they are stable in biological and buffered solutions. It has previously been reported that SPIOs degrade in both buffered and

acidic solutions, with the degradation being due to the iron oxide dissolving in the acid or buffer. As the particles are charged they are effectively pulled apart in solutions containing ions which can hydrolyse the bonds between the iron and oxygen atoms.

Bearing in mind that these particles would be coated with a material that could potentially degrade them, the HCl salt coatings were assessed to confirm whether or not they had an effect on degradation of the coated SPIOs. A degradation study using the MRI MOUSE was carried out with both T_1 and T_2 being measured every minute for the duration of the experiment. The results are shown in the graphs below (Figure 54 and 55), which illustrate how the relaxation times changed over time.

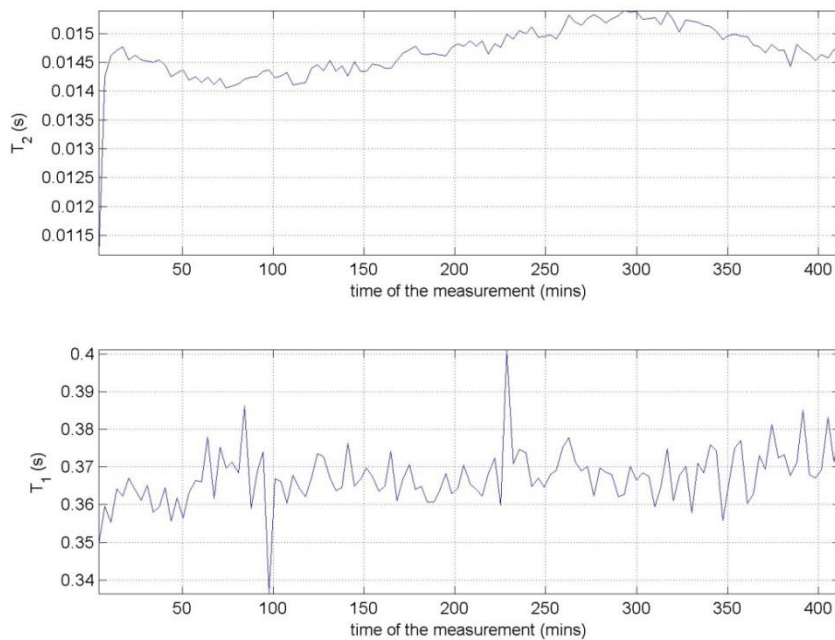


Figure 54. Graphs showing how T_1 and T_2 changed over time for SPIOs coated with ascorbic acid (non-salt). These graphs indicate little or no degradation only fluctuation in readings due to inhomogeneities in the magnetic field.

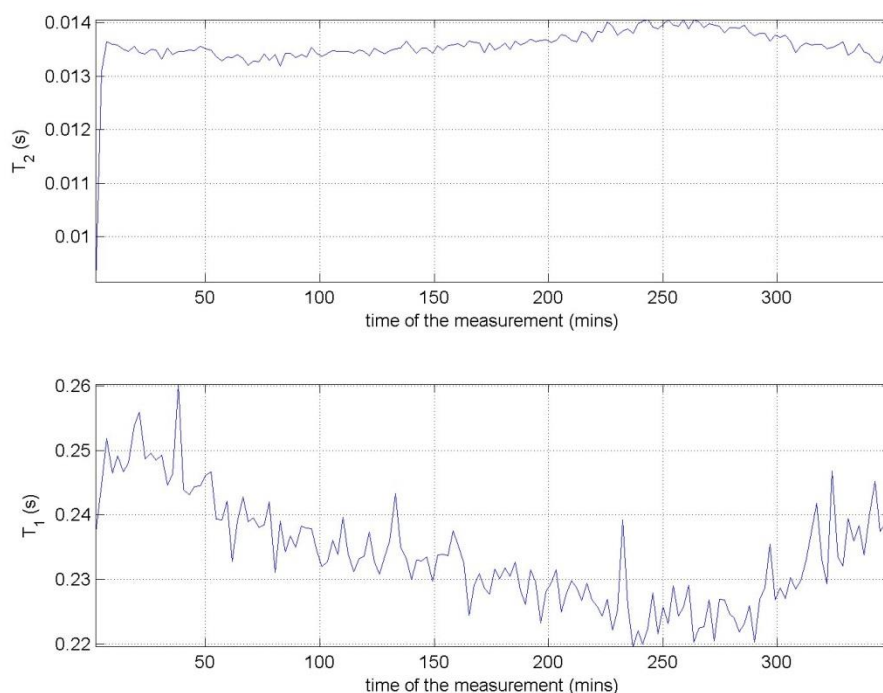


Figure 55. Graphs showing how T_1 and T_2 change over time for SPIOs coated with the HCl salt of ascorbic acid. Any fluctuations are due to inhomogeneities in the magnetic field.

What these graphs show is that there is little or no change in the relaxation times for these coated particles. The T_1 decreases slightly but the change is negligible. So, it is unlikely that the salt form of a coating material would have any adverse effect on SPIOs relative to the neat coating material, although this should be assessed on a case by case basis for certain applications as this may not always be the case.

One possibility is that as the coating material binds *via* the aforementioned functional groups, they form a protective layer around the particle, much in the same way as when Gd is chelated by EDTA. In this way the salt would dissociate in water but the particle would be shielded from any changes in pH in the surrounding solution, and so would not degrade. Stability of particles will be further explored in a comparison with commercially available alternatives.

As previously mentioned, it is possible to bind materials to SPIOs *via* several functional groups, but liquids have not been explored. To primarily determine if $-OH$ was able to facilitate binding to SPIOs hexadecanediol was used as a coating material *via* the solvent-free grinding method. The resultant hexadecanediol-SPIO solution (in chloroform) was pale brown, indicating an attachment. TEM results indicated that there were particles of 78 nm with lots of agglomeration. The agglomeration

can be attributed to the effect of the chloroform evaporating from the disc and causing the particles to clump together, or due to hydrophobic interactions forcing the coated SPIOs to form micelles. As there were no other functional groups present on the hexadecanediol, and the chloroform itself was not able to bind to SPIOs it can be concluded that it is the –OH group that is responsible for the binding. This was further supported during investigation of the suitability of liquids for solvent-free grinding.

To allow grinding to occur, a viscous alcohol was chosen, in this case glycerol. The mixture formed was solubilised in water, and on filtering the glycerol-SPIO solutions they were observed to be dark yellow/brown in colour, an initial indication that the attachment had been successful and the solution contains iron oxide. In addition to this the TEM results indicated particles of *ca.* 15 nm with an organic coating; the clear area observed in previous TEM samples. ICP results showed that there was an iron concentration of 103.1 mg.l⁻¹, confirming that the particles had been coated with glycerol prior to filtration. Attempts with a less viscous alcohol: ethanol, were unsuccessful, indicating that the viscosity of the sample is important for efficient grinding and thus attachment.

1.8 Determining optimum mass ratio for solvent free grinding method

If the solvent free method is to be scaled up or used for other applications, then in order to waste materials it is useful to know the optimum ratio that should be used for the process. As can be seen from the results in Figure 56 where Histidine.HCl was used as the coating material, as the mass of coating relative to SPIO increases the iron content of the resultant solution decreases, with the concentration of iron in solution dropping from *ca.* 1250 mg.l⁻¹ to *ca.* 450 mg.l⁻¹ as we increase the mass of coating material. This is attributed to mixing effects as at larger quantities there will be less complete contact between SPIO and coating. This indicates a possible problem for scale-up, as at even larger quantities there will be even less complete contact and therefore lower concentrations of SPIOs coated (and taken up into solution). A chemical engineer would need to be consulted in order to overcome this problem.

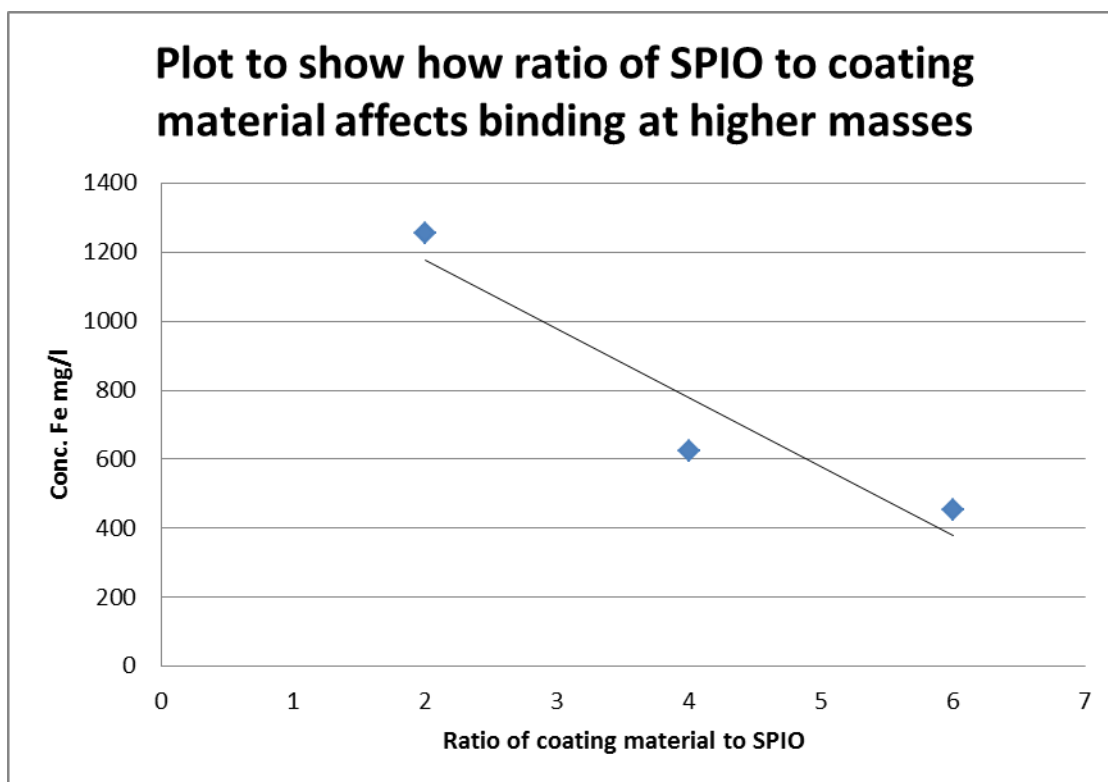


Figure 56. Preliminary results into how mass ratio of coating material to SPIO affects preparation.

Working on the assumption that coating would be more effective at lower ratio's the experiment was repeated with ratios from 4:1 to 1:2, also using histidine.HCl as the coating agent. These findings were less conclusive as illustrated in Figure 57. The results still show a general decrease in effectiveness of coating as the mass of coating material relative to SPIO increases. However it does show a large degree of variability. It is possible that the variation is due to large inhomogeneities in the mixing method. The pestle and mortar method is difficult to reproduce exactly as it is done by hand, and conditions such as pressure and speed are difficult to control.

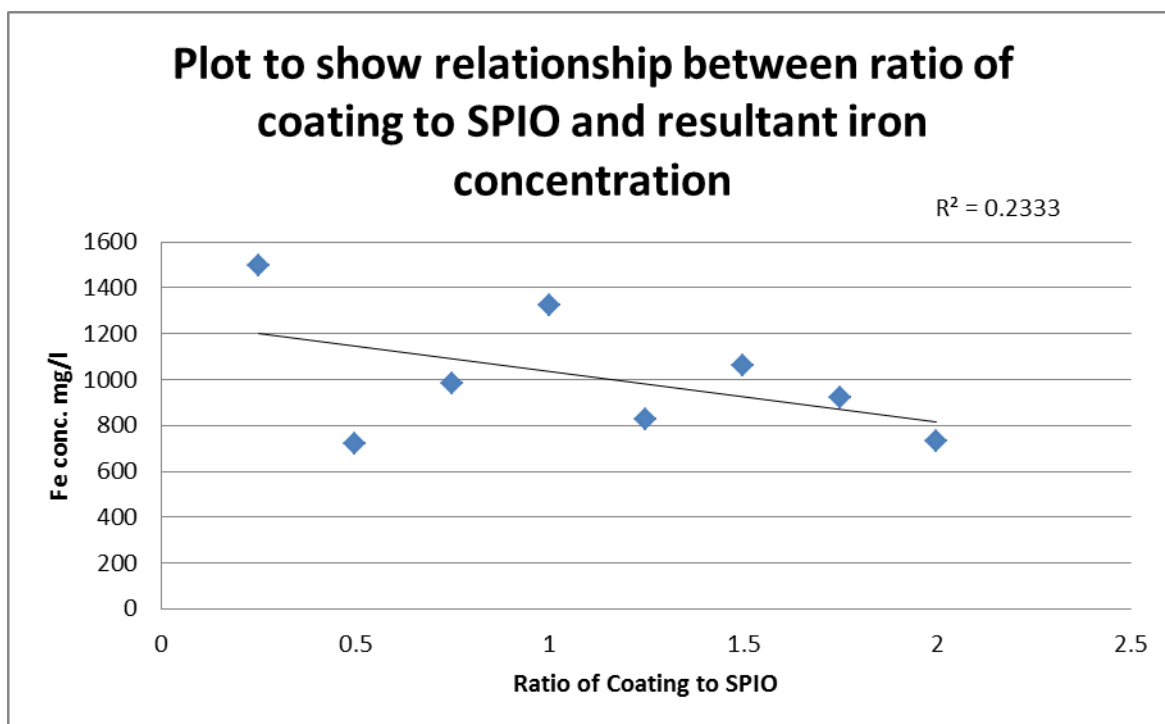


Figure 57. Graph showing ICP results for experiment to determine optimum ratio for coating SPIOs via solvent-free grinding method.

The coffee grinder method was previously mentioned in relation to scaling up the process, but it could also be used to increase reproducibility and produce a more homogeneous sample, although the same machine would have to be used due to possible differences in burr size, rotation speed, and groove size affecting results. When SPIOs and HCl histidine salt were processed together ten times each with either a mortar and pestle or a coffee grinder, it was found that the coffee grinder was better at producing a homogeneous sample than the pestle and mortar. Standard Deviation for pestle and mortar samples was 11.28 with a mean value of 100.301 mg.l⁻¹. The coffee grinder sample had a standard deviation of 4.18 with a mean value of 55.483 mg.l⁻¹. These results indicate that although the yield using the coffee grinder is lower, confirming that with the current design there is a large amount of the materials wasted, the coffee grinder increases precision and produces a more homogeneous sample, with a range of only 13.50 mg.l⁻¹ vs. 32.16 mg.l⁻¹ for coffee grinder vs. human grinding respectively.

1.9 Calculation of the number of molecules of ascorbic acid coating each SPIO

Further to the aim of using coating SPIOs for biomedical applications it was essential to determine how much material was bound to the particles. This is particularly important for cancer immunotherapy where the concentration of immunogenic peptide delivered is crucial.

Using the Oxford Crystal Database the unit cell for magnetite was found. This was applied to the following calculations:

There are 8 Fe₃O₄ units per unit cell of the inverse spinel structure, with each cell having a volume of 8.3967 Å³ (or 0.83967 nm). Each SPIO is found by TEM, to have a mean diameter of 15 nm, giving each SPIO a mean volume of 1.415 x 10⁷ Å³.

So, if each SPIO has a volume of ~ 1.415 x 10⁷ Å³ and each unit has a volume of 8.3967 Å³, each containing 32 Fe atoms, then:

$$\begin{aligned}\text{Number of Fe atoms per SPIO} &= (1.415\text{E}^{07}/8.3967)32 \\ &= 4.044 \text{E}^7\end{aligned}$$

$$\text{Number of moles} = \text{Number of atoms} \div \text{Avogadro's constant}$$

$$\begin{aligned}\text{Number of moles Fe per SPIO} &= 4.044 \text{E}^7 \div 6.023 \text{E}^{23} \\ &= 6.714 \text{E}^{-17}\end{aligned}$$

From the ICP results the concentration of iron per ml was found to be 149.2 mg.l⁻¹. A 10 ml sample was used, so the actual mass of iron present in the original sample was 1.492 mg.

$$\begin{aligned}\text{Moles Fe} &= 1.492\text{E}^{-3} \div 56 \\ &= 2.664 \text{E}^{-5}\end{aligned}$$

Given the number of moles it is now possible to calculate the number of SPIO particles in the sample:

$$\begin{aligned}\text{Number of SPIOs in 129 mg} &= 2.664 \text{E}^{-5} \div 6.714 \text{E}^{-17} \\ &= 3.968 \text{E}^{11}\end{aligned}$$

Moles of O in this sample can be calculated as follows:

If there are 2.664×10^{-5} moles Fe then:

$$\text{Moles O} = 2.664 \text{ E}^{-5} \div 3 \times 4$$

$$= 3.552 \text{ E}^{-5}$$

$$\text{Mass of O} = 3.552 \text{ E}^{-5} \times 16.00$$

$$= 5.6832 \text{ E}^{-4}$$

Now having the mass of oxygen and the mass of iron it is possible to calculate the mass of ascorbic acid, and thus the number of moles and molecules present in this sample, and the approximate number of ascorbic acid molecules binding to each SPIO.

$$\text{Mass Fe} = 1.492 \text{ mg}$$

$$\text{Mass O} = 0.568 \text{ mg}$$

$$\therefore \text{Mass Fe}_3\text{O}_4 = 2.06 \text{ mg}$$

$$\text{Mass Ascorbic acid} = 129 - 2.06 = 126.94 \text{ mg}$$

$$\text{Moles Ascorbic Acid} = 126.94 \text{ E}^{-3} \div 176 = 7.2125 \text{ E}^{-4}$$

$$\text{Molecules Ascorbic Acid} = 7.2125 \text{ E}^{-4} \times 6.023 \text{ E}^{23} = 4.344 \text{ E}^{20}$$

$$\therefore \text{Ratio of SPIOs to Ascorbic acid molecules} = 4.344 \text{ E}^{20} \div 3.968 \text{ E}^{11}$$

$$= 10.95 \text{ E}^9$$

So, according to these calculations there are 1095 million ascorbic acid molecules per SPIO particle.

A repeat of this experiment gave a value of 930 million ascorbic acid molecules per SPIO particle, close to the original value.

The total surface area of each SPIO can be estimated using the following:

$$4\pi r^2 = 4 \times 3.14 \times (10)^2 = 1256.6 \text{ nm}^2$$

Assuming that the molecules are binding at the carboxylic acid group this would mean that each binding site requires an area of 1.52\AA to bind successfully. The maximum number of molecules that could bind, not taking into account any repulsion or steric effects, is 82,671; over 11,000 times less than calculated. This suggests one of the following possibilities:

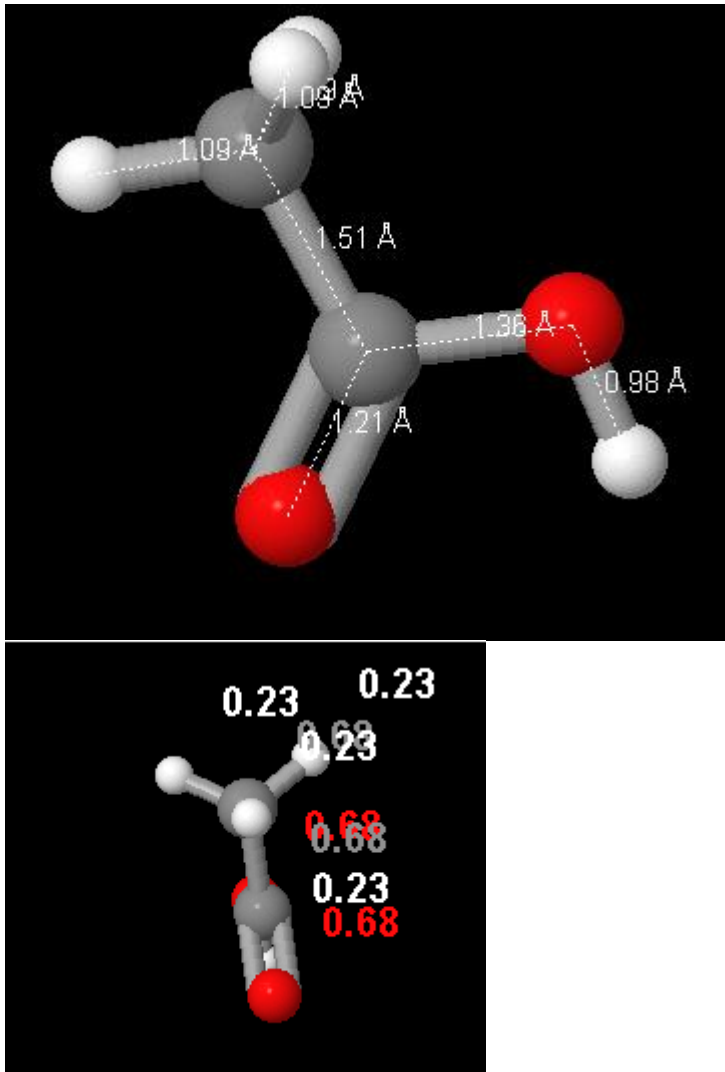


Figure 58. Dimension of a molecule of acetic acid to show dimension on binding carboxyl group.

- 1) The coating formed on the surface of the particle is not a monolayer and so the results are higher than expected, as monolayer coverage was assumed.
- 2) There is free coating material present in the sample due to insufficient separation.
- 3) Many of the coated particles are larger than was observed by TEM.
- 4) The sample was not completely dry and so the mass measured was incorrect.

Regardless of the reason, this measurement tool is still effective for calculating the mass of “active ingredient” in a SPIO preparation, assuming that the sample is completely dry. It is also worth considering that even after separation steps have been carried out, there will still be a certain amount of free coating material in any solutions prepared as the coating agent, only joined by an electrostatic interaction with the particle, is able to dissociate in equilibrium with the solution. This

makes a separation step less important and illustrates the importance of quantifying and controlling the total amount of coating material, bound or unbound, in the sample.

Due to the equilibrium effects of the coating agent in solution it is important to determine the effect of this dissociation, and if it has any effect on degradation of the particle or on the T_1 or T_2 relaxation times. pH buffers were used to investigate these effects, which could be applied to the biological aspects of the research.

1.10 Results of pH study

To determine if the functionalised particles would be stable enough in biological buffers, the effects of different buffers were investigated. The plot for T_1 shows that changes in T_1 for all amino acid coated SPIOs are slightly larger than that of water, represented in these graphs as buffer pH 0, regardless of the pH with the exception of pH 9.00 which will be discussed in further detail later on (Figure 59). Other exceptions are the acidic coating, glutamic acid, at pH 4.00, and the basic coating, histidine, at pH 11.00. These findings suggest that in pH solutions with pH similar to that of the coating material there may be more interactions between the coated SPIOs and the solutions which leads to either an enhancement or dampening of the superparamagnetic effect. This has caused a larger increase in T_1 for histidine and a smaller increase in T_1 for glutamic acid in comparison with the other amino acids. However, as explained previously any inconsistencies could be explained away as inhomogeneities in the magnetic field. So we turn to the results for T_2 to confirm or reject these findings.

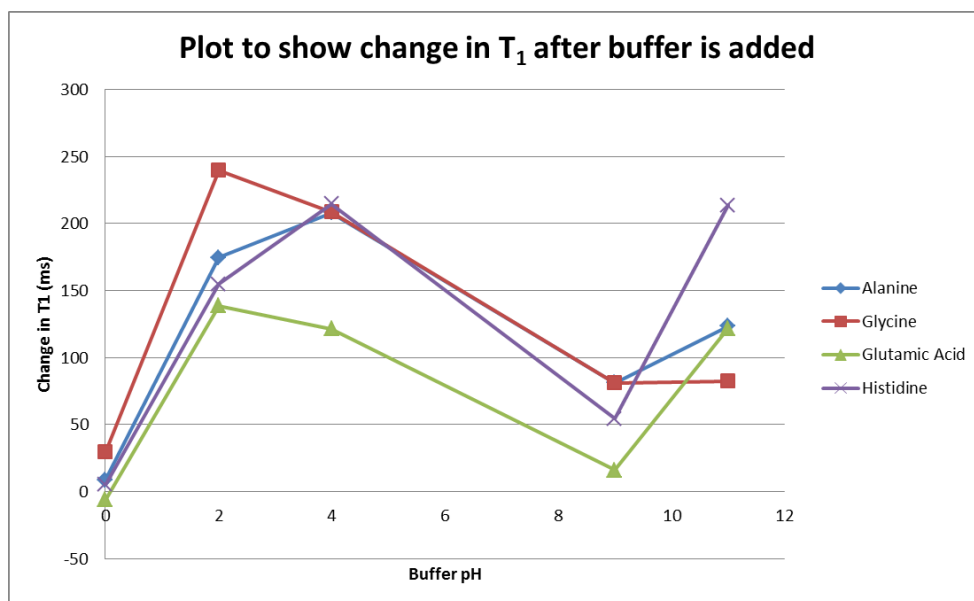
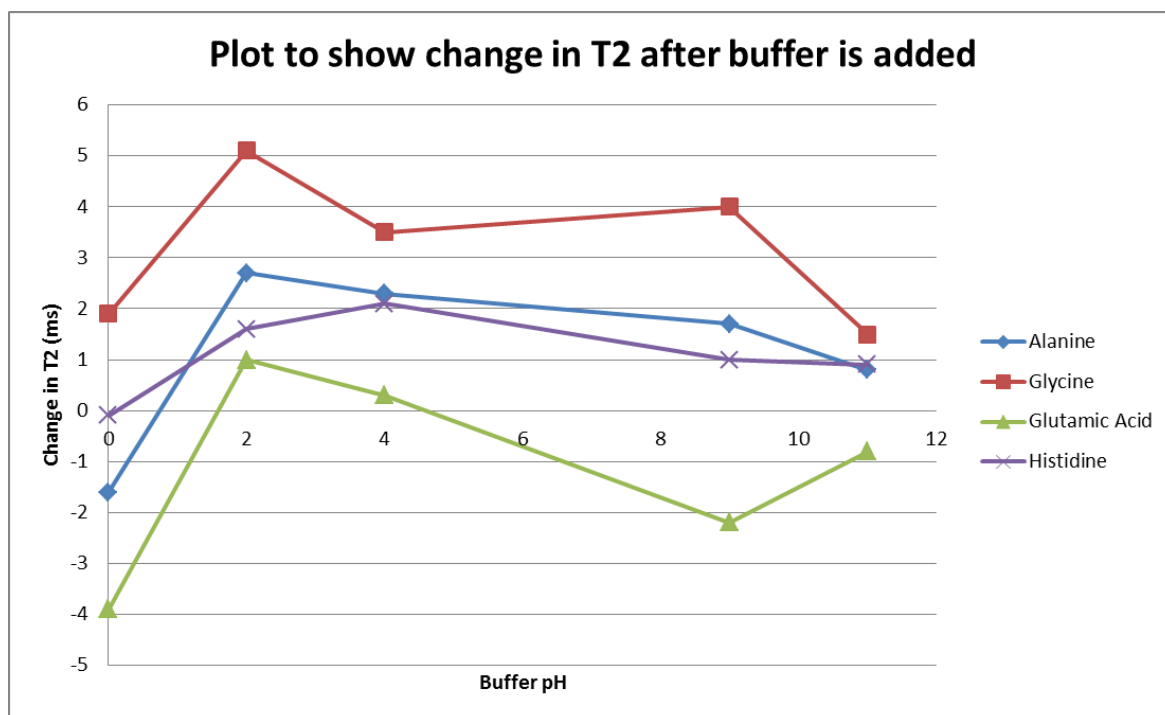


Figure 59. Graph showing T₁ when different amino acids are put into buffers of different pH.

Analysis of the data for T₂, displayed in the graph in Figure 60, shows that changes in T₂ are again slightly higher than for dilution with water alone. Also of note is the absence of consistency both overall at pH 9.00, and with glutamic acid and histidine at low and high pH respectively. This supports the theory of inhomogeneities in the magnetic field being the cause of fluctuations in T₁, which is much more susceptible to these inhomogeneities. This sensitivity is also the likely cause of the effects at pH 9.00. It is likely that an error occurred during dilution of the buffer which has in turn affected the results. It was not considered necessary to repeat the results as T₂ results did not show the same inconsistency, and the aim of the experiment was to determine if there were any large adverse effects in the presence of buffers, which there were not.



*Buffer pH 0 is the amino acids diluted with 1 ml water rather than placed into 1 ml buffer.

Figure 60. Graph showing T2 when different amino acids are put into buffers of different pH.

From these results it can be concluded that when placed into buffers the coating material does not undergo a degree of dissociation significant enough to expose the SPIOs to degradation, and so SPIOs coated by this method appear to be stable in biological solutions. This goes some way to meeting the aim of using the particles for biomedical applications.

1.11 Autoclaving

If these particles are to be used *in vivo* then it is essential that they are sterile to meet FDA regulations. The easiest method available to us was to autoclave the particles, but it was not clear if this would have any adverse effects on the particles themselves.

On completion of autoclaving it was noticed that the SPIOs had become brown in colour. This suggests that oxidation had taken place which would lead to a reduction in formation of Fe₂O₃ (hematite). In addition to this, any samples containing ascorbic acid appeared to have melted or decomposed slightly. The TEM results (Figure 61) indicated that there was more agglomeration of

particles that had been autoclaved, although all particles still seemed to be spherical in shape and to be sufficiently coated. MRI measurements gave T_1 of 1103.95 ms and T_2 of 12.84 ms for the non-autoclaved sample, and T_1 of 927.24 ms and T_2 of 12.84 ms for the autoclaved sample, with both samples being dissolved 12 mg of ascorbic acid coated SPIOs in 3 ml distilled water. These results indicated that the autoclaving process did not produce any deleterious effects and so can be used to sterilise these types of particles, adding to the case for their suitability for biomedical applications.

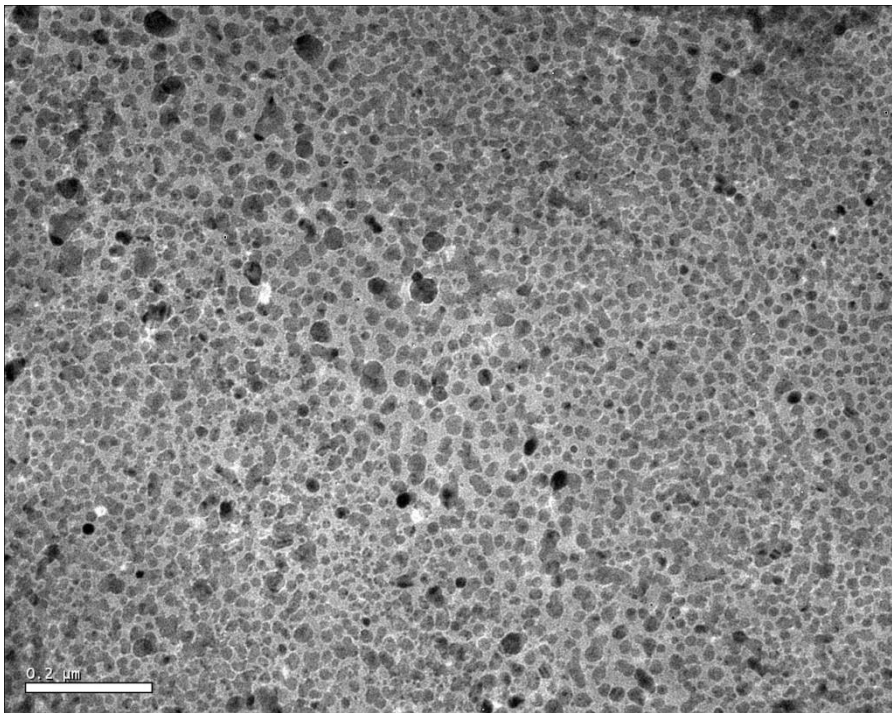


Figure 61. TEM image showing agglomeration of ascorbic acid coated SPIOs rehydrated following autoclaving. Particles appear to be ca. 20 nm and above in diameter but have not formed large aggregates.

1.12 Separation of particles using size exclusion chromatography

Particularly when aiming to use particles for applications such as cancer vaccines, or anything else *in vivo*, the particles need to be pure to meet regulations. The first method of separation trialled was size exclusion, working on the principle that the coated particles would elute later than the free

coating materials. G50 sephadex was used as it was deemed to have the perfect pore size, and distilled water was used for elution in case buffer solution caused some of the particles to fall out of solution. The ICP data for each fraction collected was plotted against fraction number to give Figure 62.

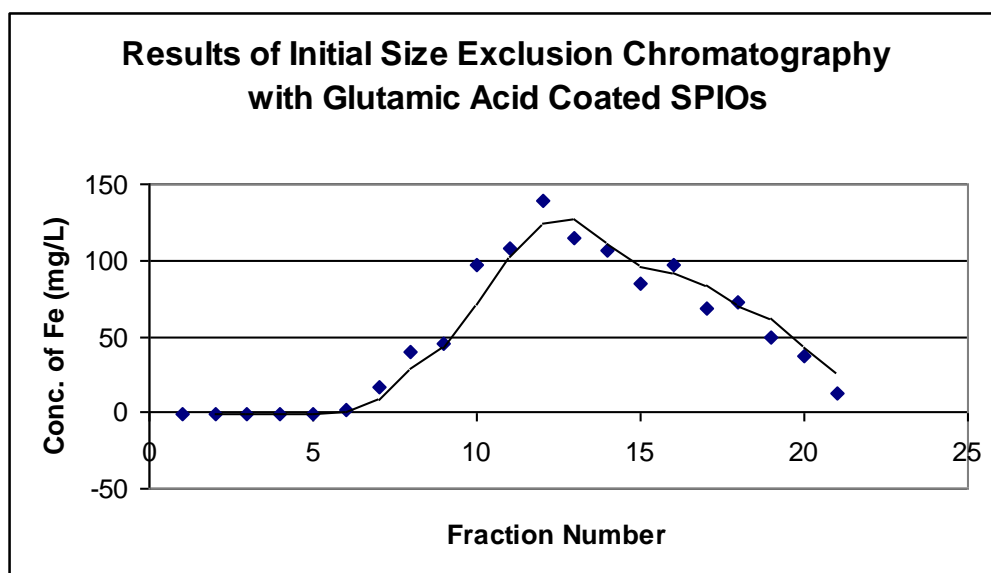


Figure 62. This plot shows how the iron oxide nanoparticles are eluted from the column containing G50 Sephadex

This graph shows that the SPIOs started to elute around fraction 5 but there were insufficient fractions to collect all of the SPIOs, as indicated by the line not returning back to 0 mg.l⁻¹ of iron. It was therefore decided that in future experiments a minimum of 30 fractions would be collected. It was predicted that the SPIOs would elute first followed in later fractions by the free glutamic acid due to the size of the particles. Larger particles, in this case the coated SPIOs, pass around the porous beads of the Sephadex. The smaller coating materials will take a longer path through the beads and so elute later. As an insufficient number of fractions were collected it was not possible to test this theory by removing the solvent *in vacuo* to reveal if free coating material was present in later fractions. It is predicted that there will be a number of fractions between the iron containing fractions and the glutamic acid containing fractions so that a good separation can be guaranteed. This could be adjusted in further experiments by either using a longer column, different beads, or by using a slower flow rate.

When the separation was repeated using more fractions (Figure 63), it can be seen that the concentration of Fe returns to 0 mg.l⁻¹. This confirms that the separation method can be effective although results are indicative of three sets of coated SPIOs, each of which will differ in size either due to coverage of coating material or due to variability of the particles themselves. The presence of different peaks with particles showing such small variation illustrates the sensitivity of this method, which when developed could be exploited.

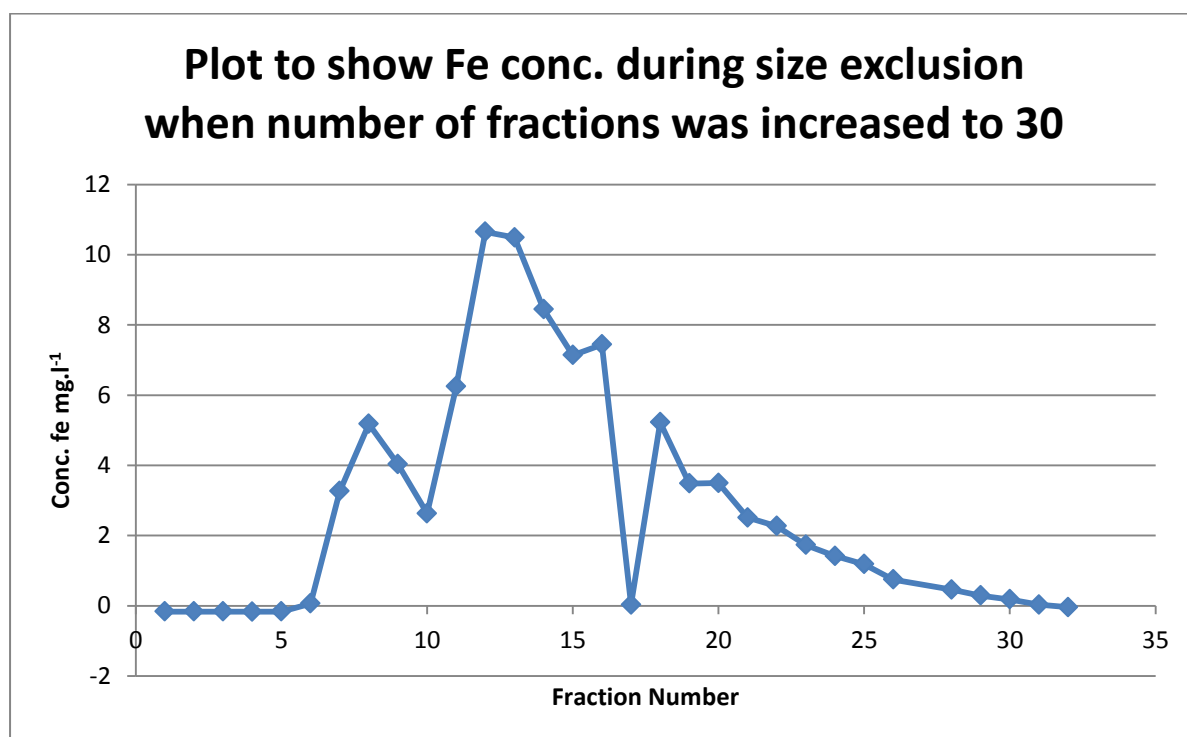


Figure 63. Plot to show conc. of Fe in each fraction collected when number of fractions was increased

Disappointingly this method was not successful for the larger coatings such as the immunogenic peptides. What was observed in these cases, was that irrespective of the packing material, column length or solvent used for elution, SEC was ineffective. In all cases the sample stuck at the top of the column and did not move down the column at all. Initially it was assumed that this was due to the size of the particles but trialling of different sized beads soon eliminated this possibility. So, it was decided that other methods should be trialled for separation of free peptide from peptide coated SPIOs.

1.13 Eppendorf and centrifuge

Before moving on to the alternative separation methods, a system was devised with the possibility of increasing the efficiency of the size exclusion method. For each of the conditions in which the Sephadex was used in a centrifuge column, the Sephadex dried out before any separation could take place as there was no way of keeping the top of the column wet. Even with the lowest speed and shortest spin time the column was completely dry. In addition to this the length of the column was too short, thus not allowing sufficient separation to take place and so any SPIO solution collected would also contain free coating agent. In conclusion this is not a suitable method for separation of SPIOs from free coating material in solution.

1.14 Separation using antisolvents

Although for this research the aim was to avoid solvents as much as possible, the importance of obtaining a pure product for medical applications led to the investigation of antisolvents as a means of separation. This type of separation produced some mixed results. When SPIO solutions were mixed with solvents that were miscible with water, namely Acetone, Ethanol, ACN or THF, each mixture should have led to a certain amount of coated SPIO precipitating out of solution. The results show that the mixture of water and solvent in some instances did not lead to the desired effect. Both ethanol and THF did not produce any precipitate, even when left in the freezer overnight, marking them as unsuitable antisolvents for this experiment. The most effective antisolvent was acetone, producing a large amount of precipitate on initial addition, and further precipitate when left in the freezer. This was effective for all of the amino acid coated SPIOs trialed. It should be noted however that due to its effectiveness as an antisolvent it was difficult to add acetone, even in 100 μ l increments, without leading to a small amount of white precipitate (characterised as the coating material by NMR and IR). It is possible that the acetone is too effective and so the next best antisolvent, ACN should be considered. ACN was also effective in producing the desired brown precipitate but did not produce such a large quantity of unwanted free coating material. It was thus much easier to tailor the ACN method to give the desired product, although again at 100 μ l increments a small amount of white solid was observed (characterised as the coating material by NMR and IR).

Overall, despite the use of antisolvents being cited as a method for purifying nanoparticles, it was both unreliable and inconsistent for the particles coated *via* this method. So, this method was abandoned and magnetic separation investigated as the alternative.

1.15 Separation by Magnetic Force

The literature suggests that SPIOs in solution are too small to be affected by the magnetic field of even a strong magnet. However, if the mixture of free SPIO, coating material and coated SPIO could be separated when not in solution, then it could become a useable method. In this instance a solvent in which the coated SPIOs and coating material would not be soluble was used as illustrated in Figure 64.

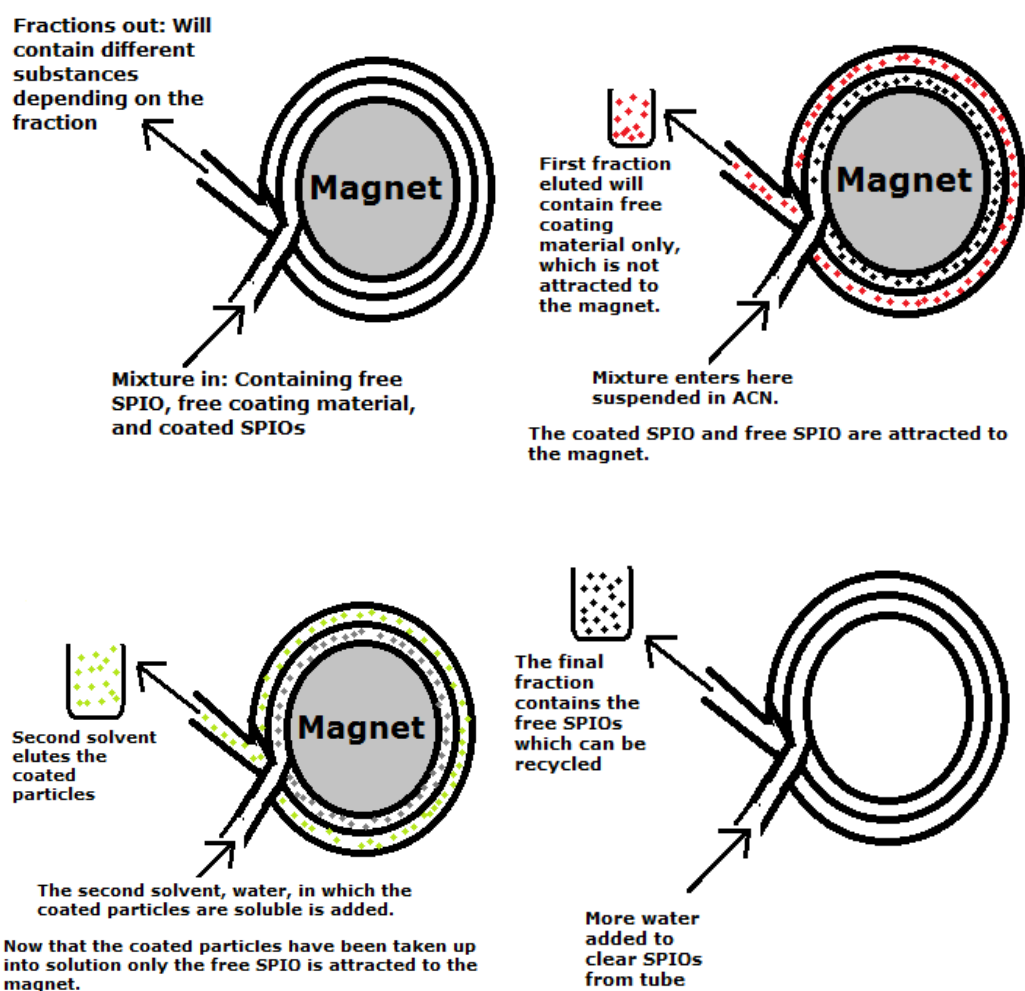


Figure 64. Schematic to show process of separation using magnetic force and a variety of solvents.

The SPIOs showed considerable magnetic properties prior to coating, so working on this principle a device was constructed consisting of a magnet with a piece of thin tubing wrapped tightly around it and a needle at one end through which a solution could be passed. The principle was that as the SPIO solution was forced through the tubing the SPIOs would remain around the magnet and any free coating (amino acid or peptide) would pass through the tubing without attraction, leading to a pure sample of the coated SPIOs with no free coating.

However, it was found that once in solution the SPIOs were not attracted to the magnet, as predicted in the literature, and so passed through the tubing together with the free coating. It was decided that this method was ineffective for SPIOs in solution.

Following this, a system was devised in which the SPIOs were coated with histidine HCl salt and the mixture suspended in acetonitrile. The aim of this was to provide a mobile phase in which both the coating material and coated SPIOs were insoluble, with the aim that it would carry along any particles that were not attracted to the magnet. The coated SPIOs and free SPIOs would therefore remain attached to the magnet until the second solvent, in which the coating material and thus the coated SPIOs were soluble, was passed through. As the magnetic field is not strong enough to hold the SPIOs in solution onto the magnet, the coated SPIOs would dissolve in the second solvent and be carried through the tubing to the collecting syringe. All that would remain on the magnet would be uncoated SPIOs which could be removed upon removal of the magnetic field.

The fractions collected when water was passed through the tubing were found to have iron by ICP, but the fractions collected with acetonitrile did not contain any free coating material, as discovered when the solvent was removed *in vacuo*. This could mean that either the separation step was ineffective, or there was no free coating material in solution. During further experiments it was found that the flow of solvent was sufficient to push the larger and magnetically attracted SPIOs through the tubing and so it could reasonably be assumed that the coating agent would pass through the tubing with more ease. As such, it was assumed that the grinding method, using the ratio of 1:1 led to an excess of SPIO, but not any free coating material.

This method was found to be effective for amino acid salt coated SPIOs but was not suitable for the ascorbic acid coated particles, showing that it could not be applied to all coatings. The solvent was altered for a less dense, less viscous solvent, as some of the SPIOs were being carried through on the primary solvent. However, this was not effective for all coatings and this method was therefore stopped in favour of an alternative method.

1.16 Separation using a Magnetic Separation Rack

A random variety of samples were chosen from what was most readily available. These are detailed in Table 29. For each of the samples trialled, the magnets showed some effectiveness in attracting the coated SPIOs in solution, which had not proved possible when using the neodymium magnet. However despite this promising start the force had not been effective enough to pull the particles completely out of solution, merely creating a “bubble” of ferrofluid. It was also not possible to separate this ferrofluid, as the effects of either gravity when tipping the supernatant from the eppendorfs, or the suction from a pipette was enough to pull the fluid away from the magnet. The limitation in this equipment was the strength of the magnet and it could be speculated that with a stronger magnet this method would have been effective.

1.17 Separation using centrifugal force



Figure 65. Showing the pellet formed during high speed centrifugation. The samples that show no defined pellet had a very high concentration of iron and so a more dilute sample or several centrifugation steps may have been required for separation.

A reliable method of purification is essential for the application of nanoparticles in biomedical fields. As the previous methods described were unsuccessful overall, this final method was investigated. The centrifugal force at 60 000 rpm was expected to be effective at separating the particles in solution, and could have been further investigated by using solvent gradients. However, due to a

technical error it was not possible to analyse the samples from the high speed centrifugation experiment. What was noticed though, was that on removal from the rotor (Figure 76) the tubes contained a pellet of dark material and a colourless solvent separated from this. The only dark material present in the sample was the SPIOs and the solvent was water. Therefore, we can assume that the pellet contains SPIOs that are separated from the solvent. Due to the aforementioned problems it was not possible to determine if the solvent still contained the free amino acid or if the free coating material is inside the pellet as on defrosting the pellet became re-suspended in the solvent. Due to damages to the equipment it was not possible to repeat this experiment and so no conclusive results could be drawn.

As this method has been reported previously for separation of similar particles, it can be assumed that, had the equipment been in full working order, the particles and coating material would have been separated out. However, it is likely that a gradient would increase the degree of separation observed. This could utilise the antisolvents that have been previously described, or alternatively solvents of different viscosity which would separate different sized particles out according to their density and the density of solvents used.

1.18 Iron (III) tin (II) oxide particles

The research hypothesis states that metal and metal oxide particles will be synthesised, but the results so far are from iron oxide particles only. As the other aim was for biomedical applications including medical imaging, the idea arose for a particle consisting of iron oxide, which would provide the desired NMR contrast, and tin, which with an Ar of $118.71 \text{ g} \cdot \text{mol}^{-1}$ would provide sufficient contrast for CT. The results shown in Table 4 and Figure 66 combined indicate that spherical nanoparticles with the chemical formula $\text{Fe}_3\text{Sn}_2\text{O}_9$ have been successfully formed, as was the general aim of the experiment, although it was assumed that the Sn would occupy the Fe(II) site leading to particles with the chemical formula Fe_2SnO_4 . The crystal structure of this compound could not be determined, which would confirm the suggested formula. What has been successfully illustrated is that a nanocomposite containing both tin and iron can be formed, which has the potential to be useful for both CT and MRI. It also shows that these mixed metal oxide particles can also be coated successfully using the solvent-free grinding method.

The MRI results indicate that the particles formed are magnetically active, or even superparamagnetic, which is possibly due to the presence of both Fe²⁺ and Fe³⁺ ions. The T₁ of 236.91 ms and T₂ of 5.19 ms are comparable with iron oxide nanoparticles (SPIOs).

Element	Weight%	Atomic%
O K	50.36	83.20
Cl K	0.53	0.39
Fe K	21.83	10.33
Sn L	27.29	6.08
Totals	100.00	

Table 4. Showing the EDX results for analysis of the iron tin oxide nanocomposite.

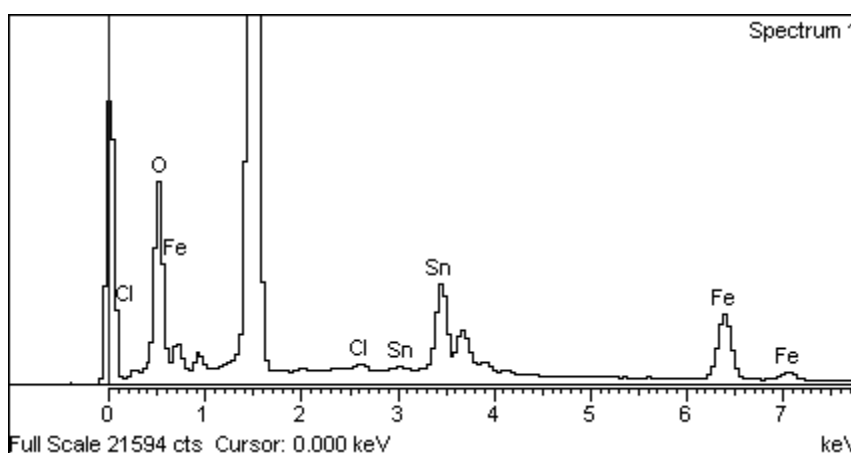


Figure 66. Graph of EDX results showing the elemental composition of the iron tin oxide nanocomposite

1.19 Calcium Oxide Nanoparticles

As has been previously mentioned, the research hypothesis aims to investigate more than one type of particle. Calcium oxide was investigated as it is possible that the calcium in the particle could be used as a vitamin supplement, and a further vitamin or drug molecule attached to the surface of the

particle making it multifunctional. Figures 67 and 68 show TEM picture and the relative EDX results respectively. TEM results indicate that spherical particles of *ca.* 5-10 nm have been formed from the spinning disc reaction, and the EDX data proves that these particles are composed of calcium and oxygen. The EDX shows chlorine in the ratio of 1:2 with oxygen. This equates to a 1:1 ratio of oxygen to chlorine on the histidine as illustrated in Figure 80. This leaves 1 equivalent which is present in the form of oxygen in the CaO nanoparticle. The ratio of calcium to oxygen is 1:2.5 respectively, leaving an excess of oxygen, which could mean that the sample had not completely dried before analysis, leading to a small amount of residual water and thus oxygen in the sample.

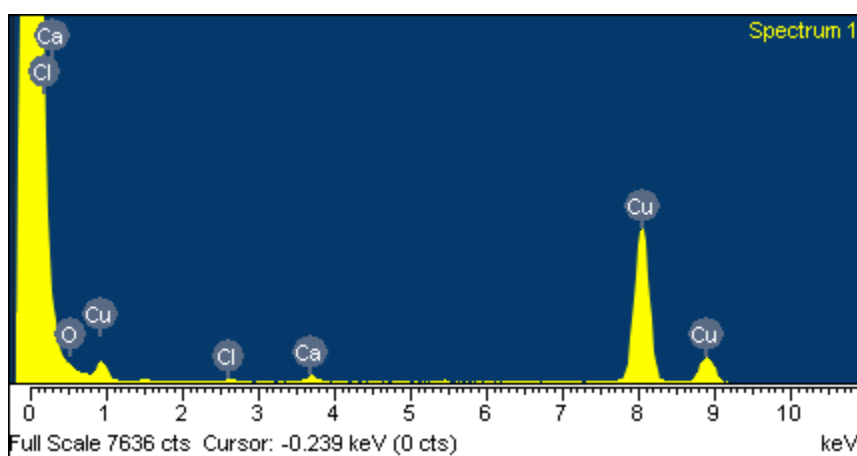
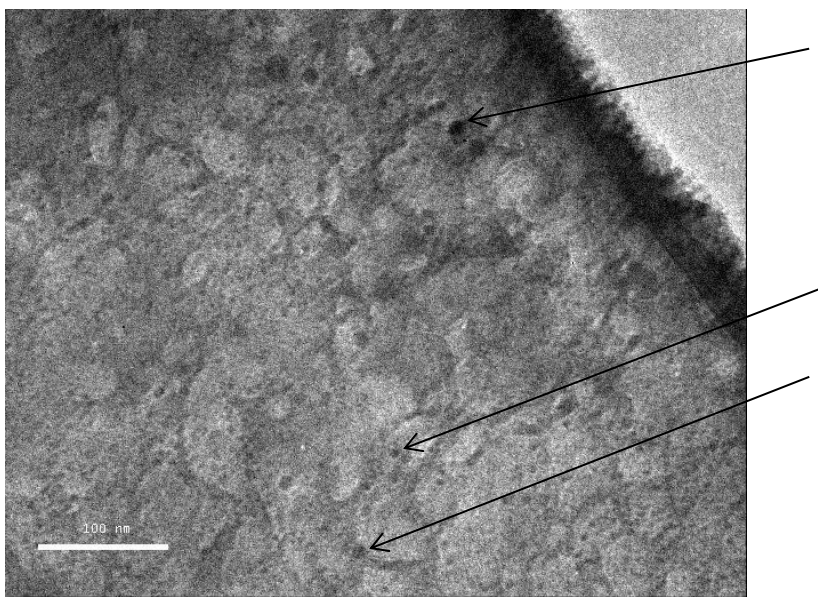


Figure 67. EDX result for CaO nanoparticles. The grid is made of Cu accounting for the Cu peaks. Other peaks show Ca, O and Cl, with the large peak on the left showing the presence of organic matter (mostly a mixture of H, C and N present in the organic coating)



*Figure 49. TEM image of CaO nanoparticles showing spherical particles of ca. 5-10 nm. Arrows are pointing to individual nanoparticles. *Poor image is due to limitations of the transmission electron microscope.*

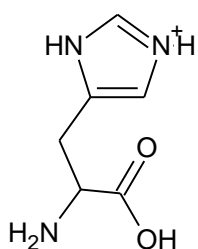


Figure 69. Structural formula for Histidine indicating one protonated site at pH 4

In addition to confirmation that CaO nanoparticles can be formed using an SDR method, these results also indicate that the solvent-free grinding method is also effective for coating of CaO nanoparticles. CaO NP's were not soluble in water themselves and aggregated, thus stopping them from passing through the filter. This means that any particles present in the resultant solution must have been coated successfully coated prior to filtration. This has implications for other metal oxide particles, suggesting that there are a plethora of nanoparticles that can be coated using this method.

1.20 Gold nanoparticles

Finally, in order to meet the research aims the gold nanoparticles were synthesised with the aim of proving that coating methods would be successful for naked metal nanoparticles as well as metal oxide. Using EDX and TEM at a magnification of 100K the images shown in Figure 70 indicate that gold nanoparticles were successfully formed *via* the methods described in the previous chapter. The product was isolate at 30 sec, 60 seconds and 90 seconds after the reducing agent was added as there was a distinct colour change from pale yellow to purple and then to red as the reaction progressed. It was found that the particles isolated at 30 seconds (purple) were smaller in diameter at around 5 nm, than the particles isolated at 60 and 90 seconds (red), which were > 10 nm in diameter. It was also found that the red particles were subject to a degree of agglomeration.

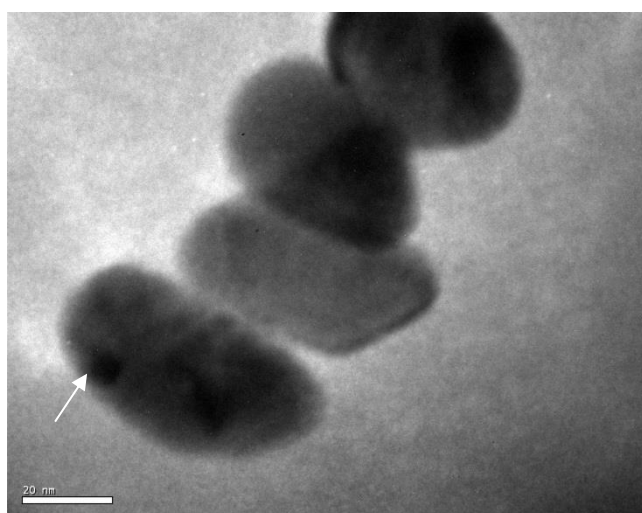


Figure 70. TEM image showing gold nanoparticles of 40 nm length and 20 nm width. Arrow indicated a smaller particle of ~ 5 nm suggesting that these particles are made up of smaller particles.

When higher concentrations of HAuCl_4 were used, a black precipitate formed. This was the case from 0.02 – 0.10 %. The particles would not suspend in solution, indicating that they were aggregated rather than agglomerated (Figure 71). The reason for this, is that the high surface energy on the gold nanoparticles will lead to them clumping together in order to increase their stability. At

lower concentrations the water molecules separate the molecules and keep them far enough apart that the high surface energy is not enough to overcome the distance. At higher concentrations the distance between molecules is reduced and so they attract each other and form larger particles in a process similar to Ostwald ripening. However, in order to increase the concentration of gold in the solution some of the solvent was removed *in vacuo*, leading to the particles being closer together in the solution, and in this case no aggregation was observed. So, it could be suggested that the environment of the gold ions prior to reduction and coating is more important to dispersion than their environment following synthesis, and also that the coating material reduces or masks the high surface energy, thus protecting the particle from aggregation.

When the peptide (p53(108)) was added to the solution as the reducing agent in place of the citrate, it was found that at higher concentrations it led to the particles aggregating as characterised by a black solid precipitating out of the solution. This shows that it is not only the concentration of gold but that of the coating material itself that can lead to aggregation.

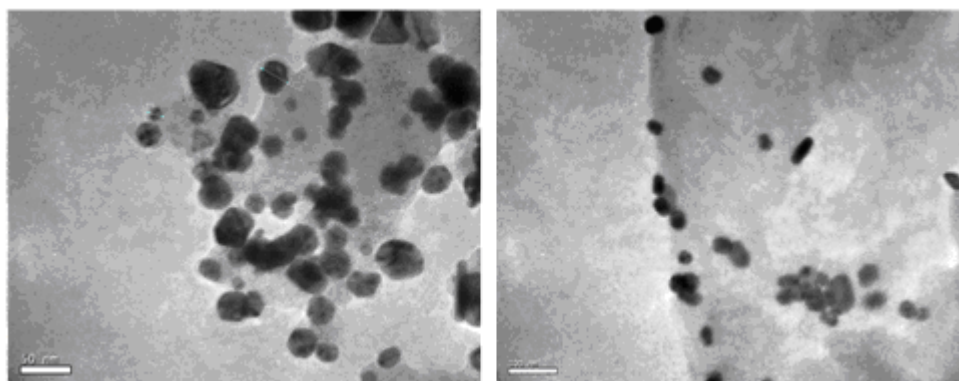


Figure 71. Images to show appearance of peptide (p53(108)) coated GNPs when peptide added at high concentration (left) and at low concentration (right)

Whilst the particles have been successfully synthesised and coated, it was not possible to isolate the gold nanoparticles in sufficient quantities to trial the solvent free grinding method. Reagents were expensive and no more than 2 mg of particles were made during each experiment; these quantities cannot be manipulated with the pestle and mortar.

Section 2: Medical Imaging

2.1 Preliminary test with gold nanoparticles

This project aims to prove that nanoparticles synthesised and functionalised using these methods can be used for biomedical applications. This includes CT scanning, which was kept in mind during the design of the iron tin oxide nanoparticle. However, as the literature leans towards the potential for gold nanoparticles as CT contrast, the focus was on these.

To determine a starting point for the synthesis of gold nanoparticles (GNPs) for X-ray contrast, glass vials containing solutions of dodecylamine capped GNPs dissolved by weight in methyl methacrylate (MMA), were placed into plastic tubes so that they fit into a CT Phantom. However, on attempting to measure the CT number of these solutions it was found that they could not be measured if there were any air bubbles inside the tube. So, it was suggested that a block of polymer that would not interact strongly with the X-Rays, should be cut into tubes that would fit into the phantom, and vials milled into each end of the tube, to hold 1 ml of solution each. When imaging was attempted it was found that CT measurements were inaccurate for this low volume of solution due to pixilation where each pixel of the image is so large that they overlap and it is not possible to distinguish the area with the solution in it apart from the rest of the vial. It was suggested that a larger volume be used. For this reason the containers were drilled to a volume of 2 ml and the experiments repeated. These vessels were found to be suitable for measuring CT number of various solutions and can also be cleaned with ease using dilute nitric acid.

2.2 CT testing with citrate capped gold nanoparticles

If these particles are to be used as contrast agents then the optimum concentration for that application must be found. The first experiments to determine the concentration of gold that would be required for *in vivo* use of GNPs as a contrast agent were carried out using the dodecylamine capped GNPs dissolved in methylmethacrylate (MMA). Figure 72 shows that the CT number, which increases linearly with increasing concentration of gold, for these preparations was very low but the experiments were successfully used to devise a vessel for use in the phantom.

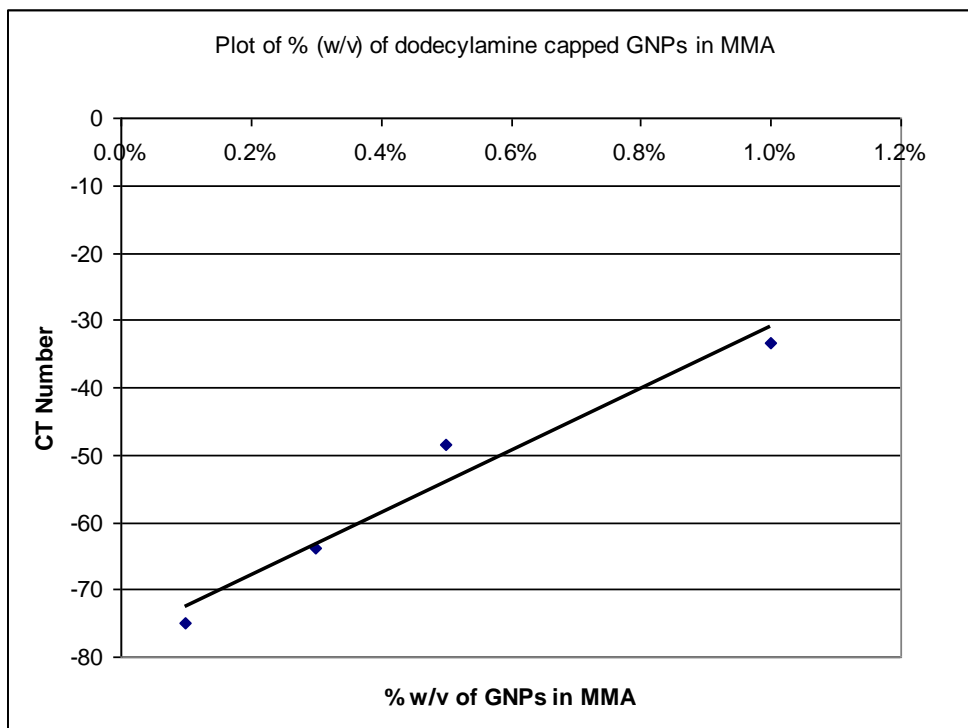


Figure 72. Plot of CT number vs % w/v of dodecylamine capped GNPs dissolved in methylmethacrylate when measured using tailored vessel for phantom.

The GNPs were synthesised *via* the sodium citrate reduction method and samples of different concentrations placed into the phantom vessels and sealed. These were then analysed and given a CT number (Figure 73)

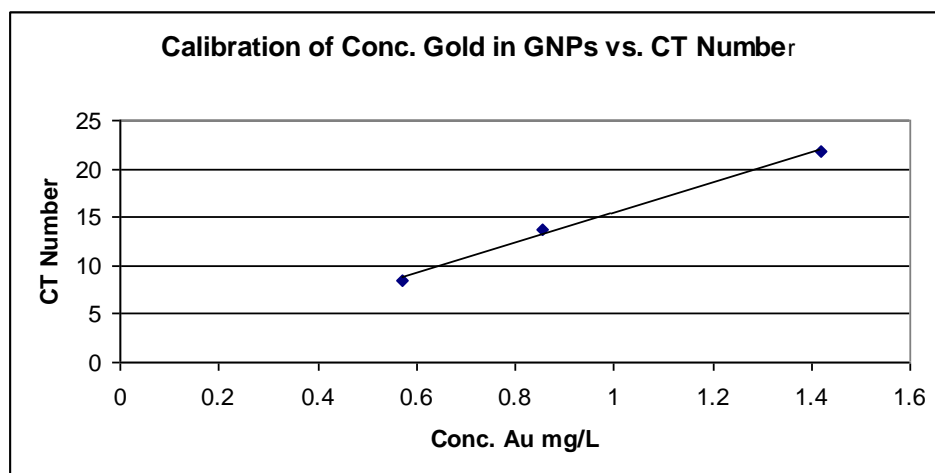


Figure 73. Plot to show CT number for citrate capped GNPs at various concentrations in water.

A CT number of 500 is needed for *in vivo* contrast which would mean a gold concentration of 3700 mg.l⁻¹, indicating the GNPs at the concentrations currently being synthesised, are not suitable. It is possible to remove solvent *in vacuo* to increase the gold concentration but this will prove to be both time consuming and expensive so other options may need to be pursued.

2.3 Determining optimum concentration of SPIO solutions for MRI experiments

As with the CT studies, in order to use the SPIOs for MRI imaging, the optimum concentration of SPIOs functionalised *via* the solvent free method must be found. To do this we first created a calibration graph for concentration vs. NMR relaxation times. Calibration standards were analysed using the 0.25 T MRI MOUSE to determine the T₁ and T₂ relaxation times for each standard. The results are shown in Figure 74 below. T₂ time decreases in a linear manner as concentration of iron increases. Due to limitations of the machine it is very difficult to measure relaxation times that fall below 5 ms. For this reason the optimum concentration was chosen to be between 50 and 250 mg.l⁻¹. Another factor to take into consideration is the quantification of any sedimentation that may occur as the SPIOs fall out of solution, either due to aggregation or pH effects. For this reason, the highest workable concentration was determined to be 250 mg.l⁻¹.

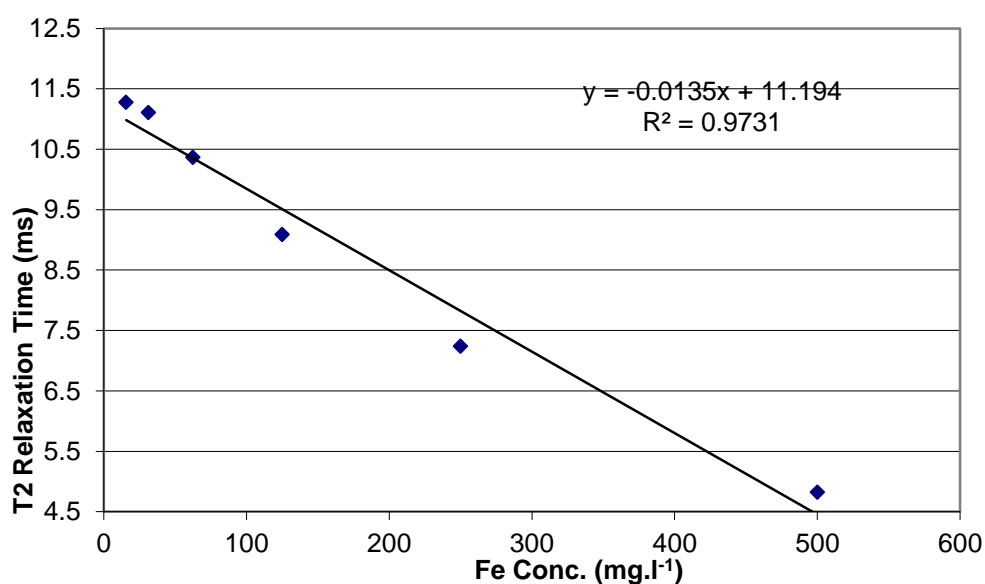


Figure 74. Showing calibration for T₂ with SPIOs from which optimum concentration can be found.

2.4 Lysosome simulation experiment

On entry into the body it is very likely that the particles will be taken up by macrophages as the site of entry, and will be put into lysosomes which have an acidic environment typically used to kill microbes. As has been previously mentioned these kinds of acidic environments can potentially decompose SPIOs, and so it was important to test if the coated SPIOs could withstand these harsh conditions. To simulate the environment that encapsulation in a lysosome would present to a SPIO a buffer solution of pH 4 was used, as this most closely matches the pH inside the lysosome. Within the scope of the project it was not possible to exactly recreate the complete lysosomal environment (enzymes and other chemicals).

Over a period of 6 hours the Histidine coated SPIOs were kept at room temperature in the buffered solution. The degradation of signal is shown in Figure 75. The loss of signal shown is 6×10^{-3} seconds for T_2 . As has been previously discussed, SPIOs are used mainly for T_2 weighted images and so for the purposes of this experiment the T_1 results can be ignored although they also show a minimal change. The small change in signal would not result in any change in image resolution and so it can be concluded that as far as the pH is concerned, SPIOs coated in this way can withstand the conditions and still produce a good signal.

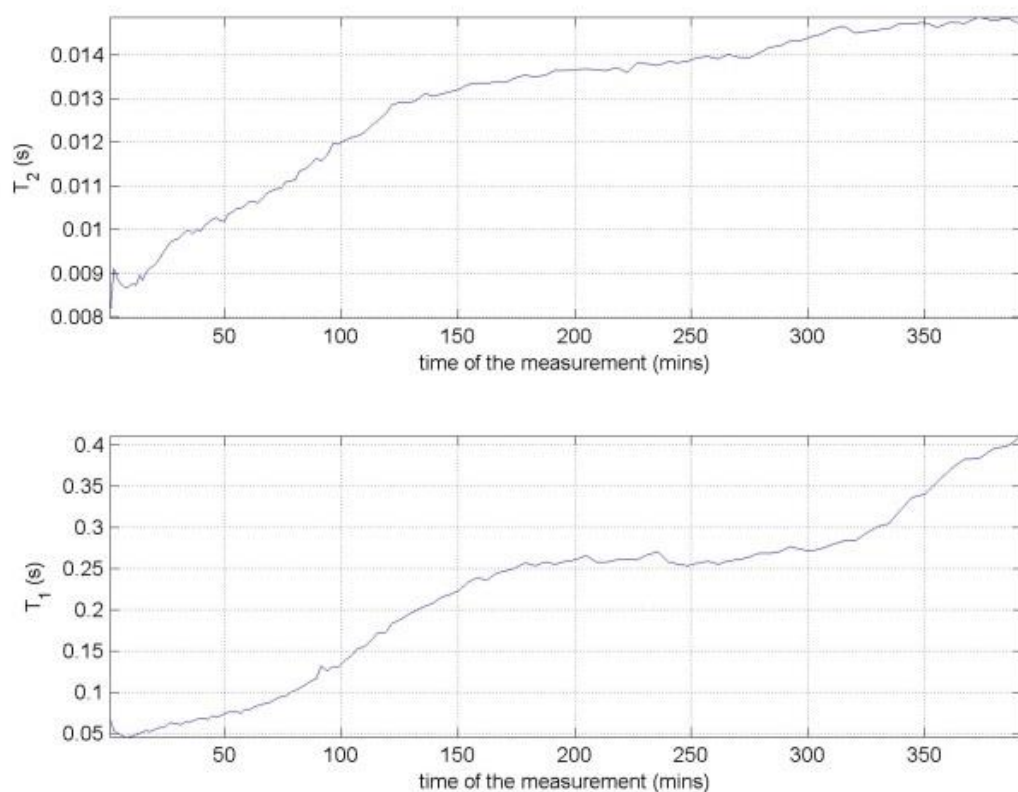


Figure 75. T₁ and T₂ relaxation time lapse study for histidine HCl coated SPIOs in pH4 buffer over a period of 6 hours.

It is generally considered that SPIOs are not suitable for oral administration as an MRI imaging agent due to the degradation they would undergo in the acidic conditions in the stomach. In a similar study at pH 2 it was shown that, again, the SPIOs coated in this manner were not degraded and instead showed good stability over the 6 hours they were studied. (Figure 76).

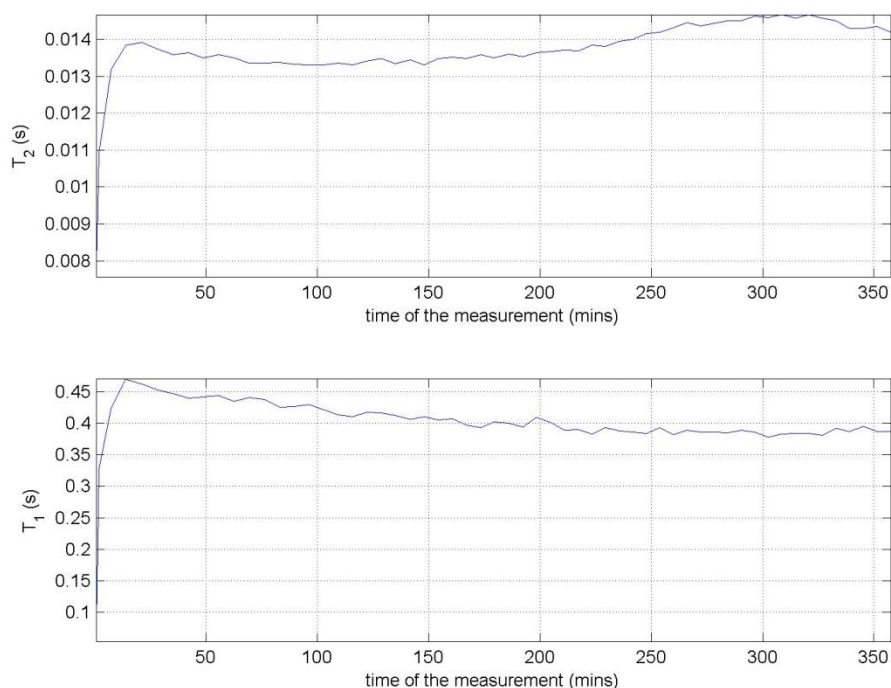


Figure 76. T₁ and T₂ relaxation time lapse study for Histidine HCl coated SPIOs in pH2 buffer over a period of 6 hours.

2.5 Comparison of prepared particles with Endorem[®]

If the SPIOs are to become a commercially viable alternative to current technologies it is essential for them to be able to compete and in some way outperform what is already available. When compared with Endorem[®], both at a concentration of 250 mg.l⁻¹, it was found that the SPIOs had a comparable relaxation effect to Endorem[®] (Table 35), with both T₁ and T₂ relaxation times being very similar. What is of more significance is the observed stability of the particles. Whilst the particles prepared *via* the solvent free grinding method have been shown to be stable as both a powder or solution for a matter of weeks with some handling and exposure to air, it was found that once the vial to the Endorem[®] was opened the solution was very unstable and even in a sealed vial the solid particles dropped out of solution and soon could not be used.

These findings suggest that the coated SPIOs prepared using these methods could be an improvement on the Endorem[®] as it is much more stable and so could have a longer shelf-life

leading to less waste and easier preparation. The particles can also be dehydrated and then rehydrated when required, providing ease of storage and a possible longer shelf-life.

What should be noted is that the dehydrated particles did not completely re-dissolve in water, and that in PBS there were further solubility issues. In PBS the same quantity of SPIO gave a T_2 of 1113.4 ms, which is over 10 times longer than the rehydrated histidine coated SPIOs. This could present problems in a clinical setting, where water cannot be used due to osmotic effects. However, these experiments were carried out using very low concentrations of SPIO and at larger concentrations it is likely that the diluting effects of PBS would be lessened.

2.6 Blood Studies

Before thinking about using these particles *in vivo* it is essential to know how they behave in blood as well as the other physiological solutions that have been previously discussed. When SPIOs were added to blood samples, the results were surprising, with the blood coagulating. It is likely that the ethylenetriaminetetraacetic acid (EDTA) which is present as an anticoagulant preferentially binds to the SPIOs instead of the blood. Without the anticoagulant being active in the blood, the blood is free to coagulate and so the NMR relaxation time is increased due to restricted movement of molecules in the blood. Despite this, the SPIO solution and dehydrated SPIOs led to a significant decrease in T_1 from 1000.2 ms for blood alone, to 62.7 ms with blood and SPIO. There was also a small decrease in T_2 from 11.9 ms to 5.6 ms. This means that SPIOs synthesised *via* the solvent free grinding method would be suitable for T_1 weighted MRI imaging, but do not produce a large enough decrease in T_2 for a T_2 weighted image. However, it is possible that if the blood had not coagulated then the difference in T_2 may have been significant enough to produce a T_2 weighted image.

As different organs in the body have different proton density and so different relaxation times, it is possible that the SPIOs will have a greater relaxation effect on other tissues as it passes through the circulatory system. This would need to be further investigated *in vivo* or using an MRI phantom.

Section 3: Transdermal drug delivery

3.1 Analysis of CPP

MALDI-TOF gave a molecular ion peak with m/z 1661.96. This corresponds to the CPP described in the experimental section, and show below (Figure 77). It would have been beneficial to carry out amino acid sequencing for the peptide but due to the large quantity of Arginine present there were large interference peaks and fragments that could be isolated for sequencing were near impossible to produce. For this reason the only confirmation that the correct peptide was synthesized is the molecular ion peak.

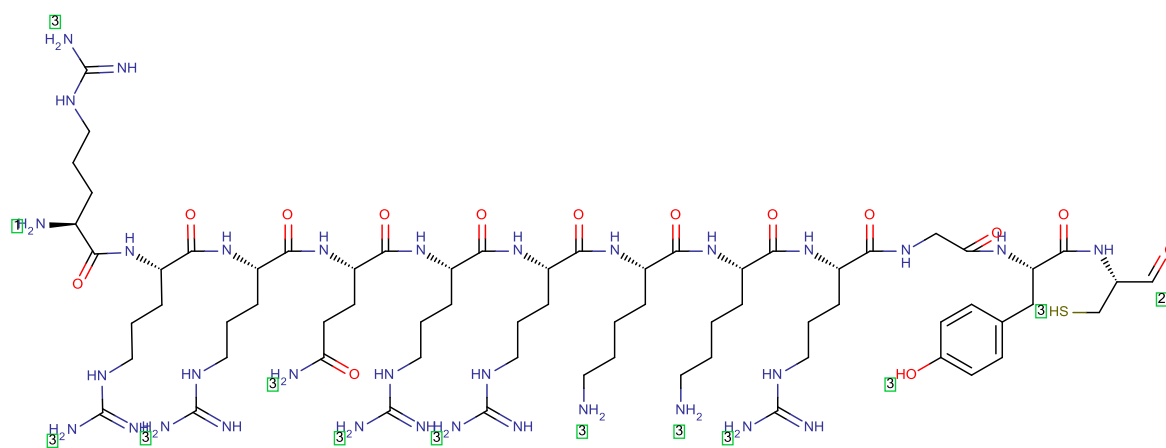


Figure 77. Structural formula of the cell-penetrating peptide

HPLC of the peptide showed a peak accounting for 89.95 % of the sample at 13.22 minutes. As previously mentioned this could not be confirmed by MALDI-TOF due to poor fragmentation but was taken to be the true value as there was a correlation between the main peak HPLC and the molecular ion peak from MS.

3.2 Characterisation of SPIOs coated with CPP

The SPIO-CPP complex was analysed using ICP, TEM and DLS and particles were found to be on average around 50 nm in diameter by TEM and 10 nm in diameter by DLS containing an average of 9.4 mg.l⁻¹ of Fe. Distribution of particles on the grid was sparse and so it was not possible to determine if there was a clear coating area around the particles. However, if the particles had not been coated then they would not have been taken up into solution and so could not be analysed by either ICP, DLS or TEM following microfiltration. This suggests that on drying the particles clump together on the TEM disc to give larger agglomerates of 50 nm. Regardless of the size of these particles, these images and measurements indicate that the particles are within the desired range of 40-60 nm for cell uptake and thus transdermal delivery. These results again confirm the effectiveness of the coating method with peptides.

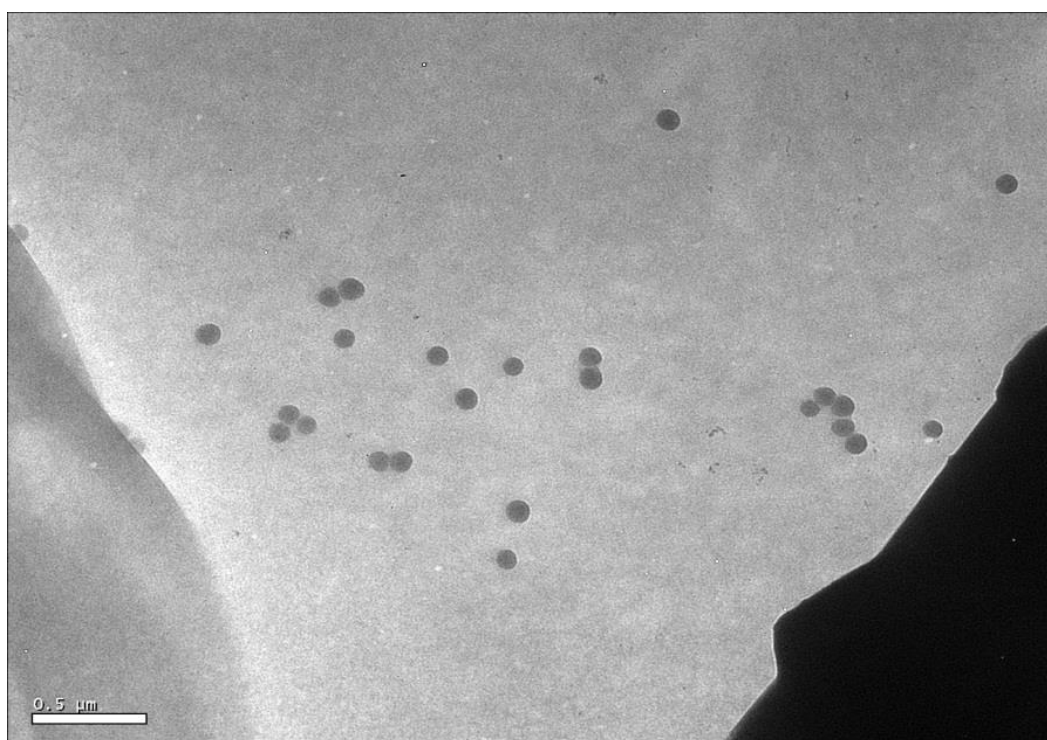


Figure 78. TEM image of CPP coated SPIOs showing diameters of ca. 50 nm.

	Size (r.nm...)	% Number	Width (r.n...
Z-Average (r.nm): 130.5	Peak 1: 11.82	100.0	2.926
Pdl: 0.311	Peak 2: 0.000	0.0	0.000
Intercept: 0.824	Peak 3: 0.000	0.0	0.000

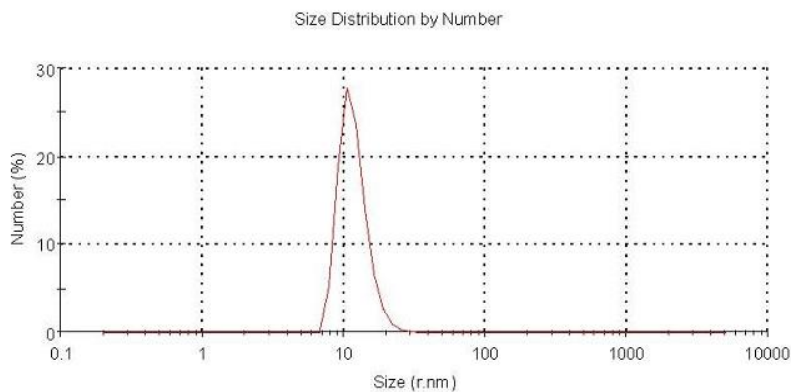


Figure 79. DLS graph indicating CPP coated SPIOs to be ca. 10 nm in diameter.

3.3 Optimisation of conditions for pig skin incubation

After application of the gel preparations it was unclear which methods might be suitable for optimal uptake of gel and preservation of pig skin so several conditions were trialed; on a glass slide at room temperature, glass slide in an incubator at 37°C, glass slide in 50 ml centrifuge tube at 37°C, glass slide in 50 ml centrifuge tube with 10 ml PBS underneath slide at 37°C.

In all but the final condition the pig skin began to curl up at the edge which made performing a depth profile on the MOUSE difficult, and the results unreliable. In some conditions the pig skin also dried out during the incubation period meaning that it would not simulate the real conditions of the skin and thus would not show reliably if uptake would occur. For all experiments henceforth the pig skin was placed on a glass slide which was inserted into a 50 ml centrifuge tube, with the glass slide suspended above 10 ml of PBS (Figure 80), and kept in an incubator at 37°C for the desired incubation time. These skin samples were still warm and moist after incubation, more closely representing a true skin sample.

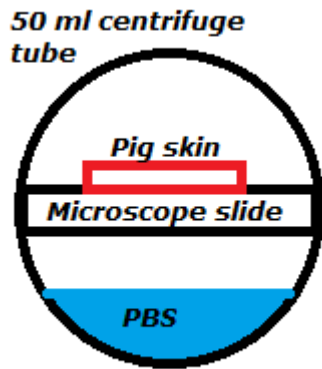


Figure 80. Schematic of optimised pig skin incubation set up.

3.3 MRI Imaging to determine SPIO-CPP uptake

The 2.45 T BIOSPEC imaging system was used to determine if the SPIO-CPP had been taken up by the skin. Following incubation the pieces of skin had been washed in PBS to remove any remaining gel preparations on the surface of the skin. Figure 81 shows the control piece of skin. The large spot shows the position in which the gel was positioned on the skin. This indicates that the gel itself has been soaked into the skin, thus altering its relaxivity. It can be seen that the area of skin without gel has been unaffected during incubation.

Figure 82 shows the same dark red/blue spot at the bottom of the skin where gel alone has been applied in the spot. It also shows a smaller light blue/yellow spot. This is from an area where the same volume of gel was applied but this one containing the SPIO-CPP mixture. This is promising as it shows that the SPIOs, as expected, have reduced the signal intensity of the gel as they have penetrated along with the gel. As the skin has been washed thoroughly prior to imaging it can be concluded that the SPIOs have been able to penetrate the skin along with the gel, indicating that the experiment was a success.

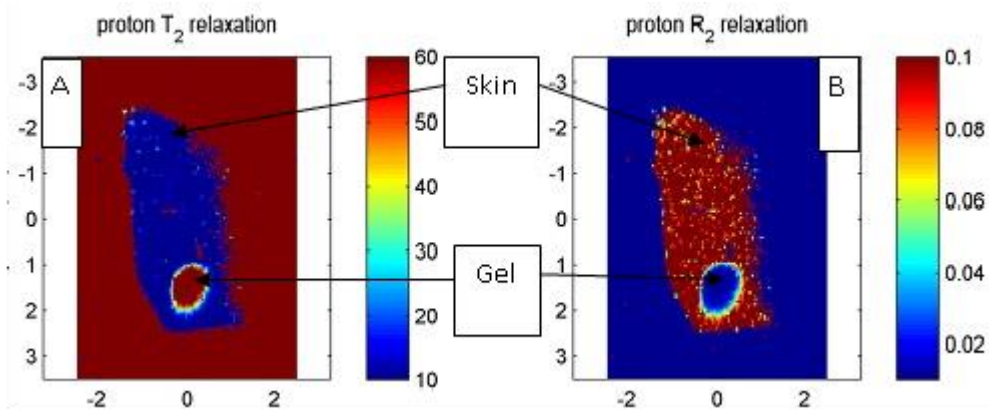


Figure 8150. BIOSPEC Image indicating the position of the gel control on the skin. The large red/blue spot indicates a difference in relaxivity between the skin itself and the area into which the gel has soaked, showing that the gel itself is able to penetrate.

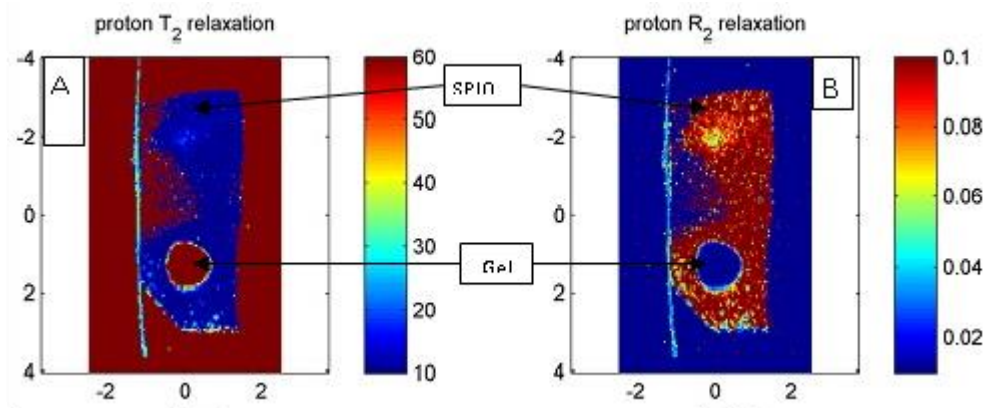


Figure 82. BIOSPEC Image indicating the position of the gel control (blue/red) and further up, the diminished signal from the penetrating gel which contains SPIOs. This image shows that the SPIOs are reducing the image produced by the gel and so must have soaked

To further clarify the success of these preparations in penetrating the skin, further experiments were carried out on the same skin samples, under the same conditions but in this case using the 0.25 T MRI MOUSE. Here the T_1 and T_2 relaxation at different cross sections through the skin, referred to as a depth profile, were measured and these plotted on a graph. The difference in the graphs produced are due to optimisation of the instrument and do not reflect different conditions being used before and after the application of the gel. Figure 83 shows the profile through the skin prior to incubation with the SPIO-CPP gel. Figure 84 shows a profile through the same piece of skin which was treated with gel only. As can be seen, there has been no significant change in signal through the

depth profile and so we can conclude that the gel itself does not cause any difference that can be observed using this type of instrumentation.

However, what we can see from the depth profile for the skin incubated with CPP-SPIO gel preparation (Figure 85), is that there is a marked decrease in signal at 800-1400 μm . This indicates that the SPIO-CPP has penetrated to between 400 – 1000 μm into the skin. This corresponds to a penetration all the way through the porcine *stratum corneum* (20 μm).

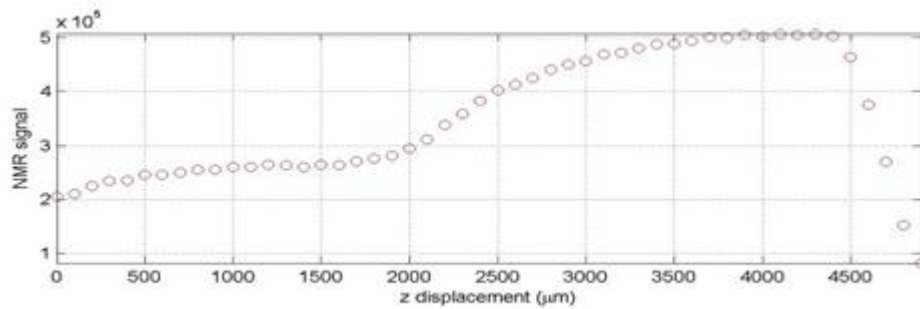


Figure 83. Depth profile showing relaxivity at 100 μm slices through a section of pig skin prior to treatment with any type of gel preparation.

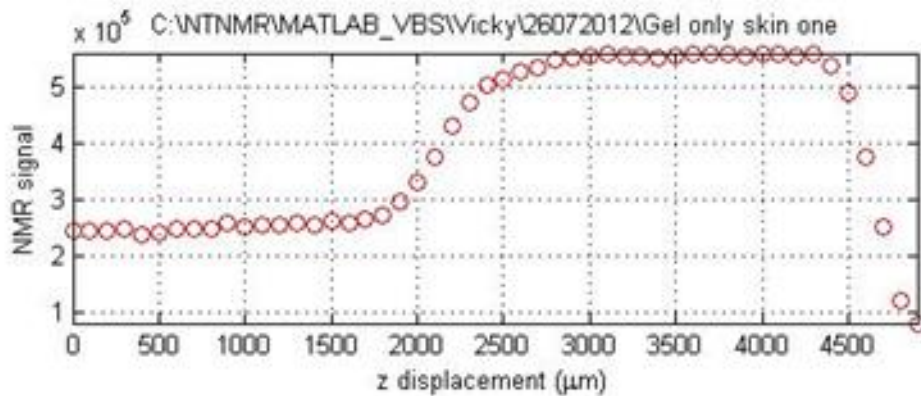


Figure 84. Depth profile showing relaxivity at 100 μm slices through a section of pig skin after incubation with gel only.

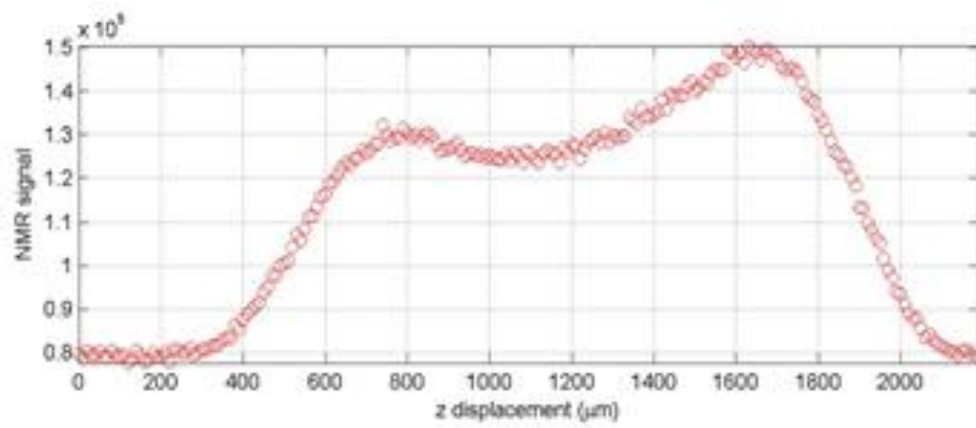


Figure 85. Depth profile showing relaxivity at 50 μm slices through a section of pig skin after incubation with SPIO-CPP

Section 4: Immunotherapy

4.1 Synthesis of peptides

4.1.1 Optimisation

Through repeated synthesis of p53(108) it had been found that purity was variable and often lower than expected. Peptides whose synthesis was interrupted by storage in the freezer between couplings were found to have much lower purity than those synthesised without stopping. This could be due to the beads shrinking during storage and not successfully swelling before continuing synthesis. This means that many of the peptides would not be sufficiently exposed to the reagents and so reaction would be stopped, leading to some deletion sequences. It could be assumed that a second swelling step prior to continuing synthesis would overcome this problem. However, despite trialling a second swelling step the purity continued to remain low (*ca.* 40 %) so it was concluded that peptides should be synthesised from start to finish without stopping.

Certain amino acids are known to be problematic in terms of coupling. A suggested solution to this is longer coupling times for these amino acids, such as 10 minutes at 50 °C rather than 5 minutes at 75 °C for histidine and cysteine, and two couplings for arginine (30 mins room temperature followed by 5 minutes at 75 °C). Using this approach it was decided that longer coupling times could be of benefit for increasing purity of peptides known to give low purity such as p53(108). So, for all amino acids the coupling times were doubled, with the exception of the 30 minutes at room temperature for the first addition of arginine.

The peptides were analysed by HPLC (Figure 86 and 87) and those synthesised using regular coupling times were found to have lower yield and purity than those synthesised using longer coupling times.

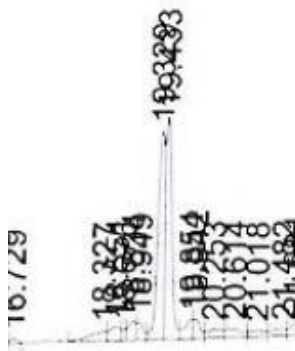


Figure 86. Showing a section of the HPLC graph for p53(108) synthesised using standard 5 minute coupling times, indicating purity of ca. 45 % (MS results were in agreement)

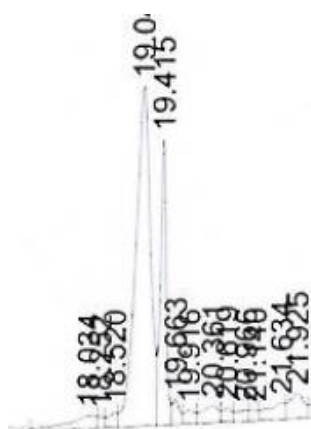


Figure 87. Showing part of the HPLC graph for p53(108) synthesised using longer coupling times and without long gaps between couplings, indicating purity of ca. 75 % by HPLC (MS results were in agreement).

4.1.2 p53(108)

For the desired application of SPIOs for cancer immunotherapy adjuvants, it was important to choose a peptide that was being used in current research. The John van Geest cancer research group were using this peptide and were in the process of developing a tumor model for it during the

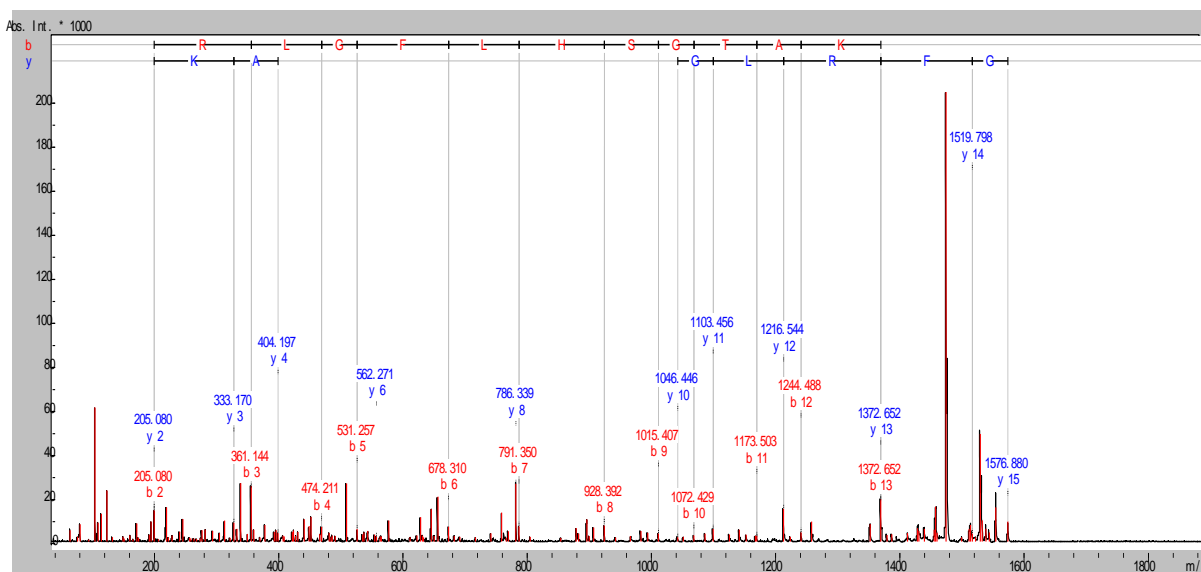


Figure 89. MS-MS results showing the molecular ion at 1576.880, and the fragments formed from this peak proving that the correct peptide had been formed.

4.1.3 p53(105)

p53(105) (Figure 90) was synthesised *via* SPPS and analysed by HPLC.

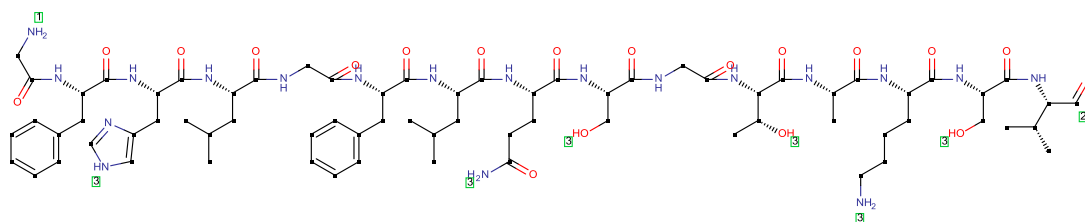


Figure 90. Structural formula of p53(105) (Mass: 1547.81 g.mol⁻¹).

HPLC on the sample was carried out as in general experimental. There was a peak at 30.206 minutes corresponds to p53(105), with this peak accounting for 71.23 % of the total product injected onto the column. Unfortunately the zip tip preparation could not be carried out for MS and so there are both Na and K adducts of the peptide present in the spectra making it difficult to determine purity of the peptide alone. However, by combining the Na and K adducts along with the peak for the peptide alone the total comes to 53 % supporting identification of the HPLC peak at 30.206 minutes

corresponds to p53(105). For the purpose of the rest of the experiments using p53(105) the purity was taken as 70 % by HPLC.

4.2 Checking immunogenicity following recrystallisation

In order to determine if the p53(108) was still immunogenically active following recrystallisation with hydrochloric acid and also in part to check whether or not the peptide had been successfully synthesised, it was tested against the commercially purchased peptide *via* ELISPOT using spleenocytes from DR1 mice (kept in sterile conditions – *barrier*, conventional conditions – *conventional*, and taken from the barrier into the conventional – “barrier-conventional”) previously immunised with the commercially bought peptide. The results are shown in Figures 91 and 92.

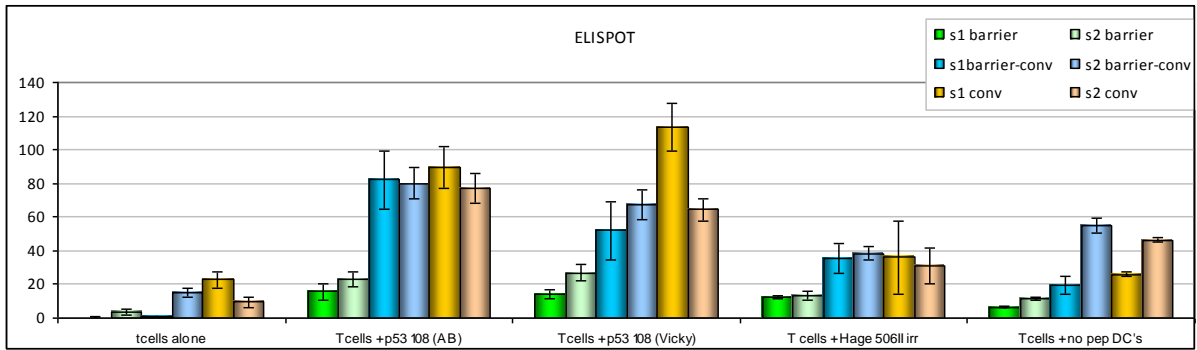


Figure 91. Complete ELISPOT results for all conditions of mice for checking immunogenicity of recrystallized peptides. The left hand bars are for T cells without any stimulating agent or DCs. The second set of bars shows the number of spots when the T cells are re-stimulated with the DCs that have taken up the commercial p53(108). The third set of bars shows the number of spots when the T cells are re-stimulated with DCs that have taken up the recrystallized p53(108). The fourth set of bars shows the number of spots when the T cells are re-stimulated with DCs that have taken up a non-specific peptide to which they should not show an immune response. The final set of bars shows the number of spots when the T cells are re-stimulated with DCs that have not taken any peptide up. Each differently coloured bar represents a different mouse immunised. X-axis shows number of spots.

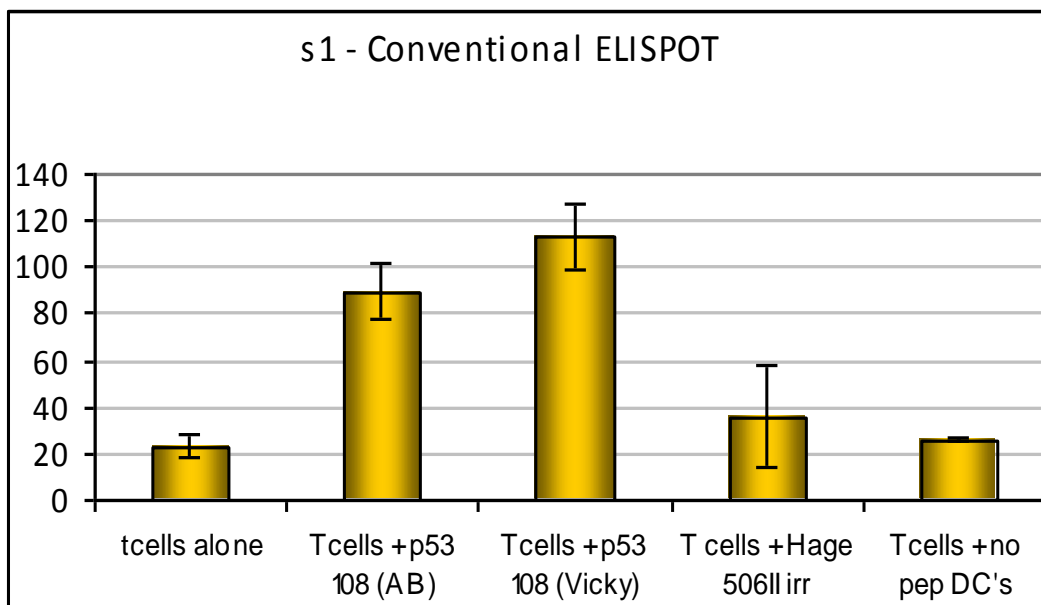


Figure 92. ELISPOT results for mice kept in the conventional conditions showing a higher response for the processed peptide (p53 108 (Vicky)) than for the commercially bought peptide (p53 108 (AB))

These results show that the recrystallized p53(108) produces an immune response when used to stimulate spleenocytes from mice immunised with commercially bought p53(108), and this response is significantly larger than that for the irrelevant peptide. This is promising as it shows that the recrystallization process does not affect the immunogenicity of the peptide and so for sparingly soluble peptides it could be a suitable option to use this method to increase attachment to SPIOs or even solubility in general.

4.3 Formation and analysis of SPIO-Peptide Complexes

Peptides contain a number of side chains and groups that could potentially bind to SPIOs. The p53(105) used in the immunology studies contains many amine and hydroxyl side chains along with its terminal carboxylic acid and amine; groups like this have been shown to bind well to the surface of the positively charged SPIOs. On recrystallization the binding of the peptide to SPIO improves as has been previously discussed, so that the particles coated with peptide can easily be taken up into both water and DMSO (used to solubilise difficult materials prior to injection). The iron content of the particles by ICP was found to be 15.03 mg.l^{-1} for 3 mg of the powder dissolved in 6 ml of water. This means that the iron content of the particles can be calculated as follows:

$$15.03 \text{ mg.l}^{-1} \therefore 15.03 \div 1000 \times 6 = 0.090 \text{ mg}$$

$$\text{Moles Fe} = 9.0 \text{ e}^{-5} \div 56 = 1.61 \text{ e}^{-6}$$

$$\therefore \text{Moles O} = 1.61 \text{ e}^{-6} \div 3 \times 4 = 2.14 \text{ e}^{-6}$$

$$\therefore \text{Mass O} = 2.14 \text{ e}^{-6} \times 16 \times 1000 = 3.43 \text{ e}^{-2} \text{ mg}$$

$$\text{Mass of SPIO} = 3.43 \text{ e}^{-2} \text{ mg} (.0343 \text{ mg})$$

This means that the remainder of the 3 mg of sample is made up of peptide which gives 2.97 mg p53(108). As it is difficult to control the content of iron, the experiment was controlled by mass of peptide, and so the SPIO-peptide was dissolved to give 10 mg/ml of peptide. This technique was also used to successfully quantify the mass of peptide in the SPIO-peptide complex used for p53(105) immunisations.

This technique is beneficial as it allows control of peptide concentration. However, as there is the possibility of free peptide in the mixture it is difficult to fully assess the effectiveness of the SPIOs in

any application as ideally all peptide present would be bound to SPIO. Due to equilibrium effects some peptide will always be free in solution due to dissociation, but this could be greatly reduced by further development of a suitable separation step. The centrifugation process looks like the most promising option but further experimentation would be required to develop this fully.

4.4 U937 Uptake Study

In order for the coated SPIOs to be used successfully in cancer immunotherapy it must be possible for them to be engulfed by phagocytes. To this end the cell line U937 was selected and used for some preliminary studies. The cells were incubated with the SPIOs coated with histidine.HCl, as described in the experimental section before analysis to determine if they were indeed taking up the SPIOs.

T_1 and T_2 relaxation times of the cells following incubation was measured and results indicated an anomaly with the cells incubated for 1.5 hrs and also that the concentration of SPIOs in the cells is too low to be detectable using this low field MRI (Figure 93).

As the uptake of SPIO could not be determined by MRI the cells were digested in nitric acid and diluted for ICP analysis as displayed in Figure 94.

The results show a general trend, with the amount of iron in the cells following incubation being higher than in the control cells; however, there are large fluctuations so results are inconclusive. The result was much more exaggerated in the repeat experiment when experimentation had been optimised, however in this case only two samples were successful and so again results are inconclusive. Combining the sets of results together, there is a general increase in the concentration of iron with increased incubation times although the difference between the times is very small. This would need further investigation in order for any conclusive results to be drawn. Saying this, it was decided on the limited evidence that the optimum incubation time for further experiments should be 2 hrs.

To increase the reliability of this study an NMR with a larger magnetic field could have improved the sensitivity to SPIOs inside the cells and so produced valid results. The MRI and ICP-AES results in

combination would have been preferential. Alternatively using a Prussian blue would have allowed quantitative results by colorimetry, for how much SPIO had been taken up into the cells. Unfortunately at this point in the experiment the cells had been destroyed through digestion in nitric acid and so this was not possible.

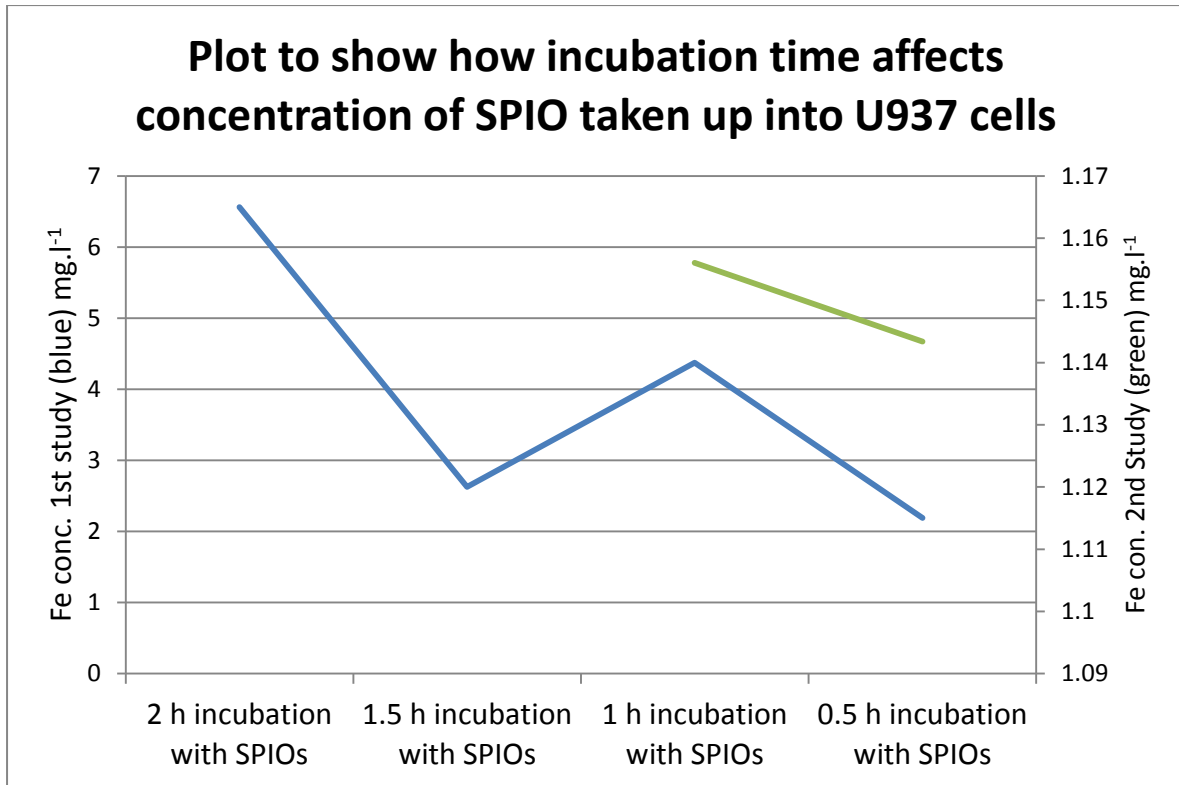


Figure 93. Plot to show iron concentration in U937 cells incubated with SPIOs *Cells with media only have an average Fe conc. of 0.818 mg.l-1

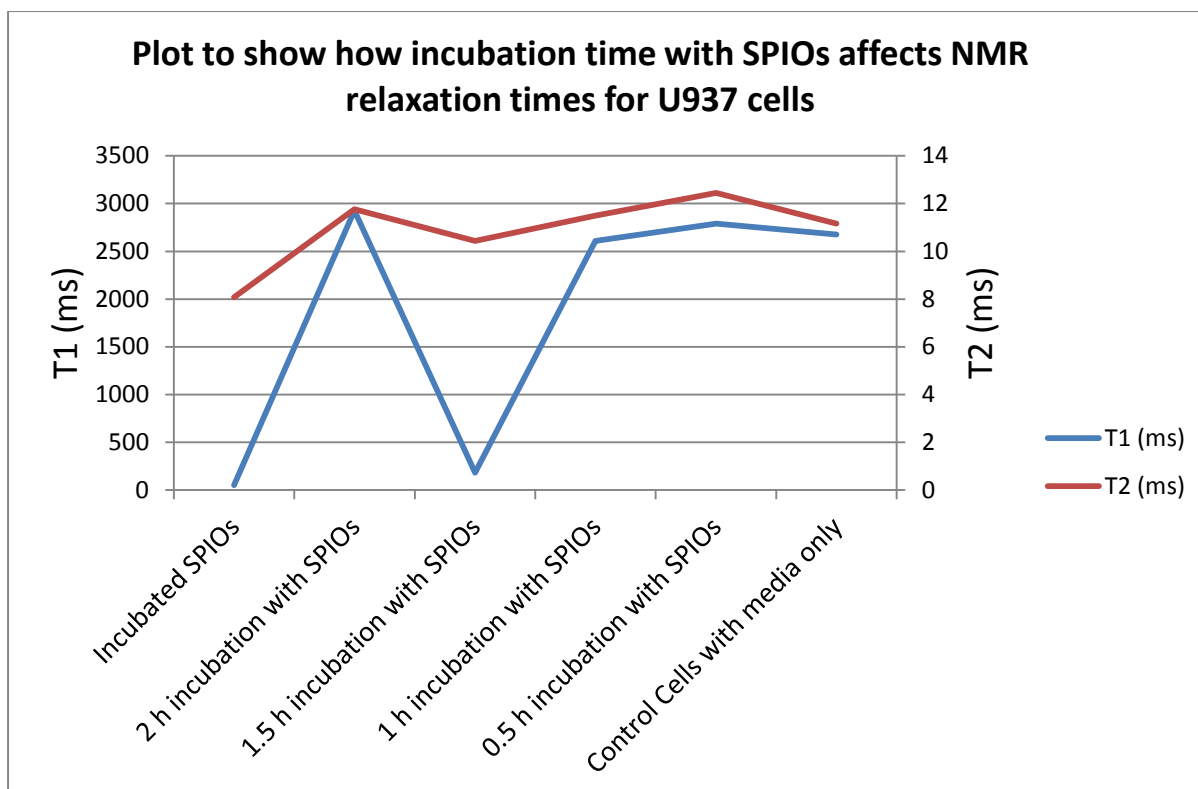


Figure 94. Graph to show NMR relaxation times for U937 incubated for varying times with SPIOs

4.5 Investigation into uptake of coated SPIOs by bone marrow dendritic cells (BMDCs)

4.5.1 Culturing of BMDCs

Moving the studies on from simple uptake studies *in vitro* we moved on to test the SPIOs using dendritic cells from mice with humanised immune systems. For the first stage of this BMDCs were harvested from mouse bone marrow and cultured as described in the General Experimental section. Figure 95 shows a light microscope image of BMDCs grown as described. These were adhered to the well plate, as confirmed by their elongated shape. The fact that these cells are adhered means they are alive and healthy; unhealthy or dead D's do not adhere to the plate and so are not elongated. This is essential for the uptake study as the membranes of these cells change as they become unhealthy and cell death occurs. These cells were grown from cells isolated from mouse hind legs, and so were part of an impure population as illustrated in Figure 96 which shows the BMDCs to be only *ca.* 45 % of the total population. In order to obtain a pure population the cells were passed

through a CD11c+ MACS column in subsequent experiments. By ensuring a pure population the accuracy of the results is increased, ensuring any results are specific to BMDCs.

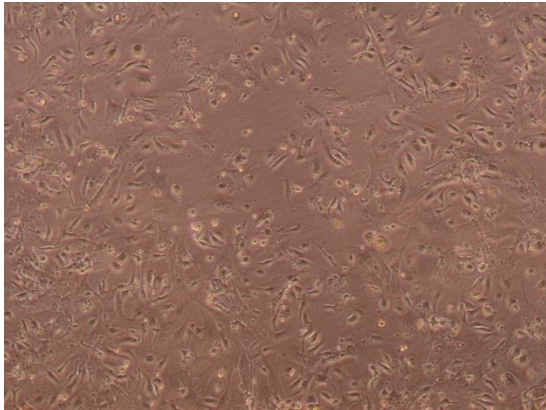


Figure 95. Light microscope image of adhered BMDCs

CD11c+ population in BMDC

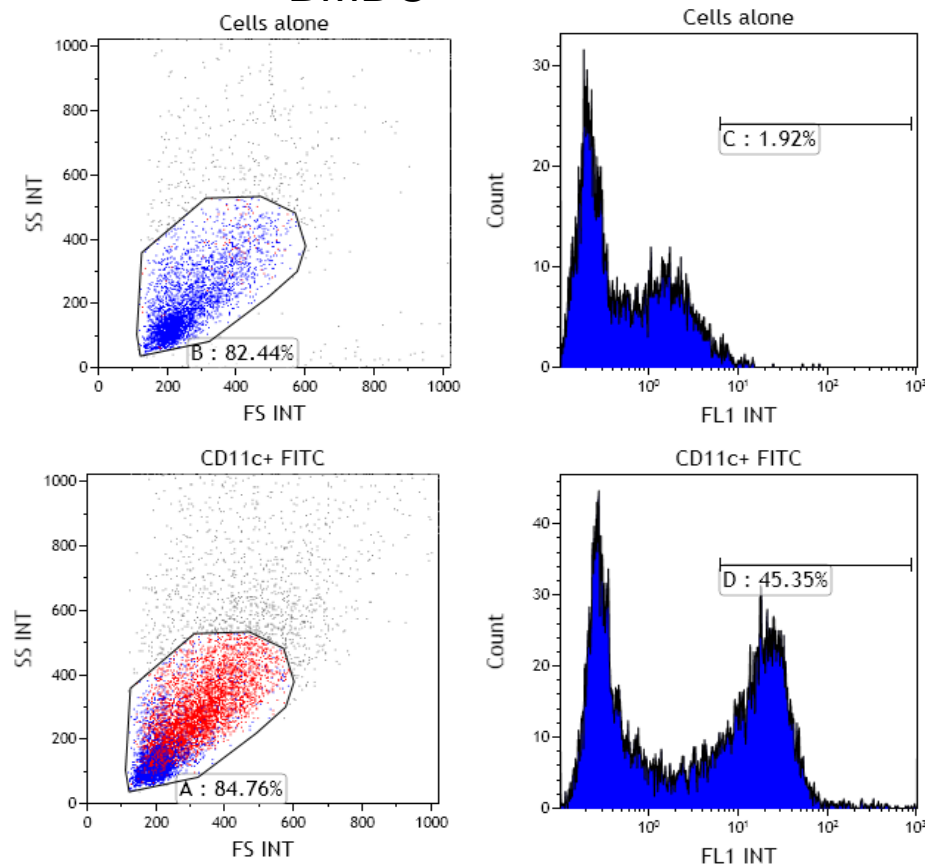


Figure 96. FACS data showing population of BMDCs prior to purification using CD11c+ column.

4.5.2 Culture of BMDC's on different types of plate

Before it was viable to take the immunology section to the next stage it was essential to get some reliable results on a slightly larger scale. However, whenever any attempt was made to culture BMDCs a very small impure population was found. This hampered results as repeats and statistical analysis was not possible on a such a small number of cells. The suggestions for overcoming this problem were i) to grown the cells on different plates and ii) to grow the cells in T25 flasks which could be vacuated using a cell scraper rather than a pipette tip, thus reducing the chance of killing cells during the scraping process.

Three different plates were trialled: Normal coating, amine coating and carboxyl coating. At first glance the results seem to indicate that the carboxyl coated plates are much better for growing BMDCs (Figure 97). However this may not mean a larger quantity of BMDCs as the number of any type of cell grown on the carboxyl plates is larger than for the normal or amine plates. It is logical to assume there will be more BMDCs overall, as the total number of cells is much larger and so if the % population of BMDCs remains the same regardless of plate then the number of BMDCs should increase with increasing cell number. This is confirmed when the data is normalised (i.e. the number of BMDCs is divided by the total number of cells for each plate). The graph in Figure 98 shows that the relative number of BMDCs overall is not higher on the carboxyl plates than for any of the other plates and in fact for plate 1 the normal plate has more BMDC's present on it than the carboxyl plate.

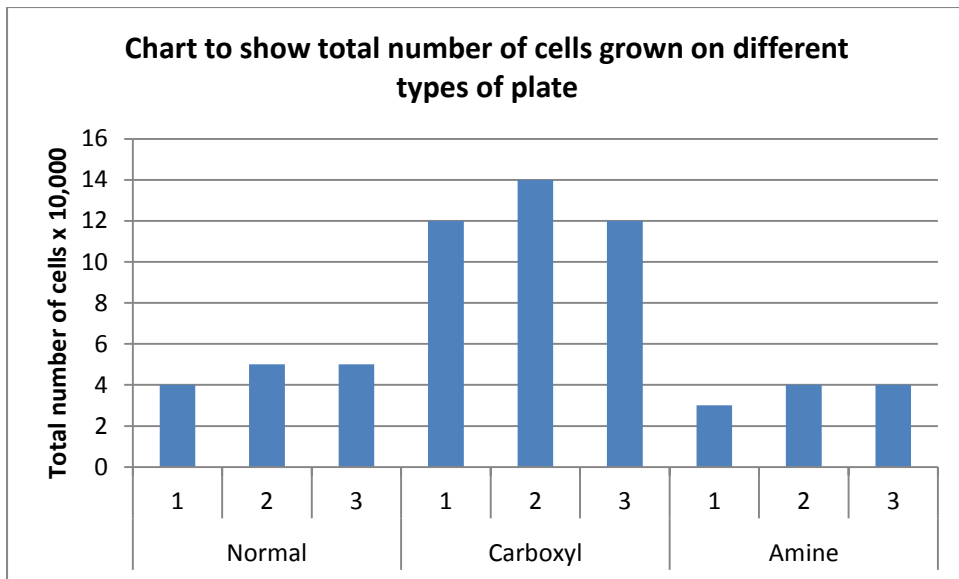


Figure 97. Graph to show difference in total number of cells grown on different types of plate.

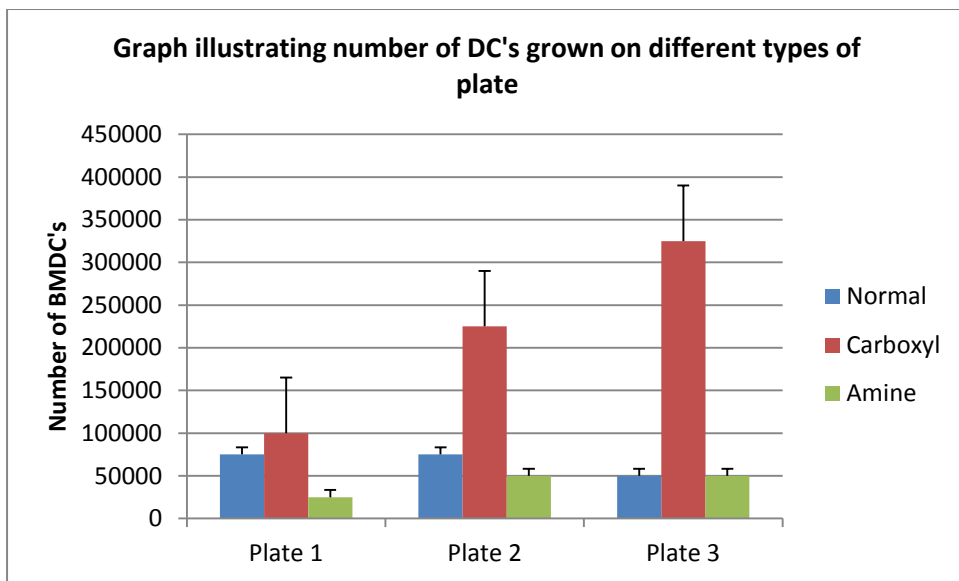


Figure 98. Graph to show total number of BMDC's grown on different types of plate.

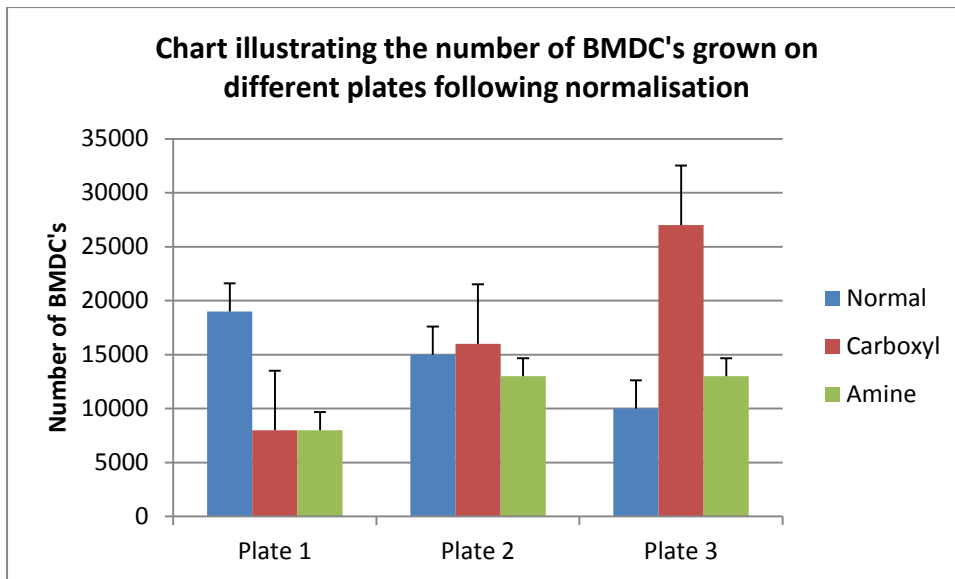


Figure 99. Graph showing normalisation of number of BMDC's grown on different plates relative to total number of cells grown on plates.

T Test	
Normal vs Carboxyl	0.173
Normal vs Amine	0.225
Amine vs Carboxyl	0.094

Table 5. T Test results showing no significant difference between the number of BMDC's on different plates following normalisation.

Statistical tests carried out on the number of BMDCs following CD11c+ isolation (Table 5) indicates that there is no significant difference between the results obtained from the different plates, however there were significantly more cells overall on the carboxyl plates relative to the normal plates and amine plates ($p = 0.005$ and $p = 0.004$ respectively). A possible explanation for the overall increase in the number of cells may be that they adhere better on the carboxyl plates and so fewer cells are lost during the washing steps. This would require further investigation but in the meantime carboxyl plates can be used to generate more cells overall.

4.5.3 Uptake results

Whilst the preliminary results into uptake of coated SPIOs by U937 cells were reasonably successful, it was not repeated enough times to make it reliable. It was also not possible to determine if the SPIOs had actually entered the cell and so further investigations relying on coating of SPIOs with a peptide containing fluorescein, were carried out. Here we incubated the SPIOs with BMDCs and observed them under the microscope following the 6 hour incubation process.

BMDCs were isolated, cultured and incubated with SPIO-peptide complex, and uptake of the complexes determined by fluorescence microscopy with DAPI stain being used to highlight the nucleus of the cell and the presence of FITC (green stain) inside the cell being used as the positive result.

These images (Figure 100) clearly show the nuclei of the cells, with the blue nuclear stain (DAPI) highlighting them in the image. What can also be seen is the green colour of the fluorescein, which is attached to the peptide, in some of the cells. This colour spreads out to the edges of each cell that it is present in, picking out the shape of the cells. It could be assumed that this confirms that the peptide has been delivered into the cell, however fluorescein has a tendency to stick to the outside of the cell membrane.

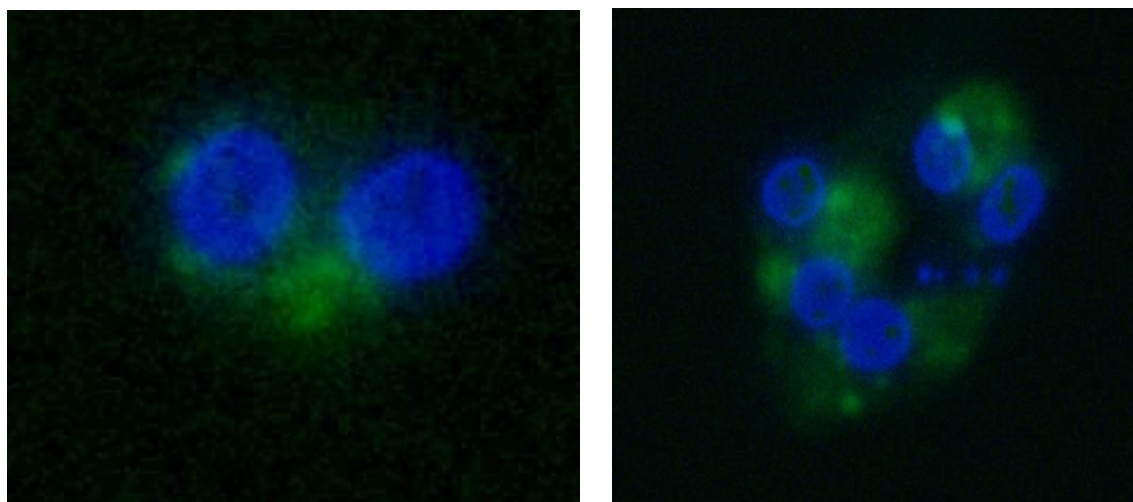


Figure 100. Fluorescence microscope images of cells incubated with SPIO-peptide where peptide has been synthesised with fluorescein at the end. Blue colour is nuclear stain DAPI and green colour is FITC attached to peptide.

One of the conditions in this experiment was the p53(108) peptide-fluorescein without SPIO attached to it. If binding was occurring on the outside of the membrane only, then this would happen irrespective of whether SPIO was bound to the peptide or not. What was observed was that in this condition there was not a single cell observed that exhibited the green fluorophore.

The green colour was only observed when both p53(108) peptide-fluorescein and SPIO were present. This suggests that the p53(108) peptide alone cannot enter the cell, but with the SPIO acting as a vector entry is possible. This is promising for applications such as vaccinations, as uptake of antigens (in this case the peptide is the antigen) is essential for a full immune response.

The uptake of these complexes is most likely occurring due to the optimal size of the SPIO-peptide. As seen in TEM images, the longer peptides such as p53(108) form small clusters of particles that have a diameter in the range of 40-60 nm. As has been previously mentioned, the literature suggests that 50 nm is the optimum size for a particles to be engulfed by endocytosis as it is neither too small to be energetically favourable, nor too large to be too sterically restricted.

4.6 Maturation of BMDC's using SPIOs

Whilst it was not the primary aim of the experiment, it was decided that the SPIOs would be tested for their ability to induce maturation of the immune cells. Following incubation with SPIO-p53(108) peptide complexes, maturation of DCs with and without lipopolysaccharide (LPS) was monitored using fluorescence microscopy with the red stain phycoerythrin (PE) being used as a positive result.

During the majority of studies using BMDC's Poly-IC and LPS are used to mature BMDC's. This is necessary to activate the BMDC's to produce the required signalling molecules to illicit an immune response, and must be carried artificially *in vitro* as it would usually occur in the lymph nodes. Using the cell marker CD86 the possibility that SPIO-peptide preparations, or more SPIOs themselves, might be able to induce cell maturation was explored.

What was observed was a very small number of cells that had been fluorescently labelled by the red fluorophore (PE) but many with the blue nuclear stain (DAPI) was still visible, showing the location of cells on the slide (Figure 101). This indicates that there were very few cells that had matured to express the CD86 molecule, and so it is not possible to confirm whether or not the SPIOs caused maturation. Given the small numbers it is possible that another factor such as maturation prior to isolation, or maturation due to an impurity in any of the media or reagents was responsible. Bearing

this in mind, this experiment should be repeated with larger numbers of cells and higher concentrations of SPIO.

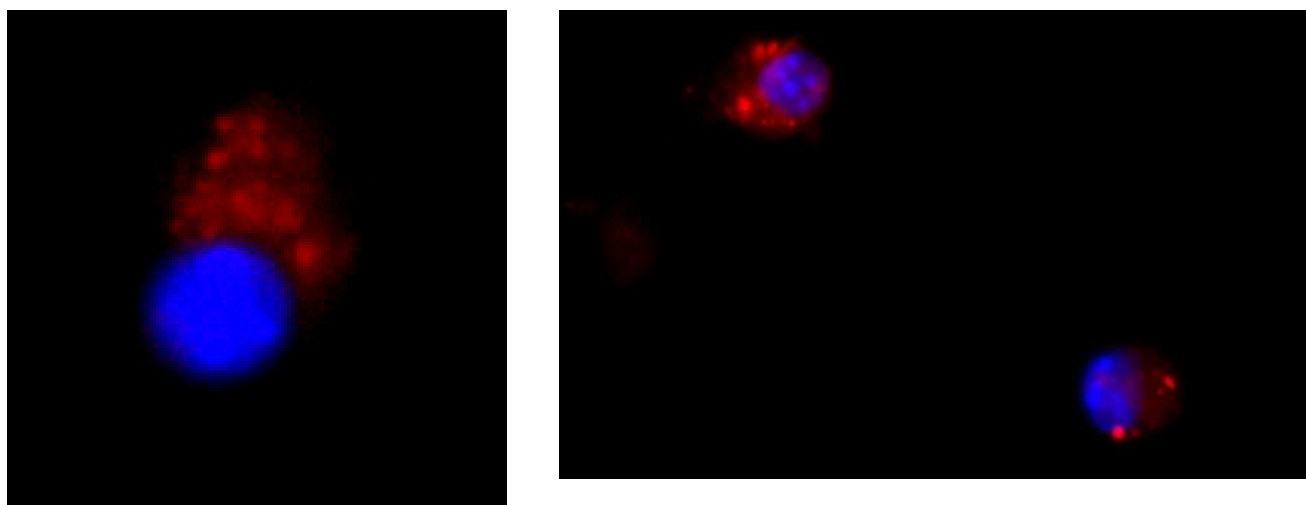


Figure 101. Cells incubated without LPS but with p53(108)- SPIO complex at 50 $\mu\text{g} / \text{ml}$. Blue colour indicates the nuclear stain DAPI, and red colour indicates CD86 linked to the red stain PE.

4.7 Cytotoxicity Assay

If the particles are to be successfully applied to biomedical applications then it is of the utmost importance that they are not toxic to cells in the doses in which they will be administered. Simple cytotoxicity assays looking at the viability of cells after incubation with the coated SPIOs was carried out in the hope of proving that the particles were benign. The results of the cell count showed all conditions to contain similar numbers of cells after incubation from the same original cell count of 250 000 cells (Table 49) with the mean cell count being 1.24×10^5 cells with a standard deviation of 3.97×10^4 . So, it can be deduced that the complexes have little or no toxicity to cells. However, this study was carried out using an impure population of dendritic cells and so all cells present will be taken into account. Also, this method only takes into account complete cell death, ignoring cells undergoing apoptosis, and so could be painting an incomplete picture of how harmful the preparations are. In future studies markers for cells that are undergoing apoptosis but have not yet died should be used, such as those in the Annexin V kit. This will give a more complete picture of the cytotoxicity of these compounds.

4.8 Quantum™ FITC kit

Quantum™ FITC MESF (Molecules of Equivalent Soluble Fluorochrome) beads are microspheres that contain a known quantity of fluorescent molecules, in this case fluorescein isothiocyanate (FITC). As there is a known quantity it is possible to use the intensity of their fluorescence along with the known concentrations to create a calibration graph from which it is possible to determine the concentration and so quantity of fluorescent molecules within cells. The beads for the Quantum™ FITC MESF kit were diluted as directed, and the graphs below created from these standards using a fluorescence assisted cell sorting system. This was going to be carried out on a culture of BMDCs that had been incubated with either fluorescent peptide and alone or fluorescent peptide attached to SPIO, as a measure of how effective the SPIOs are as vectors. As the peptides, namely p53(105) and p53(108) have been synthesised with a 1:1 ratio of peptide to fluorescein it would be possible from the concentration of fluorescein to determine the concentration, and so number of peptide molecules within a cell. This would be a useful tool for studying immunology, as the number of molecules taken into a macrophage may have an effect on the type of immune response and whether or not long-lived T-Cells are formed.

Unfortunately due to problems during cell culture it was not possible to carry out any measurements on the cells themselves. Due to time constraints there was not an opportunity to repeat the cell culture and conclude how effective a vector the SPIOs are. However, Figure 102 shows the initial calibration graph created that could have potentially been used to determine the average number of peptide molecules in each cell.

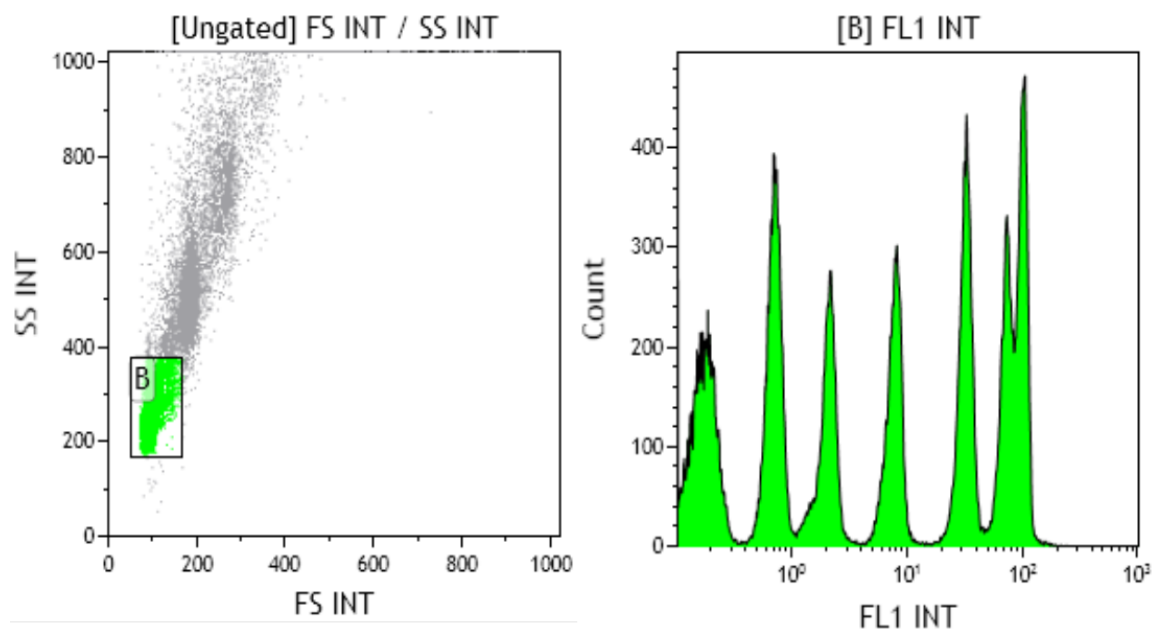


Figure 102. Quantum FITC MESF 5 Kit preliminary calibration results

4.9 Mouse immunisations with p53(105) SPIOs

Mice were immunised with either p53(105) in the adjuvant IFA or with p53(105)-SPIO complex. As has been discussed it is very difficult to find adjuvants that enhance the immune response to weak antigens without creating side effects. SPIOs are FDA approved and degrade in the body to produce iron ions which can be used to make haemoglobin, and so if they could be used as adjuvants these properties would be beneficial. The aim of the immunisations was to determine if SPIOs could be used as an adjuvant and if so, could they produce a stronger immune response than the current alternative, in this case IFA.

Following immunisations the splenocytes were harvested and analysed by ELISpot, with the spots being counted using a C.T.L. Immunospot counter. The counter was calibrated to only take into account spots of a certain darkness, so as to avoid false positive results. Figure 103 and 104 shows the key findings from this experiment, and the T Test results shown in Table 6 which show whether or not the results are significantly different.

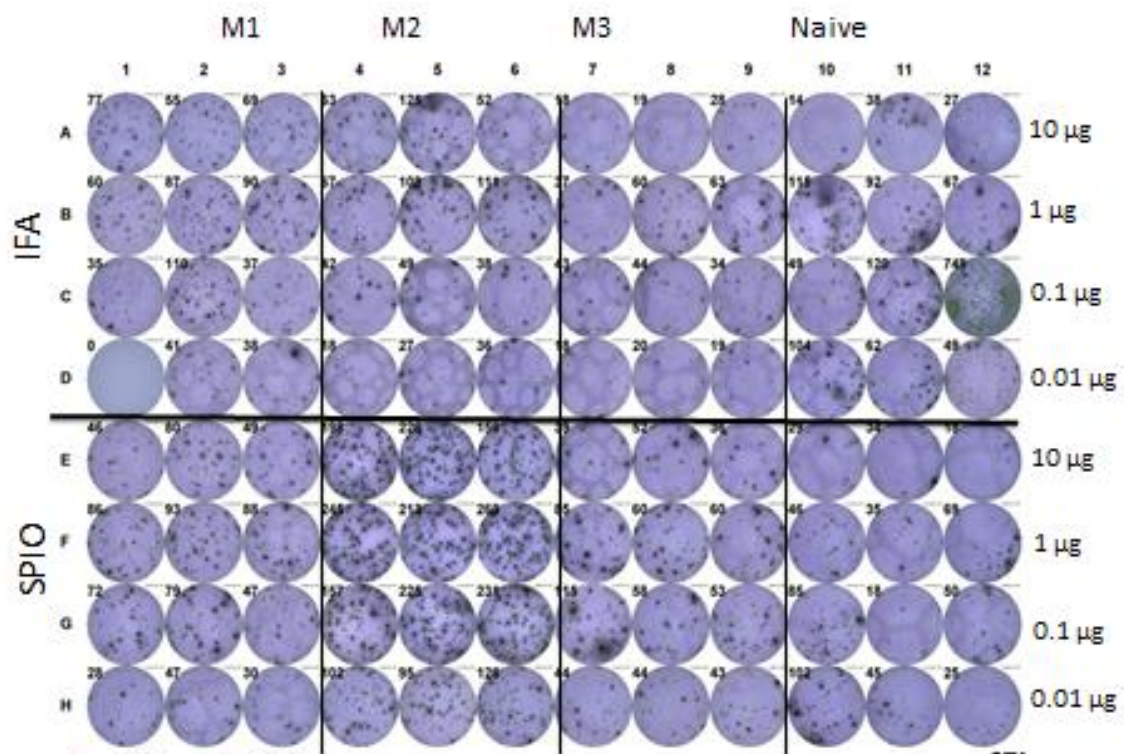


Figure 103. Photograph of ELISPOT plate showing spots for each positive result

From this image it appears that there has been a much larger immune response in the second mouse, specifically to the p53(105) complex at 0.1, 1 and 10 µg of peptide, as shown by the much darker colour of the wells in question due to a larger number of spots. Each spot indicates one antibody that has been produced that is specific to p53(105) showing that immunisation has been effective. There are inconsistencies elsewhere in the plate but here each well shows a large increase. This is the first piece of evidence to suggest that the SPIOs are a suitable vector for delivery of immunogenic peptides.

This graph (Figure 104) also supports those results, with the peaks for Mouse 2 immunised with peptide-SPIO showing a much larger immune response than all of the other mice. However, it should be noted that this same large immune response has not been exhibited by either Mouse 1 or Mouse 3 with respect to the peptide-SPIO immunisations, and so it may be that the results for Mouse 2 are due to chance.

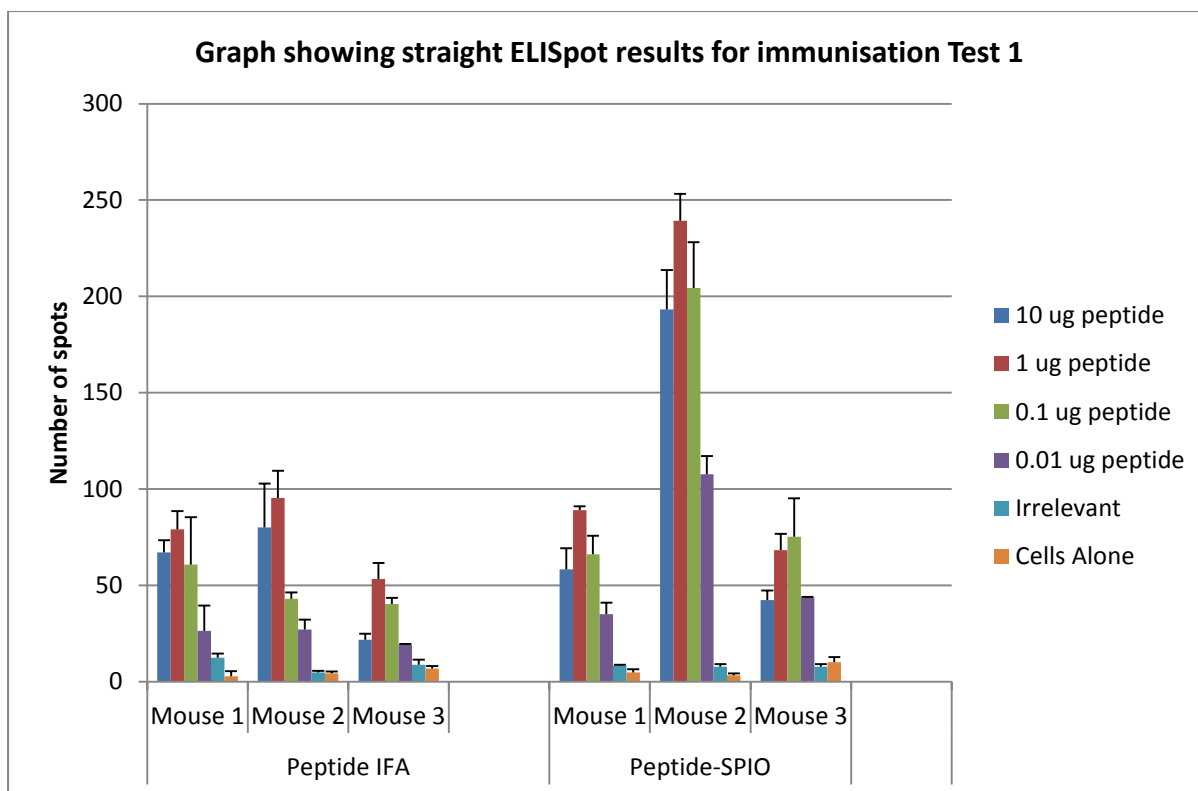


Figure 104. Graph showing the results for comparison between IFA and SPIO as vectors for immunisation with p53(105)

T Test	Mouse 1	Mouse 2	Mouse 3	Naïve
10	0.33158	0.009071	0.103424	0.935651
1	0.176351	0.021035	0.459788	0.200283
0.1	0.812606	0.020873	0.199917	0.716
0.01	0.247561	0.00656	0.00073	0.157834

Table 6. T Test results for immunisation showing difference between IFA and SPIO as vector.

The T Test results indicate that overall there is no significant difference, in either direction, between the SPIOs and the IFA, although there is a significant different for M2, in favour of mice immunised with the SPIO complex. This result was matched when the experiment was repeated, with there being no significant difference in the immune response from either type of immunisation.

Whilst this does not show the desired result, that the SPIOs would work better than IFA as an adjuvant, the results are very promising and show that the SPIOs are at least equivalent to the IFA as an adjuvant. It was noticed that some of the SPIO-p53(105) had fallen out of solution on storage, which may have reduced the effectiveness of the SPIO as an adjuvant. It may be possible that if all of the SPIO had remained in solution the results may have shown a significant difference in favour of the SPIO. It is also possible that Mouse 2 received a larger dose than Mouse 1 and Mouse 3, possibly having the only injection to contain the desired amount of p53(105)-SPIO complex.

To overcome this problem it is suggested that the SPIO-p53(105) or other relevant peptide, should not be dissolved in DMSO and diluted until immediately prior to injection, to reduce the chance of sedimentation. It is also possible that solubility is an issue and so the original formulation needs to be adjusted to make it easier to dissolve the complex in DMSO rather than water.

Restimulation results (Figure 105) do not show an increased immune response to DC's pulsed with the peptide for mice immunised with the SPIO complex. This is in keeping with the results from the ELISPOT which indicate that there is not an increase in the strength of the immune response.

However, there is a significant decrease in non-specific response, meaning that the cells are not significantly responsive to peptides other than the peptide that was used for immunisation. Additionally there is a significant decrease in response to peptide without DC's as indicated by statistical T Test analysis (Table 7).

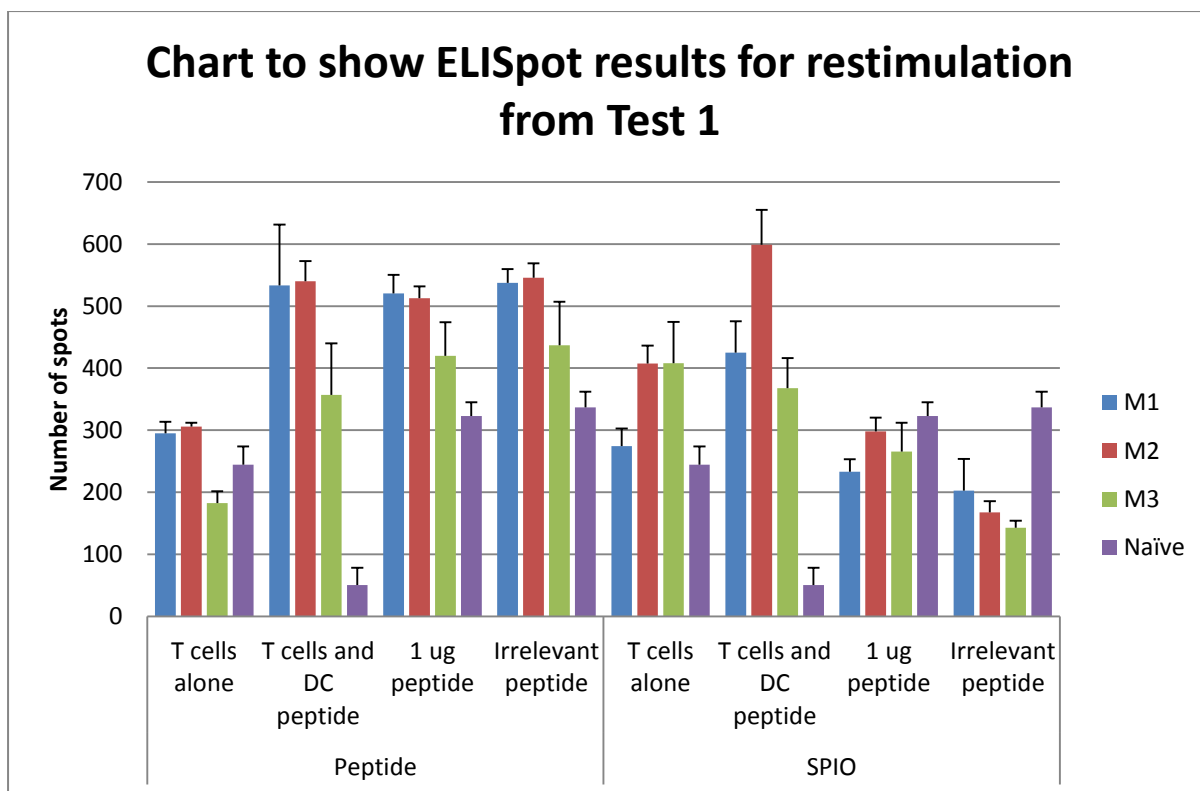


Figure 105. ELISpot results for restimulation of splenocytes from mouse immunisations.

	M1	M2	M3
T cells alone	0.496841	0.056288	0.017233
T cells and DC Peptide	0.11348	0.500241	0.921297
1 ug peptide	0.00393	0.003146	0.030783
Irrelevant peptide	0.004659	0.001273	0.023178

Table 7. Showing T Test results for restimulation with Peptide-IFA vs Peptide-SPIO

A T Test for T cells plus peptide pulsed DC's vs. T cells with a) irrelevant peptide and b) peptide alone, was carried out and the results shown in Tables 8 and 9. These results show that the number of spots produced by T cells from mice immunised using IFA adjuvant when stimulated with either peptide only, irrelevant peptide or DC's pulsed with peptide. This shows that any response generated by these cells is non-specific and so the response to p53(105) on APC's cannot be taken as a true response but rather that they are reacting to any type of antigen.

In contrast the T cells taken from mice immunised using SPIO as the adjuvant showed a significantly larger response to DC's pulsed with peptide compared to either peptide only or the irrelevant peptide. This shows that the T cells activated/produced when SPIO is used as an adjuvant respond specifically to the relevant antigen (peptide, p53(105)). This is significant as it goes some way to proving that not only is SPIO successful as an adjuvant, but also that it is superior to IFA in the response that it produces. In order for an immunisation to be effective it needs to create a response that is specific to that antigen, and it appears that the IFA is not helping to create this scenario, but is rather stimulating the T-cells to produce a non-specific immune response similar to inflammation or an allergic reaction. What the SPIOs are doing is producing a specific immune response so that the cells will only be affected by p53(105). As cancer cells are so specific in their nature and their antigens so similar to that of healthy cells, the specificity of the immune response is exceptionally important.

Peptide			
	M1	M2	M3
DC peptide vs irrelevant peptide	0.966316	0.563394	0.152127
DC peptide vs peptide only	0.661825	0.672573	0.511865

Table 8. Showing T Test results for DC peptide stimulated T cells vs. Irrelevant peptide or peptide only stimulated T cells for T cells isolated from mice immunised with IFA-p53(105). Flu-DR1 is used as the irrelevant peptide.

SPIO			
	M1	M2	M3
DC peptide vs. irrelevant peptide	0.006997	0.027468	0.023875
DC peptide vs. peptide only	0.031612	0.021272	0.004625

Table 9. Showing T Test results for DC peptide stimulated T cells vs. Irrelevant peptide or peptide only stimulated T cells for T cells isolated from mice immunised with SPIO-p53(105). Flu-DR1 is used as the irrelevant peptide.

In addition to the realisation that SPIOs can be used as adjuvants, these results also support the theory that SPIOs can be used as vectors for delivery of peptide into BMDC's as without the vector

peptide would not be taken up into the cells sufficiently and so a significant immune response could not be mounted. This can be tied in with previous results in which the results of the fluorescence microscopy were ambiguous owing to fluorescein's ability to bind to the outer membrane. So it is clear that SPIOs have the potential to be useful and versatile vectors.

Chapter 3: Materials and Methodology

Section 1: General Experimental

All chemicals were used as received by the suppliers (Sigma Aldrich, Acros, Alfa Aesar) unless stated otherwise. All other solvents were used as supplied (Laboratory, Analytical or HPLC grade), without further purification.

Microwave experiments were performed on CEM Discover[®]-SP microwave (CEM Corporation, UK), dynamic with temperature or pressure control, 30 sec pre-stirring, power max function (simultaneous air cooling). Peptides syntheses were carried out on CEM Discover[®]-SPS Microwave peptide synthesiser (CEM Corporation, UK).

Mass spectra were obtained using a Bruker MALDI-TOF mass spectrometer using a raster mode and 1000 averages, using 1 α -cyano-4-hydroxy-cinnamic acid (CHCA) as a matrix with only molecular ions and major peaks reported. Molecular ion peaks were isolated and run back through the spectrometer to further fragment and identify amino acid sequence.

UV-vis spectrometry was achieved on a JASCO V530 (Jasco, USA)

TEM images were generated on a JEOL JEM-2010, accelerating voltage 200 keV, tungsten filament, electron beam current 10 μ A; using a Gatan SC1000 ORIUS CCD camera.

SEM were performed on JEOL JSM-A840A scanning electron microscope (SEM), (Jeol Ltd, UK).

T₁ and T₂ measurements were made using a 0.25 T NMR MOUSE[®].

Dynamic light scattering (DLS) and Zeta potential measurements were carried out using a Malvern Nano Zetasizer using low volume sizing cuvettes at 4 °C for DLS and zeta cuvettes at 25 °C for zeta potential measurements.

1.1 Culture of U937 Cells

RPMI media (500 ml containing foetal calf serum (FCS) (50 ml) and L-glutamine (2%)) was freshly prepared. Frozen U937 cells were allowed to defrost at room temperature and then suspended in the media (10 ml). Cells were centrifuged (3 min, 2500 rpm). The pellet was re-suspended in media

(2 ml) and counted using trypan blue and haemocytometry. Cells were then re-suspended (5×10^6 cells, 20 ml media) and incubated at (37 °C, 5.1 % CO₂).

Cells were split down by removing half of the media containing cells and replacing this with fresh media every three days.

1.2 General method for solid phase peptide synthesis (SPPS)

All Fmoc amino acids and resins were purchased from Merck4Biosciences and used without further purification.

The Fmoc amino acids used:

Fmoc-Ala-OH.H₂O

Fmoc-Arg(Pbf)-OH

Fmoc-Asn(Trt)-OH

Fmoc-Asp(O^tBu)-OH

Fmoc-Cys-(Trt)-OH

Fmoc-Gln(O^tBu)-OH

Fmoc-Gly-OH

Fmoc-His(Trt)-OH

Fmoc-Ile-OH

Fmoc-Leu-OH

Fmoc-Lys(Boc)-OH

Fmoc-Met-OH

Fmoc-Phe-OH

Fmoc-Pro-OH

Fmoc-Ser(^tBu)-OH

Fmoc-Thr(^tBu)-OH

Fmoc-Trp(Boc)-OH

Fmoc-Tyr(Boc)-OH

Fmoc-Val-OH

In a SPPS reaction vessel, Fmoc protected Wang resin (0.1 mmol) was swelled in a dimethyl formamide (DMF)/ dichloromethane (DCM) mixture (2.5 ml/2.5 ml) for 30 min and was then drained and rinsed with DMF (5 ml).

Resin deprotection was carried out by addition of piperazine (4.1 mmol, 0.58 M, 7 ml) and reacted for 30 sec at 75 °C (+/- 5 °C, 50 W), drained and piperazine added (4.1 mmol, 0.58 M, 7 ml) and reacted for further 3 min at 75 °C (+/- 5 °C, 50 W). The deprotected resin was then drained under vacuum and rinsed with DMF (3 x 5 ml).

Fmoc protected amino acid (0.25 mmol, 2.5 equiv.) dissolved in DMF (2.5 ml) was added to the deprotected resin with O-Benzotriazole-N,N,N',N'-tetramethyl-uronium-hexafluoro-phosphate (HBTU) (0.47 mmol, 1 ml, 0.474 M, 4.7 equiv.) and diisopropylethylamine (DIEA) in *N*-methyl pyrrolidine (NMP) (1.3 mmol, 0.5 ml, 2.58 M, 13 equiv.). The reaction was performed under microwave irradiation using different temperature and coupling time depending on the amino acid used (details included in peptide synthesis tables). Typically all amino acids except arginine, histidine and cysteine, were reacted for 5 min at 75 °C (+/- 5 °C, 25W). Arginine was reacted for 30 min at 25 °C (+/- 5 °C, 0W) drained and more amino acid (0.25 mmol, 2.5 equiv.) was added and reacted for further 5 min at 25 °C (+/- 5 °C, 0W). Histidine and cysteine were reacted for 10 min at 50 °C (+/- 5 °C, 25W).

Final deprotection was done by addition of piperazine (4.1 mmol, 0.58 M, 7 ml) which was reacted for 30 sec for the first deprotection, then the same quantities added and reacted for 3 min at 75 °C (+/- 5 °C, 50 W), then repeated. The reaction mixture was drained and washed with DMF (3 x 5 ml) and rinsed with DCM (3 x 5 ml) and left to dry under air for 15 min.

The resin was then transferred into a cleavage mix solution containing H₂O (0.25 ml), triisopropylsilane (TIS) (4.86 mmol, 0.1ml), 3,6-dioxa-1,8-octanedithiol (DODT) (3.1 x mmol, 0.5ml) and trifluoroacetic acid (TFA) (0.13 mol, 9.4 ml) and stirred at room temperature for 1 – 3 hrs depending on the peptide.

The peptide was filtrated into a chilled solution of diethylether (100 ml), and the resin washed with DCM (2 x 5 ml). The ether solution was placed in the freezer for a minimum of 1 hr, to yield a white precipitate.

The mixture was centrifuged (10 min, 3000 rpm, <10 °C), the supernatant removed and clean, chilled diethyl ether (30 ml) was added. This was repeated three times to ensure a clean product.

The recovered white waxy solid was left to dry in air overnight, or freeze-dried using liquid nitrogen under vacuum. Peptide purity was analysed using HPLC and MALDI-TOF MS (see standard procedures).

*Note: The method used has since been discovered to be incorrect. The correct procedure for any future peptides requires exactly 2.5 molar equivalents of HBTU (0.25 mmol, 1 ml, 0.25 M, 2.5 equiv.).

1.3 FACS staining protocol

Cells were seeded at 2×10^5 cells per fluorescence assisted cell sorting (FACS) tube (2 ml suspension per tube) and washed with FACS buffer. To the cell pellet was added 10 μ l of primary antibody (1:100) and incubated on ice for 30 min. Samples then washed once with FACS buffer and secondary antibody added to the pellet (1:1000) and incubated for a further 30 min on ice. Isotone (500 μ l) added and samples run through FACS as in general procedure.

1.4 CD86 – with PE (Red)

A solution containing phosphate-buffered saline (500 ml), bovine serum albumin (2.5 ml) and EDTA (2 mM) was prepared and kept cold (2 – 8 °C). Cells were counted and resuspended at 10^7 cells per 100 μ l of buffer. The CD86 antibody (10 μ l) was added, mixed well and incubated for 10 min in the dark at 2 – 8 °C. Cells washed with buffer (1-2 ml) and centrifuged (1500 rpm, 10 min) before aspiration. Cells were re-suspended in buffer (*ca.* 2 ml) for further analysis by FACS or fluorescence microscopy.

1.5 DAPI Nuclear Staining

Cell sample to be analysed was washed with PBS (*ca.* 5 ml). DAPI stock solution was diluted to 300 nM in PBS and added (300 μ l) to the coverslip preparation, making sure all cells were covered. Sample was incubated (1 – 5 min) before rinsing three times with PBS (3 x 5 ml). Excess buffer was drained and the coverslip mounted ready for microscopy.

1.6 Cell Counting by haemocytometry using trypan blue

Cells were centrifuged (5 min, 1500 rpm), and supernatant discarded. The cell pellet was re-suspended in RPMI media. Cell suspension (50 μ l) was added to acetic acid (450 μ l) and mixed by pipette. The mixture (50 μ l) was added to trypan blue (450 μ l) and mixed by pipette to give a dilution of 100. This mixture was plated on a haemocytometer slide and number of cells per 1 mm corner square (see Figure 106) counted and averaged over the four squares taking into account cells within the 16 corner squares but not touching the top line or left hand line. Number of cells counted was multiplied by 10^4 then multiplied by the dilution factor of 10^2 to give number of viable cells per 1 ml of cell suspension.

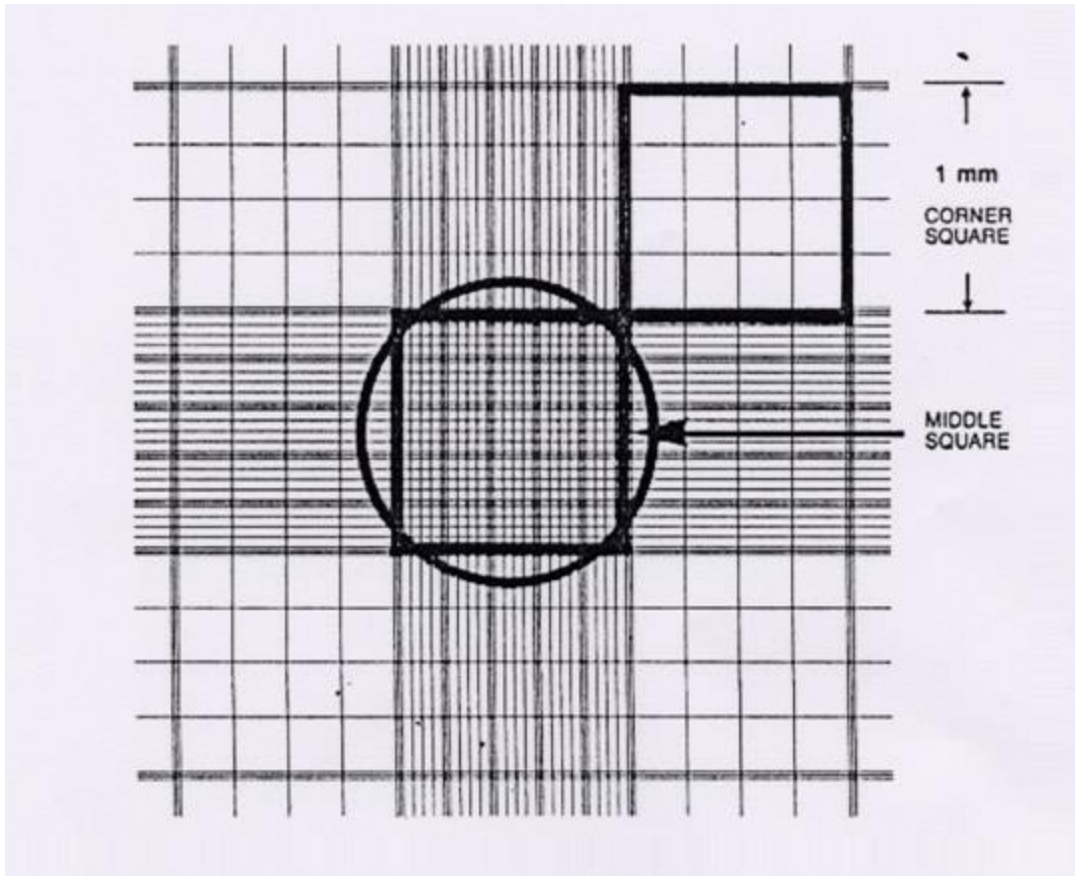


Figure 106. Picture of haemocytometer indicating corner squares used for cell counting.

1.7 High performance liquid chromatography (HPLC)

All HPLC herein was carried out using an Agilent HPLC system

Column: Hypersil Gold 250 x 4.6 mm, 5 μm particles size, C18 column

Flow rate: 1.500 ml/min

Injection: 10 μl

UV detection: 220 nm

HPLC Buffer: 5 % Triethanolamine (TEA), 7.5 % Trifluoroacetic acid (TFA), 25 % HPLC Grade Acetonitrile (ACN), 62.5 % HPLC Grade Water.

Solvent A: 1 % HPLC Buffer, 10 % ACN, 89 % H₂O

Solvent B: 1 % HPLC Buffer, 75 % ACN, 24 % H₂O

Gradient:

Time (mins)	% A	% B
0	100	0
20	70	30
30	65	35
39	65	35
40	100	0

Table 9. Gradient for HPLC

Samples were dissolved 2 mg/ml in 50:50 ACN:H₂O and processed through a 0.2 µm filter.

1.8 Zip-tip preparation of samples for Mass Spectrometry

All samples were dissolved in an aqueous solution containing 10% acetonitrile (ACN) in 0.1 % TFA. 80 % ACN containing 0.1 % TFA (2 x 10 µl) was used to wash the zip tip (C₁₈ silica). 0.1 % TFA (2 x 10 µl) was then used to rinse the zip-tip. The sample (10 µl) was then loaded onto the tip by repeatedly taking up and ejecting the solution to provide optimum binding. The tip was then washed with 0.1 % TFA (10 µl x 3) and the peptide then eluted using 80 % ACN in 0.1 % TFA (4 µl), by taking up and ejecting the solution twenty times.

The sample was then mixed with recrystallised 1α-cyano-4-hydroxy-cinnamic acid (CHCA) matrix on a target plate and left to dry.

1.9 Mass Spectrometry of Samples

Peptide samples were processed and then analysed by MALDI-TOF MS using an Ultraflex 3158A by adjusting the laser power to the lowest power producing fragments (*ca.* 30 % but variable). MS-MS was carried out by isolating the peak of interest, filtering for this peak only and increasing laser power to further fragment the peak. Amino acids sequences were identified manually.

Section 2: Synthesis, functionalization and purification of iron oxide nanoparticles (SPIOs)

2.1 Co-precipitation General Route

To FeCl₂·4H₂O (10 g, 0.05 mol) was added FeCl₃·6H₂O (24.3 g, 0.09 mol) both dissolved in distilled water (100 ml). 35 % aqueous NH₃ solution (50 ml, 0.90 mol) was added dropwise with stirring (*ca.* 5 min) then sonicated in a sonic bath (1 hr). The mixture was filtered using a sintered funnel and washed (2 x 50 ml distilled water, 2 x 50 ml diethyl ether) and allowed to dry in air before storing in a sealed vial. The solution was found to be stable in a sealed vial 2 months from the time of storage. See Table 10 for other methods trialled.

Moles FeCl ₂	Moles FeCl ₃	Base (50 ml)	Conditions	Result
0.05	0.09	NH _{3(aq)}	No sonication	Black solid responsive to magnetic stimuli formed, particles by TEM 10-60 nm. Size not uniform.
0.05	0.09	NH _{3(aq)}	Sonication for 10 minutes	Black solid responsive to magnetic stimuli formed, particles by TEM 10-40 nm. Size not uniform.
0.05	0.09	NH _{3(aq)}	Sonication for 30 minutes	Black solid responsive to magnetic stimuli formed, particles by TEM 10-40 nm. Size not uniform.
0.05	0.09	NH _{3(aq)}	Sonication for 60 minutes	Black solid responsive to magnetic stimuli formed, particles by TEM 10-20 nm, fairly uniform in size.*
0.05	0.09	NH _{3(aq)}	Base added in one addition rather than dropwise; sonication for 60 minutes	Black solid responsive to magnetic stimuli formed, particles by TEM indistinguishable, very clumped together. Particles could not be coated by solvent free route.
0.05	0.09	NH _{3(aq)}	Base added dropwise; sonication for 60 minutes	Black solid responsive to magnetic stimuli formed, particles by TEM 10-20 nm, fairly uniform in size. Successfully coated <i>via</i> solvent free grinding route.
0.05	0.09	NaOH _(aq) 1.0M	Alternative base added dropwise	Black solid responsive to magnetic stimuli formed, particles by TEM indistinguishable, very clumped together. Particles could not be coated by solvent free route.
0.05	0.09	NaOH _(aq) 0.25M	Alternative weaker base added dropwise	Black solid responsive to magnetic stimuli formed, particles by TEM indistinguishable, very clumped together. Particles could not be coated by solvent free route.

Table 10. Conditions trialled for synthesis of SPIOs by co-precipitation

*For these conditions there was a yield of 10.8 g giving a % yield of 93.3 %. Other methods yielded similar results although they were not repeated due to the highlighted method being better optimised. The size of these particles was found to be 8-10 nm by TEM when suspended in ethanol. The IR results indicated that there were no hydroxyl groups present, indicating that the particles were not in the hydrated form. The appearance of these particles was as a black solid, responsive to magnetic stimuli.

2.2 Spinning Disc Reactor

2.2.1 Ammonia solution

$\text{FeCl}_2 \cdot 4\text{H}_2\text{O}_{(s)}$ (50.0 g, 0.25 mol) and $\text{FeCl}_3 \cdot 6\text{H}_2\text{O}_{(s)}$ (121.3g, 0.45 mol) were dissolved in distilled water to make 1.0 L of stock solution. This was fed into the spinning disc reactor with the addition of ammonia solution (500 ml, 35 %, 9.0 mol). The resultant black precipitate was washed thrice with distilled water, twice with ethyl acetate, filtered under *vacuum* and air dried to yield a crystalline black powder. This powder was stored at room temperature in a sealed vial for a period of 2 months. Samples were analysed for TEM for size and morphology. Observations showed spherical particles with significant agglomeration, and that the spin rate has no effect on the size of the particles, with large overlaps in particles sizes over all rates.

Spin speeds were altered as shown in Table 11.

Voltage (V)	60V	80V	100V	120V	140V	160V	180V	200V	220V	240V
Spin-rate (rpm)	352.9	705.9	1000.0	1250.0	1578.9	1818.2	2069.0	2307.7	2449.0	2727.3
Particle Size (nm)	15-30	10-30	12-35	10-35	8-40	10-35	10-35	10-30	8-25	7-25

Table 11. Conditions for SPIO synthesis using SDR with ammonia solution

2.2.2 Ammonia gas

$\text{FeCl}_2 \cdot 4\text{H}_2\text{O}_{(s)}$ (50.0 g, 0.25 mol) and $\text{FeCl}_3 \cdot 6\text{H}_2\text{O}_{(s)}$ (121.3g, 0.45 mol) were dissolved in distilled water to make 1.0 L of stock solution. This was fed into the spinning disc reactor with the addition of ammonia gas. The resultant black precipitate was washed thrice with distilled water (50 ml per 50 g of reactants), twice with ethyl acetate (50 ml per 50 g of reactants), filtered under vacuum and air dried to yield a crystalline black powder. This powder was stored at room temperature in a sealed vial for a period of 2 months.

Spin speeds were altered as shown in Table 12. Particles were analysed using TEM to determine size and morphology. Observations showed spherical particles that were well separated displaying minimal agglomeration.

Voltage (V)	60V	80V	100V	120V	140V	160V	180V	200V	220V	240V
Spin-rate (rpm)	352.9	705.9	1000.0	1250.0	1578.9	1818.2	2069.0	2307.7	2449.0	2727.3
Particle Size (nm)	19-25	18-25	19-25	16-28	18-24	16-35	20-42	15-35	17-27	15-30

Table 12. Conditions for SPIO synthesis using SDR with ammonia gas.

2.3 Using a ball mill to attach coatings onto SPIOs

Typically coating material and SPIO were placed in a micro ball mill and processed (5 mins, 25 Hz). The resultant powder was taken up into water, filtered (0.2 μm microfilter) and analysed. Alternative methods are detailed in Table 13. Mass was used rather than moles as the grinding method is subject to mixing effects which are more affected by mass of reactants. The method also consistently leads to multilayer coverage.

Mass of SPIO (g)	Mass of histidine coating (g)	Other conditions	Observations
0.100	0.100	None	No iron observed in resultant solution and no particles by TEM.
0.100	0.200	None	No iron observed in resultant solution and no particles by TEM.
0.200	0.100	None	No iron observed in resultant solution and no particles by TEM.
0.200	0.200	None	No iron observed in resultant solution and no particles by TEM.
0.200	0.200	Heated with heat gun during milling	The container exploded during this reaction as the pressure build up from heating a sealed vial could not be contained. The SPIO-coating materials mixture expanded during the reaction.

Table 13. Conditions trialled for coating of SPIOs using a ball mill

2.4 Incubation of SPIOs with coating material

Threonine (0.5 g, 4.2 mmol) was vortexed in 5 ml distilled water until dissolved. To this solution was added SPIO powder (0.25 g, 1.1 mmol). The mixture was stirred overnight before being processed through a 0.2 μm microfilter. A clear brown solution was obtained and analysed. Table 14 indicates other methods trialled. The only successful method was using threonine. The success is attributed to the high solubility of this amino acid.

TEM indicated for threonine only there were clusters of particles of 10-20 nm in size with a clear area around them. DLS confirmed particles of 18 nm in size. ICP showed iron in the sample.

Amino Acids	Observations	Analysis
Alanine, Cysteine, Aspartic Acid, Glutamic Acid, Phenylalanine, Glycine, Histidine, Isoleucine, Lysins, Leucine, Methionine, Asparagine, Proline, Glutamine, Arginine, Serine, Valine, Tryptophan, Tyrosine	Insoluble/sparingly soluble. Colourless solution produced.	No particles by TEM or DLS. ICP indicated no iron present in the solution
Threonine	Highly soluble in water. Pale brown solution produced.	Spherical particles of 8-10 nm by DLS and TEM observed. TEM images show a clear area around the particles indicating a layer of organic coating material.

Table 14. Conditions trialled for incubation to coat SPIOs

2.5 Sonication

Typically 0.5 g of coating material (Table 15) was dissolved in distilled water (20 ml) and SPIO (0.25 g, 1.1 x mmol) added. The mixture was then sonicated for 180 min before being filtered (0.2 µm microfilter).

Coating material	Observations	Analysis
Threonine	Colourless solution	No particles by TEM or DLS. No iron present in the solution by ICP.
Glutamic acid	Not fully soluble in the water. Colourless solution formed	No particles by TEM or DLS. No iron present in the solution by ICP.
Aspartic acid	Not fully soluble in water. Colourless solution formed	No particles by TEM or DLS. No iron present in the solution by ICP.

Table 15. Conditions trialled for coating SPIOs using sonication

2.6 Heating method for coating particles

Typically SPIOs (0.500 g, 2.2 mmol) and coating material (see Table 16) were placed into a vial and heated until a change from solid to liquid was observed. The resultant black/brown solid was then taken up into water, filtered (0.2 µm microfilter) and analysed by TEM, DLS, ICP and MRI MOUSE.

Coating material	Mass (g)	Moles	DLS/TEM	Iron present by ICP Y/N?	T ₁ (ms)	T ₂ (ms)
Alanine	0.500	5.61 x 10 ⁻⁰³	Large aggregates of ~ 1000 nm, no individual particles observed	Y	Could not be measured (too long)	Could not be measured (too long)
Cysteine	0.500	4.13 x 10 ⁻⁰³	Large aggregates of ~ 1000 nm, no individual particles observed	Y	Could not be measured (too long)	Could not be measured (too long)
Aspartic Acid	0.500	3.76 x 10 ⁻⁰³	Large aggregates of ~ 1000 nm, no individual particles observed	Y	Could not be measured (too long)	Could not be measured (too long)
Glutamic Acid	0.500	3.40 x 10 ⁻⁰³	Large aggregates of ~ 1000 nm, no individual particles observed	Y	Could not be measured (too long)	Could not be measured (too long)
Phenylalanine	0.500	3.03 x 10 ⁻⁰³	Large aggregates of ~ 1000 nm, no individual particles observed	Y	Could not be measured (too long)	Could not be measured (too long)
Glycine	0.500	6.66 x 10 ⁻⁰³	Large aggregates of ~ 1000 nm, no individual particles observed	Y	Could not be measured (too long)	Could not be measured (too long)
Histidine	0.500	3.22 x 10 ⁻⁰³	Large aggregates of ~ 1000 nm, no individual particles observed	Y	Could not be measured (too long)	Could not be measured (too long)
Isoleucine	0.500	3.81 x 10 ⁻⁰³	Large aggregates of ~ 1000 nm, no individual particles observed	Y	Could not be measured (too long)	Could not be measured (too long)
Lysine	0.500	3.42 x 10 ⁻⁰³	Large aggregates of ~ 1000 nm, no individual particles observed	Y	Could not be measured (too long)	Could not be measured (too long)
Leucine	0.500	3.81 x 10 ⁻⁰³	Large aggregates of ~ 1000 nm, no individual particles observed	Y	Could not be measured (too long)	Could not be measured (too long)
Methionine	0.500	3.35 x 10 ⁻⁰³	Large aggregates of ~ 1000 nm, no individual particles observed	Y	Could not be measured (too long)	Could not be measured (too long)
Asparagine	0.500	3.78 x 10 ⁻⁰³	Large aggregates of ~ 1000 nm, no individual particles observed	Y	Could not be measured (too long)	Could not be measured (too long)
Proline	0.500	4.34 x 10 ⁻⁰³	Large aggregates of ~ 1000 nm, no individual particles observed	Y	Could not be measured (too long)	Could not be measured (too long)

Glutamine	0.500	3.42×10^{-03}	Large aggregates of ~ 1000 nm, no individual particles observed	Y	Could not be measured (too long)	Could not be measured (too long)
Arginine	0.500	2.87×10^{-03}	Large aggregates of ~ 1000 nm, no individual particles observed	Y	Could not be measured (too long)	Could not be measured (too long)
Serine	0.500	4.76×10^{-03}	Large aggregates of ~ 1000 nm, no individual particles observed	Y	Could not be measured (too long)	Could not be measured (too long)
Threonine	0.500	4.20×10^{-03}	Large aggregates of ~ 1000 nm, no individual particles observed	Y	Could not be measured (too long)	Could not be measured (too long)
Valine	0.500	4.27×10^{-03}	Large aggregates of ~ 1000 nm, no individual particles observed	Y	Could not be measured (too long)	Could not be measured (too long)
Tryptophan	0.500	2.45×10^{-03}	Large aggregates of ~ 1000 nm, no individual particles observed	Y	Could not be measured (too long)	Could not be measured (too long)
Tyrosine	0.500	2.76×10^{-03}	Large aggregates of ~ 1000 nm, no individual particles observed	Y	Could not be measured (too long)	Could not be measured (too long)

* Samples showed significant sedimentation and measurements were not possible due to limitations of the MRI MOUSE®. T_1 and T_2 were too long to be measured.

Table 16. Conditions trialled for coating SPIOs using heat

2.7 Solvent-free grinding of aqueous soluble substances with SPIOs

2.7.1 Pestle and Mortar

Typically, SPIO (0.25 g, 1.1 mmol) and coating agent (see Table 17) were vigorously agitated using a mortar and pestle (*ca.* 5 min). The homogeneous brown powder was vigorously agitated with distilled water (*ca.* 10 ml) before filtration (0.2 μm disposable microfilter) to yield a colourless – dark brown solution free of visible particles. The equipment is illustrated in Figure 107.



Figure 107. Mortar and Pestle with SPIOs and ascorbic acid pre-grinding

TEM indicated Spherical particles of 8-10 nm in diameter with clear area indicating coating agent.

ICP and DLS showed various iron concentrations and size distributions depending on the coating agent and variable between experiments (see Table 17). There was no consistent pattern other than that spherical particles coated with an organic coating were found for all experiments.

Coating Agent	Mass (g)	Moles	Observations	Iron present in ICP Y/N?	Size by DLS and TEM
Alanine	0.500	5.61×10^{-03}	Colourless solution	N	No particles observed
Cysteine	0.500	4.13×10^{-03}	Colourless solution	N	No particles observed
Aspartic Acid	0.500	3.76×10^{-03}	Pale brown solution	Y	Spherical particles 10-20 nm in diameter in small clusters
Glutamic Acid	0.500	3.40×10^{-03}	Pale brown solution	Y	Spherical particles 10-20 nm in diameter in small clusters
Phenylalanine	0.500	3.03×10^{-03}	Colourless solution	N	No particles observed
Glycine	0.500	6.66×10^{-03}	Colourless solution	N	No particles observed
Histidine	0.500	3.22×10^{-03}	Colourless solution	N	No particles observed
Isoleucine	0.500	3.81×10^{-03}	Colourless solution	N	No particles observed
Lysine	0.500	3.42×10^{-03}	Colourless solution	N	No particles observed
Leucine	0.500	3.81×10^{-03}	Colourless solution	N	No particles observed
Methionine	0.500	3.35×10^{-03}	Colourless solution	N	No particles observed
Asparagine	0.500	3.78×10^{-03}	Colourless solution	N	No particles observed
Proline	0.500	4.34×10^{-03}	Colourless solution	N	No particles observed
Glutamine	0.500	3.42×10^{-03}	Colourless solution	N	No particles observed
Arginine	0.500	2.87×10^{-03}	Colourless solution	N	No particles observed
Serine	0.500	4.76×10^{-03}	Colourless solution	N	No particles observed
Threonine	0.500	4.20×10^{-03}	Pale brown solution	Y	10-20 nm particles with clear area around each particle, in small clusters.
Valine	0.500	4.27×10^{-03}	Colourless solution	N	No particles observed
Tryptophan	0.500	2.45×10^{-03}	Colourless solution, amino acid not soluble in water	N	No particles observed
Tyrosine	0.500	2.76×10^{-03}	Colourless solution	N	No particles observed
Palmitic Acid	0.500	1.95×10^{-03}	Brown solution when taken up into chloroform	Y	Particles in large clusters. 10-20 nm in diameter where not clustered.
Paracetamol	0.500	3.31×10^{-03}	Colourless solution	N	No particles observed
Ascorbic Acid	0.500	2.84×10^{-03}	Pale brown solution	Y	Particles of 10-20 nm in diameter in small clusters with clear area around each particle
Glycerol	0.500	5.43×10^{-03}	Dark brown solution	Y	Particles equally distributed, 10-20 nm in diameter with clear area around each particle
Diclofenac	0.500	1.69×10^{-03}	Pale brown solution when taken up into chloroform	Y	Particles clumped together and indistinguishable
Aspirin	0.500	2.78×10^{-03}	Colourless solution	N	No particles observed
Hexadecanediol	0.500	1.93×10^{-03}	Colourless solution	N	No particles observed

Table 17. Conditions trialled for solvent-free grinding using pestle and mortar

2.7.2 Using a coffee grinder to carry out solvent free coating of SPIOs

A Kitchen Aid™ Artisan Coffee Grinder was set with the metal burrs as close together as possible. To the top of the coffee grinder SPIO (1.00 g, 4.4 mmol) and a coating agent were added as detailed in Table 18. The grinder was switched on and the mixture passed through the coffee grinder in accordance with Table 12. The resultant homogeneous brown powder was dissolved in distilled water (10 ml), filtered (0.2 µm microfilter) and analysed for iron content by ICP. The T_1 and T_2 relaxation times of the samples were measured, to ensure that the coffee grinder process had not altered the activity of the SPIOs.

Coating material	Mass (g)	Moles	Observations	Fe present by ICP Y/N?	TEM/DLS
Aspirin	1.00	5.55×10^{-03}	Colourless solution	N	No particles observed
Paracetamol	1.00	6.62×10^{-03}	Colourless solution	N	No particles observed
Diclofenac	1.00	3.38×10^{-03}	Brown solution when taken up into chloroform	Y	Particles in large clusters. 10-20 nm in diameter where not clustered.
Ascorbic Acid	1.00	5.68×10^{-03}	Brown solution	Y	Spherical particles 10 -20 nm diameter in small clusters
Histidine	1.00	6.44×10^{-03}	Brown solution	Y	Spherical particles 10 -20 nm diameter in small clusters

Table 18. Conditions trialled for coating SPIOs using a coffee grinder

Although this method was found to be successful certain drawbacks would need to be addressed before further investigations carried out. The size of the burrs, the size of the grooves in the burrs (0.8 mm for the Artisan®) and the speed at which the burrs spin must all be reproducible. There will also be an issue during scale-up as with larger quantities of SPIO the feed rate, burr speed, and groove size may need to be altered.

2.8 Processing of amino acids / peptides

For amino acids and peptides presenting aqueous solubility problems, coating agent (2 g) was dissolved in HCl_{aq} (20 ml, 4M) aided by vortex (see Table 19). Solvent removed *in vacuo* to yield a dry white/off-white crystalline powder (5 mbar, 40/60°C peptide/amino acid respectively). Alternatively acetone was added to the solution and kept at – 20 °C for 24 hours to yield an off-white precipitate. Mixture centrifuged (10 min, 3000 rpm), supernatant removed and solid product washed with diethyl ether (3 x 50 ml) then dried in air before grinding with SPIO *via* solvent free route and analysis by ICP, DLS and TEM.

Coating Agent	Mass (g)	Moles	Observations	Iron present in ICP Y/N?	Size by DLS and TEM
Alanine.HCl	0.500	5.61 x 10 ⁻⁰³	Dark brown solution	Y	10-20 nm particles with clear area around each particle. Many distinguishable particles clustered together
Cysteine.HCl	0.500	4.13 x 10 ⁻⁰³	Dark brown solution, precipitation occurred over 24 hrs	Y	Particles no distinguishable from each other
Aspartic Acid.HCl	0.500	3.76 x 10 ⁻⁰³	Dark brown solution	Y	10-20 nm particles with clear area around each particle. Many distinguishable particles clustered together
Glutamic Acid.HCl	0.500	3.40 x 10 ⁻⁰³	Dark brown solution	Y	10-20 nm particles with clear area around each particle. Many distinguishable particles clustered together
Phenylalanine.HCl	0.500	3.03 x 10 ⁻⁰³	Dark brown solution	Y	10-20 nm particles with clear area around each particle. Many distinguishable particles clustered together
Glycine.HCl	0.500	6.66 x 10 ⁻⁰³	Dark brown solution	Y	10-20 nm particles with clear area around each particle. Many distinguishable particles clustered together
Histidine.HCl	0.500	3.22 x 10 ⁻⁰³	Dark brown solution	Y	10-20 nm particles with clear area around each particle. Many distinguishable particles clustered together
Isoleucine.HCl	0.500	3.81 x 10 ⁻⁰³	Dark brown solution	Y	10-20 nm particles with clear area around each particle. Many distinguishable particles clustered together

Coating Agent	Mass (g)	Moles	Observations	Iron present in ICP Y/N?	Size by DLS and TEM
Lysine.HCl	0.500	3.42×10^{-03}	Dark brown solution	Y	10-20 nm particles with clear area around each particle. Many distinguishable particles clustered together
Leucine.HCl	0.500	3.81×10^{-03}	Dark brown solution	Y	10-20 nm particles with clear area around each particle. Many distinguishable particles clustered together
Methionine.HCl	0.500	3.35×10^{-03}	Dark brown solution, precipitation occurred over 24 hrs	Y	10-20 nm particles with clear area around each particle. Many distinguishable particles clustered together
Asparagine.HCl	0.500	3.78×10^{-03}	Dark brown solution	Y	10-20 nm particles with clear area around each particle. Many distinguishable particles clustered together
Proline.HCl	0.500	4.34×10^{-03}	Dark brown solution	Y	10-20 nm particles with clear area around each particle. Many distinguishable particles clustered together
Glutamine.HCl	0.500	3.42×10^{-03}	Dark brown solution	Y	10-20 nm particles with clear area around each particle. Many distinguishable particles clustered together
Arginine.HCl	0.500	2.87×10^{-03}	Dark brown solution	Y	10-20 nm particles with clear area around each particle. Many distinguishable particles clustered together
Serine.HCl	0.500	4.76×10^{-03}	Dark brown solution	Y	10-20 nm particles with clear area around each particle. Many distinguishable particles clustered together
Threonine.HCl	0.500	4.20×10^{-03}	Dark brown solution	Y	10-20 nm particles with clear area around each particle. Many distinguishable particles clustered together
Valine.HCl	0.500	4.27×10^{-03}	Dark brown solution	Y	10-20 nm particles with clear area around each particle. Many distinguishable particles clustered together
Tryptophan.HCl	0.500	2.45×10^{-03}	Very pale brown solution	Y	10-20 nm particles in small clusters. Very few particles
Tyrosine.HCl	0.500	2.76×10^{-03}	Dark brown solution	Y	10-20 nm particles with clear area around each particle. Many distinguishable particles clustered together
Pap-161.HCl	0.050	2.78×10^{-05}	Very pale brown solution	Y	10-20 nm particles with clear area around each particle. Few small clusters of particles

Coating Agent	Mass (g)	Moles	Observations	Iron present in ICP Y/N?	Size by DLS and TEM
p53(108).HCl	0.050	3.17 x 10 ⁻⁰⁵	Very pale brown solution	Y	10-20 nm particles with clear area around each particle. Few small clusters of particles
p53(105).HCl	0.050	3.23 x 10 ⁻⁰⁵	Very pale brown solution	Y	10-20 nm particles with clear area around each particle. Few small clusters of particles
Flu DR1.HCl	0.050	3.32 x 10 ⁻⁰⁵	Very pale brown solution	Y	10-20 nm particles with clear area around each particle. Few small clusters of particles
TRP2.HCl	0.050	4.25 x 10 ⁻⁰⁵	Very pale brown solution	Y	10-20 nm particles with clear area around each particle. Few small clusters of particles

Table 19. Results for grinding of SPIOs with HCl salts of amino acids and peptides

Zeta potential measurements show neat amino acid coatings give *ca.* + 10 mV and HCl salt amino acid coatings give *ca.* – 15 mV.

2.9 Assessing inorganic salts as a coating

SPIO (0.25 g, 1.1 mmol) and salts were ground in 1:1 mass ratio in a mortar (5 min) then taken up into distilled water (10 ml), filtered (0.2 µm microfilter), and the resultant solution analysed by ICP (Table 20).

Compound	Mass (g)	Moles	Observations	Fe present by ICP Y/N?	Size by DLS/TEM
NaCl	0.250	4.28 x 10 ⁻⁰³	Colourless solution formed	N	No particles observed
NH ₄ Cl	0.250	4.67 x 10 ⁻⁰³	Colourless solution formed	N	No particles observed.

Table 20. Results for trialling inorganic salts as coatings

2.10 Determining if using the HCl salt will lead to degradation of the particle

SPIO coated with a) ascorbic acid and b) HCl salt of ascorbic acid was prepared as in 2.8, analysed for Fe content by ICP, diluted to 400 mg.l^{-1} using distilled water and the relaxation time (T_1 and T_2) measured every 10 min for a period of 350-400 min.

2.11 Determining if alcohols bind to the SPIOs *via* the solvent free grinding method

2.11.1 Solids

Hexadecanediol (100 mg, 3.87 mmol) was added to SPIO (100 mg, 4.31 mmol). The mixture was ground in a mortar for *ca.* 5 min, dissolved in chloroform and centrifuged to remove free particles. The supernatant was then removed and used for analysis by TEM which showed aggregates of 78 nm.

2.11.2 Liquids

Glycerol (1 g, 1.09×10^{-2} mol, 0.79 ml) was added to SPIO (1 g, 4.31 mmol). The mixture was ground in a mortar for five minutes and taken up into distilled water before being processed through a $0.2 \mu\text{m}$ filter. The resultant brown solution was analysed by TEM and ICP showing spherical particles of 15-20 nm and Fe conc. of 103.1 mg.l^{-1} .

2.12 Determining the Optimum Mass Ratio for solvent free grinding

SPIOs synthesised as described previously were ground (*ca.* 5 min) with aspartic acid hydrochloride in the mass ratios indicated in Table 21. The resultant powder was taken up into 5 ml of distilled water and processed through a filter ($0.2 \mu\text{m}$) and analysed for iron content by ICP.

Mass SPIO (mg)	Mass Coating (mg)	Mass Ratio	Fe Conc. mg.l ⁻¹
50	100	1:2	1253.3
50	200	1:4	625.6
50	300	1:6	454.8

Table 213. Showing mass ratio of coating to SPIO investigated; 1:2 – 1:6

This experiment was repeated for different ratios of SPIO to histidine hydrochloride salt as described in Table 22 and the final solution analysed for Fe concentration by ICP-AES.

Mass SPIO (mg)	Mass Coating (mg)	Ratio SPIO:Coating	Fe Conc. mg.l ⁻¹
100	25	4:1	1497.8
100	50	2:1	717.8
100	75	4:3	985.5
100	100	1:1	1326.2
100	125	4:5	828.4
100	150	2:3	1059.7
100	175	4:7	923.7
100	200	1:2	729.6

Table 22. Showing mass ratio of coating to SPIO; 4:1 – 1:2

2.13 Determining if the mortar and pestle or coffee grinder produces a more homogeneous sample

HCl salt of histidine (0.100 g, 0.706 m mol)) and SPIO (0.100 g, 0.431 mmol) were weighed and mixed either through the coffee grinder five times, or using a pestle and mortar for ca. 5 min. Samples were then taken up into distilled water (10 ml) and filtered (0.2 µm microfilter). The resultant solutions were analysed for Fe content by ICP and size by TEM and DLS (Table 23).

Sample	Fe conc. mg.l ⁻¹	Sample	Fe conc. mg.l ⁻¹
P1	115.5	C1	53.1
P2	84.24	C2	48.62
P3	94.15	C3	54.02
P4	116.4	C4	50.59
P5	96.75	C5	55.58
P6	98.12	C6	56.99
P7	89.88	C7	62.12
P8	91.27	C8	56.08
P9	111.6	C9	60.96
P10	105.1	C10	56.77

Table 23. Results to test homogeneity of pestle and mortar (P) vs. coffee grinder (C).

2.14 Calculating the amount of coating material relative to the mass of SPIO

A sample of ascorbic acid coated SPIOs (10 ml) prepared *via* the solvent free grinding method was analysed by ICP and found to contain 129 mg.l⁻¹ of iron. Using mole calculations and Avogadro's constant the amount of coating material in both grams, moles and molecules was calculated.

2.15 pH Buffer Experiments

All buffers were purchased as concentrated FIXANAL® buffers from Sigma Aldrich, and were made up to 500 ml with deionised water and kept at room temperature.

One of each type of amino acid; acidic, basic, hydrophobic, and hydrophilic was chosen. Each of these was attached to SPIOs *via* the solvent free grinding method, taken up into distilled water and filtered. Following determination of Fe content by ICP, all samples were diluted to 25 mg.l⁻¹ of iron with distilled water and their initial T₁ and T₂ relaxation times measured using a 0.25 T NMR MOUSE. The repetition time was initially set to 500 ms with 32 Echoes and 32 Averages, although this was altered to obtain the most accurate results for each condition.

1 ml each of the solutions containing coated SPIOs as the desired concentration was placed into vials, with three repeats for each condition. To each vial was added a buffer (1 ml), as indicated in Table 24. After 30 min T_1 and T_2 were measured for each solution.

Amino Acid	NMR Measurement	Neat (no buffer)	pH of buffer solution					Water added (cm ³)
			2.00	4.00	7.00	9.00	11.00	
Alanine.HCl	T1 (ms)	42.6	217.2	250.6	58.6	123.8	166.1	51.3
	T2 (ms)	7.9	10.6	10.2	6.9	9.6	8.7	6.3
Glycine.HCl	T1 (ms)	31.4	271.2	240.1	117.4	112.7	113.9	61.0
	T2 (ms)	6.2	11.3	9.7	6.9	10.2	7.7	8.1
Glutamic Acid.HCl	T1 (ms)	53.7	192.5	175.2	53.2	69.8	175.4	47.8
	T2 (ms)	9.4	10.4	9.7	7.0	7.2	8.6	5.5
Histidine.HCl	T1 (ms)	51.9	206.7	266.7	86.8	106.2	265.7	57.0
	T2 (ms)	8.9	10.5	11.0	8.3	9.9	9.8	8.8

Table 24. Showing the amino acids used and the pH of buffer used.

2.16 Autoclaving of samples

SPIOs were synthesised as previously described and Ascorbic Acid purchased from Sigma Aldrich. Samples were prepared as detailed in Table 25. One set of samples was kept at room temperature overnight, and the other samples autoclaved (121°C, 103 KPa). The samples were then analysed by TEM to determine if the particles had undergone adverse changes during the autoclaving process, and any visual and microscopic observations recorded. MRI measurements were also taken to determine if the magnetic activity of the particles had been affected.

Sample	T ₁ (ms)	T ₂ (ms)	Observations
Ascorbic acid	-	-	Free flowing white crystalline powder.
Ascorbic acid autoclaved	-	-	Clumpy off-white/pale yellow crystalline powder.
SPIOs	-	-	Black powder responsive to magnetic stimuli
SPIOs autoclaved	-	-	Brown powder responsive to magnetic stimuli
Ascorbic acid coated SPIOs	1103.95	12.84	Black powder
Ascorbic acid coated SPIOs autoclaved	927.24	12.84	Brown powder

Table 25. Showing the conditions trialled for autoclaving.

2.17 Size Exclusion Chromatography

G50 Sephadex (10 g) was swelled in water (100 ml) at 37 °C for two hours and then packed into a 1 x 15 cm glass size exclusion column. The column was kept flowing with distilled deionised water. An aqueous solution containing histidine coated SPIO (1 ml, 250 mg.l⁻¹ Fe) was added to the top of the column and run through with distilled deionised water. Fractions (1.5 ml) were collected with a total of 20 fractions collected. Each fraction was analysed by ICP-AES to find Fe content. This was repeated for other samples (Table 26).

Coating material	Observation	Successful Y/N?
Histidine.HCl	Fractions collected were pale brown and indicated separation had occurred. 20 fraction was not sufficient.	Y
Glutamic Acid.HCl	Fractions collected were pale brown and indicated separation had occurred. 20 fraction was not sufficient.	Y
p53 (105).HCl	Sample was stuck at the top of the column and did not separate at all. Experiment repeated with G25 Sephadex which was also unsuccessful.	N

Table 26. Samples used for size exclusion chromatography

2.18 Finding a suitable antisolvent for coated SPIOs

A solution containing glutamic acid hydrochloride coated SPIOs (125 mg.l^{-1} of iron) was prepared and 1 ml transferred to each of seven vials. 3 ml of solvent was added as detailed in Table 27.

Vial	Solvent	Condition	Observations
1	Acetone	Room temperature	Some brown precipitate with small amount of white precipitate
1a	Acetone	6 hours at -2°C (freezer)	Some brown precipitate with large amount of white precipitate
2	Ethanol	Room temperature	No precipitate
2a	Ethanol	6 hours at -2°C (freezer)	No precipitate
3	Acetonitrile	Room temperature	Brown precipitate with very small amount of white precipitate
4	THF	Room temperature	No precipitate
4a	THF	6 hours at -2°C (freezer)	No precipitate

Table 27. Antisolvents and conditions used to precipitate amino acid coated SPIOs

2.19 Separation using a Neodymium magnet

SPIO mixture was prepared as in section 2.8 containing coated SPIOs, free SPIO, free coating material as in Table 28 and water was forced through tubing wrapped around a neodymium magnet, as illustrated in Figure 108. Fractions of the liquid exiting the tube were collected. This was repeated with different solvents to remove the free coating agent, followed by water to solubilise the coated SPIOs to elute them from the tubing.



Figure 108. Syringe containing SPIO mixture is attached to tubing wrapped around neodymium magnet, with a collecting syringe on the other end of the tubing

Fractions were analysed for Fe content using ICP. Initial fractions had their solvent removed *in vacuo* to determine if they contained free coating agent.

Coating on SPIOs	Solvent used	Observation
Ascorbic acid	Water	Magnetic particles moved through the tube and were not separated
Glutamic acid.HCl	Water	Magnetic particles moved through the tube and were not separated
p53(105).HCl	Water	Magnetic particles moved through the tube and were not separated
Ascorbic acid	Acetonitrile	Magnetic particles moved through the tube and were not separated
Glutamic acid.HCl	Acetonitrile	All magnetic particles were separated and stayed on the magnet, colourless solvent eluted. Following addition of water magnetic particles were solubilised and a brown solution eluted. Colourless solvent did not contain free coating agent.
p53(105).HCl	Acetonitrile	Magnetic particles moved through the tube and were not separated
Ascorbic acid	Ethyl acetate	Magnetic particles moved through the tube and were not separated
Glutamic acid.HCl	Ethyl acetate	Magnetic particles moved through the tube and were not separated
p53(105).HCl	Ethyl acetate	Magnetic particles moved through the tube and were not separated

Table 284. Conditions used for trialling magnetic separation method

2.20 Separation using a Magnetic Separation Rack

A magnetic separation rack from BioLabs was used as supplied (Figure 109). The eppendorfs were filled with coated SPIO solutions as in Table 29 (2 ml, 250 mg.l⁻¹) and left for 10 min to separate.



Figure 109. Magnetic separation rack

Coating material	Observation
Histidine.HCl	A mass of SPIO appearing as a “bubble” collected at the magnetic points. On removal of supernatant the SPIOs did not remain on the side of the tube.
Ascorbic Acid	A smaller mass of SPIO appearing as a “bubble” collected at the magnetic points. On removal of supernatant the SPIOs did not remain on the side of the tube.
Glutamic Acid.HCl	A mass of SPIO appearing as a “bubble” collected at the magnetic points. On removal of supernatant the SPIOs did not remain on the side of the tube.

Table 29. Samples used for trial of magnetic separation rack

2.21 High Speed Centrifugation for separating SPIOs from free coating material in solution

An Optima L-100 XP Ultracentrifuge was used, with 70 I rotor and tubes. The samples were centrifuged for 15 minutes (including time taken to put the rotor under vacuum and build up speed)

at a maximum speed of 60, 000 RPM. The samples were spun at the maximum speed for approximately 5 minutes (Table 30).

Sample	Observation
Histidine coated SPIOs	Brown pellet and clear supernatant
Ascorbic acid coated SPIOs	Brown pellet and clear supernatant
p53(105) coated SPIOs	Brown pellet and clear supernatant
Concentrated Histidine coated SPIOs	Dark brown/black pellet and brown supernatant

Table 30. Samples used for separation by high speed centrifugation

Section 3: Synthesis and functionalization of other nanoparticles

3.1 Synthesis of iron (III) tin (II) oxide nanoparticles

Tin (II) chloride (5.3 mmol, 1.00g) and iron (III) chloride (9.5 mmol, 2.57 g) were dissolved separately in the minimum amount of distilled water. These solutions were then combined and ammonia solution (30 %, 30 ml, 0.48 mol) was added slowly whilst stirring. The mixture was then sonicated (1 hr) and filtered. The resultant brown solid was then washed with distilled water (3 x 50 ml) followed by ethyl acetate (2 x 50 ml), and left to dry in air.

Tin (II) chloride (5.3 mmol, 1.00g) and iron (III) chloride (9.5 mmol, 2.57 g) were dissolved separately in the minimum amount of distilled water. These solutions were then combined and ammonia solution (30 %, 30 ml, 0.48 mol) was added whilst stirring. The mixture was then heated at 100 °C for 20 minutes, then filtered. The resultant brown solid was washed with distilled water (3 x 50 ml) followed by ethyl acetate (2 x 50 ml) and allow to dry in air. Yield: 1.82 g (68 % yield).

A portion of the brown powder (200 mg) was then ground with glutamic acid hydrochloride salt (200 mg) using a solvent free grinding method. This was taken up into water (5 ml) and processed through a filter (0.2 µm). The resultant pale brown solution was analysed by TEM, EDX and ICP showing spherical particles of 4-10 nm containing Sn and Fe in the molar ratio of approximately 2:3.

EDX: Atomic concentration 10 % Fe and 6 % Sn.

ICP: Fe = 118.32 mg.l⁻¹, Sn = 168.50 mg.l⁻¹

Moles Fe = 2.12 x 10⁻³

Moles Sn = 1.42 x 10⁻³

3.2 Synthesis of calcium oxide nanoparticles *via* Spinning Disc Reactor (SDR)

Calcium nitrate tetrahydrate (47.24 g, 0.20 mol), was dissolved in ethylene glycol (1000 ml). In a separate container sodium hydroxide (16.8 g, 0.42 mol) was dissolved in distilled water (100 ml). The two solutions were fed into a spinning disc reactor with a feed rate of 10:1 calcium nitrate to

sodium hydroxide at a speed of 1818.2 rpm. The white paste formed was left overnight and then washed with distilled water (500 ml). A sample of the mixture (250 ml) was sonicated for 60 min and analysed by TEM showing spherical particles of 5-10 nm diameter.

3.3 Synthesis of aqueous soluble gold nanoparticles (GNPs)

Typically H₂AuCl₄ hydrate (10 mg, 25 μmol) was dissolved in distilled water (100 ml). Sodium citrate (1 g, 4.67 mmol) was dissolved in distilled water (100 ml). The gold solution (50 ml, 0.01%) was heated to boiling under N₂. Sodium citrate solution (1 ml, 1%) was then added and the mixture boiled until a colour change from yellow to purple was observed (*ca.* 1 min.).

This was repeated at higher concentrations as in Table 31.

% H ₂ AuCl ₄ in solution	Observation
0.01	Purple solution, particles 4-10 nm by TEM with very little agglomeration.
0.02	Black precipitate formed, aggregated and would not go back into solution.
0.05	Black precipitate formed, aggregated and would not go back into solution.
0.075	Black precipitate formed, aggregated and would not go back into solution.
0.10	Black precipitate formed, aggregated and would not go back into solution.

Table 31. Conditions for synthesis of citrate capped gold nanoparticles

3.4 Coating of gold nanoparticles with peptide.

Peptide was dissolved in water (10 mg in 10 ml of distilled water). Peptide solution was heated to boiling point and H₂AuCl₄(aq.) (1 ml, 0.01%) was added. The solution was kept at boiling temperature for 1 minute then left to cool.

The resultant purple solution was found to contain particles of 4-10 nm by TEM and DLS.

To increase the concentration of the gold nanoparticles solvent was removed *in vacuo*.

Section 4: Medical Imaging

4.1 CT analysis of gold nanoparticles

Citrate capped gold nanoparticles were synthesised as previously described and concentrated down *in vacuo*. Au concentration was determined using ICP and the solution diluted as shown in Table 32. The solutions were then scanned in a CT phantom (5mm slice, 120kV, 300 mA 1sec std recon algorithm rmi electron density phantom) to determine their CT number and the results compared against required CT number, using a specially designed PTFE holder.

Conc. mg.l ⁻¹	CT Number
1.42	21.77
0.856	13.75
0.571	8.37

Table 32. Dilutions for CT phantom scanning for citrate capped H₂AuCl₄(aq.)

4.2 Calibration study for SPIOs

SPIOs coated with histidine were prepared *via* the standard route and diluted to different concentrations with distilled water (see Table 33). The T₁ and T₂ relaxation times were then measured using the MRI MOUSE.

Concentration Fe (mg.l ⁻¹)	Maximum Repetition Time (ms)	NEchoes	Number of averages	T ₁ (ms)	T ₂ (ms)
500.00	50	64	284	15.92	4.82
250.00	100	64	192	35.98	7.24
125.00	150	64	192	71.85	9.09
62.50	200	64	96	148.31	10.37
31.25	400	64	48	280.00	11.11
15.63	1500	64	12	655.50	11.28

Table 33. Table for calibration study for SPIOs using NMR MOUSE®

4.3 Lysosome simulation

A solution of HCl histidine coated SPIOs (2 ml, 250 mg.l⁻¹) was added to buffer at pH 4.00, which is similar to the pH inside a lysosome. The T₁ and T₂ relaxations times were measured every minute for a period of 6 hours at room temperature.

4.4 Comparison with commercially available

SPIOs coated with a) Histidine and b) p53(108), prepared *via* the standard method were analysed by ICP and diluted to give a total iron concentration of 250 mg.l⁻¹. The relaxation rates of these solutions were then measured using the 0.25 T NMR MOUSE (Table 34).

Endorem (dextran coated SPIOs) purchased from Guerbet, Sulzbach was also diluted to give a total iron concentration of 250 mg.l⁻¹ and the relaxation rates determined in the same way.

SPIO Coating	T ₁ (ms)	T ₂ (ms)
Dextran (Endorem [®])	14.2662	3.0424
Histidine	3.3637	1.3399
Histidine (+43 days)	9.4887	2.6079
Histidine following dehydration and rehydration	75.4144	8.5825
Histidine diluted with PBS	1113.3641	14.0335
Flu DR1	5.7752	1.4897
Flu DR1 (+43 days)	4.8246	1.5813
Water	~2500	~100

Table 34. NMR measurements for SPIO preparations vs. commercially available

4.5 Blood Studies

Fresh human whole blood (5 ml) with EDTA (as per collection tube) to prevent coagulation was mixed with preparations as described in Table 35. Observations were made and the relaxation times of the different preparations were recorded.

Condition	T ₁ (ms)	T ₂ (ms)
Neat SPIO (300 mg.l ⁻¹)	12.4071	4.0744
SPIO + EDTA	43.8523	10.5295
Blood only	1000.2365	11.9032
Blood + SPIO Solution (1 ml)	62.6773	5.6386
Blood + 0.2 g dehydrated SPIO complex	58.9634	6.9221

Table 35. NMR measurements of SPIOs in blood

Section 5: Transdermal drug delivery

5.1 Synthesis of CPP

Peptide sequence: RRRQRRKRGYC

Peptide was synthesised *via* the standard method using the optimised peptide synthesis protocol. Reagents and coupling times are outlined in Table 36. The peptide was analysed for purity *via* HPLC (see General Experimental section for HPLC conditions and gradient) and MALDI-TOF MS.

0.1639 g of Cysteine resin was swelled for 30 min in 50: 50: DCM: DMF then drained and the following added:

Amino Acid	Mass (g)	DMF (ml)	Coupling conditions
Arginine	3.900	30	2.5 ml amino acid, 1.0 ml HBTU, 0.5 ml DIEA a) As above, 30 minutes at room temperature b) As above, 10 minutes at 75° C
Glutamine	0.305	2.5	2.5 ml amino acid, 1.0 ml HBTU, 0.5 ml DIEA
Glycine	0.150	2.5	2.5 ml amino acid, 1.0 ml HBTU, 0.5 ml DIEA
Lysine	0.470	5.0	2.5 ml amino acid, 1.0 ml HBTU, 0.5 ml DIEA
Tyrosine	0.230	2.5	2.5 ml amino acid, 1.0 ml HBTU, 0.5 ml DIEA

Table 36. Conditions for synthesis of CPP

HPLC retention time: 13.127 minutes. Purity was ca. 60 % by HPLC, but due to the high number of arginine residues in the peptide it was not possible to characterise by MALDI-TOF. Due to time constraints and limitations of available equipment it was not possible to purify the peptide.

5.2 Coating onto SPIO

Peptide was coated onto freshly prepared SPIOs *via* the standard method. The resultant solution was analysed for iron concentration *via* ICP then diluted and used as required. TEM and DLS confirmed spherical particles of 15-20 nm diameter with a clear area of coating material around each particle.

5.3 Distribution in gel

SPIO or SPIO solution (see Table 37) was added to glucosamine gel (10 ml), and was mixed thoroughly using a pipette and pipette filler (1000 μ l) to give a homogeneous mixture. This was repeated for each desired preparation and applied to skin as required.

SPIO preparation to add to gel	Mass (mg)	Volume (ml)	Mass of Fe (mg)	Additional preparations	Final Fe concentration of gel preparation
SPIOs Neat	10	-	7.2	Diluted 10 μ l in 100 μ l gel to give 72 mg.l ⁻¹ Fe	72 mg.l ⁻¹
SPIOs coated with CPP in solution 100 mg.l ⁻¹ Fe	-	10	0.72	-	72 mg.l ⁻¹
Histidine coated SPIOs inside liposomes 100 mg.l ⁻¹ Fe	-	10	0.72	-	72 mg.l ⁻¹
Histidine coated SPIOs inside liposomes with CPP functionalization 100 mg.l ⁻¹	-	10	0.72	-	72 mg.l ⁻¹ Fe

Table 37. Preparations used for CPP transdermal drug delivery trials

5.4 Preparation of pig skin

The skin of a porcine ear, taken within 24 hrs of butchering, was stripped of any fat and cut into sections of 1.0 cm by 3.0 cm from the same area of the ear. These were placed onto a microscope slide under various conditions and the quality of the resultant skin sample assessed (Table 38).

Conditions	Observation
Placed on slide at room temperature.	Skin dried out and curled up at the edges making it very difficult to image.
Placed on a microscope slide in a 50 ml centrifuge tube at room temperature.	Skin dried out and curled up at the edges slightly making it unreliable for imaging.
Placed on a microscope slide in a 50 ml centrifuge tube above 10 ml PBS at room temperature.	Skin slightly dried out and curled at the edges so less reliable for imaging.
Placed on microscope slide in incubator at 37°C	Skin dried up and curled slightly making it less reliable for imaging.
Placed on a microscope slide in a 50 ml centrifuge tube at 37°C.	Skin was very slightly curled at the edges and slightly drier than prior to incubation.
Placed on a microscope slide in a 50 ml centrifuge tube above 10 ml of PBS at 37°C.	Skin moist, uncurled and in optimal condition for imaging.

Table 38. Conditions trialled for pig skin

5.5 Trialling different SPIO preparations on pig skin

When required, the skin was removed and 100 µl of the preparation to be tested administered to the centre of the skin on the stratum corneum side (see Table 39 and Figure 110).

Pig skin was then incubated (37°C) on a microscope slide in a 50 ml centrifuge tube above PBS (10 ml) at for a period of 2.5 hrs to allow the test preparation time to be absorbed.

Following the incubation period pig skin was removed from the incubator and placed immediately onto the NMR MOUSE to obtain accurate readings. Where the skin began to curl, a second slide was administered on top of the skin to keep a flat profile.

Sample Number	Gel used	Extra additive	Observations
1	Yes	None	No change in NMR MOUSE profile. Contrast seen on Biospec with lightening of image.
2	Yes	SPIO-CPP	Decrease in NMR MOUSE profile at 400 μm . BIOSPEC also showed a decrease in signal.
3	No	No	No change in NMR MOUSE profile OR Biospec.

Table 39. Showing the different samples incubated with pig skin samples to test transdermal penetration.



Figure 110. Image of slides with prepared pig skin prior to MRI measurements. From left to right: Slide 1: SPIO-gel only; Slide 2: Skin only; Slide 3: SPIO-gel on skin; Slide 4: skin with gel only; Slide 5: Two pieces of skin with SPIO-gel in between.

5.6 Skin penetration profile with NMR MOUSE 0.25 T

Preliminary measurements (T_1 and T_2) were taken at intervals of 100 μm through the skin to determine where the top and bottom of the skin lay with respect to the magnetic field. The measurements were then repeated, starting at the top of the skin and moving down at 20 μm intervals.

These measurements were carried out on both the nude skin and on the same piece of skin following incubation with sample. The skin was also imaged in 2D using the Biospec 2.45 T MRI.

Section 6: Immunotherapy

6.1 Optimisation of peptide synthesis to obtain higher purity peptides

The following adjustments were made to the peptide synthesis protocol:

The peptide p53(108) was synthesised without storage in freezer between couplings.

Regular amino acid couplings were carried out for 10 minutes at 75 °C. Histidine and cysteine couplings were carried out for 20 minutes at 50 °C. Arginine couplings were carried out at room temperature for 30 minutes followed by the second coupling for 10 minutes at 75 °C.

A comparison of p53(108) synthesised *via* the standard method and the optimised method showed the revised method to be superior (Table 40).

Coupling Conditions	Yield (mg)	Purity by HPLC %	Purity by MALDI-TOF %
5 minute couplings recommended by manufacturer	130	50	45-50
10 minute extended couplings	150	75	70

Table 405. Conditions for optimisation of peptide synthesis

6.2 Synthesis of Immunogenic Peptide(s)

All peptides were synthesised *via* the standard solid phase peptide synthesis protocol using CEM Discover microwave. For peptide sequences and reagents see tables below.

6.2.1 Pap 161

Sequence: CPRFQELESETLKSE

Resin: 0.3448 g Glutamic acid resin swelled.

Amino Acid	Mass (g)	Volume DMF (ml)	Coupling Conditions per amino acid
Arginine	0.650	5.0	Double coupling, each with 0.5 ml DIEA, 1.0 ml HBTU and 2.5 ml of amino acid : a)30 min at room temperature b)5 min 75°C
Cysteine	0.295	2.5	2.5 ml of amino acid, 0.5 ml DIEA, 1 ml HBTU, 10 min 75 °C
Glutamine	0.305	2.5	2.5 ml of amino acid, 0.5 ml DIEA, 1 ml HBTU, 5 min 75 °C
Glutamic Acid	0.645	7.5	2.5 ml of amino acid, 0.5 ml DIEA, 1 ml HBTU, 5 min 75 °C
Leucine	0.350	5.0	2.5 ml of amino acid, 0.5 ml DIEA, 1 ml HBTU, 5 min 75 °C
Lysine	0.235	2.5	2.5 ml of amino acid, 0.5 ml DIEA, 1 ml HBTU, 5 min 75 °C
Phenylalanine	0.195	2.5	2.5 ml of amino acid, 0.5 ml DIEA, 1 ml HBTU, 5 min 75 °C
Proline	0.170	2.5	2.5 ml of amino acid, 0.5 ml DIEA, 1 ml HBTU, 5 min 75 °C
Serine	0.380	5.0	2.5 ml of amino acid, 0.5 ml DIEA, 1 ml HBTU, 5 min 75 °C
Threonine	0.200	2.5	2.5 ml of amino acid, 0.5 ml DIEA, 1 ml HBTU, 5 min 75 °C

Yield: 63 mg. Purity by HPLC: ca. 55 %

Table 41. Reagents and conditions for synthesis of Pap 161

6.2.2 Flu DR1

Sequence: PKYVKQNTLKLAT

0.1639 g Threonine resin swelled, 30 min, 5 ml DMF/DCM (50:50)

Amino Acid	Mass (g)	Volume DMF (ml)	Coupling Conditions per amino acid
Alanine	0.155	2.5	2.5 ml of amino acid, 0.5 ml DIEA, 1 ml HBTU, 5 min 75 °C
Asparagine	0.300	2.5	2.5 ml of amino acid, 0.5 ml DIEA, 1 ml HBTU, 5 min 75 °C
Glutamine	0.305	2.5	2.5 ml of amino acid, 0.5 ml DIEA, 1 ml HBTU, 5 min 75 °C
Leucine	0.350	5.0	2.5 ml of amino acid, 0.5 ml DIEA, 1 ml HBTU, 5 min 75 °C
Lysine	0.705	7.5	2.5 ml of amino acid, 0.5 ml DIEA, 1 ml HBTU, 5 min 75 °C
Proline	0.170	2.5	2.5 ml of amino acid, 0.5 ml DIEA, 1 ml HBTU, 5 min 75 °C
Threonine	0.200	2.5	2.5 ml of amino acid, 0.5 ml DIEA, 1 ml HBTU, 5 min 75 °C
Tyrosine	0.230	2.5	2.5 ml of amino acid, 0.5 ml DIEA, 1 ml HBTU, 5 min 75 °C
Valine	0.170	2.5	2.5 ml of amino acid, 0.5 ml DIEA, 1 ml HBTU, 5 min 75 °C

Yield: 63 mg

Table 42. Reagents and conditions for synthesis of Flu-DR1

Unfortunately the Flu-DR1 synthesised was of very low purity (> 20 % by HPLC) and so commercially available peptide at a purity of 80 % was used (purchased from Peptidecs). This was analysed for purity *via* both HPLC and MALDI-TOF prior to use and was confirmed to be 80 % pure.

6.2.3 P53(108)

Sequence: GFRLGFLHSGTAKSV

0.1639 g of Valine resin swelled, 30 min, 5 ml DMF/DCM (50:50)

Amino Acid	Mass (g)	Volume DMF (ml)	Conditions for coupling per amino acid
Serine	0.380	5.0	2.5 ml of amino acid, 0.5 ml DIEA, 1 ml HBTU, 5 min 75 °C
Lysine	0.235	2.5	2.5 ml of amino acid, 0.5 ml DIEA, 1 ml HBTU, 5 min 75 °C
Alanine	0.155	2.5	2.5 ml of amino acid, 0.5 ml DIEA, 1 ml HBTU, 5 min 75 °C
Threonine	0.200	2.5	2.5 ml of amino acid, 0.5 ml DIEA, 1 ml HBTU, 5 min 75 °C
Glycine	0.450	7.5	2.5 ml of amino acid, 0.5 ml DIEA, 1 ml HBTU, 5 min 75 °C
Histidine	0.310	2.5	2.5 ml of amino acid, 0.5 ml DIEA, 1 ml HBTU, 10 min 75 °C
Leucine	0.350	5.0	2.5 ml of amino acid, 0.5 ml DIEA, 1 ml HBTU, 5 min 75 °C
Phenylalanine	0.390	5.0	2.5 ml of amino acid, 0.5 ml DIEA, 1 ml HBTU, 5 min 75 °C
Arginine	0.650	5.0	Double coupling, each with 0.5 ml DIEA, 1.0 ml HBTU and 2.5 ml of amino acid : a)30 min RTP b)5 min 75°C

**In order to synthesise this peptide with fluorescein on the terminal amine, following arginine coupling, 0.100 g of fluorescein was dissolved in 2.5 ml of DMF and coupled using 0.5 ml DIEA, 1 ml HBTU, for 5 minutes at 75 °C.*

Yield: 45 mg. Purity: 75 % by HPLC and MALDI-TOF

Table 43. Reagents and conditions for synthesis of p53(108)

6.2.4 Synthesis of p53(105)

Sequence: GFHLGFLQSGTAKSV

0.1639 g of Valine resin swelled, 30 min, 5 ml DMF/DCM (50:50)

Amino Acid	Mass (g)	DMF (ml)	Coupling conditions
Serine	0.380	5	2.5 ml amino acid, 1.0 ml HBTU, 0.5 ml DIEA
Lysine	0.235	2.5	2.5 ml amino acid, 1.0 ml HBTU, 0.5 ml DIEA
Alanine	0.155	2.5	2.5 ml amino acid, 1.0 ml HBTU, 0.5 ml DIEA
Threonine	0.200	2.5	2.5 ml amino acid, 1.0 ml HBTU, 0.5 ml DIEA
Glycine	0.450	7.5	2.5 ml amino acid, 1.0 ml HBTU, 0.5 ml DIEA
Glutamine	0.305	2.5	2.5 ml amino acid, 1.0 ml HBTU, 0.5 ml DIEA
Leucine	0.350	5	2.5 ml amino acid, 1.0 ml HBTU, 0.5 ml DIEA
Phenylalanine	0.390	5	2.5 ml amino acid, 1.0 ml HBTU, 0.5 ml DIEA
Histidine	0.310	2.5	2.5 ml amino acid, 1.0 ml HBTU, 0.5 ml DIEA. 20 minute coupling at 50 °C

Yield: 49 mg. Purity: ca. 80 % by HPLC and MALDI-TOF

Table 44. Reagents and conditions for synthesis of p53(105)

*Note: The immunogenic peptides were all synthesised as the peptide acids as these were the available reagents. In future studies the peptide amides should be synthesised for comparison.

6.3 Determining if HCl peptides were still immunogenic

HCl salt of p53(108) was dissolved in DMSO to give a stock solution of 10 mg/ml. This was used to restimulate spleenocytes from mice previously immunised with commercially bought p53(108) (Pepceuticals). An ELISpot assay was performed and the spots counted using a C.T.L. Immunospot counter.

6.4 Synthesis of peptide-SPIO complex

SPIOs were synthesised *via* the standard method and coated with p53 peptide using the pestle and mortar solvent free grinding method. No further purification was carried out. Solvent was removed from the solution *in vacuo* (60 °C, *ca.* 5 mbar). Typically SPIO peptide (2 mg) was dissolved in distilled water (5 ml) and analysed for Fe content using ICP with the result being used to calculate mass of peptide to SPIO using the method previously described. SPIO-peptide was then dissolved in sterile DMSO to give a stock solution of 10 mg/ml which could be further diluted with cell culture media for immunisations. (Note: peptides are measured in mg rather than moles due to the large molar excess used in immunological studies).

6.5 Preliminary cell uptake study with U937

U937 cells grown in RPMI with L-glutamine (10 %) and Foetal Calf Serum (1 %) were counted by haemocytometry as detailed in the general experimental section. The cells were then plated in a sterile 24-well plate at a concentration of 1×10^6 cells per ml of media per well. SPIOs at Fe concentration of 500 mg.l^{-1} were added at a volume of 1 ml per well at different times (see Figure 111 and the corresponding Table 45) and incubated (37°C). A sample of the SPIO solution was incubated (37°C) for the duration of the experiment as a control.

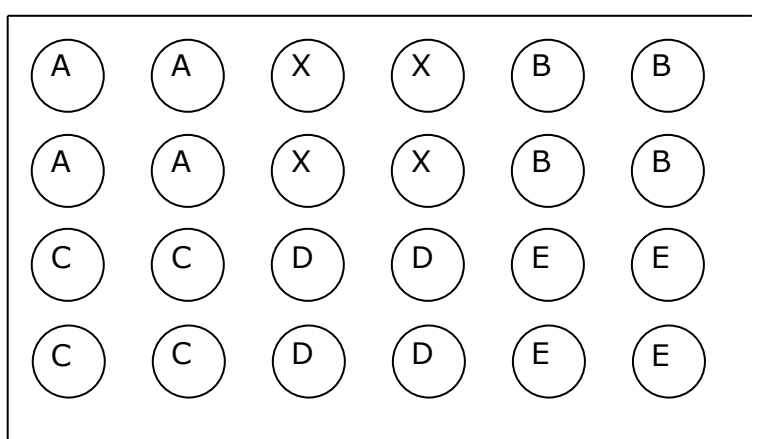


Figure 111. Schematic of 24-well plate for preliminary studies for SPIO uptake by U937. Wells marked "X" were empty.

At 0 hours the cells were removed from the wells and centrifuged (1500 rpm, 4°C for 3 minutes), and washed with PBS (3 x 5 ml). The cells were then placed into glass vials (cells from condition A combined, B combined, C combined, D combined and E combined) and their T_1 and T_2 relaxation times measured. The cells were then digested in nitric acid (1 ml) and diluted with distilled water (to 5 ml), and analysed for Fe concentration by ICP.

Well Identities	Number of cells per ml	Volume of 500 mg.l ⁻¹ SPIO solution added	Time at which SPIO solution added (h)	Fe conc. mg.l ⁻¹	T_1 (ms)	T_2 (ms)
A	1000000	0 (Control, 1 ml of media added instead of SPIOs)	-2	0.975	2675.29	11.1588
B	1000000	1 ml	-2	1.65	2928.8632	11.7707
C	1000000	1 ml	-1.5	1.120	181.0506	10.4381
D	1000000	1 ml	-1.0	1.140	2608.4202	11.4964
E	1000000	1 ml	-0.5	1.115	2790.6152	12.4531

*Incubated SPIOs T_1 : 51.4773 ms; T_2 : 8.0734 ms

Table 45. Shows conditions present in each well depicted in Figure 111.

6.6 Uptake study with bone marrow dendritic cells (BMDCs)

6.6.1 Culturing BMDCs

6.6.1.1 Culturing on standard plates

Sarstedt non-pyrogenic, non-cytotoxic standard 24-well plates were used for culture of BMDC's. BMDC media containing (RPMI (500 ml), glutamine (1 %, 5 ml), FCS (5 %, 25 ml), HEPES buffer (10 mM, 10 ml), 2-mercaptoethanol (50 µM, 500 µl), PEN-STREP (25 µg / ml, 5 ml) and Fungizone (0.25 µg / ml, 500 µl)) was freshly prepared and stored in fridge. On day one hind legs of DR1 mice were cut at the joint and muscle and fat removed. Bone marrow was flushed into a Petri dish using a syringe of BMDC media (10 ml) and a needle. Media containing cells was filtered and resultant media centrifuged (1500 rpm, 10 min, 4 °C) to give a cell pellet. Cells counted using trypan blue and plated at 1 million cells per ml per well in 24-well plate with GMCSF (1 ng per million cells). These were incubated (37 °C, 5.1 % CO₂) and washed with fresh BMDC media (750 µl) on day 3 and 6 and harvested using a pipette tip, before being counted, purified using CD11c⁺ column or number of

BMDCs present determined by CD11c FACS. On day 8 these were recounted and cells could then be re-plated as desired.

6.6.1.2 Culturing in T 25 flasks

Standard T 25 flasks were purchased from Sarstedt and used as received. BMDCs were re-suspended in media with GMCSF and transferred to a T25 flask, washed as described in the general experimental section, and harvested using a cell scraper.

6.6.2 Trialling of different plates for optimal BMDC culturing

Sarstedt standard 24-well plates were used along with BD Purecoat amine and carboxyl coated 24-well plates.

24-well plates with either normal, carboxyl or amine coating were seeded with BMDC's and these were cultured as in section 6.6.1.1. Following culture a total cell count and a BMDC specific cell count following MACS CD11c+ sorting was carried out (Table 46).

	Plate Number	Number of cells after harvesting (x 10 ⁵)	Number of cells following CD11c column (x 10 ⁵)	Number of BMDC's normalised (x10 ⁵)
Normal	1	4	0.75	0.19
	2	5	0.75	0.15
	3	5	0.5	0.1
Carboxyl	1	12	1	0.08
	2	14	2.25	0.16
	3	12	3.25	0.27
Amine	1	3	0.25	0.08
	2	4	0.5	0.13
	3	4	0.5	0.13

Table 46. Results for culturing BMDCs on different plates

Cells were harvested from mice hind legs as in section 6.6.1.1 and seeded at a concentration of 1×10^6 cells per ml of media per well into 3 x non-coated 24-well plate, 3 x carboxyl coated 24-well plate, and 3 x amine coated 24-well plate. The cells were incubated (37 °C, 5.1% CO₂) and washed with fresh media on day 3 and 5, and harvested and counted by haemocytometry on day 7. The cells from each plate were then passed through a CD11c+ column to isolated BMDC's and these also counted by haemocytometry.

6.7 Incubation of BMDCs with SPIOs

Peptide-SPIO solutions were prepared as previously described. This stock solution was diluted to varying concentrations (see Figure 112 and Table 47) and these each added to preparations of cells in a 24-well plate at a volume of 500 µl per well. Each well contained 500,000 cells in BMDC media (1 ml) and GMCSF (1 ng/ml), and were left to incubate (37°C, 4 hours). After 4 hours LPS was added (ca. 1 ml) and the cells left to incubate (37 °C) over night. The following day poly-IC (0.5 ml) was added and the cells left to incubate (37°C, 2 hours) and then harvested by scraping from the 24-well plate using a pipette tip.

Cells were then counted by haemocytometry as in experimental and imaged by fluorescence microscopy.

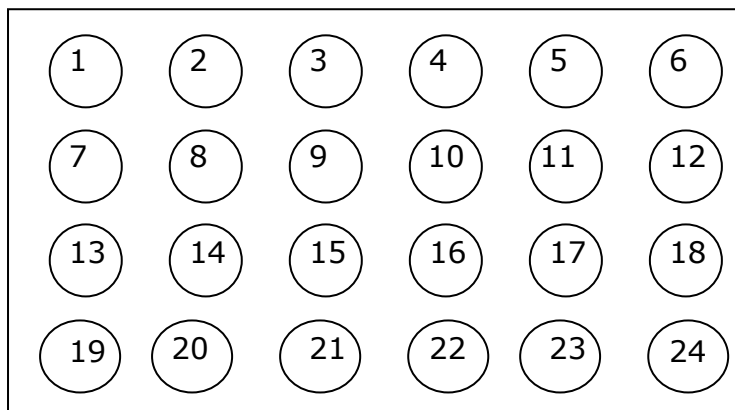


Figure 111. Schematic of 24-well plate used for BMDC uptake of SPIO experiments

Well Number(s)	Conditions	Number of cells ($\times 10^5$)	Observations with fluorescence microscope
1, 2, 3	50 $\mu\text{g/ml}$ SPIO – Peptide - Fluorescein	1.80	Green colour inside cells and blue stain on nuclei. Some cells with only blue nuclear stain.
4, 5, 6	25 $\mu\text{g/ml}$ SPIO – Peptide - Fluorescein	1.10	Green colour inside cells and blue stain on nuclei. Some cells with only blue nuclear stain.
7, 8, 9	10 $\mu\text{g/ml}$ SPIO – Peptide - Fluorescein	0.90	Green colour inside cells and blue stain on nuclei. Some cells with only blue nuclear stain.
10, 11, 12	50 $\mu\text{g/ml}$ SPIO – Peptide	1.50	Blue colour of nuclei observed. Absence of green as no fluorescein present.
13, 14, 15	25 $\mu\text{g/ml}$ SPIO – Peptide	1.00	Blue colour of nuclei observed. Absence of green as no fluorescein present.
16, 17, 18	10 $\mu\text{g/ml}$ SPIO – Peptide	1.20	Blue colour of nuclei observed. Absence of green as no fluorescein present.
19, 20	Control Cells, RPMI media only	1.00	Blue colour of nuclei observed. Absence of green as no fluorescein present.
21, 22	Peptide – Fluorescein, 10 $\mu\text{g/ml}$	0.80	Blue colour of nuclei observed. No green fluorescent stain.
23, 24	Peptide only, 10 $\mu\text{g/ml}$	1.90	Blue colour of nuclei observed. Absence of green as no fluorescein present.

Table 47. Showing conditions for each cell indicated in Fig. 9 with each cell holding 500, 000 BMDC cells in 1 ml BMDC media with 1 ng of GMCSF

6.8 Determining maturation of cells with SPIO-peptide

BMDCs were cultured and incubated (37°C, 24 hrs) with various concentrations of peptide-SPIO complexes with and without adding LPS and poly-IC to mature cells (see Figure 113 and Table 48). Following this, cells were incubated with CD86 (a biomarker for BMDC maturation) linked to fluorophore PE as described in experimental section, with uptake of the fluorophore being the marker for cell maturity. The cells were then imaged *via* fluorescence microscopy to determine if cells had matured.

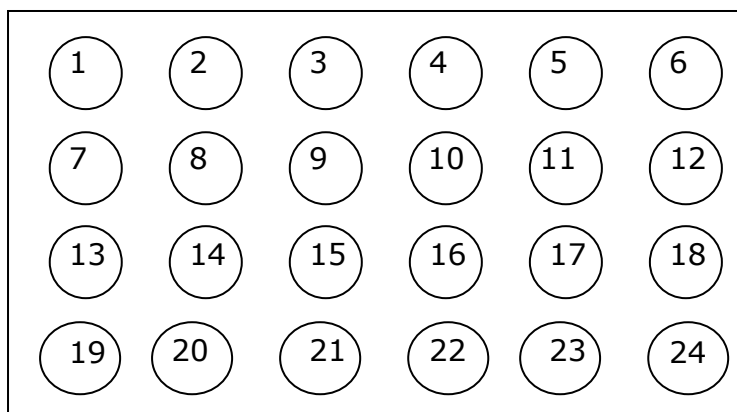


Figure 113. Plan of 24-well plate for BMDC maturation studies

Well Identities	Number of cells per ml	Conditions in Wells	LPS and Poly-IC added (Y/N)?
1 – 3	150 000	50 µg / ml Peptide only	N
7 – 9	150 000	50 µg / ml SPIO - peptide	N
13 – 15	150 000	10 µg / ml Peptide-SPIO	N
19 – 21	150 000	Control Cells	N
4 - 6	150 000	50 µg / ml Peptide only	Y
10 – 12	150 000	50 µg / ml SPIO - peptide	Y
16 – 18	150 000	10 µg / ml Peptide-SPIO	Y
22 - 24	150 000	Control Cells	Y

Table 48. Showing conditions present in each well depicted in Fig. 56 for maturation of BMDCs using SPIOs.

6.9 Cytotoxicity Assay

Cytotoxicity of SPIO-peptide solutions to the cells was determined by incubating BMDCs (2.5×10^5 cells per ml per well) in BMDC media containing GM-CSF (1 ng per ml) for 24 hrs with various concentrations of SPIO-peptide and peptide only (p53(108)) in triplicate as described in Figure 115 and Table 49 and carrying out a cell count by haemocytometry using trypan blue.

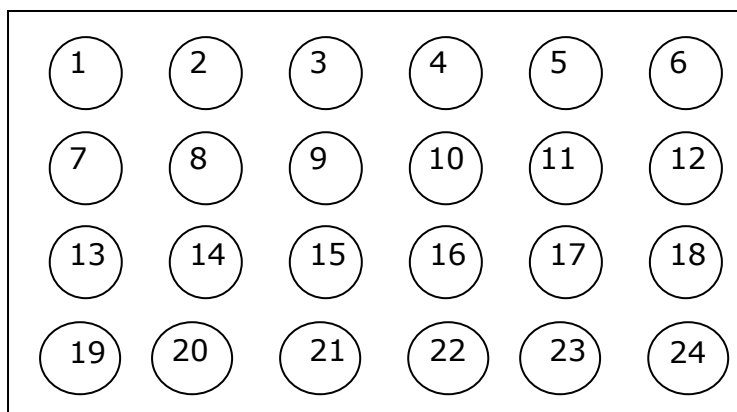


Figure 51. Diagram of 24-well plate for cytotoxicity study

Condition	Cell Count
50 µg/ml p53(108)-Fluorescein	1.80E+05
25 µg/ml p53(108)-Fluorescein	1.10E+05
10 µg/ml SPIO - p53(108)-Fluorescein	9.00E+04
50 µg/ml SPIO - p53(108)-Fluorescein	1.50E+05
25 µg/ml SPIO - p53(108)-Fluorescein	1.00E+05
10 µg/ml p53(108)-Fluorescein	1.20E+05
10 µg/ml p53(108)	1.00E+05
10 µg/ml SPIO - p53(108)	8.00E+04
Control cells with 1 ml BMDC media	1.90E+05
Mean	1.24E+05
Standard Deviation	3.97E+04

Table 49. Showing contents of each well on 24-well plate for assessing cytotoxicity of peptide and peptide-SPIO complex on BMDC's.

6.10 Mouse immunisations

For these experiments female C57BL/6 mice aged 7-9 weeks were used following purchase from Charles River Laboratories, Margate, Kent, UK. Animals were kept at 19 – 23 °C at a humidity of 40 – 70 % and had artificial light for 12 hours out of every 24 hour period, and with air changes a

minimum of fifteen times per hour. Animals were housed in accordance with the Code of Practice for the Housing and Care of Animals Used in Scientific Procedures and in alignment with the United Kingdom Home Office recommendations and requirements. Animals were fed Rodent 2018C Tekland Global Certified Diet (Harlan Laboratories U.K. Ltd., Oxon, UK) and tap or pouched water ad libitum. Animals were acclimatised for one week prior to experimentation.

6.10.1 Immunisation schedule for mice

For each mouse for immunisation with peptide only, stock peptide solution (30 μ l) containing of p53(105) (10 mg/ml) was diluted with PBS (170 μ l) and mixed with IFA (200 μ l). For each immunisation with peptide-SPIO stock peptide-SPIO solution (30 μ l) containing peptide (10 mg/ml) was diluted with PBS (370 μ l). The preparation (100 μ l) was used to give a total of 75 μ g of peptide per mouse per injection.

Mice were immunised by subcutaneous injection at the tail base on day 0, boosted using the same preparations on day 14, and killed and spleens and hind legs harvested on day 21.

The experiment was repeated once staggered by one week.

For each experiment three mice were immunised with p53(105) in IFA, three mice with p53(105)-SPIO and a control naïve mouse was kept under the same conditions.

6.10.2 Harvesting of spleens

Spleens of immunised mice were isolated and all fat removed. These were then flushed with 10 ml of CTL media to remove spleenocytes. The spleen was crushed to remove any remaining spleenocytes. Larger particles from the spleen were allowed to settle (120 sec) then the supernatant removed and spun (10 mins, 1500 RPM). The cell pellet was resuspended in T cell media (2 ml) (RPMI 500 ml, 10% FCS, 2 mM L-glutamine, 20 mM HEPES buffer, 50 μ M 2-mercaptoethanol, 25 mg streptomycin, 12.5 mg Fungizone) and counted using haemocytometry. Cells were then be diluted and/or seeded as required.

6.10.3 Culturing of spleenocytes

Spleenocytes harvested as in section 3.11.7.2 were seeded at 30×10^6 cells per 8 ml T cell media into T25 flasks. These were incubated (37 °C, 5.1 % CO₂) for 1 week.

6.10.4 ELISpot Assay

ELISpot assays were carried out using Mabtech ELISpot kit for mouse IFN- γ on 96-well plates.

On day zero the plate was first wet with ethanol (50 μ l, 70 %) per well for 2 minutes, before washing (5 x 200 μ l sterile water per well). The capture antibody (monoclonal antibody AN18) was diluted to 15 μ g/ml with sterile PBS, then 100 μ l added per well and incubated at 4-8 °C overnight.

On day 1 the antibody was tipped off the plate and each well washed with sterile water (5 x 200 μ l), before adding CTL media (200 μ l per well) and leaving (30 min, 37 °C). The media was then removed and cells (1×10^6 per well) and stimulatory agents added as in Figure 115, before incubation (37 °C, 5.1 % CO₂, 24 hrs).

		M1			M2			M3					
Peptide Concentration in ug / ml	10										Peptide-IFA	Mouse	Spleenocytes
	1												
	0.1												
	0.01												
	10										Peptide-SPIO	Mouse	Spleenocytes
	1												
	0.1												
	0.01												

		Irrelevant Peptide Flu-DR1			Cells Alone						
M1									Peptide-IFA	Mouse	Spleenocytes
M2											
M3											
SEB	M1	M2	M3	Media Alone							
M1									Peptide-SPIO	Mouse	Spleenocytes
M2											
M3											
SEB	M1	M2	M3	Media Alone							

Figure 115. Plate plan for ELISpot following mouse immunisation with p53(105)-SPIO. Shaded cells contain cells and stimulants as indicated. For peptides at different concentrations experiments were run in triplicate for each mouse and all conditions were repeated

To develop the plate cells were removed and each well washed with PBS (5 x 200 µl) before adding monoclonal biotinylated detection antibody (100 µl per well) (1 µg/ml in PBS with 0.5 % FCS) and leaving for 2 hrs at room temperature in the absence of light. Wells were then washed with PBS (5 x 200 µl) and Streptavidin-Alkaline Phosphatase (100 µl) (1:1000 in PBS with 0.5 % FCS) added and left at room temperature for 1 hr in the absence of light. Finally the wells were washed with PBS (5 x 200 µl) before the substrate solution was added (100 µl per well). Plates were allowed to develop until distinct spots emerged before being washed thoroughly with tap water to prevent over-development.

Once the plates were dry they were read using an C.T.L Immunospot counter (Table 50).

	Peptide IFA				Peptide-SPIO			
	Mouse 1	Mouse 2	Mouse 3	Naïve	Mouse 1	Mouse 2	Mouse 3	Naïve
10 ug peptide	67	80	21.7	26.3	58.3	193.3	42.3	27
1 ug peptide	79	95.3	53.3	91.3	89	239.3	68.3	50
0.1 ug peptide	60.7	43	40.3	84.5	66	204.3	75.3	51
0.01 ug peptide	26.3	27	19	71.7	35	107.7	43.7	57.3
Irrelevant	12.33	4.67	8.67		8.33	7.67	7.67	
Cells Alone	2.67	4.33	6.67		4.67	3.33	10	

Table 50. ELISPOT results following mouse immunisation with p53(105)-SPIO

6.10.5 Restimulation and proliferation assay

For restimulation ELISpot the protocol was followed as described. Spleenocytes were seeded at 30×10^6 cells per 8 ml T cell media in T25 flasks. To this was added $1 \mu\text{l/ml}$ of the 10 mg/ml stock peptide solution (total $10 \mu\text{g}$) along with $1 \mu\text{l/ml}$ of vitamin E and kept in the dark for 1 week.

On Day 1 naïve BMDC's were pulsed with the peptide ($1 \mu\text{l}$, $10 \mu\text{g}$ per ml per well) and incubated (37°C , $5.1\% \text{ CO}_2$) for 4 hours before adding LPS for cell maturation ($100 \mu\text{l}$ per well or stock diluted 1:100 with BMDC media) and incubating overnight.

BMDC's were then harvested and counted before resuspension in BMDC media (1 ml). PolyIC ($12.5 \mu\text{l}$) was then added to further mature the cells, and incubated (2 hrs, 37°C).

BMDCs and Spleenocytes previously stimulated with peptide were counted and seeded at 1×10^4 BMDC's per well and 1×10^5 T cells per well on the ELISpot plate at the point in the protocol requiring cells and stimulating agents (see Figure 116 and Table 51).

Spots were counted using a C.T.L. Immunospot counter.

		M1				M2				M3			
Peptide-IFA Mouse Spleenocytes	T cells alone												
	T Cells and DC peptide												
	1 µg peptide												
	Irrelevant peptide												
Peptide-SPIO Mouse Spleenocytes	T cells alone												
	T Cells and DC peptide												
	1 µg peptide												
	Irrelevant peptide												

Naive	T cells alone				
	T Cells and DC peptide				
	1 µg peptide				
	Irrelevant peptide				

Figure 116. 96- well plate plan for restimulation ELISpot following mouse immunisations. Wells not shown were left empty, shaded wells were filled as shown.

		T cells alone	T cell and DC peptide	1 ug peptide	Irrelevant Peptide
Peptide	M1	295.25	533.5	520.25	537.25
	M2	306	540	512.5	545.5
	M2	182.5	356.75	420	437
SPIO	M1	274.5	425	233.25	203
	M2	407.5	598.75	298.25	167.5
	M3	408	367.75	265.5	143
	Naïve	244.5	50.75	323	336.75

Table 51. Results for ELISPOT following restimulation of spleenocytes from mine immunised with p53(105)-SPIO

Chapter 4: Conclusion

Section 1: Synthesis of Particles

SPIO's were successfully synthesised *via* both co-precipitation and SDR methods with co-precipitation forming the most uniform particles of 10-15 nm. The SDR produced particles that had a wide size range from 8-42 nm and due to excess reagents some rod shaped particles were formed. However, the SDR appeared to be the most suitable method for scaling up the reaction and so the method should be improved. As the size of the particles is determined by nucleation, spin speed, feed rate and concentration of reagents, all of these things could be further explored. The size of the grooves on the disc could also affect particle size as these affect micro-mixing effects. In keeping with the effects of micro-mixing, the feed rate plays an important factor. The results showed that excess reagents led to nucleation and the formation of rods, and so the effects of lower volumes of reagents, possibly by flow rate, should be investigated.

The results from using the SDR also show that using gaseous ammonia rather than liquid ammonia can improve the quality of SPIOs, leading to less aggregation. Again, this can be affected by the concentration of the reagents and the feed flow rate so these factors need to be explored in more detail.

Calcium oxide nanoparticles were also formed using the SDR, yielding spherical particles of 5-10 nm in diameter that appeared uniform by TEM. These particles had a much narrower size distribution showing that under the right conditions the SDR is suitable for forming uniform particles.

An iron tin oxide complex was also synthesised using a co-precipitation, yielding spherical particles of 4-10 nm in diameter with a suggested chemical formula of $\text{Fe}_5\text{Sn}_2\text{O}_9$, taken from a combination of ICP and EDX results. In order to clarify if this is the correct formula, x-ray powder diffraction should be carried out.

Gold nanoparticles (citrate capped) were also synthesised, in this case *via* a reduction method with sodium citrate as the reducing agent. This was also successful, yielding spherical particles of 4-10 nm in diameter with the colour of the solution being dependent on the size of the majority of the particles. The smaller particles (4 nm) gave a purple solution, with the larger particles (10 nm) giving a red solution. What was also noticed was that at higher concentrations the particles quickly aggregated to give black particles that would not go back into solution.

Section 2: Coating of particles

The solvent-free grinding method was found to be hugely successful, with the method being successful for SPIOs, CaO, and FeSnO particles. In each case particles were coated, solubilised and when imaged by TEM showed that there were spherical particles with a coating, shown as a clear area around particles.

For this method, the pestle and mortar is currently the best method, giving rise to higher yields. However, the coffee grinder method produced more homogeneous particles and so would be more suitable for scale-up. To optimise the method, a machine similar to the coffee grinder could be designed, with the burrs having smaller grooves and being closer together.

Investigations into the effect of mass ratio of the SPIOs to coating material were inconclusive, but there seemed to be a very weak negative correlation between mass ratio of coating material and the concentration of iron in the resultant preparations. This was attributed to mixing effects, with larger quantities of coating leading to less interaction between coating and particle. This has implications for future synthesis, with a recommendation that the coating material be kept to a minimum.

A heating method was trialled and this produced SPIO-coating complexes with very large concentrations of iron, although the particles were heavily aggregated with sizes of ~ 1000 nm. As the method proved so successful for binding SPIO and coating together it stands to reason that once optimised this would be the best method. To do this, the particles should be kept as separate as possible during coating so as to avoid aggregation. Further investigation will be needed in this area.

A combination of investigation and literature showed that $-\text{COOH}$, $-\text{NH}_2$, and $-\text{OH}$ were responsible for binding to the SPIOs. This is through electrostatic interactions which, it was found, are enhanced by using salts of the coating materials. This was proven for all 20 naturally occurring amino acids, although it was not clear if this was due to increased solubility or enhancement of the electrostatic interactions themselves. Further investigation is required in this area.

The actual coverage of the particle with coating was assessed and by calculations into the maximum number of coating molecules for monolayer coverage vs. the number of molecules present on a particle as analysed by ICP, it was clear to see that several layers of coating material have been bound to the particle. In order for the results of this to be conclusive modelling software could be used. This would show what kind of coverage would be expected on such a particle, and would either confirm or reject the idea that there are ~ 1000 more coating molecules present than are necessary for a monolayer to form. The actual number of coating materials has implications for

future use, as the number /concentration of particle molecules is important for accuracy and consistency in biological applications.

When autoclaving was carried out, with a view to using the particles for biological applications such as immunisations, results showed that although the particles has visibly changed colour from black to brown. The amino acid coating showed a very small amount of degradation, but NMR measurements showed that there had been no adverse effects and the SPIOs were still potentially suitable for use in MRI imaging. To further clarify these findings the x-ray diffraction of all particles could be carried out, as this is a more accurate method of looking at the microstructure.

Additionally, buffer experiments showed the coated SPIOs to be very stable in buffered solution. Previously the literature had suggested that SPIOs underwent rapid degradation on exposure to buffers, but these particles remained stable in buffered solution for a period of 1 week. However, this experiment was only carried once with some conditions repeated. For this reason it should be repeated to show that results were accurate and the SPIOs prepared *via* the solvent free grinding route, were very stable in both aqueous and buffered solutions.

Section 3: Separation and purification of particles

Size exclusion was the first method trialled and this proved to be effective for smaller sized coatings such as single amino acids, but was unsuitable for larger coating such as immunogenic peptides (12-15 amino acids long). The longer coatings caused the SPIOs to become stuck on the column, possibly because they were too large to pass around the beads, or because they were too small to avoid the pores, but too large to pass through.

As size exclusion was effective for the smaller coatings, it is possible that with tailoring it could be effective for larger ones. Further studies could include using different packing materials with larger or smaller bead sizes and different pore sizes. The flow rate could also be investigated as it may be the case that with a slower flow rate the materials would pass through the column successfully.

The investigation into antisolvents had mixed success with acetonitrile being identified as the most effective for the majority of organic coatings. This solvent was able to cause precipitation of coated SPIOs whilst avoiding the majority of the coating falling out of solution. Acetone caused precipitation of too much of the free coating material to be considered successful although it could be further investigated.

When taking this method into consideration as a whole, the use of large volumes of solvents leads to high volumes of waste solvents. It seems pointless to have developed a solvent-free approach to coating the particles if large volumes of solvents are then going to be used in the separation/purification step, so this method does not seem very viable.

Further work could include looking at using antisolvents but in a way that allows recycling following use. By reclaiming the solvents there is not real waste and so the process remains essentially "green".

The magnetic separation method was largely unsuccessful, and the SPIOs, due to their small size were able to overcome the magnetic forces of attraction. In these cases the forces of Brownian motion were larger than that of the magnetic field, thus allowing particles to remain suspended in solution.

When using the magnetic separation with tubing and a neodymium magnet there was limited success with HCl histidine coated particles. These were able to separate into free coating material, coated SPIOs and uncoated SPIOs. However, all other samples trialled failed even with different solvents. It would be beneficial to repeat this experiment but with a wide variety of different

coatings in order to determine which of the coatings make particles suitable for the magnetic separation method. Additionally stronger magnets could be used, thereby determining the minimum magnetic field strength required for successful magnetic separation.

The final method trialled, centrifugal force, had the most potential for both a small and large scale separation. When spun at a speed of 60 000 rpm, the SPIO solution separated into a brown pellet and a colourless supernatant. Whilst results are not conclusive due to machinery being damaged during the experiment, when combined with the literature it can be assumed that this method is the most reliable and effective. Further investigations should be carried out into the use of density gradients, and when repeated the supernatant should be tested for free coating material by removing the solvent *in vacuo*.

Overall this part of the project was the most inconclusive and would require the most additional investigation.

Section 4: Medical Imaging

For CT imaging gold nanoparticles were synthesised and concentrated *in vacuo* to give concentrations that could be detected by CT. These were placed into a CT phantom for comparison with body tissues, and the resultant CT values showed that if these particles were to be used for CT a concentration of 3700 mg.l⁻¹ would be required. For this reason the use of gold for CT was abandoned. During the course of this research it was also reported in the literature that gold accumulates in the liver and cannot be removed by the body, thus making it unsuitable for medical imaging. What it could be used for however, is OCT imaging, where the particles could be delivered under the skin for imaging of subcutaneous disorders.

Another route that could be taken is to use iodinated peptides, or possibly the iron tin oxide particles, as tin has a high atomic number and so would be suitable for x-ray imaging. It may also be possible to attach a drug molecule such as iodipamide to SPIOs or to the peptides, thus creating a complex containing atoms with a high atomic number.

Studies into incubation of cells with SPIO complexes indicated that for studies into cells *in vitro* the concentration of iron in SPIO solutions needed to be higher, or alternatively the magnetic field strength needed to be higher. These studies were carried out using a 0.25 T NMR MOUSE but higher field strengths such as 2.45 T exhibited by the BIOSPEC would be more suitable.

What was shown however, was that SPIOs attached to cell-penetrating peptides were able to penetrate porcine skin to layers below the stratum corneum, with a reduction in the relaxation time of the skin in that area being shown to have decreased. This shows that SPIOs can successfully cross the skin, which has applications for use in hyperthermia for treating skin melanoma.

One key problem with the skin studies was the use of non-comparable skin samples. As they were taken from a pig butchered for meat rather than research the skin was uneven and results are not likely to be reproducible. For future studies either a skin model or animals for research should be used to ensure uniformity of samples.

In order for these preparations to be used in medical applications, they must be stable in buffered solutions, and studies into stability in buffers led to the conclusion that in contrast with findings reported in the literature these particles are very stable in both water and buffered solutions. It can be assumed then that these particles would be retained in the body long enough for imaging to be carried out although further *in vivo* studies would need to be carried out. What is promising for these preparations is that the cytotoxicity assay indicated that the coated SPIO's were not toxic up to and including a peptide concentration of 50 µg/ml.

Promisingly the blood studies also showed that SPIOs coated *via* the solvent free grinding method would also be stable in blood, although in the presence of EDTA the blood clotted and firm conclusions could not be drawn. It is suggested that further studies on blood plasma rather than whole blood should be carried out to produce more reliable results with respect to stability in blood.

When compared to commercially available alternatives, the SPIOs gave comparable NMR relaxation times, but were considered to be superior as they were more stable when in solution. Endorem® quickly came out of solution to form brown crystals that could not be taken back up into solution, when removed from the protective atmosphere of the vial despite being transferred to another closed vial. In stark contrast the coated SPIOs remained stable both in powder form and in solution at room temperature for 1 month +. As there are currently issues with the safety of SPIO preparations for MRI, coated particles formed by solvent free grinding methods may be able to overcome any issues, and this should be further researched.

Section 5: Cell Studies for uptake of coated SPIOs

U937 cells were used for preliminary investigations into the uptake of SPIOs by monocytes. The results were inconclusive due to low concentrations of SPIOs and low field strength of the NMR MOUSE used for imaging. Unfortunately due to time limitations and technical problems it was not possible to repeat this experiment using a higher magnetic field but this could be done in further work.

When studies progressed to BMDC's a different approach was taken, using SPIOs with a fluorescently labelled coating to track uptake. The images obtained showed that fluorescently labelled material had passed into the cytoplasm of the cells, but only when SPIO was present. So it can be concluded that the SPIOs act as a successful vector for delivery of materials into dendritic cells. This could be further quantified using a Quantum MESF FITC kit, which would show how many molecules of the coating material were entering the cell.

For the biological applications of SPIOs cell culture was an integral part, and the successful culture of sufficient numbers of BMDC's was essential. Due to problems with culturing the type of plate was investigated, with the variations being standard plates, carboxyl coated and amine coated. It was found that although carboxyl coated plates led to a general increase in the number of all cells it did not increase the number of BMDC's specifically. It was suggested that the washing steps were responsible for loss of BMDC's as this would remove any cells that were not completely adhered. T25 flasks were trialled for this but did not show any increase in the number of BMDC's. However, there is less likelihood of killing cells during the scraping process so T25 flasks would be better to use. As an increased number of BMDC's would be beneficial to this type of research, time should be taken to investigate other coatings in this way, as there are currently no suggestions by any of the suppliers.

Section 6: Mouse Immunisations

Before peptides can be used for immunisations they need to meet certain purity expectations, with the minimum being 75 % purity. The standard peptide synthesis route was producing peptides with variable purity averaging at ~ 50 %. An optimised method was devised using double coupling times and continuous synthesis, and this was found by both MALDI-TOF MS and HPLC to give peptides a purity of ~ 75 %. To further increase purity (some protocols require 80 % plus purity) a purification step could be added. This could not be carried out during the scope of this project as with the equipment available a minimum of three weeks would have been required to collect a 10 mg sample. A much larger column would be required for this purification step to be viable.

As has been mentioned, in order to increase solubility the peptides had to be recrystallized from $\text{HCl}_{(\text{aq})}$ and it was not clear if this would affect immunogenicity. An ELISPOT assay was carried out using splenocytes from mice immunised with commercially available p53(108), and it was found that the recrystallized p53(108) created the desired immune response, thus indicating that the recrystallization process had not affected the immunogenicity of the peptide. This needs to be checked for any peptides that are to be used, as this would not necessarily be the case with all peptides.

SPIOs were tested against IFA as a vector for delivery of peptides for immunisation. The results indicate that the SPIOs were equivalent to IFA in terms of the immune response produced, but produced a significantly more specific immune response than IFA. The IFA- peptide immunised mice showed no difference in its response to the irrelevant peptide vs. the p53(105) whereas the SPIO-peptide immunised mice showed a significantly higher response to the p53(105) compared with the irrelevant peptide. This confirms that not only is SPIO suitable as a vector for peptide delivery, but that it also creates a much more specific immune response in the case of p53(105). Further studies on other peptides should be carried out, as this may be a phenomenon specific to just one peptide, although the preliminary studies with BMDC's do indicate that SPIOs can act as vectors.

The major improvement that is required for this method is improvement of the solubility of peptide-SPIOs in DMSO, which has already been brought up in the SPIO coating section.

References

- 1 R. P. Feynman, *Plenty of room at the bottom*, Americal Physical Society, United States of America, 1959.
- 2 No author, *What is nanotechnology?*, www.nano.gov/nanotech-101/what/definition, United States of America, 2013.
- 3 B. I. Kharisov, *Recent Patents on Nanotechnology*, 2008, **2**, 190.
- 4 E. Drexler, *Engines of creation: The coming era of nanotechnology*, Anchor books, United States of America, 1986.
- 5 S. Lohse, *Nanoparticles are all around us*, Sustainable Nano, <http://sustainable-nano.com/2013/03/25/nanoparticles-are-all-around-us/>, 15th March, 2013.
- 6 G. Sharma and P. Jeevanandam, *Appl. Surf. Sci.*, 2012, **258**, 3679-3688 (DOI:10.1016/j.apsusc.2011.12.005).
- 7 E. Darezereshki, M. Alizadeh, F. Bakhtiari, M. Schaffie and M. Ranjbar, *Appl. Clay. Sci.*, 2011, **54**, 107-111 (DOI:10.1016/j.clay.2011.07.023).
- 8 S. Farhadi and Z. Roostaei-Zaniyani, *Polyhedron*, 2011, **30**, 971-975 (DOI:10.1016/j.poly.2010.12.044).
- 9 F. Davar, M. Salavati-Niasari, N. Mir, K. Saberyan, M. Monemzadeh and E. Ahmadi, *Polyhedron*, 2010, **29**, 1747-1753 (DOI:10.1016/j.poly.2010.02.026).
- 10 D. Maity, S. Choo, J. Yi, J. Ding and J. M. Xue, *J Magn. Magn. Mater.*, 2009, **321**, 1256-1259 (DOI:10.1016/j.jmmm.2008.11.013).
- 11 P. K. Sahoo, S. S. Kalyan Kamal, M. Premkumar, T. Jagadeesh Kumar, B. Sreedhar, A. K. Singh, S. K. Srivastava and K. Chandra Sekhar, *Int. J. Refract. Met. H.*, 2009, **27**, 784-791 (DOI:10.1016/j.ijrmhm.2009.01.005).
- 12 M. Salavati-Niasari and F. Davar, *Mater. Lett.*, 2009, **63**, 441-443 (DOI:10.1016/j.matlet.2008.11.023).

- 13 C. Yang, N. K. van der Laak, K. Chan and X. Zhang, *Electrochim. Acta*, 2012, **75**, 262-272 (DOI:10.1016/j.electacta.2012.04.107).
- 14 L. Han, H. Liu and Y. Wei, *Powder Technol.*, 2011, **207**, 42-46 (DOI:10.1016/j.powtec.2010.10.008).
- 15 M. R. Housaindokht and A. N. Pour, *J. Nat. Gas Chem.*, 2011, **20**, 687-692 (DOI:10.1016/S1003-9953(10)60234-4).
- 16 M. F. Nazar, O. Myakonkaya, S. S. Shah and J. Eastoe, *J. Colloid Interface Sci.*, 2011, **354**, 624-629 (DOI:10.1016/j.jcis.2010.11.017).
- 17 D. Sarkar, S. Tikku, V. Thapar, R. S. Srinivasa and K. C. Khilar, *Colloids Surf. Physicochem. Eng. Aspects*, 2011, **381**, 123-129 (DOI:10.1016/j.colsurfa.2011.03.041).
- 18 T. Aubert, F. Grasset, S. Mornet, E. Duguet, O. Cador, S. Cordier, Y. Molard, V. Demange, M. Mortier and H. Haneda, *J. Colloid Interface Sci.*, 2010, **341**, 201-208 (DOI:10.1016/j.jcis.2009.09.064).
- 19 R. K. Keswani, H. Ghodke, D. Sarkar, K. C. Khilar and R. S. Srinivasa, *Colloids Surf. Physicochem. Eng. Aspects*, 2010, **369**, 75-81 (DOI:10.1016/j.colsurfa.2010.08.001).
- 20 A. Bumajdad, J. Eastoe, M. I. Zaki, R. K. Heenan and L. Pasupulety, *J. Colloid Interface Sci.*, 2007, **312**, 68-75 (DOI:10.1016/j.jcis.2006.09.007).
- 21 A. B. Chin and I. I. Yaacob, *J. Mater. Process. Technol.*, 2007, **191**, 235-237 (DOI:10.1016/j.jmatprotec.2007.03.011).
- 22 W. Zhang, X. Qiao and J. Chen, *Mater. Sci. Eng. B-Adv.*, 2007, **142**, 1-15 (DOI:10.1016/j.mseb.2007.06.014).
- 23 A. C. Sintov and S. Botner, *Int. J. Pharm.*, 2006, **311**, 55-62 (DOI:10.1016/j.ijpharm.2005.12.019).
- 24 J. Vidal-Vidal, J. Rivas and M. A. López-Quintela, *Colloids Surf. Physicochem. Eng. Aspects*, 2006, **288**, 44-51 (DOI:10.1016/j.colsurfa.2006.04.027).
- 25 M. A. Lopez-Quintela, *Curr. Opin. Colloid In.*, 2003, **8**, 137.
- 26 E. J. Kim and S. Hahn, *Mater. Lett.*, 2001, **49**, 244-249 (DOI:10.1016/S0167-577X(00)00382-7).

- 27 M. Gobe, K. Kon-No, K. Kandori and A. Kitahara, *J. Colloid Interface Sci.*, 1983, **93**, 293-295 (DOI:DOI: 10.1016/0021-9797(83)90411-3).
- 28 S. Anandan, G. Lee, C. Yang, M. Ashokkumar and J. J. Wu, *Chem. Eng. J.*, 2012, **183**, 46-52 (DOI:10.1016/j.cej.2011.12.018).
- 29 P. Banerjee, S. Chakrabarti, S. Maitra and B. K. Dutta, *Ultrason. Sonochem.*, 2012, **19**, 85-93 (DOI:10.1016/j.ultsonch.2011.05.007).
- 30 M. Darroudi, A. Khorsand Zak, M. R. Muhamad, N. M. Huang and M. Hakimi, *Mater. Lett.*, 2012, **66**, 117-120 (DOI:10.1016/j.matlet.2011.08.016).
- 31 G. Marchegiani, P. Imperatori, A. Mari, L. Pilloni, A. Chiolerio, P. Allia, P. Tiberto and L. Suber, *Ultrason. Sonochem.*, 2012, **19**, 877-882 (DOI:10.1016/j.ultsonch.2011.12.007).
- 32 A. Hassanjani-Roshan, M. R. Vaezi, A. Shokuhfar and Z. Rajabali, *Particuology*, 2011, **9**, 95-99 (DOI:10.1016/j.partic.2010.05.013).
- 33 N. Wongpisutpaisan, P. Charoonsuk, N. Vittayakorn and W. Pecharapa, *Energy Procedia*, 2011, **9**, 404-409 (DOI:10.1016/j.egypro.2011.09.044).
- 34 P. S. S. Kumar, A. Manivel, S. Anandan, M. Zhou, F. Grieser and M. Ashokkumar, *Colloids Surf. Physicochem. Eng. Aspects*, 2010, **356**, 140-144 (DOI:10.1016/j.colsurfa.2010.01.004).
- 35 J. Jang, J. Kim, Y. Lee, C. Pak and Y. Kwon, *Electrochim. Acta*, 2009, **55**, 485-490 (DOI:10.1016/j.electacta.2009.08.061).
- 36 K. Okitsu, Y. Mizukoshi, T. A. Yamamoto, Y. Maeda and Y. Nagata, *Mater Lett*, 2007, **61**, 3429-3431 (DOI:10.1016/j.matlet.2006.11.090).
- 37 E. Hee Kim, H. Sook Lee, B. Kook Kwak and B. Kim, *J Magn Magn Mater*, 2005, **289**, 328-330 (DOI:DOI: 10.1016/j.jmmm.2004.11.093).
- 38 A. Ramadoss and S. J. Kim, *J. Alloys Compounds*, (DOI:10.1016/j.jallcom.2012.08.005).
- 39 B. de Caprariis, M. Di Rita, M. Stoller, N. Verdone and A. Chianese, *Chem. Eng. Sci.*, 2012, **76**, 73-80 (DOI:10.1016/j.ces.2012.03.043).

- 40 H. Liu, Y. Wang, C. Li and C. Y. Tai, *Chem. Eng. J.*, 2012, **183**, 466-472 (DOI:10.1016/j.cej.2011.12.035).
- 41 C. Y. Tai, Y. H. Wang, Y. W. Kuo, M. H. Chang and H. S. Liu, *Chem. Eng. Sci.*, 2009, **64**, 3112-3119 (DOI:10.1016/j.ces.2009.03.041).
- 42 E. K. Goharshadi and M. Hadadian, *Ceram. Int.*, 2012, **38**, 1771-1777 (DOI:10.1016/j.ceramint.2011.09.063).
- 43 L. M. Fang, X. T. Zu, Z. J. Li, S. Zhu, C. M. Liu, W. L. Zhou and L. M. Wang, *J. Alloys Compounds*, 2008, **454**, 261-267 (DOI:10.1016/j.jallcom.2006.12.014).
- 44 C. Suci, A. C. Hoffmann, A. Vik and F. Goga, *Chem. Eng. J.*, 2008, **138**, 608-615 (DOI:10.1016/j.cej.2007.09.020).
- 45 Q. Li, L. Wang, B. Hu, C. Yang, L. Zhou and L. Zhang, *Mater Lett*, 2007, **61**, 1615-1618 (DOI:10.1016/j.matlet.2006.07.113).
- 46 F. Chen, K. Zhu, L. Huang, Y. Chen and F. Kooli, *Mater. Res. Bull.*, 2006, **41**, 10-18 (DOI:10.1016/j.materresbull.2005.07.041).
- 47 Y. X. Pang and X. Bao, *J. Eur. Ceram. Soc.*, 2003, **23**, 1697-1704 (DOI:10.1016/S0955-2219(02)00413-2).
- 48 Y. H. Kim, D. K. Lee, B. G. Jo, J. H. Jeong and Y. S. Kang, *Colloids Surf. Physicochem. Eng. Aspects*, 2006, **284-285**, 364-368 (DOI:10.1016/j.colsurfa.2005.10.067).
- 49 H. Shao, H. Lee, Y. Suh, J. Kim, Y. Li and C. Kim, *J. Iron Steel Res., Int.*, 2006, **13**, **Supplement 1**, 205-208 (DOI:10.1016/S1006-706X(08)60183-1).
- 50 S. Lee and M. T. Harris, *J. Colloid Interface Sci.*, 2006, **293**, 401-408 (DOI:10.1016/j.jcis.2005.06.062).
- 51 Z. Li, B. Hou, Y. Xu, D. Wu, Y. Sun, W. Hu and F. Deng, *J. Solid State Chem.*, 2005, **178**, 1395-1405 (DOI:10.1016/j.jssc.2004.12.034).
- 52 D. Maity, S. N. Kale, R. Kaul-Ghanekar, J. Xue and J. Ding, *J. Magn. Magn. Mater.*, 2009, **321**, 3093-3098 (DOI:<http://dx.doi.org/10.1016/j.jmmm.2009.05.020>).

- 53 K. Melghit and K. Bouziane, *Mater. Sci. Eng. B-Adv.*, 2006, **128**, 58-62 (DOI:10.1016/j.mseb.2005.11.024).
- 54 S. L. Easo and P. V. Mohanan, *Carbohydr. Polym.*, 2013, **92**, 726-732 (DOI:<http://dx.doi.org/10.1016/j.carbpol.2012.09.098>).
- 55 Y. Yang, H. Chen, B. Zhao and X. Bao, *J. Cryst. Growth*, 2004, **263**, 447-453 (DOI:10.1016/j.jcrysgr.2003.12.010).
- 56 R. Muñoz-Espí, C. K. Weiss and K. Landfester, *Curr. Opin. Colloid In.*, 2012, **17**, 212-224 (DOI:10.1016/j.cocis.2012.04.002).
- 57 G. Guo, Y. Sun, Z. Wang and H. Guo, *Ceram. Int.*, 2005, **31**, 869-872 (DOI:10.1016/j.ceramint.2004.10.003).
- 58 J. Zhi, Y. Wang, Y. Lu, J. Ma and G. Luo, *React Funct Polym*, 2006, **66**, 1552-1558 (DOI:10.1016/j.reactfunctpolym.2006.05.006).
- 59 K. Petcharoen and A. Sirivat, *Mater. Sci. Eng. B Int.*, 2012, **177**, 421-427 (DOI:10.1016/j.mseb.2012.01.003).
- 60 K. Petcharoen and A. Sirivat, *Mater. Sci. Eng. B Int.*, 2012, **177**, 421.
- 61 S. Wu, A. Sun, F. Zhai, J. Wang, W. Xu, Q. Zhang and A. A. Volinsky, *Mater Lett*, 2011, **65**, 1882-1884 (DOI:10.1016/j.matlet.2011.03.065).
- 62 W. Hsu, S. C. Chen, P. C. Kuo, C. T. Lie and W. S. Tsai, *Mater. Sci. Eng. B Int.*, 2004, **111**, 142-149 (DOI:10.1016/j.mseb.2004.04.009).
- 63 H. Yang, X. Song, X. Zhang, W. Ao and G. Qiu, *Mater Lett*, 2003, **57**, 3124-3127 (DOI:10.1016/S0167-577X(03)00008-9).
- 64 J. Lu, Y. Huang, W. Zhao, Y. Chen, J. Li, X. Gao, R. Venkataramanan and S. Li, *Mol. Pharm.*, 2013, **10**, 2880.
- 65 B. Jiang, L. Hu, C. Gao and J. Shen, *Int. J. Pharm.*, 2005, **304**, 220-230 (DOI:10.1016/j.ijpharm.2005.08.008).

- 66 T. J. Mason and D. Peters, *Practical Sonochemistry: Power Ultrasound Uses and Applications 2nd ed.*, Harwood Publishing, Chichester, 2004.
- 67 S. F. Chin, K. S. Iyer, C. L. Raston and M. Saunders, *Adv. Funct. Mater.*, 2008, **18**, 922.
- 68 C. Y. Tai, C. T. Tai, M. H. Chang and H. S. Liu, *Ind. Eng. Chem. Res.*, 2007, **46**, 5539.
- 69 R. G. Moharir, P. R. Gogate and V. K. Rathod, *Can. J. Chem. Eng.*, 2012, **90**, 996.
- 70 H. Qu, H. Ma, W. Zhou and C. J. O'Connor, *Inorg. Chim. Acta*, 2012, **389**, 60-65 (DOI:10.1016/j.ica.2012.01.058).
- 71 W. Cho, M. Cho, J. Jeong, M. Choi, H. Cho, B. S. Han, S. H. Kim, H. O. Kim, Y. T. Lim, B. H. Chung and J. Jeong, *Toxicol. Appl. Pharmacol.*, 2009, **236**, 16-24 (DOI:DOI: 10.1016/j.taap.2008.12.023).
- 72 P. Kalimuthu and S. A. John, *Mater. Chem. Phys.*, 2010, **122**, 380-385 (DOI:10.1016/j.matchemphys.2010.03.009).
- 73 S. Laurent, S. Dutz, U. O. Häfeli and M. Mahmoudi, *Adv. Colloid Interface Sci.*, 2011, **166**, 8-23 (DOI:10.1016/j.cis.2011.04.003).
- 74 M. Carmen Bautista, O. Bomati-Miguel, M. del Puerto Morales, C. J. Serna and S. Veintemillas-Verdaguer, *J. Magn. Magn. Mater.*, 2005, **293**, 20-27 (DOI:DOI: 10.1016/j.jmmm.2005.01.038).
- 75 N. T. K. Thanh and L. A. W. Green, *Nano Today*, 2010, **5**, 213-230 (DOI:10.1016/j.nantod.2010.05.003).
- 76 Z. P. Xu, Q. H. Zeng, G. Q. Lu and A. B. Yu, *Chem. Eng. Sci.*, 2006, **61**, 1027-1040 (DOI:10.1016/j.ces.2005.06.019).
- 77 M. Song, Y. Zhang, S. Hu, L. Song, J. Dong, Z. Chen and N. Gu, *Colloids Surf. Physicochem. Eng. Aspects*, 2012, **408**, 114-121 (DOI:10.1016/j.colsurfa.2012.05.039).
- 78 M. Kallumadil, M. Tada, T. Nakagawa, M. Abe, P. Southern and Q. A. Pankhurst, *J. Magn. Magn. Mater.*, 2009, **321**, 1509-1513 (DOI:10.1016/j.jmmm.2009.02.075).
- 79 C. E. Sjögren, C. Johansson, A. Nævestad, P. C. Sontum, K. Briley-Sæbø and A. K. Fahlvik, *Magn. Reson. Imaging*, 1997, **15**, 55-67 (DOI:10.1016/S0730-725X(96)00335-9).

- 80 D. A. Scheinberg, C. H. Villa, F. E. Escorcia and M. R. McDevitt, *Nat. Rev. Clin. Oncol.*, 2010, **7**, 266.
- 81 *Gold chemistry : applications and future directions in the life sciences*, Wiley-VCH, Weinheim, 2009.
- 82 J. Gao, X. Huang, H. Liu, F. Zan and J. Ren, *Langmuir*, 2012, **28**, 4464.
- 83 J. W. Kim, L. U. Kim and C. K. Kim, *Biomacromolecules*, 2007, **8**, 215.
- 84 N. Venkatathri, *Ind. J. Chem.*, 2007, **46**, 1955.
- 85 K. L. Vigor, P. G. Kyrtatos, S. Minogue, K. T. Al-Jamal, H. Kogelberg, B. Tolner, K. Kostarelos, R. H. Begent, Q. A. Pankhurst, M. F. Lythgoe and K. A. Chester, *Biomaterials*, 2010, **31**, 1307-1315 (DOI:DOI: 10.1016/j.biomaterials.2009.10.036).
- 86 R. Y. Hong, B. Feng, L. L. Chen, G. H. Liu, H. Z. Li, Y. Zheng and D. G. Wei, *Biochem. Eng. J.*, 2008, **42**, 290-300 (DOI:DOI: 10.1016/j.bej.2008.07.009).
- 87 J. Hradil, A. Pisarev, M. Babič and D. Horák, *China Particuology*, 2007, **5**, 162-168 (DOI:DOI: 10.1016/j.cpart.2007.01.003).
- 88 Y. Fukumori, T. Nomura, T. Adschiri, S. Ohara, F. Scuito, M. Naito, K. Okuyama, M. Kawahara, H. Suzuki, T. Sasaki, M. Fuji, S. Inagaki, H. Takeuchi and Y. Ando, in *Nanoparticle technology handbook*, ed. M. Hosokawa, K. Nogi, M. Ncuito and T. Yokoyama, Elsevier, Netherlands, 2007, p. 51.
- 89 B. Zhang, Z. Tu, F. Zhao and J. Wang, *Appl. Surf. Sci.*, 2013, **266**, 375-379 (DOI:<http://dx.doi.org/10.1016/j.apsusc.2012.12.032>).
- 90 E. B. Denkbaş, E. Kiliçay, C. Birlikseven and E. Öztürk, *React Funct Polym*, 2002, **50**, 225-232 (DOI:10.1016/S1381-5148(01)00115-8).
- 91 D. L. J. Thorek, J. Czupryna, A. K. Chen and A. Tsourkas, in *Cancer Imaging*, ed. M.A. Hayat, Academic Press, San Diego, 2008, p. 85-95.
- 92 L. Cademartiri and G. A. Ozin, *Concepts of nanochemistry*, Wiley-VCH; John Wiley distributor, Weinheim; Chichester, 2009.

- 93 P. An, F. Zuo, Y. P. Wu, J. H. Zhang, Z. H. Zheng, X. B. Ding and Y. X. Peng, *Chinese Chem. Lett.*, 2012, **23**, 1099-1102 (DOI:10.1016/j.ccllet.2012.06.039).
- 94 Q. Zhang, K. Song, J. Zhao, X. Kong, Y. Sun, X. Liu, Y. Zhang, Q. Zeng and H. Zhang, *J. Colloid Interface Sci.*, 2009, **336**, 171-175 (DOI:10.1016/j.jcis.2009.04.024).
- 95 A. Kraus, K. Jainae, F. Unob and N. Sukpirom, *J. Colloid Interface Sci.*, 2009, **338**, 359-365 (DOI:10.1016/j.jcis.2009.06.045).
- 96 N. Doan, K. Kontturi and C. Johans, *J. Colloid Interface Sci.*, 2010, **350**, 126-131 (DOI:10.1016/j.jcis.2010.06.024).
- 97 Z. Zhang, J. Jia, Y. Lai, Y. Ma, J. Weng and L. Sun, *Bioorg. Med. Chem.*, 2010, **18**, 5528-5534 (DOI:DOI: 10.1016/j.bmc.2010.06.045).
- 98 BioPhysics Assay Laboratory Inc., *Receptor mediated endocytosis: Conjugation of spermidine to CL-30Q02-6C, a carboxyl containing USPIO.*, BioPal, www.biopal.com, 2013.
- 99 A. Ulman, *Chem. Rev.*, 1996, **96**, 1533.
- 100 F. Laffineur, J. Delhalle and Z. Mekhalif, *Mater. Sci. and Eng. C*, 2002, **22**, 331-337 (DOI:10.1016/S0928-4931(02)00212-6).
- 101 L. Srisombat, A. C. Jamison and T. R. Lee, *Colloids Surf. Physicochem. Eng. Aspects*, 2011, **390**, 1-19 (DOI:10.1016/j.colsurfa.2011.09.020).
- 102 L. Chen, W. Zhao, Y. Jiao, X. He, J. Wang and Y. Zhang, *Spectrochimica Acta Part A: Molecular and Biomolecular Spectroscopy*, 2007, **68**, 484-490 (DOI:<http://dx.doi.org/10.1016/j.saa.2006.12.014>).
- 103 P. Roonasi and A. Holmgren, *Appl. Surf. Sci.*, 2009, **255**, 5891-5895 (DOI:<http://dx.doi.org/10.1016/j.apsusc.2009.01.031>).
- 104 N. Purdie, K. A. Swallows, L. H. Murphy and R. B. Purdie, *J. Pharm. Biomed. Anal.*, 1989, **7**, 1519-1526 (DOI:[http://dx.doi.org/10.1016/0731-7085\(89\)80160-8](http://dx.doi.org/10.1016/0731-7085(89)80160-8)).
- 105 T. Doane and C. Burda, *Adv. Drug Deliv. Rev.*, (DOI:10.1016/j.addr.2012.05.012).

- 106 X. Zhang, X. Xu, N. Bertrand, E. Pridgen, A. Swami and O. C. Farokhzad, *Adv. Drug Deliv. Rev.*, (DOI:10.1016/j.addr.2012.08.005).
- 107 J. Liu, S. Yu, Y. Yin and J. Chao, *TrAC Trend. Anal. Chem.*, 2012, **33**, 95-106 (DOI:10.1016/j.trac.2011.10.010).
- 108 B. Kowalczyk, I. Lagzi and B. A. Grzybowski, *Curr. Opin. Coll. In.*, 2011, **16**, 135-148 (DOI:10.1016/j.cocis.2011.01.004).
- 109 M. F. Nazar, S. S. Shah, J. Eastoe, A. M. Khan and A. Shah, *J. Colloid Interface Sci.*, 2011, **363**, 490-496 (DOI:10.1016/j.jcis.2011.07.070).
- 110 Q. Xie, J. Liu, X. Xu, G. Han, H. Xia and X. He, *Sep. Purif. Technol.*, 2009, **66**, 148-152 (DOI:10.1016/j.seppur.2008.11.016).
- 111 M. Hanauer, S. Pierrat, I. Zins, A. Lotz and C. Sonnichsen, *Nano Lett.*, 2007, **7**, 2881.
- 112 X. Xu, K. K. Caswell, E. Tucker, S. Kabisatpathy, K. L. Brodhacker and W. A. Scrivens, *J. Chroma. A*, 2007, **1167**, 35-41 (DOI:10.1016/j.chroma.2007.07.056).
- 113 I. Limayem, C. Charcosset and H. Fessi, *Sep. Purif. Technol.*, 2004, **38**, 1-9 (DOI:10.1016/j.seppur.2003.10.002).
- 114 A. M. Gole, C. Sathivel, A. Lachke and M. Sastry, *J. Chroma. A*, 1999, **848**, 485-490 (DOI:10.1016/S0021-9673(99)00408-2).
- 115 C. K. Knox, S. D. Fillmore, D. M. Call, D. G. Allen, B. C. Hess, R. C. Davis, W. E. Evenson and R. G. Harrison, *J. Colloid Interface Sci.*, 2006, **300**, 591-596 (DOI:10.1016/j.jcis.2006.04.029).
- 116 Thermo Scientific, *Thermo Scientific Pierce High-Performance Dialysis, Desalting and Detergent Removal Technical Handbook Version 2*, Thermo Scientific, United States, 2009.
- 117 *Introduction to the science of medical imaging*, Cambridge University Press, Cambridge, 2010.
- 118 N. E. Fearnot, C. F. Babbs, J. D. Bourland and L. A. Geddes, *Ultrason. Imaging*, 1980, **2**, 78-83 (DOI: 10.1016/0161-7346(80)90205-9).

- 119 T. R. Nelson and D. H. Pretorius, *Ultrasound Med. Biol.*, 1998, **24**, 1243-1270 (DOI: 10.1016/S0301-5629(98)00043-X).
- 120 A. U. Desai, W. E. Pienaar, D. C. Howlett and A. C. Andi, *The Foundation Years*, 2008, **4**, 287-292 (DOI: 10.1016/j.mpfou.2008.06.015).
- 121 M. J. O. Taylor, *Early Hum. Dev.*, 2006, **82**, 365-370 (DOI: 10.1016/j.earlhumdev.2006.03.008).
- 122 G. A. Badtram, J. D. Gaines, C. B. Thomas and W. T. K. Bosu, *Theriogenology*, 1991, **35**, 1153-1167 (DOI: 10.1016/0093-691X(91)90362-H).
- 123 R. Dammers, A. F. Krisht and S. Partington, *Clin. Neurol. Neurosurg.*, 2009, **111**, 758-761 (DOI: 10.1016/j.clineuro.2009.05.012).
- 124 B. Chen, P. Liang, K. Liu, J. Hsiao, J. Huang, J. Wong, P. Lee, C. Shun and Y. Ming-Tsang, *J. Formosan Med. Assoc.*, 2007, **106**, 943-952 (DOI: 10.1016/S0929-6646(08)60065-0).
- 125 C. K. Hoh, *Nucl. Med. Biol.*, 2007, **34**, 737-742 (DOI: 10.1016/j.nucmedbio.2007.07.001).
- 126 C. C. Wagner and O. Langer, *Adv. Drug Deliv. Rev.*, 2011, **63**, 539-546 (DOI: 10.1016/j.addr.2010.09.011).
- 127 R. Tarawneh and D. M. Holtzman, *Neuropharmacology*, 2010, **59**, 310-322 (DOI: 10.1016/j.neuropharm.2010.04.006).
- 128 T. Grimmer, G. Henriksen, H. Wester, H. Förstl, W. E. Klunk, C. A. Mathis, A. Kurz and A. Drzezga, *Neurobiol. Aging*, 2009, **30**, 1902-1909 (DOI:DOI: 10.1016/j.neurobiolaging.2008.01.016).
- 129 D. Weishaupt, V. Kochli and B. Marincek, *How does MRI work?: an introduction to the physics and function of magnetic resonance imaging*, Springer, Berlin ; London, 2003.
- 130 J. W. M. Bulte, A. S. Arbab, T. Douglas and J. A. Frank, in *Methods in Enzymology*, ed. P. Michael Conn, Academic Press, 2004, p. 275-299.
- 131 D. Baumjohann and M. B. Lutz, *Immunobiology*, 2006, **211**, 587-597 (DOI:10.1016/j.imbio.2006.05.011).

- 132 J. W. M. Bulte, P. G. Laughlin, E. K. Jordan, V. A. Tran, J. Vymazal and J. A. Frank, *Acad. Radiol.*, 1996, **3**, S301-S303 (DOI: 10.1016/S1076-6332(96)80564-2).
- 133 F. Winau, O. Westphal and R. Winau, *Microb. Infect.*, 2004, **6**, 786-789 (DOI: 10.1016/j.micinf.2004.04.003).
- 134 K. B. Hartman, L. J. Wilson and M. G. Rosenblum, *Mol. Diagn. Ther.*, 2008, **12**, 1-14.
- 135 G. Sternbach and J. Varon, *J. Emerg. Med.*, 1993, **11**, 743-745 (DOI: 10.1016/0736-4679(93)90635-K).
- 136 Author Unknown, *How to read a seismogram*, Berkeley Seismological Lab, Online, 2009.
- 137 W. P. Pais, S. S. Tekwani, P. Tiwari, N. M. Szary, M. L. Bechtold, J. A. Ibdah, J. B. Marshall and M. R. Antillon, *Gastroenterology*, 2009, **136**, A-644 (DOI:http://dx.doi.org/10.1016/S0016-5085(09)62971-1).
- 138 C. Ho, M. Chern, M. Wu, H. Wu, W. Lin, C. Chang, M. C. Chen and T. Chou, *Kaohsiung J. Med. Sci.*, 2003, **19**, 599-606 (DOI: 10.1016/S1607-551X(09)70513-3).
- 139 J. G. Caridi, I. F. Hawkins Jr, S. D. Klioze and R. F. LeVeen, *Techniques in Vascular and Interventional Radiology*, 2001, **4**, 57-65 (DOI:http://dx.doi.org/10.1053/tvir.2001.22006).
- 140 I. F. Hawkins Jr, J. G. Caridi, R. F. LeVeen, S. D. Khoze and C. R. J. Mladinich, *Techniques in Vascular and Interventional Radiology*, 2000, **3**, 130-138 (DOI:http://dx.doi.org/10.1053/tvir.2000.9148).
- 141 T. Prangé, F. Gaudey, J. Ohanessian, D. Avenel, A. Neuman, C. Corot and D. Meyer, *FEBS Lett.*, 1995, **357**, 247-250 (DOI:http://dx.doi.org/10.1016/0014-5793(94)01356-6).
- 142 I. A. Sproat, F. T. Lee Jr, A. H. Rappe and S. G. Chosy, *Journal of Vascular and Interventional Radiology*, 1996, **7**, 889-895 (DOI:http://dx.doi.org/10.1016/S1051-0443(96)70867-9).
- 143 P. A. Jackson, W. N. W. A. Rahman, C. J. Wong, T. Ackerly and M. Geso, *Eur. J. Radiol.*, 2010, **75**, 104-109 (DOI: 10.1016/j.ejrad.2009.03.057).
- 144 Nanoprobes.com, , Nanoprobes Inc., New York, 2013.

- 145 E. Sadauskas, G. Danscher, M. Stoltenberg, U. Vogel, A. Larsen and H. Wallin, *Nanomed. Nanotechnol.*, 2009, **5**, 162-169 (DOI: 10.1016/j.nano.2008.11.002).
- 146 J. K. Aronson, in *Meyler's Side Effects of Drugs: The International Encyclopedia of Adverse Drug Reactions and Interactions*, ed. : Editor: J.K. Aronson, Elsevier, Amsterdam, 2006, p. 1848-1896.
- 147 M. Kishimoto, S. Doi, J. Shimizu, K. Lee, T. Iwasaki, Y. Miyake and K. Yamada, *Eur. J. Radiol.*, 2010, **76**, 135-139 (DOI: 10.1016/j.ejrad.2009.05.018).
- 148 T. Asao, K. Fujita, J. Nakamura, N. Morinaga, H. Shoji, M. Ide, I. Hirayama and H. Kuwano, *Clin. Radiol.*, 2002, **57**, 488-491 (DOI:http://dx.doi.org/10.1053/crad.2002.0953).
- 149 P. Dawson, C. Heron and J. Marshall, *Clin. Radiol.*, 1984, **35**, 173-175 (DOI: 10.1016/S0009-9260(84)80126-9).
- 150 R. J. Dray, A. C. Winfield, C. A. Muhletaler and F. K. Kirchner Jr., *Urology*, 1984, **24**, 297-299 (DOI: 10.1016/0090-4295(84)90366-2).
- 151 J. Kleefield, J. Chirico-Post, H. L. Levine, M. K. Srinivasan, J. McA. Harris III, A. J. Rommel and A. H. Robbins, *Surg. Neurol.*, 1983, **20**, 165-170 (DOI: 10.1016/0090-3019(83)90471-8).
- 152 A. La Noce, F. Bertani, V. Lorusso, F. Luzzani, P. Tirone and C. de Haën, *Eur. J. Radiol.*, 1994, **18**, S43-S50 (DOI: 10.1016/0720-048X(94)90093-0).
- 153 A. Heuck, H. Bonél, A. Stäbler and R. Schmitt, *Eur. J. Radiol.*, 1997, **26**, 2-15 (DOI: 10.1016/S0720-048X(97)01174-1).
- 154 D. W. McRobbie, *MRI from picture to proton*, Cambridge University Press, Cambridge, 2003.
- 155 G. Sosnovsky and N. U. Maheswara Rao, *Eur. J. Med. Chem.*, 1988, **23**, 517-522 (DOI:http://dx.doi.org/10.1016/0223-5234(88)90094-3).
- 156 A. Makino, H. Harada, T. Okada, H. Kimura, H. Amano, H. Saji, M. Hiraoka and S. Kimura, *Nanomed. Nanotechnol.*, 2011, **7**, 638-646 (DOI:10.1016/j.nano.2011.01.015).
- 157 Y. Liu and N. Zhang, *Biomaterials*, 2012, **33**, 5363-5375 (DOI:10.1016/j.biomaterials.2012.03.084).

- 158 M. Bellin and A. J. Van Der Molen, *Eur. J. Radiol.*, 2008, **66**, 160-167 (DOI: 10.1016/j.ejrad.2008.01.023).
- 159 K. W. Chan and W. Wong, *Coord. Chem. Rev.*, 2007, **251**, 2428-2451 (DOI:10.1016/j.ccr.2007.04.018).
- 160 E. Sausseureau, C. Lacroix, A. Cattaneo, L. Mahieu and J. P. Gouille, *Forensic Sci. Int.*, 2008, **176**, 54-57 (DOI:10.1016/j.forsciint.2007.06.026).
- 161 H. Lu, S. Demny, Y. Zuo, W. Rea, L. Wang, S. I. Chefer, D. B. Vaupel, Y. Yang and E. A. Stein, *Neuroimage*, 2010, **50**, 7-14 (DOI: 10.1016/j.neuroimage.2009.12.053).
- 162 P. S. Tofts, A. Porchia, Y. Jin, R. Roberts and B. A. Berkowitz, *Brain Res. Bull.*, 2010, **81**, 333-338 (DOI: 10.1016/j.brainresbull.2009.06.002).
- 163 A. Figuerola, R. Di Corato, L. Manna and T. Pellegrino, *Pharmacol. Res.*, 2010, **62**, 126-143 (DOI: 10.1016/j.phrs.2009.12.012).
- 164 R. G. Pautler, *Neuroimage*, 2002, **16**, 441.
- 165 J. M. Starr, A. J. Farrall, P. Armitage, B. McGurn and J. Wardlaw, *Psychiat. Res. - Neuroim.*, 2009, **171**, 232-241 (DOI: 10.1016/j.psychresns.2008.04.003).
- 166 N. G. Harris, V. Gauden, P. A. Fraser, S. R. Williams and G. J. M. Parker, *Magn. Reson. Imaging*, 2002, **20**, 221-230 (DOI: 10.1016/S0730-725X(02)00498-8).
- 167 P. Savranoglu, F. Obuz, S. Karasu, A. Coker, M. Secil, O. Sagol, E. Igci, O. Dicle and I. Astarcioglu, *Clin. Imaging*, 2006, **30**, 377-381 (DOI:10.1016/j.clinimag.2006.06.001).
- 168 C. Corot, P. Robert, J. Idée and M. Port, *Adv. Drug Deliv. Rev.*, 2006, **58**, 1471-1504 (DOI:DOI: 10.1016/j.addr.2006.09.013).
- 169 W. K. Johnson, C. Stoupis, G. M. Torres, E. B. Rosenberg and P. R. Ros, *Magn. Reson. Imaging*, 1996, **14**, 43-49 (DOI:10.1016/0730-725X(95)02044-T).
- 170 J. T. Smith, J. Ward, J. A. Guthrie, M. B. Sheridan, S. Boyes, D. Wilson, J. I. Wyatt, D. Treanor and P. J. Robinson, *Magn. Reson. Imaging*, (DOI:10.1016/j.mri.2012.04.016).

- 171 A. Yilmaz, S. Rösch, K. Klingel, R. Kandolf, X. Helluy, K. Hiller, P. M. Jakob and U. Sechtem, *Int. J. Cardiol.*, (DOI:10.1016/j.ijcard.2011.06.004).
- 172 N. C. Balci, M. Şirvancı, C. Duran and A. Akıncı, *Clin. Imaging*, 2002, **26**, 35-38 (DOI: 10.1016/S0899-7071(01)00352-7).
- 173 F. Yang, C. Jin, S. Subedi, C. L. Lee, Q. Wang, Y. Jiang, J. Li, Y. Di and D. Fu, *Cancer Treat. Rev.*, 2012, **38**, 566-579 (DOI:10.1016/j.ctrv.2012.02.003).
- 174 Y. Liu, Z. Chen, C. Liu, D. Yu, Z. Lu and N. Zhang, *Biomaterials*, 2011, **32**, 5167-5176 (DOI: 10.1016/j.biomaterials.2011.03.077).
- 175 X. Huang and M. A. El-Sayed, *J. Adv. Res.*, 2010, **1**, 13-28 (DOI: 10.1016/j.jare.2010.02.002).
- 176 I. Brigger, C. Dubernet and P. Couvreur, *Adv. Drug Deliv. Rev.*, 2002, **54**, 631-651 (DOI: 10.1016/S0169-409X(02)00044-3).
- 177 I. R. Bell, G. E. Schwartz, N. N. Boyer, M. Koithan and A. J. Brooks, *Eur. J. Integ. Med.*, 2013, **5**, 126-140 (DOI:http://dx.doi.org/10.1016/j.eujim.2012.11.002).
- 178 A. A. M. Elsherbini, M. Saber, M. Aggag, A. El-Shahawy and H. A. A. Shokier, *Magn. Reson. Imaging*, 2011, **29**, 272-280 (DOI:10.1016/j.mri.2010.08.010).
- 179 *Hyperthermia in cancer treatment*, National Cancer Institute, 31st August, 2011.
- 180 M. Sharma, S. Mantri and D. Bahadur, *J. Magn. Magn. Mater.*, 2012, **324**, 3975-3980 (DOI:10.1016/j.jmmm.2012.05.059).
- 181 P. Cherukuri, E. S. Glazer and S. A. Curley, *Adv. Drug Deliv. Rev.*, 2010, **62**, 339-345 (DOI: 10.1016/j.addr.2009.11.006).
- 182 A. Ito, Y. Kuga, H. Honda, H. Kikkawa, A. Horiuchi, Y. Watanabe and T. Kobayashi, *Cancer Lett.*, 2004, **212**, 167-175 (DOI: 10.1016/j.canlet.2004.03.038).
- 183 C. S. S. R. Kumar and F. Mohammad, *Adv. Drug Deliv. Rev.*, 2011, **63** (9), 789-808 (DOI: 10.1016/j.addr.2011.03.008).

- 184 S. Laurent, S. Dutz, U. O. Häfeli and M. Mahmoudi, *Adv. Colloid Interface Sci.*, 2011, **166**, 1–2, 8-23 (DOI: 10.1016/j.cis.2011.04.003).
- 185 X. Zhu, Y. J. Wang, K. C. Leung, S. Lee, F. Zhao, D. Wang, J. M. Lai, C. Wan, C. H. Cheng and A. T. Ahuja, *Int. J. Nanomedicine*, 2012, **7**, 953.
- 186 A. K. Gupta and M. Gupta, *Biomaterials*, 2005, **26**, 3995-4021 (DOI:10.1016/j.biomaterials.2004.10.012).
- 187 D. Thacharodi and K. P. Rao, *Biomaterials*, 1995, **16**, 145-148 (DOI:10.1016/0142-9612(95)98278-M).
- 188 A. Davidson, B. Al-Qallat and D. B. Das, *Chem. Eng. Res. Des.*, 2008, **86**, 1196.
- 189 G. Jiang, D. Zhu, J. Zan and F. Ding, *Chin. J. Chem. Eng.*, 2007, **15**, 397.
- 190 A. G. Doukas and N. Kollias, *Adv. Drug Deliv. Rev.*, 2004, **56**, 559-579 (DOI:10.1016/j.addr.2003.10.031).
- 191 J. W. Lee, P. Gadiraju, J. Park, M. G. Allen and M. R. Prausnitz, *J. Controlled Release*, 2011, **154**, 58-68 (DOI:10.1016/j.jconrel.2011.05.003).
- 192 I. Lavon and J. Kost, *Drug Discov. Today*, 2004, **9**, 670-676 (DOI:10.1016/S1359-6446(04)03170-8).
- 193 J. Park, M. G. Allen and M. R. Prausnitz, *J. Controlled Release*, 2005, **104**, 51-66 (DOI:10.1016/j.jconrel.2005.02.002).
- 194 B. W. Barry, *Drug Discov. Today*, 2001, **6**, 967-971 (DOI:10.1016/S1359-6446(01)01938-9).
- 195 R. Tong, H. D. Hemmati, R. Langer and D. S. Kohane, *J. Am. Chem. Soc.*, 2012, **134**, 8848.
- 196 D. G. Cameron, E. H. Bensley, P. Wood and V. Grayston, *Canad. M. A. J.*, 1951, **64**, 27.
- 197 R. Weissleder, D. D. Stark, B. L. Engelstad, B. R. Bacon, C. C. Compton, D. L. White, P. Jacobs and J. Lewis, *Am. J. Roenten.*, 1989, **152**, 167.
- 198 M. Mahmoudi, S. Sant, B. Wang, S. Laurent and T. Sen, *Adv. Drug Deliv. Rev.*, 2011, **166**, 1–2, 8-23 (DOI:DOI: 10.1016/j.addr.2010.05.006).

- 199 S. Purushotham and R. V. Ramanujan, *Acta Biomaterialia*, 2010, **6**, 502-510 (DOI:10.1016/j.actbio.2009.07.004).
- 200 R. Lawaczeck, M. Menzel and H. Pietsch, *Appl. Organomet. Chem.*, 2004, **18**, 506-513 (DOI:10.1002/aoc.753).
- 201 P. W. Atkins and D. F. Shriver, *Shriver & Atkins inorganic chemistry*, Oxford University Press, Oxford, 2006.
- 202 P. Arnold, J. Ward, D. Wilson, J. Ashley Guthrie and P. J. Robinson, *Magn. Reson. Imaging*, 2003, **21**, 695-700 (DOI:http://dx.doi.org/10.1016/S0730-725X(03)00101-2).
- 203 Y. Asahina, N. Izumi, M. Uchihara, O. Noguchi, K. Ueda, K. Inoue, Y. Nishimura, K. Tsuchiya, K. Hamano, J. Itakura, Y. Himeno, M. Koike and S. Miyake, *Hepatol. Res.*, 2003, **27**, 196-204 (DOI:http://dx.doi.org/10.1016/S1386-6346(03)00261-4).
- 204 R. Lencioni, F. Donati, D. Cioni, A. Paolicchi, A. Cicorelli and C. Bartolozzi, *Magn. Reson. Mater. Phys.*, 1998, **7**, 76-87 (DOI:http://dx.doi.org/).
- 205 C. W. Jung and P. Jacobs, *Magn. Reson. Imaging*, 1995, **13**, 661-674 (DOI:http://dx.doi.org/10.1016/0730-725X(95)00024-B).
- 206 M. D. Hammerstingl, M. D. Schwarz and M. D. Vogl, *Liver-specific contrast agent for MRI of focal liver lesions: Detection and characterisation in a single diagnostic work-up*, Schering, Germany, 2002.
- 207 A. Bjornerud, L. O. Johansson and H. K. Ahlstron, *Magn. Reson. Mater. Phys.*, 2001, **12**, 99.
- 208 S. J. Soenen, U. Himmelreich, N. Nuytten and M. De Cuyper, *Biomaterials*, 2011, **32**, 195-205 (DOI:10.1016/j.biomaterials.2010.08.075).
- 209 W. Li, J. Luo and Z. Chen, *Inorg. Chem. Commun.*, 2011, **14**, 1898-1900 (DOI:10.1016/j.inoche.2011.09.006).
- 210 D. Hanahan and R. A. Weinberg, *Cell*, 2000, **100**, 57-70 (DOI: 10.1016/S0092-8674(00)81683-9).
- 211 *CancerStats: Cancer Worldwide*, Cancer Research UK, UK, 2011.

- 212 D. Hanahan, *Eur. J. Cancer Supp.*, 2010, **8**, 20-20 (DOI: 10.1016/S1359-6349(10)71737-7).
- 213 D. Hanahan and R. Weinberg, *Cell*, 2011, **144**, 646-674 (DOI: 10.1016/j.cell.2011.02.013).
- 214 L. Pecorino, *Molecular Biology of Cancer: Mechanisms, Targets and Therapeutics*, OUP, Oxford, 2008.
- 215 P. Fedi, D. Basso, C. Pasquali, C. De Paoli, C. Sperti, G. Roveroni, G. Pedrazzoli and M. Plebani, *In Cancer Medicine*, 1997, , 41.
- 216 D. J. Slamon, G. M. Clark, S. G. Wong, W. J. Levin, A. Ullrich and W. L. McGuire, *Science*, **235**, 177-182.
- 217 M. Skobe and N. E. Fusenig, *Proc. Natl. Acad. Sci. USA*, 1998, **92**, 1050-1055.
- 218 R. A. Weinberg, *Cell*, 1995, **81**, 323-330.
- 219 J. F. Kerr, A. H. Wyllie and A. R. Currie, *Br. J. Cancer*, 1972, **26**, 239-257.
- 220 C. C. Harris, *Carcinogenesis*, 1996, **17**, 1187-1198.
- 221 L. Hayflick, *Biochemistry*, 1997, **62**, 1180-1190.
- 222 J. W. Shay and S. Bacchetti, *Eur. J. Cancer*, 1997, **33**, 787-791.
- 223 T. M. Bryan and T. R. Cech, *Curr. Opin. Cell Biol.*, 1999, **11**, 318-324.
- 224 K. J. Kim, B. Li, J. Winer, M. Armanini, N. Gillett, H. S. Phillips and N. Ferrara, *Nature*, 1993, **362**, 841-844.
- 225 S. V. Rajkumar and T. E. Witzig, *Cancer Treat. Rev.*, 2000, **26**, 351-362 (DOI:DOI: 10.1053/ctrv.2000.0188).
- 226 O. V. Volpert, K. M. Dameron and N. Bouck, *Oncogene*, 1997, **14**, 1495-1502.
- 227 R. K. Singh, M. Gutman, C. D. Bucana, R. Sanchez, N. Llansa and I. J. Fidler, *Proc. Natl. Acad. Sci. USA*, 1995, **92**, 4562-4566.
- 228 K. M. Dameron, O. V. Volpert, M. A. Tainsky and N. Bouck, *Science*, 1994, **265**, 1582-1584.

- 229 M. B. Sporn, *Lancet*, 1996, **347**, 1377-1381.
- 230 W. G. Stetler-Stevenson, *J. Clin. Invest.*, 1999, **103**, 1237-1241.
- 231 Z. Werb, *Cell*, 1997, **91**, 439-442.
- 232 M. G. Vander Heiden, L. C. Cantley and C. B. Thompson, *Science*, 2009, **324**, 1029.
- 233 C. Liang, J. Lee and J. U. Jung, *Semin. Cancer Biol.*, 2008, **18**, 423-436 (DOI: 10.1016/j.semcancer.2008.09.003).
- 234 P. R. Lee, J. E. Cohen and R. D. Fields, *Neurosci. Lett.*, 2006, **397**, 126-129 (DOI: 10.1016/j.neulet.2005.12.027).
- 235 M. Gary-Bobo, O. Hocine, D. Brevet, M. Maynadier, L. Raehm, S. Richeter, V. Charasson, B. Loock, A. Morère, P. Maillard, M. Garcia and J. Durand, *Int. J. Pharm.*, 2012, **423**, 509-515 (DOI:<http://dx.doi.org/10.1016/j.ijpharm.2011.11.045>).
- 236 D. Magda and R. A. Miller, *Semin. Cancer Biol.*, 2006, **16**, 466-476 (DOI:10.1016/j.semcancer.2006.09.002).
- 237 M. R. Hilleman, *Vaccine*, 2000, **18**, 1436-1447 (DOI:[http://dx.doi.org/10.1016/S0264-410X\(99\)00434-X](http://dx.doi.org/10.1016/S0264-410X(99)00434-X)).
- 238 J. Kuby, *Immunology; 4th Edition*, W.H. Freeman and Co Ltd., US, 2000.
- 239 K. Todar, *Immune Defense against Bacterial Pathogens: Adaptive or Acquired Immunity*, http://textbookofbacteriology.net/adaptive_2.html, 2012.
- 240 P. J. Gearhart, *J. Immunol.*, 2004, **173**, 4259.
- 241 U. Sahin, O. Tureci, H. Schmitt, B. Cochlovius, T. Johannes, R. Schmits, F. Stenner, G. Luo, I. Schobert and M. Pfreundschuh, *Proc. Natl. Acad. Sci. USA*, 1995, **92**, 11810-11813.
- 242 A. K. Miles, B. Matharoo-Ball, G. Li, M. Ahmad and R. C. Rees, *Cancer Immunol. Immunother.*, 2006, **55**, 996-1003.
- 243 A. K. Miles, A. Rogers, G. Li, R. Seth, D. Powe, S. E. B. McArdle, T. A. McCulloch, M. C. Bishop and R. C. Rees, *The Prostate*, 2007, **67**, 274-287.

- 244 K. H. Vousden and X. Lu, *Nature*, 2002, **2**, 594.
- 245 K. H. Vousden and D. P. Lane, *Nature*, 2007, **8**, 275.
- 246 M. Hollstein, D. Sidransky, B. Vogelstein and C. C. Harris, *Science*, 1991, **253**, 49.
- 247 M. Amblard, J. Fehrentz, J. Martinez and G. Subra, *Mol. Biotechnol.*, 2006, **33**, 239-254.
- 248 B. Merrifield, in *Method. Enzymol.*, ed. Gregg B. Fields, Academic Press, 1997, p. 3-13.
- 249 R. B. Merrifield, *J. Am. Chem. Soc.*, 1963, **85**, 2149.
- 250 S. -. Wang, *J. Am. Chem. Soc.*, 1973, **95**, 1328.
- 251 S. -. Wang, J. P. Tam, B. S. H. Wang and R. B. Merrifield, *Int. J. Pept. Protein Res.*, 1981, **18**, 459.
- 252 D. A. Wellings and E. Atherton, in *Methods in Enzymology*, ed. Gregg B. Fields, Academic Press, 1997, p. 44-67.
- 253 J. Chromik, E. Schnürer, R. Georg Meyer, T. Wehler, T. Tüting, T. Wölfel, C. Huber and W. Herr, *J. Immunol. Methods*, 2006, **308**, 77-89 (DOI: 10.1016/j.jim.2005.09.021).
- 254 B. Ludewig, F. Barchiesi, M. Pericin, R. M. Zinkernagel, H. Hengartner and R. A. Schwendener, *Vaccine*, 2000, **19**, 23-32 (DOI: 10.1016/S0264-410X(00)00163-8).
- 255 R. Audran, K. Peter, J. Dannull, Y. Men, E. Scandella, M. Groettrup, B. Gander and G. Corradin, *Vaccine*, 2003, **21**, 1250-1255 (DOI: 10.1016/S0264-410X(02)00521-2).
- 256 W. R. Usinger, *Vaccine*, 1997, **15**, 1902-1907 (DOI: 10.1016/S0264-410X(97)00136-9).
- 257 G. Guillén, J. C. Aguilar, S. Dueñas, L. Hermida, M. G. Guzmán, E. Penton, E. Iglesias, J. Junco, I. Torrens, Y. Lobaina, V. Muzio and L. Herrera, *Procedia in Vaccinology*, 2010, **2**, 128-133 (DOI:10.1016/j.provac.2010.07.004).
- 258 M. Osorio, M. D. Bray and R. I. Walker, *Vaccine*, 2007, **25**, 1581-1592 (DOI: 10.1016/j.vaccine.2006.11.012).
- 259 C. D. Thomas, A. Ehrhardt and M. A. Kay, *Nat. Rev.*, 2003, **4**, 346.

- 260 A. Aris and A. Villaverde, *Trends Biotechnol.*, 2004, **22**, 371.
- 261 A. Agarwal, R. Unfer and S. K. Mallapragada, *J. Controlled Release*, 2005, **103**, 245-258 (DOI:10.1016/j.jconrel.2004.11.022).
- 262 D. Li, G. Li, P. Li, L. Zhang, Z. Liu, J. Wang and E. Wang, *Biomaterials*, 2010, **31**, 1850-1857 (DOI:DOI: 10.1016/j.biomaterials.2009.11.027).
- 263 A. Bajaj, S. K. Mishra, P. Kondaiah and S. Bhattacharya, *Biochimica et Biophysica Acta (BBA) - Biomembranes*, 2008, **1778**, 1222-1236 (DOI:10.1016/j.bbamem.2007.12.010).
- 264 S. H. Choi, S. Jin, M. Lee, S. Lim, J. Park, B. Kim, W. S. Ahn and C. Kim, *Eur. J. Pharm. Biopharm.*, 2008, **68**, 545-554 (DOI:10.1016/j.ejpb.2007.07.011).
- 265 W. Ding, Y. Hattori, K. Higashiyama and Y. Maitani, *Int. J. Pharm.*, 2008, **354**, 196-203 (DOI:10.1016/j.ijpharm.2007.10.051).
- 266 Y. Wang, C. Ke, C. Weijie Beh, S. Liu, S. Goh and Y. Yang, *Biomaterials*, 2007, **28**, 5358-5368 (DOI:10.1016/j.biomaterials.2007.08.013).
- 267 T. Wang, H. Jiang, Q. Zhao, S. Wang, M. Zou and G. Cheng, *Int. J. Pharm.*, 2012, **436**, 351-358 (DOI:10.1016/j.ijpharm.2012.06.028).
- 268 B. Kateb, K. Chiu, K. L. Black, V. Yamamoto, B. Khalsa, J. Y. Ljubimova, H. Ding, R. Patil, J. A. Portilla-Arias, M. Modo, D. F. Moore, K. Farahani, M. S. Okun, N. Prakash, J. Neman, D. Ahdoot, W. Grundfest, S. Nikzad and J. D. Heiss, *Neuroimage*, 2011, **54**, S106-S124 (DOI: 10.1016/j.neuroimage.2010.01.105).
- 269 F. A. Gallagher, *Clin. Radiol.*, 2010, **65**, 557-566 (DOI: 10.1016/j.crad.2010.04.006).
- 270 E. A. Osborn and F. A. Jaffer, *JACC: Cardiovascular Imaging*, 2010, **3**, 1181-1195 (DOI: 10.1016/j.jcmg.2010.09.009).
- 271 N. G. Bastus, M. J. Kogan, R. Amigo, D. Grillo-Bosch, E. Araya, A. Turiel, A. Labarta, E. Giralt and V. F. Puntès, *Mater. Sci. Eng. C*, 2007, **27**, 1236-1240 (DOI: 10.1016/j.msec.2006.08.003).

- 272 R. Bhattacharya, C. R. Patra, A. Earl, S. Wang, A. Katarya, L. Lu, J. N. Kizhakkedathu, M. J. Yaszemski, P. R. Greipp, D. Mukhopadhyay and P. Mukherjee, *Nanomed. Nanotechnol.*, 2007, **3**, 224-238 (DOI:10.1016/j.nano.2007.07.001).
- 273 A. K. Gupta and A. S. G. Curtis, *J. Mater. Sci. - Mater. M.*, 2004, **15**, 493.
- 274 D. Pissuwan, T. Niidome and M. B. Cortie, *J. Controlled Release*, 2011, **149**, 65-71 (DOI:10.1016/j.jconrel.2009.12.006).
- 275 B. Mastelic, S. Ahmed, W. M. Egan, G. Del Giudice, H. Golding, I. Gust, P. Neels, S. G. Reed, R. L. Sheets, C. Siegrist and P. Lambert, *Biologicals*, 2010, **38**, 594-601 (DOI:10.1016/j.biologicals.2010.06.002).
- 276 M. L. Mbow, E. De Gregorio, N. M. Valiante and R. Rappuoli, *Curr. Opin. Immunol.*, 2010, **22**, 411-416 (DOI:10.1016/j.coi.2010.04.004).
- 277 A. M. Harandi, D. Medaglini and R. J. Shattock, *Vaccine*, 2010, **28**, 2363-2366 (DOI:10.1016/j.vaccine.2009.12.084).
- 278 T. W. Dubensky Jr and S. G. Reed, *Semin. Immunol.*, 2010, **22**, 155-161 (DOI:10.1016/j.smim.2010.04.007).
- 279 R. Cramer and C. Rhyner, *Curr. Opin. Immunol.*, 2006, **18**, 761-768 (DOI:10.1016/j.coi.2006.09.001).
- 280 N. Garçon, L. Segal, F. Tavares and M. Van Mechelen, *Vaccine*, 2011, **29**, 4453-4459 (DOI:10.1016/j.vaccine.2011.04.046).
- 281 P. López, I. González-Rodríguez, B. Sánchez, M. Gueimonde, A. Margolles and A. Suárez, *Vaccine*, 2012, **30**, 825-829 (DOI:10.1016/j.vaccine.2011.11.115).
- 282 J. M. Grange, O. Bottasso, C. A. Stanford and J. L. Stanford, *Vaccine*, 2008, **26**, 4984-4990 (DOI:10.1016/j.vaccine.2008.06.092).
- 283 E. F. McCarthy, *Iowa Orthop. J.*, 2006, **26**, 154.
- 284 B. H. Segal, X. Wang, C. G. Dennis, R. Youn, E. A. Repasky, M. H. Manjili and J. R. Subjeck, *Drug Discov. Today*, 2006, **11**, 534-540 (DOI:10.1016/j.drudis.2006.04.016).

285 H. Takita, A. C. Hollinshead, R. H. Adler, J. Bhayana, M. Ramundo, R. Moskowitz, U. N. Rao and S. Raman, *J. Surg. Oncol.*, 1991, **46**, 9.

286 R. Rettner, *Swine flu vaccine linked with small risk of paralysis disorder*, MyHealthNewsDaily, <http://www.livescience.com/36872-swine-flu-vaccine-guillain-barre-syndrome.html>, 2013.

287 S. Gómez, C. Gamazo, B. San Roman, A. Grau, S. Espuelas, M. Ferrer, M. L. Sanz and J. M. Irache, *J. Immunol. Methods*, 2009, **348**, 1-8 (DOI:10.1016/j.jim.2009.06.005).

288 *Prescribing information for Cervarix*, GlaxoSmithKline, Belgium, 2011.

289 F. Fu, H. Tian, X. Li, Y. Lang, G. Tong, S. Liu, H. Li, W. Wang, X. Li and X. Chen, *The Veterinary Journal*, (DOI:10.1016/j.tvjl.2012.06.005).